Water Quality

BIGHT'03

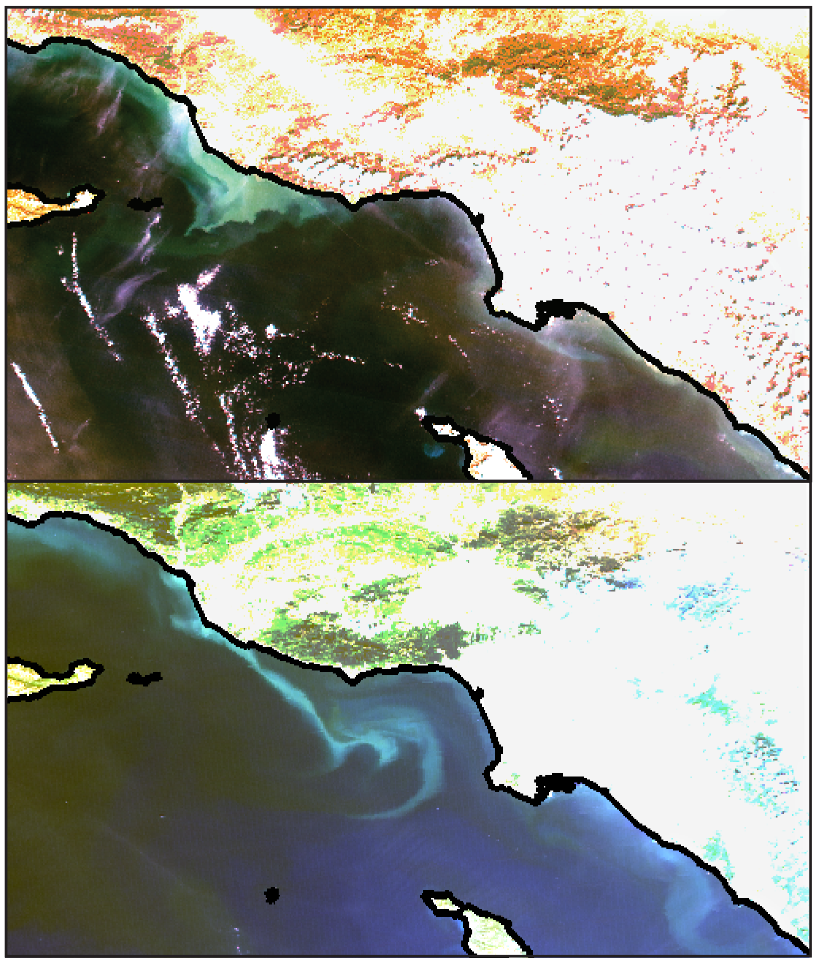

Southern California Bight
2003 Regional Monitoring
Program
Vol. V

Southern California Bight 2003 Regional Monitoring Program: V. Water Quality

August 2007

Nikolay P. Nezlin[1], Paul M. DiGiacomo[2], Stephen B. Weisberg[1], Dario W. Diehl[1], Jonathan A. Warrick[3], Michael J. Mengel[4], Burton H. Jones[5], Kristen M. Reifel[5], Scott C. Johnson[6], J. Carter Ohlmann[7], Libe Washburn[7], Eric J. Terrill[8]

[1]Southern California Coastal Water Research Project
3535 Harbor Blvd, #110
Costa Mesa, CA 92626

[2]NESDIS Center for Satellite Applications and Research (STAR)
5200 Auth Road
Camp Springs, MD 20746

[3]USGS Coastal and Marine Geology Program
400 Natural Bridges Drive
Santa Cruz, CA 95060

[4]Orange County Sanitation District
10844 Ellis Avenue
Fountain Valley, CA 92728

[5]Department of Biological Sciences, University of Southern California
3616 Trousdale Parkway
Los Angeles, CA 90089

[6]Aquatic Bioassay and Consulting Laboratories
29 N Olive Street
Ventura, CA 93001

[7]Institute for Computational Earth System Science (ICESS)
University of California, Santa Barbara 3060
Santa Barbara , CA 93106

[8]Marine Physical Laboratory, Scripps Institute of Oceanography
9500 Gilman Drive
La Jolla, CA 92093

BIGHT '03 WATER QUALITY WORKING GROUP

Member	Affiliation
Bay, Steve	Southern California Coastal Water Research Project
Caron, David	University of Southern California
Cooper, Larry	Southern California Coastal Water Research Project
Diehl, Dario	Southern California Coastal Water Research Project
DiGiacomo, Paul	NOAA/NESDIS Center for Satellite Applications and Research (STAR)
Grant, Stan	University of California Irvine
Johnson, Scott	Aquatic Bioassay and Consulting Laboratories
Jones, Burt	University of Southern California
Mengel, Mike	Orange County Sanitation District
Nezlin, Nikolay	Southern California Coastal Water Research Project
Ohlmann, Carter	University of California Santa Barbara
Robertson, George	Orange County Sanitation District
Schiff, Ken	Southern California Coastal Water Research Project
Schnetzer, Astrid	University of Southern California
Steele, Alex	Los Angeles County Sanitation District
Stolzenbach, Keith	University of California Los Angeles
Terrill, Eric	Scripps Institute of Oceanography
Warrick, Jonathan	USGS Coastal and Marine Geology Program
Washburn, Libe	University of California Santa Barbara
Weisberg, Steve	Southern California Coastal Water Research Project

FOREWORD

The 2003 Southern California Bight (SCB) Regional Monitoring Program (Bight '03) is part of an effort to provide an integrated assessment of the SCB through cooperative regional-scale monitoring. Bight '03 is a continuation of regional surveys conducted in 1994 and 1998, and represents the joint effort of 58 organizations (Appendix A). Bight '03 is organized into three technical components: (1) Coastal Ecology, (2) Shoreline Microbiology, and (3) Water Quality. This report presents the results of Water Quality component. Copies of this and the other Bight '03 guidance manuals, data, and reports are available for download at www.sccwrp.org.

The proper citation for this report is: Nezlin, N.P., DiGiacomo, P.M., Weisberg, S.B., Diehl, D.W., Warrick, J.A., Mengel, M.J., Jones, B.H., Reifel K.M., Johnson, S.C., Ohlmann, J.C., Washburn, L., Terrill, E.J. 2007. Southern California Bight 2003 Monitoring Program: V. Water Quality. Southern California Coastal Water Research Project, Costa Mesa, CA.

ACKNOWLEDGEMENTS

This report is the product of the dedication and hard work of many individuals who share a common goal of improving our understanding of the environmental quality of the Southern California Bight. The authors wish to thank the members of the Bight '03 Steering Committee and all organizations participating in planning, collecting samples, processing and analysis of the collected data. This study would not have been possible without the exceptional skill of the field sampling personnel from the following organizations: City of San Diego, Orange County Sanitation District, Los Angeles County Sanitation District, City of Los Angeles, Southern California Coastal Water Research Project, Aquatic Bioassay and Consulting Laboratories, Weston Solutions (formerly MEC Analytical Systems, Inc.), Universidad Autónoma de Baja California. The authors would like to thank the National Aeronautics and Space Administration (NASA) Goddard Space Flight Center (GSFC) for the production and distribution of the MODIS satellite data and images. MODIS data were acquired as part of the NASA's Earth Science Enterprise and were processed by the MODIS Adaptive Processing System (MODAPS), archived and distributed by the Goddard DAAC.

EXECUTIVE SUMMARY

More than $30 million is expended annually on environmental monitoring in the Southern California Bight (SCB), yet only 5% of the Bight is monitored on an ongoing basis. Therefore, environmental managers in the SCB decided to expand their monitoring program and, starting in 1994, decided to conduct periodic regional assessments of ecosystem condition and assess the overall health of the SCB. Sixty-five different organizations collaborated in 2003 to create the third SCB Regional Monitoring Program (Bight '03). Bight '03 was designed to be an integrated regional monitoring program that encompassed regulatory, regulated, academic, and non-governmental agencies.

Bight '03 had three components: Coastal Ecology, Shoreline Microbiology, and Water Quality. This report addresses the purpose, approach, findings, and recommendations from the Water Quality component, which focused on contaminant-laden stormwater runoff, in particular its variability in time and space as well as its short-term ecological impacts.

Specifically, the Bight '03 Water Quality component had three primary goals, the first of which was to describe the temporal evolution of stormwater plumes produced by the major southern California rivers. Specifically, the study was intended to determine how far offshore the plumes extended, how rapidly they advected, how long before the plumes dispersed and how these properties differed among storms and river systems.

The second goal was to describe how the physical properties (e.g., turbidity, temperature, salinity) of the plume related to biogeochemical and ecological properties that are of more direct concern to the water quality management community. Accomplished primarily through ship-based sampling of water quality parameters, this second goal was to describe how far offshore, and for how long after the storm, elevated bacterial concentrations, toxicity, and nutrients could be detected. Similar to the first goal, the study also addressed how these answers differed among storms and river systems.

The final goal was to determine whether relationships between environmental indicators derived from coincident satellite remote sensing and *in situ* data sets are sufficiently robust for remote sensing to become a part of routine water quality monitoring programs. Remote sensing data potentially provide coastal managers with synoptic near-real time regional information about prevailing ocean conditions and hazards that would complement existing field-based sampling protocols, but only if there is a thorough understanding of how to interpret and utilize the proxy measures, such as ocean color. The understanding of these properties through Bight '03 sampling is intended to provide the basis for developing more efficient, widespread and cost-effective coastal ocean monitoring techniques.

Water quality data were collected across eight major river systems within four geographic regions of southern California. Field measurements included the primary contaminants of interest, i.e., bacterial concentrations, water toxicity, and nutrients, as well as related parameters such as temperature, salinity, total suspended solids, transmissivitiy, chlorophyll, and colored dissolved organic material (CDOM) concentrations. For each of the four major regions, i.e., Santa Clara/Ventura Rivers, Ballona Creek/Santa Monica Bay, San Pedro Shelf, and the San

Diego/Tijuana Rivers, two stormwater events were sampled for up to three days by ship resulting in 574 water column CTD+ profiles and 705 discrete water samples during 36 ship-days. These data were analyzed in combination with MODIS ocean color satellite remote sensing, buoy meteorological observations, drifters, and HF radar current measurements to evaluate the dispersal patterns, dynamics, and impacts of the freshwater runoff plumes.

Based on these data and resulting analyses, the principal conclusions were as follow:

- Stormwater runoff turbidity plumes were found to be spatially extensive, covering up to 2500 km^2 within the Southern California Bight nearshore zone, and persisting over the entire duration of the post-storm sampling period (at least 3 days).

- The spatial and temporal extent of the portion of the plume with contaminants was far less than that of the turbidity plume, typically representing <10% of its area (30 – 70% off Tijuana); however, with contaminant impacts generally greatly reduced or absent by the third or fourth day of sampling.

- *Pseudo-nitzschia*, a harmful algae that produces domoic acid, was found to be more abundant than previously reported.

- Accurately describing stormwater runoff plumes requires a combination of *in situ* and remote sensing assessment tools, with satellite data providing valuable synoptic information.

From these conclusions, the following recommendations are provided:

- Future studies designed to describe stormwater plumes should include a combination of ship- and remote sensing-based methods.

- CDOM is a good proxy of the freshwater runoff plume and should be added as a standard measurement parameter on water quality instrument packages.

- Investigations are needed that assess on a local basis the spatial extent of ecological effects of stormwater plumes early in the storm, ideally accompanied by airborne imagery to provide improved temporal & spatial resolution, to fill in knowledge gaps.

The next Bight regional monitoring program should focus on quantifying nutrient loadings and dynamics in association with stormwater runoff and other sources, and characterize their attendant ecosystem impacts such as phytoplankton blooms.

TABLE OF CONTENTS

LIST OF FIGURES

LIST OF TABLES

I. INTRODUCTION

Southern California is a highly urbanized coastal region, containing approximately 25% of the nation's coastal population (Culliton *et al.* 1990). Population and land use in this region have changed dramatically over the last 50 years, with population more than tripling and another six million new residents expected by 2025 (Southern California Association of Governments 2003). One of the most noticeable effects of this population growth is the expansion and merging of metropolitan areas.

This urban growth significantly changes watershed properties, as agriculture and natural open space are converted into urbanized impervious surfaces (Schueler and Holland 2000). Increased impervious surface leads to greater runoff and contaminant loading to the ocean, producing up to 90% more runoff than unaltered watersheds (Miller *et al.* 2002). Continuing urbanization of southern California watersheds exacerbates the already pronounced response to episodic storm events characteristic of this region's semi-arid climate (Dailey *et al.* 1993).

Episodic storm events, typically occurring in late fall to early spring, contribute more than 95% of the total runoff volume annually in the Southern California Bight (Schiff *et al.* 2000). Stormwater runoff and associated runoff plumes affect physical stratification and circulation, nutrient distributions and concentrations, suspended sediments, and phytoplankton biomass and productivity, as well as poses health risks to human and aquatic organism via pollutant and pathogen loadings. Noble *et al*. (2003) found that 96 percent of the shoreline met water quality standards during dry weather, but 58 percent of the shoreline failed water quality standards during wet weather.

Information about the size and intensity of plumes has traditionally been collected through ship-based surveys. However, samples in the near-shore ocean zone are usually collected from small vessels that are sensitive to weather conditions, especially strong winds and wind-driven short-period waves. Typically, these conditions are unfavorable for ships during and immediately after a rainstorm. Moreover, ship based collections are expensive and slow. The size and condition of the plume is sufficiently dynamic that it cannot be synoptically described without deploying multiple ships, further adding to the expense and complicating planning and logistics.

An alternative approach for assessing plume properties and attendant coastal water quality is through use of satellite imagery, particularly ocean color (Johnson and Harris 1980, Nezlin and DiGiacomo 2005). The color of the ocean surface is typically correlated with important characteristics of freshwater plumes, such as salinity (Monahan and Pybus 1978, Vasilkov *et al.* 1999, Siddorn *et al.* 2001) and suspended matter (Mertes *et al.* 1998, Sathyendranath 2000, Mertes and Warrick 2001, Toole and Siegel 2001, Otero and Siegel 2004, Warrick *et al.* 2004b). Besides being less expensive (for users) to obtain than ship-based measurements, satellite imagery provides a more synoptic assessment than can be achieved by a slow moving ship trying to capture a rapidly evolving stormwater plume.

However, depending on the parameter of interest, satellite imagery often only provides indirect assessments of water quality, for example using ocean color to characterize fields of geophysical parameters, such as suspended solids, that may be associated with contaminants of interest within a plume. Ship based sampling typically involves collection of water samples, which can then be measured for biological and ecological parameters of most interest to managers, such as toxicity. No studies have previously evaluated the extent to which the satellite ocean color imagery can be used as a surrogate for these important biological parameters.

To help evaluate the overall ecological health of the Southern California Bight, 66 organizations representing an array of public agencies, private companies and academic institutions organized and implemented a regional monitoring project referred to as Bight '03. Bight '03 was the third such Bight-wide assessment of southern California coastal water, sediment and ecosystem health. The Water Quality Component of Bight '03 focused on acquisition and analysis of multi-sensor remote sensing data, coincident with ship-based measurements, to characterize spatio-temporal characteristics and short-term ecological effects of storm water runoff within the Southern California Bight. The sampling effort associated with Bight '03 is the most comprehensive study of stormwater plumes ever conducted within the Southern California Bight.

The Bight '03 Water Quality component had three primary goals, the first of which was to describe the temporal evolution of stormwater plumes produced by the major southern California rivers. Specifically, the study was intended to determine how far offshore the plumes extended, how rapidly they advected, how long before the plumes dispersed and how these properties differed among storms and river systems.

The second goal was to describe how the physical properties (e.g., turbidity, temperature, salinity) of the plume related to biological and biogeochemical properties that are of more direct concern to the water quality management community. Accomplished primarily through ship-based sampling of water quality parameters, this second goal was to describe how far offshore, and for how long after the storm, elevated bacterial concentrations, toxicity and nutrients could be detected. Similar to the first goal, the study also addressed how these answers differed among storms and river systems.

The final goal was to determine whether relationships between environmental indicators derived from coincident remote sensing and *in situ* data sets are sufficiently robust for remote sensing to become a part of routine water quality monitoring programs. Remote sensing data potentially provide coastal managers with near-real time regional information about prevailing ocean conditions and hazards that would complement existing field-based sampling protocols, but only if there is a thorough understanding of how to interpret the proxy measures, such as ocean color. The understanding of these properties through Bight '03 sampling is intended to provide the basis for developing more efficient, widespread and cost-effective coastal ocean monitoring techniques.

This report is structured in eight sections. Section II of this report describes historical oceanographic and meteorological conditions in southern California, to provide context for interpreting data from the storms that were studied here. Section III describes the methods used to collect and process field samples and satellite imagery. A quality assurance evaluation of the results is provided in Section IV, which addresses issues of data comparability and laboratory performance during the study. Section V describes the evolution, patterns and dynamics of stormwater plumes. Section VI is focused on the impact of stormwater runoff contaminants and the relationships among plume constituents. Section VII analyzes MODIS imagery as a tool for synoptic water quality assessments in southern California coastal ocean. Conclusions from the study are presented in Section VIII and recommendations for future studies are presented in Section IX. There are also eleven appendices that describe ancillary studies conducted as part of Bight '03.

II. METEOROLOGICAL AND OCEANOGRAPHIC CONDITIONS IN THE SOUTHERN CALIFORNIA BIGHT

Introduction

The Southern California Bight (SCB) lies along the southern part of the Pacific coast of the continental United States (Figure II-1). The continental coastline generally runs along a north-south gradient beginning at Cape Flattery, Washington (~48° 23'N), until Cape Mendocino in northern California (~40° 15'N), then turns toward a south-southeast direction. The continuum is broken by a bend or curvature in the coastline between Point Conception (~34° 34'N) and the Mexico international border (~32° 32'N; Figure II-1). A ring of coastal mountain ranges defines southern California (SC). The mountain ranges shelter the coastal area from dominating northwesterly winds and create a "coastal basin" where cool, dense air is trapped, resulting in much weaker wind and sea patterns than over the open ocean (Dorman and Winant 1995).

The SCB includes an ocean area of 78,000 km^2 (Dailey *et al.* 1993) and numerous islands offshore. The bottom topography consists of submarine mountains and valleys, neither of which could be considered a classical continental shelf nor a classical continental slope. Emery (1960) called it the Southern California Borderland.

The weather is often categorized "Mediterranean" by meteorologists. On a seasonal basis, it means a moderate temperature transitions and definable wet weather periods. Summers are normally warm and dry while winters are cool and wet. The combination of ocean, coastline shape, islands, mountains and atmospheric pressure systems cause weather features such as a marine layer and a cyclonic atmospheric circulation pattern referred to as a Catalina Eddy (Bosart 1983) to form regularly. These features help maintain moderate temperatures in the area. Generally, most of the winter storm precipitation gets captured on the coastal side of the mountain ranges and most of SC's population lives on the coastal side of the coastal mountain range.

Stormwater runoff varies in SC depending upon location, rainfall quantities, drainage area, watershed physiography and land-use. Watersheds range from large named drainages to small un-named channels on coastal terraces. The channel linings of these rivers or creeks range from natural sediment to manmade concrete and any combination in between. In urbanized areas, flood control improvements and water catchment structures have minimized damage from large rainfall events. Highly controlled channels (i.e., the Los Angeles River) can be concrete lined from the foothills to the mouth at the ocean (Gumprecht 1999). Dams throughout SC capture water and control water release. As a result, major flooding has become uncommon in urbanized SC, because stormwater runoff quickly moves from its initial deposition on land to the ocean in a controlled manner.

The goal of this section is to introduce the reader to general background information, specifically give some context to variability within the SC area. First we look at large scale Pacific coast trends. Then the focus is narrowed from large-scale trends to regional to selected watersheds or study areas. The sections include information that could aid in interpreting some of the results. Subsequent sections address specific topics of the study.

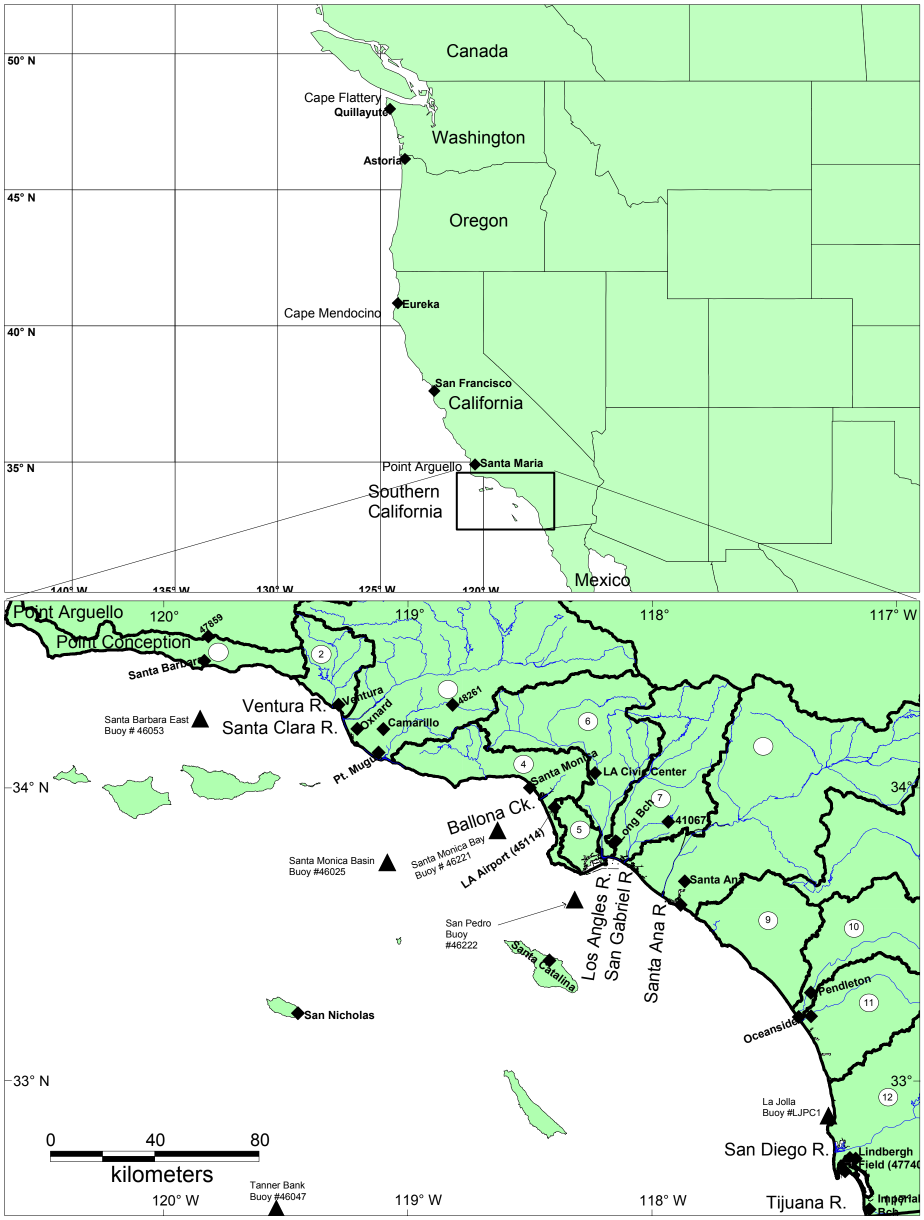

Figure II-1. Top figure shows southern California relative to the Pacific coast of the United States. The blow up shows the targeted river systems, associated coastal grouped watersheds, and NDBC moorings. The numerals in circles indicate the coastal watersheds where the rainstorm magnitude was estimated (Table II-1). Black triangles indicate buoys where wind and wave data were measured (buoys coordinates are given in Table II-2). Black diamonds indicate rain gage stations.

Table II-1. Coastal watersheds of the Southern California Bight. "#" indicates coastal watershed as shown in Figure II-1.

#	Watershed	Area (km^2)
1	Santa Barbara Creek	971
2	Ventura River	591
3	Santa Clara River	4150
	Ventura region (total)	6831
	Malibu Creek	286
	Ballona Creek	337
4	Santa Monica Bay region (total)	1170
5	Dominguez Channel	300
6	Los Angeles River	2135
7	San Gabriel River	1658
8	Santa Ana River	6340
	San Pedro Shelf region (total)	9320
9	San Juan Creek	1284
10	Santa Margarita River	1915
11	San Luis Rey River/Escondido Creek	2002
12	San Diego River	1140
	Orange County/ San Diego region (total)	8762
	Tijuana River	4303

Large Scale Latitudinal Trends

Total precipitation in SC is much smaller than in other regions of the western US coast as there are fewer rainy days. When compared with Quillayute, Washington, SC accumulates 90% less rainfall (Figure II-2a). The Pacific Northwest tends to receive measurable rainfall over half the year while SCB gets about 40 days of rain (Figure II-2b). The intensity of any given rain event in SC approximates 0.72 cm day^{-1} (San Diego: 0.60 cm day^{-1}; Los Angeles airport: 0.86 cm day^{-1}). This compares to similar values at Santa Maria 0.69 cm day^{-1}, San Francisco 0.80 cm day^{-1}, Eureka 0.81 cm day^{-1} and Astoria 0.89 cm day^{-1}. This suggests that storm rainfall quantities are comparable in California but the numbers of storms impacting the coast increase as one travels north. These are long-term averages that neglect among storm variability. The implications are that the majority of rain events are northern in nature and the SCB is at the southern end of the range with occasional storm front tails crossing the area.

One of the goals of the study was to link satellite imagery, which is available effectively during mostly clear to entirely clear days only, to ocean-based sampling. Given the precipitation trends, the cloudy or clear days exhibit expected relationships. Clear days increase with lower latitudes, comprising about 180 clear days a year at 34ºN (Figure II-2b). To the south of 34ºN (i.e., in SC) the number of cloudy days increases, resulting from the development of the Catalina Eddy features and the associated marine layer. Partly cloudy days in the SCB average over 110 days a year. These data reflect land-based sites so actual areas obscured by clouds in satellite images of coastal ocean will vary depending on patchiness and marine layer development. Another factor probably affecting satellite imagery was haze on clear or partly cloudy days. Isla *et al.* (2004) reported that San Diego averages over 140 days of haze, visibility below seven miles because of finely dispersed particles such as salt, dust, smoke, smog, etc. Overall, satellite ocean imagery for the visible light spectrum along the coast has a greater chance of success in the lower latitudes of SC as compared to northern areas.

Table II-2. The buoys in the Southern California Bight used for the analysis of wind and wave conditions.

#	NDBC identifier	Latitude	Longitude	Water depth (m)	Parameters
1	46053 (Santa Barbara East)	34° 14.17 N	119° 51.00 W	417.0	Wind vector (04/1998–12/2004) Wave height (04/1998–12/2004)
2	46221 (Santa Monica Bay)	33° 51.27 N	118° 37.96 W	363.0	Wave height and direction (01/1997–12/2004)
3	46025 Santa Monica Basin)	33° 44.70 N	119° 05.03 W	859.5	Wind vector (01/1997–12/2004) Wave height (01/1997–12/2004)
4	46222 (San Pedro)	33° 37.07 N	118° 19.02 W	457.0	Wave height and direction (02/1998–12/2004)
5	LJPC1 (La Jolla)	32° 52.00 N	117° 15.40 W	7.0	Wind vector (01/1997–11/2004) Wave height (01/1997–12/2004)
6	46047 (Tanner Bank)	32° 26.00 N	119° 31.98 W	1393.5	Wind vector (05/1999–12/2004) Wave height (05/1999–12/2004)

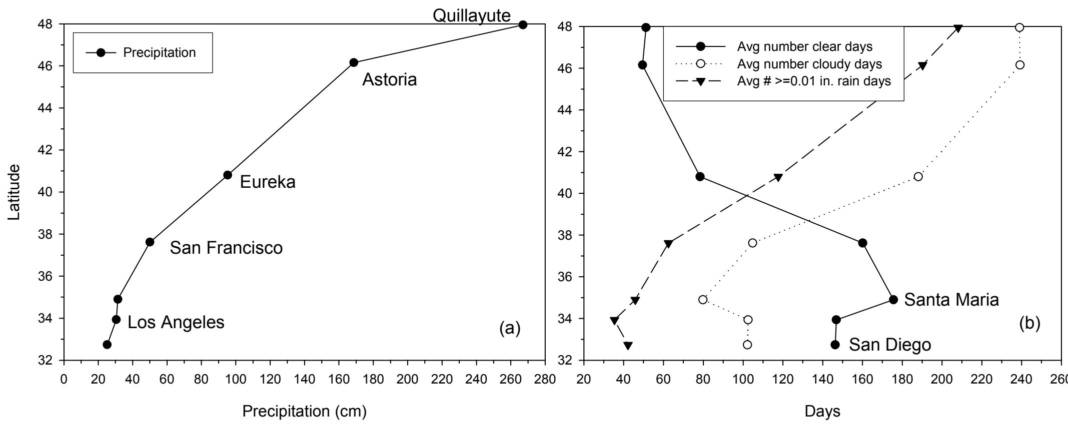

Figure II-2. Latitudinal trends along the Pacific coast for (a) precipitation, (b) days of measurable rainfall, number of cloudy days, and number of clear days. The precipitation data represent normal conditions between 1961 and 1990 as summarized by the Western Regional Climate Center. All others represent averages for Quillayute airport, Washington (29 yrs), Astoria, Oregon (40 yrs), Eureka, California (85 yrs), San Francisco, California (68 yrs), Santa Maria, California (4 – 53 yrs), Los Angeles airport, California (60 yrs), San Diego, California (55 yrs).

Regional Trends

Precipitation

Southern California's climate exhibits a relatively dry summer and wet winter season. During the dry season a semi-permanent eastern Pacific high-pressure area dominates SC. The marine layer is a prominent feature from late spring through early fall. Beginning late fall to early spring (October through March) the high-pressure ridge gets displaced and the southern margin of the polar jet stream affects SC. The probability of rain increases because the marine layer is not dominant anymore and subtropical moisture occasionally fed cold fronts crossing the SC area from Pacific storms. Over 90% of the precipitation generally occurs during this time period (Table II-3). The migratory nature of these storm front's cause alternating periods of dry and wet weather during the rainy season.

Annual rainfall decreases from the northern portion of the bight to the southern end (Table II-3). Precipitation increases as the storms near the foothills or coastal mountains. So rain measured near the coast may not reflect the actual amounts falling in any given watershed. January and February are the rainiest months. Storm intensities are frequently variable, dependent on atmospheric strength with subtropical moisture, and affected by the interannual climatic El Niño-Southern Oscillation cycles (El Niño or La Niña regimes). There are also considerable irregularities in the timing and duration of Pacific storm events.

Table II-3. Average monthly rainfall amounts (cm) for selected weather stations along the coast of Southern California. The data is presented in a water year format to highlight the rainy season.

Location	Record Period	July	Aug.	Sept.	Oct.	Nov.	Dec.	Jan.	Feb.	Mar.	Apr.	May	June	Water Year Total
Santa Barbara	1927-2004	0.05	0.08	0.38	1.32	4.34	7.85	9.32	10.29	7.11	3.05	0.79	0.23	44.81
Ventura	1948-2004	0.03	0.05	0.58	1.04	4.17	5.56	7.14	8.43	6.38	2.46	0.53	0.10	36.47
Santa Monica Pier	1948-2004	0.05	0.25	0.33	0.81	3.71	4.75	7.32	7.32	4.93	2.01	0.51	0.08	32.05
Los Angeles Airport	1944-2004	0.05	0.20	0.41	0.89	3.76	4.45	6.78	6.83	4.93	1.98	0.43	0.15	30.86
Long Beach Airport	1958-2004	0.05	0.18	0.51	0.99	3.25	4.22	6.50	7.29	4.98	1.78	0.51	0.18	30.43
Newport Bch Harb.	1934-2004	0.03	0.15	0.61	0.76	3.07	4.50	5.77	6.15	4.90	2.36	0.41	0.15	28.85
Oceanside Marina	1953-2004	0.08	0.20	0.66	0.97	2.74	3.23	5.28	5.28	4.42	2.46	0.53	0.20	26.06
San Diego Airport	1914-2004	0.05	0.15	0.46	1.27	2.44	4.47	5.16	4.98	4.29	2.01	0.53	0.15	25.96
Mean		0.05	0.16	0.49	1.01	3.44	4.88	6.66	7.07	5.24	2.26	0.53	0.16	31.94
Std Deviation		0.02	0.07	0.12	0.20	0.67	1.36	1.35	1.72	0.98	0.41	0.11	0.05	6.20

Wind

Wind, though not targeted during the study, plays an important role during regional and site-specific studies. Pressure gradients, important to satellite imagery, move storms and associated clouds through the area. Wind generated ocean waves disrupt boat based sampling. Surface ocean currents, manipulated by wind, dictate stormwater runoff direction in coastal waters. Given these factors, it becomes important to mention some of the regional variability.

Coastal winds exhibit a diurnal characteristic during most times of the year. From evening until early mornings, winds normally are moving in an offshore direction. The winds change direction to onshore usually by late morning. The heating and cooling of land next to a cool ocean causes this diurnal wind pattern. Afternoon sea breezes frequently range from 4.4 – 6.7 m s^{-1} (Morris, T.R.: The Climate of Los Angeles; http://www.wrh.noaa.gov/lox/climate/ climate_intro.php). During the wet season, the steady alongshore winds are interrupted, on the one hand, by moist precipitation-generating onshore flows (storms), and, on the other, by strong offshore flow events known as "Santa Ana winds" (extremely dry winds).

Land-based wind data are difficult to interpret on a regional scale. The wind data from airports near the SCB coast show that during winter months, wind direction often changes from westerly to easterly, or northerly or southerly, depending on the location (Table II-4). The effects of irregular topography and mountains alter the pattern of wind direction. Coastal wind speeds for SC average about 3 m s^{-1} (diurnal wind pattern effect) and do not dramatically increase during the winter storm periods. However, during December–February, standard deviations increase (Table II-4) showing higher variability due to winter conditions. San Nicholas Island is located further offshore and appears to be dominated by the prevailing oceanic northwesterly winds entering the bight. By the time the winds cross to Catalina Island and the mainland, speeds have been reduced and directions have usually changed. The decrease of northwesterly winds inshore result in an upwelling-generating positive wind curl typical to SCB (Hickey 1979, Winant and Dorman 1997, Nezlin and McWilliams 2003).

Sea-based buoy data illustrate magnitude/direction changes of winds and waves during and after rainstorms. Typically, northwesterly wind changed during rainstorms to southerly (Figure II-3). This pattern was especially evident in the open zone of SCB (Figure II-3D). In more coastal zones, including the Santa Barbara Channel (Figure II-3A), Santa Monica Bay (Figure II-3B) and San Diego (Figure II-3C) the wind pattern was less steady then offshore areas and the wind direction change associated with rainstorms was not as evident. The typical wave direction was from the west-southwest in Santa Monica Bay (Figure II-4A) and from the west in the San Pedro region (Figure II-4B). These directions are heavily influenced by the dominating wind pattern and the shape of the coastline within these two zones of SCB (see Figure II-1). Waves generated by northwesterly wind propagate to Santa Monica Bay from the open ocean and to the San Pedro Channel through the passage between the Palos Verdes Peninsula to the north and Santa Catalina Island to the south. After rainstorms, wave direction veered counterclockwise as a result of the changes in wind direction and remained atypical for two days in the San Pedro Channel (Figure II-4B) and for three to four days in Santa Monica Bay (Figure II-4A).

Table II-4. Average monthly wind speed (m s-[1]) and direction for selected airports near the southern California coast. Data represent hourly measures from 1992 to 2002. Direction is the dominant mode only. The shaded months represent the wetter periods.

Location	July	Aug.	Sept.	Oct.	Nov.	Dec.	Jan.	Feb.	Mar.	Apr.	May	June	Annual
S. Barbara	2.8	2.6	2.4	2.2	2.1	2.0	2.1	2.6	2.8	3.2	3.0	3.0	2.6
	WSW	WSW	WSW	WSW	WSW	WSW	WSW	W	WSW	WSW	WSW	WSW	
Oxnard	3.7	3.6	3.4	3.3	3.4	3.8	3.7	4.0	3.9	4.0	3.8	3.7	3.7
	W	W	W	W	W	NE	W	W	W	W	W	W	
Camarillo	2.2	2.2	2.1	2.4	2.8	3.3	2.9	3.0	2.8	2.9	2.6	2.5	2.6
	WSW	WSW	WSW	WSW	WSW	ENE	ENE	ENE	ENE	WSW	SW	SW	
Point Mugu	2.8	2.8	2.6	2.7	3.1	3.5	3.4	3.6	3.3	3.5	3.2	3.0	3.1
	W	W	W	W	NE	NE	NE	W	W	W	W	W	
LA Int'l	3.7	3.2	3.4	3.2	3.0	3.1	3.2	3.7	3.8	4.0	3.8	3.7	3.5
	WNW	WNW	WNW	WNW	WNW	E	E	WNW	WNW	WNW	WNW	WNW	
Long Beach	2.9	2.9	2.6	2.3	2.0	2.0	2.1	2.6	2.7	3.1	3.0	3.0	2.6
	S	WNW	WNW	WNW	WNW	WNW	WNW	W	S	W	S	S	
Santa Ana	3.4	3.3	2.9	2.5	2.3	2.3	2.2	2.6	3.0	3.4	3.5	3.6	2.9
	SSW	SSW	SW	SW	SW	S	S	S	S	S	S	SSW	
Pendleton	2.3	2.2	2.0	1.8	1.7	1.5	1.7	1.8	2.0	2.1	2.4	2.3	2.0
	SSW	SSW	SSW	SSW	N	N	N	SSW	SSW	SSW	SSW	SSW	
Oceanside	2.1	2.0	1.8	1.5	1.7	1.6	1.7	2.1	2.1	2.2	2.3	2.3	1.9
	WSW	WSW	WSW	WSW	WSW	NNE	W	NE	WSW	WSW	WSW	WSW	
SD Lindbergh	3.4	3.3	3.1	2.7	2.4	2.3	2.6	3.0	3.2	3.4	3.4	3.4	3.0
	WNW	WNW	WNW	WNW	WNW	WNW	WNW	WNW	WNW	WNW	WNW	WNW	
SD North Isl	3.2	3.1	3.0	2.6	2.3	2.2	2.6	3.0	3.1	3.3	3.1	3.2	2.9
	W	NW	NW	NW	NW	NW	NW	W	W	W	W	W	
Imperial Bch	4.0	3.8	3.4	3.1	2.9	3.0	3.1	3.7	3.6	3.9	3.9	4.0	3.5
	W	W	WNW	W	WNW	E	E	WNW	W	W	W	W	
Mean	3.0	2.9	2.7	2.5	2.5	2.5	2.6	3.0	3.0	3.2	3.2	3.1	2.9
SD	0.61	0.56	0.57	0.53	0.57	0.75	0.67	0.67	0.60	0.62	0.54	0.57	0.56
N	12	12	12	12	12	12	12	12	12	12	12	12	12
San Nicholas	4.9	4.8	4.7	4.2	4.5	4.3	4.2	4.4	4.6	6.1	5.4	5.3	4.8
Island	WNW	NW	WNW	WNW	NW	NW	WNW	WNW	WNW	WNW	WNW	NW	
S. Catalina	2.6	2.5	2.9	2.9	3.4	3.5	3.4	3.7	3.9	4.1	3.0	2.6	3.2
Island	WSW	WSW	WSW	W	W	W	W	W	W	W	WSW	WSW	

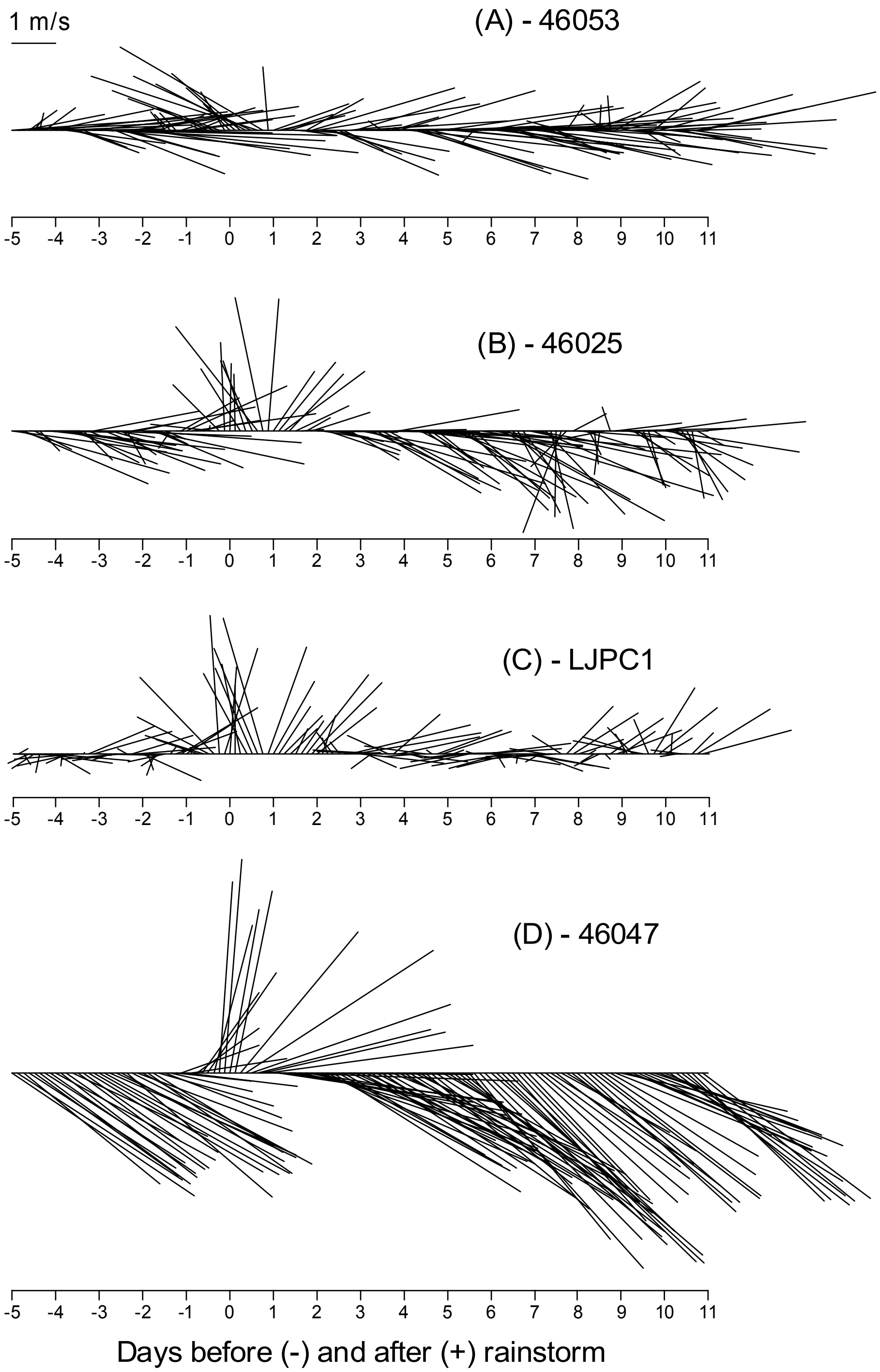

Figure II-3. Wind vectors at four NDBC buoys averaged over 3-hour periods from 5 days before rainstorm to 10 days after rainstorm.

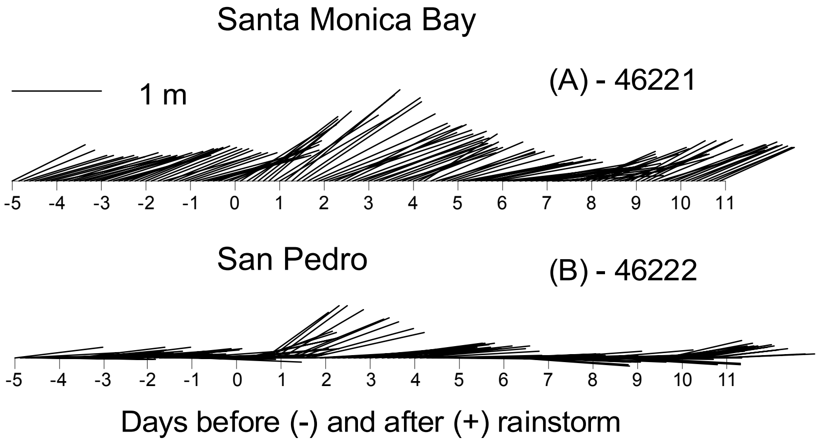

Figure II-4. Wave vectors at two NDBC buoys. Absolute wave height (m) was measured at all six SCB buoys (Figure II-1); wave direction at two of these buoys, and wind direction/speed at four buoys. Storm criterion was a rainfall accumulation exceeding 2.54 cm. Using this definition, 35 rainstorms in the Ventura region, 30 in Santa Monica, 29 in San Pedro Bay, and 29 in the San Diego watershed were grouped together (between 1997 and 2004) and used in the analysis. The time-series of wind speed/direction and wave height/direction were averaged over 3-hour time intervals and attributed to rainstorm events, from 5 days before to 10 days after each rainstorm.

Ocean Circulation

The ocean region within the SCB is dominated by the equatorward California Current (CC). The CC is a typical broad eastern boundary current (Hickey 1979, Lynn and Simpson 1987), transports cold Subarctic water from north to south throughout the year along a typically narrow (3 to 6 km) coastal continental shelf. The CC is not steady but migrates seasonally onshore and offshore, producing a rich eddy field (Burkov and Pavlova 1980, Strub and James 2000, Haney *et al.* 2001). As the CC passes Point Conception, it turns south-southeast along SC's outer continental slope then a portion branches (~32°N) eastward to northward along the coast (Hickey 1992, Harms and Winant 1998, Bray *et al.* 1999), forming a large gyre known as the Southern California Eddy. The poleward current along the coast is called the Southern California Countercurrent (Sverdrup and Fleming 1941). It transports warm southern water into Santa Monica Bay and the Santa Barbara Channel.

Surface current flows may not reflect near bottom currents. During spring, the intensity of the equatorward CC increases compared to the poleward Southern California Countercurrent. Its jet migrates onshore, and the eastward branches penetrate into the Southern California Bight through the Santa Barbara Channel and onward south of the Channel Islands (Reid and Mantyla 1976, Hickey 1979, Bray *et al.* 1999). The islands act as barriers to deflect surface currents in different directions. Near shore, over the continental shelf and borderland slope, the near surface flow is commonly equatorward while the California Undercurrent is poleward (Hickey 1993). The nearshore surface shelf flows are of special interest from the point of view of stormwater plume propagation. They may change from site to site due to local wind fields, swells, tidal motions, and larger scale basin flows. Current fluctuations over the inner shelf have significant short-period variance; these fluctuations appear to be driven predominantly by boundary forcing of the outer shelf and only secondarily by local wind stress (Winant and Bratkovich 1981, Hickey 1992, Hickey *et al.* 2003); the latter, however, may not be true for highly stratified plume waters, which are more sensitive to wind stress (see Section V).

Coastal Watersheds

Ventura/Oxnard Basin

The watersheds of the Ventura and Santa Clara Rivers drain into the ocean relatively close to the study area (Figure II-1) with the Ventura River draining the smaller area of the two. The Santa Clara River was the main focus of the study but distinguishing the two storm water plumes in the ocean may be difficult at times so the Ventura River influence can not be ruled out. The two watersheds have a high percentage of natural surroundings so significant rainfall must fall before the ground gets saturated enough for higher stream flows (Figure II-5).

The naturally lined Ventura River (50 km long) drains a 591 km^2 area of northern SC in the Transverse Mountain Range. The annual average flow approximates 16775 m^3, fluctuates significantly, and is termed an ephemeral stream because it runs normally in the winter month's "wet season". Precipitation over the Ventura River watershed can range from 12.7 to 101.6 cm per year. US Bureau of Reclamation, 2000, estimated that 98% of the total sediment load gets suspended, typical of coastal California streams. Suspended sediment was comprised primarily of sand particles (0.062 to 2 mm). Total sediment load was transported during relatively few days each year from infrequent storm events. The largest proportion of the total sediment load (i.e., suspended sediment plus bedload sediment) was transported by approximately 169.8 $m^3\ s^{-1}$ flows or equivalent to the mean annual flood (2.33 year return interval). Six dams are located within the watershed.

The Santa Clara River watershed is also unchannelized or natural. It drains an area of approximately 4150 km^2. No dams are located on the river, but four of its tributaries control 37% of the flow. During dry weather flow conditions, water gets diverted to infiltration ponds for groundwater recharge. No water flows over the diversion dam during dry conditions. During wet weather conditions, most of the flow travels through a diversion gate and over the diversion dam during high flow conditions. A barrier beach (berm) forms at the mouth of the river during low flow periods and usually breaches during high flow conditions or high wave periods. The length the inlet stays open varies with time.

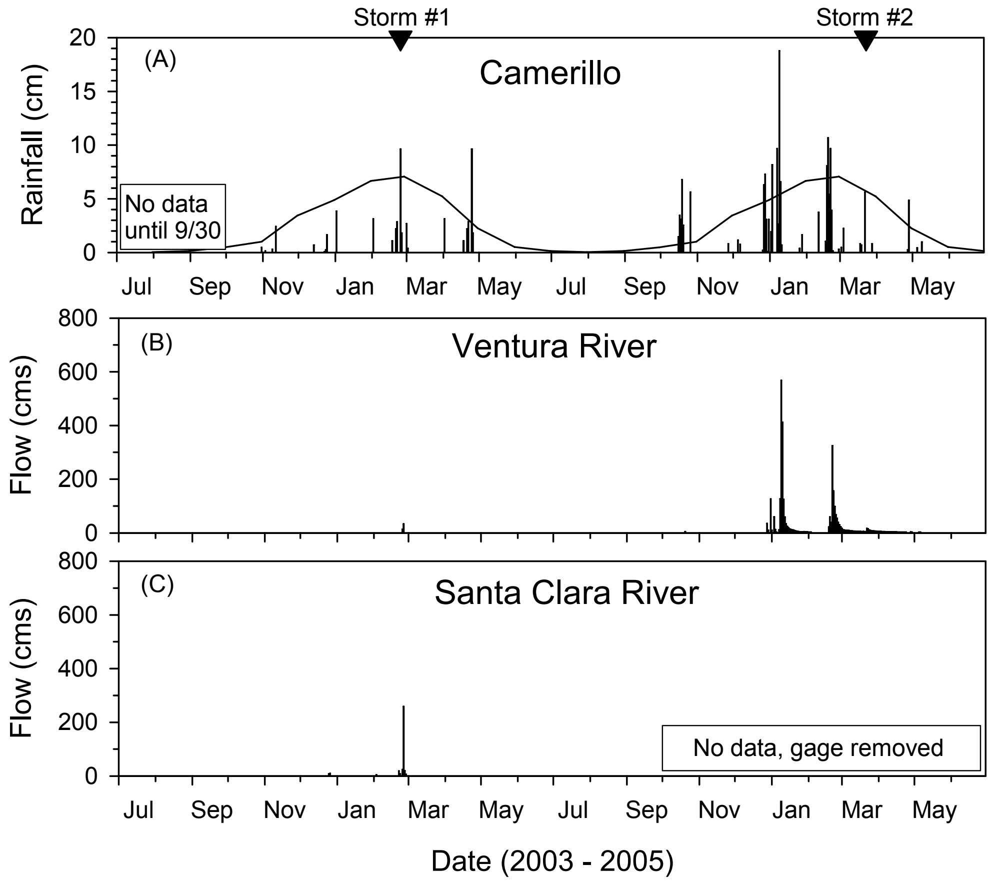

Figure II-5. Rainfall and stream flow conditions for the northern portion of SC over two water year (July 1 to June 30) period. Days of the month are located between the tick marks. (A) Daily, beginning at midnight, rainfall accumulations with a historical average curve from Table II-3 of monthly accumulations in the background. (B) Mean daily flow from USGS gage #11118500 near Ventura on the Ventura River. (C) Mean daily flow from USGS gage #11114000 at Montalov on the Santa Clara River.

Santa Monica Bay

Ballona Creek occupies the largest drainage area within the greater Santa Monica Bay (SMB) watershed. The creek drains the west central area of Los Angeles (LA), and the eastern portion of the Santa Monica Mountains. The area encompasses roughly 337 km^2. The creek should be categorized as channelized and paved. Its land use consists of 64% residential, 8% commercial, 4% industrial, and 17% open space. The study focused on Ballona Creek but influence from other watersheds cannot be ruled out. The SMB Hydrologic Unit also includes Topanga Creek, Malibu Creek, Solstice Creek, and Trancas Creek. These smaller watersheds are considered unchannelized and have a higher percentage of open space. Altogether, they drain approximately 1170 km^2 and are subdivided by 28 separate drainages. All the watersheds drain into a common ocean area known as SMB.

San Pedro Bay/Orange County

Four major watersheds are grouped into the San Pedro area. The San Pedro Bay group (SPB) sampled near discharge points for the Los Angeles River, San Gabriel River, Santa Ana River, and Newport Harbor. Distinguishing between these four storm water plumes may be difficult during a storm. All three watersheds have a high percentage of urban modification so response time between rainfall and flow are clearer to distinguish then in the northern Southern California area.

The Los Angeles River (LAR) watershed encompasses a 2135 km^2 area and contains many water catching structures (22 lakes, Devil Gates Dam, Hansen Basin, Lopez Dam, Pacoima Dam, Sepulveda Basin, and a number of spreading grounds). The watershed has diverse patterns of land use. The upper portion of the watershed, 920 km^2, has forest or open space, while the remaining portion, 1215 km^2, has highly developed commercial, industrial, or residential uses. There are eight major tributaries to LAR. The LAR empties near the Long Beach/Los Angeles Harbor complex. Virtually the entire river has been channelized and paved.

The San Gabriel River (SGR) watershed encompasses 1658 km^2. The river has been channelized and developed for much of its length. At least 26% of the total watershed area has been developed.

The Santa Ana River watershed drains approximately 6340 km^2. It has one of the largest drainage areas in southern California. This river can be categorized as channelized with high levee banks and other flood control measures upstream. Flows are composed of storm water discharge and urban run-off. Prado Dam controls 92% of the river flow and significantly affects river discharge to the ocean.

San Diego area

Two watersheds are grouped into the southern portion of the Bight. The San Diego River was sampled in 2004 while the Tijuana River had both 2004 and 2005 sampling dates. Discharge points were dissimilar and non-overlapping. The two watersheds have a higher percentage of arid surroundings so significant rainfall must fall before stream flows increase. Additionally, dams capture surface water runoff when available.

The San Diego River drains approximately 1140 km^2. There are 4 dams within the San Diego River watershed: El Capitan on the main river; San Vicente, Lake Jennings, and Cuyamaca on tributaries. The reservoirs along the river are major water storage facilities for the San Diego metropolitan area. These reservoirs store water that is primarily from the Colorado River. El Capitan stores local water while Cuyamaca Reservoir stores only local runoff. The annual precipitation ranges from less than 27.9 cm along the coast to 88.9 cm around Cuyamaca and El Capitan reservoir.

The Tijuana River watershed encompasses approximately 4303 km^2 and contains 5 dams. The watershed can be characterized as unchannelized, binational (3225 km^2 in Mexico and 1178 km^2 in the US), and located on the westernmost portion of the US - Mexico border. The basin contains three surface water reservoirs, various flood control works, and a National Estuarine

Sanctuary, which is home to several endangered species and protected by the US federal government. The major drainages include Cottonwood and Campo creeks in the US, and the Rio Las Palmas system in Mexico. Annual precipitation varies from less than 27.9 cm to 63.5 cm farther inland near the Laguna Mountains. Morena Reservoir (US), Barrett Lake (US), and Rodriquez Dam (Mexico) control 78% of the water flow in the watershed. Poor water quality continually hampers this watershed. The water quality problem has worsened in recent years with the substantial growth of Tijuana's population, along with intensive industrial development associated with an in-bond manufacturing and assembly plants program in Mexico. The international treatment plant (US) treats most of the effluent during dry weather flow periods.

Conditions During Bight '03 Program

Due to the inconsistent nature of rainfall within SC, sampling was carried out in two sub-regions, north/central and San Diego, independent of each other. As such, we analyze meteorological conditions in these two regions separately, with reference to the sampling events. Sampling event # 1 was initiated by the storms starting February 22, 2004 in San Diego area and three days later, on February 25, in the northern and central SC. Sampling event # 2 was initiated on February 11, 2005 in San Diego area and almost six weeks later, on March 23, 2005 in the northern and central SC.

Rainfall and Stream Flow

North SC

Sampling event # 1 was initiated on February 25, 2004. The National Weather Service rain gage at Camarillo recorded a 2-day storm beginning February 25 (Figure II-5). The storm totaled 11.4678 cm. One day earlier, a 3-day storm ended totaling 5.1522 cm. Two days before that storm a 1-day storm totaling 1.108 cm. There was a 14-day dry period prior to the 1.108 cm storm. After sampling was initiated, another 2-day storm began on March 1st, after which an extended dry period began.

Stormwater flow for event # 1 was sufficient to breech the berm at the Santa Clara River mouth. The stream gage measured flow beginning February 21 to March 5th (Figure II-5) with peak flow, 259 $m^3 s^{-1}$, occurring on February 26. The Ventura River flow peaked on the same day but at 34 $m^3 s^{-1}$. The gage data was different between the two rivers. While the Ventura gage continually measures low flows, not visible on Figure II-5 because of scale, the Santa Clara measured nothing. Gage placement on the Santa Clara in relationship to the diversion dam may influence the type of flow recorded at that station. In addition, large swells and surf closed the Ventura Harbor entrance for several days. Boat sampling did not begin until February 29, 2004.

Sampling event # 2 was initiated on March 23, 2005. The Camarillo rain gage recorded a 1-day storm on March 22 (Figure II-5). The storm totaled 5.6508 cm. Two days earlier, a 2-day storm occurred totaling 1.5512 cm. There was a 13-day dry period prior to that 1.5512 cm storm. After sampling was initiated, there were 5 days of little rain and a 1-day storm on March 28, after which an extended dry period began.

Stormwater flow for event # 2 peaked at 17.3 $m^3 s^{-1}$, in the Ventura River on March 22 2005. The Santa Clara River stream gage became disabled because of construction so no associated data is visible in Figure II-5. The 2004–2005 wet period was an exceptionally heavy rainfall season in Southern California. Heaviest rains and flows occurred at the beginning of January and the end of February. Ventura River flows between storms were in the single digit numbers as compared to the previous year where flows were in the tens or hundreds.

Central SC

For sampling event # 1, the National Weather Service rain gage at LA Civic Center recorded a 3-day storm beginning February 25 (Figure II-6). The storm totaled 7.2644 cm. One day earlier, a 4-day storm ended totaling 2.8194 cm. One day before that storm a 1-day storm totaled 0.4572 cm. There was a 14-day dry period prior to the 0.4572 cm storm. After sampling was initiated, another 2-day storm began on March 1, after which an extended dry period began. Differences between storms from the Camarillo gage and the LA gage appears to be higher magnitude (rainfall totals) and greater duration (more days of rain). Rainfall totals for any given storm varies from location and declines as one moves south. San Diego received the same storm a day later but 43% less in magnitude (Figure II-7).

Stormwater flow for event # 1 peaked one day after peak rainfall. On February 26 Ballona Creek, the LA River, San Gabriel River, and Santa Ana River had flows of 56, 437, 140, and 110 $m^3 s^{-1}$, respectively (Figure II-6). The following day, flows were approaching background levels except on the Santa Ana River. The Santa Ana took three additional days before approaching normal conditions. Sampling event # 1 captured the largest storm in regards to runoff for the 2003–2004 winter season.

For sampling event # 2, the Civic Center rain gage recorded a 1-day storm on March 22 (Figure II-6). The storm totaled 2.7432 cm. One day earlier, a 3-day storm ended totaling 0.7620 cm. There was a 13-day dry period prior to the 0.7620 cm storm. After sampling was initiated, there were two storms of 1-day duration on March 24, 2005 (0.0254 cm) and March 28, 2005 (0.2794 cm), after which an extended dry period began. Comparing rain gages, LA got the same storm duration but 51% less magnitude than Camarillo. San Diego got 7% more rainfall then LA but duration was extended an additional day and blended with a quick moving storm front passing on the March 24, 2005. On a final note, the National Weather Service recorded the second largest rainy season, 2004–2005, for LA Civic Center.

Stormwater flow for event # 2 peaked about the same day as peak rainfall. On March 22, 2005 Ballona Creek, the LA River, and San Gabriel River had flows of 43, 138, and 94 $m^3 s^{-1}$, respectively (Figure II-6). The Santa Ana River peaked the day after at 96 $m^3 s^{-1}$. The LA area was still recovering from heavy rains earlier in the season, so response time varied with watershed. Ballona Creek, the LA River, San Gabriel River, and Santa Ana River took 2, 6, 4, and 12 days, respectively, to return to levels before the storm. Dam releases influenced most of the response times after late December except at Ballona Creek. Additional storms passing through the area complicated flow patterns to near continuous stormwater discharge for extended periods of time.

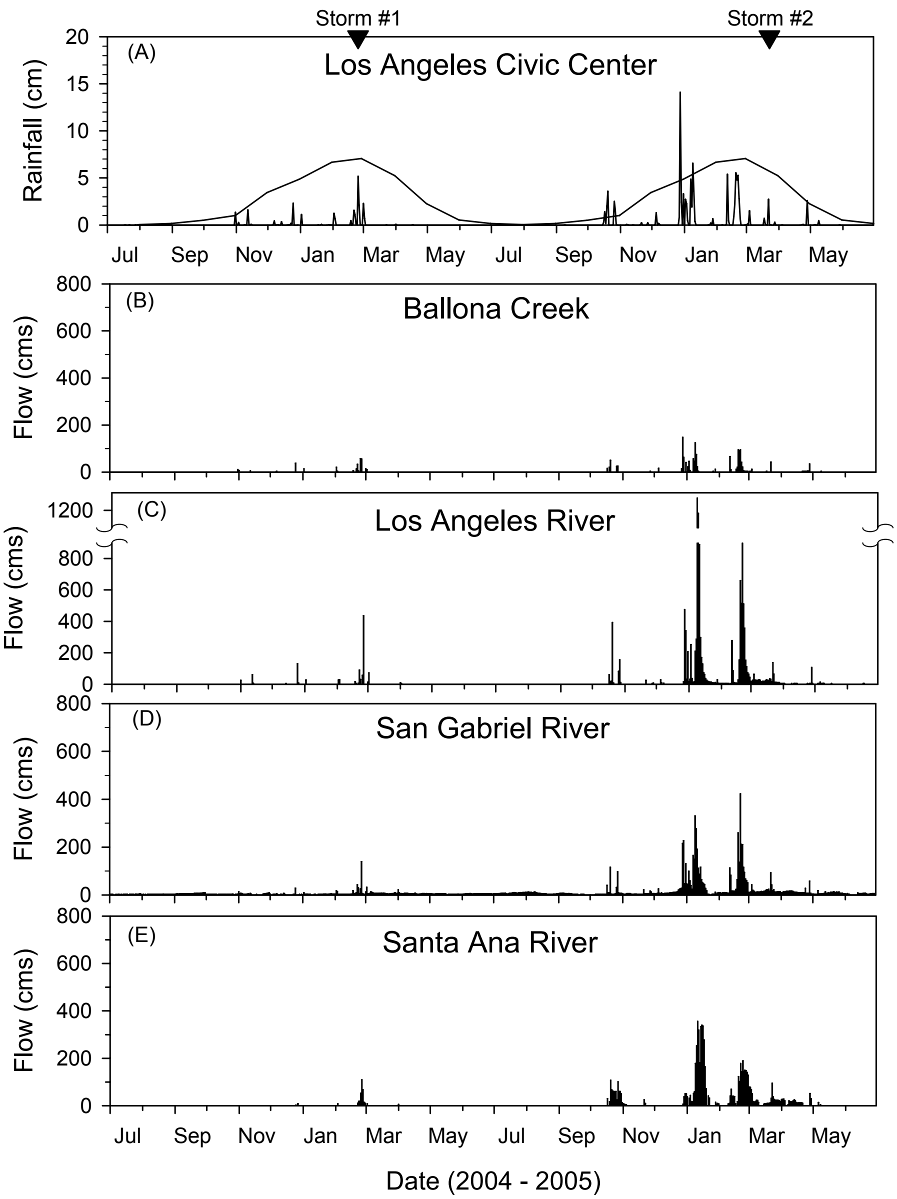

Figure II-6. Central SC rain and flow conditions for July 1, 2003 to June 30, 2005. Days of the month are located between the tick marks. (A) Daily, beginning at midnight, rain accumulations at Los Angeles Civic Center with a historical average curve from Table II-3 on monthly accumulations in the background. (B) Mean daily flow from LACDPW #F38C-R gage on Ballona Creek. (C) Mean daily flow from LACDPW #F319-R gage on the Los Angeles River. (D) Mean daily flow from combined LACDPW gages #F42B-R and F354-R on the San Gabriel River. (E) Mean daily flow from USGS gage #11078000 on the Santa Ana River.

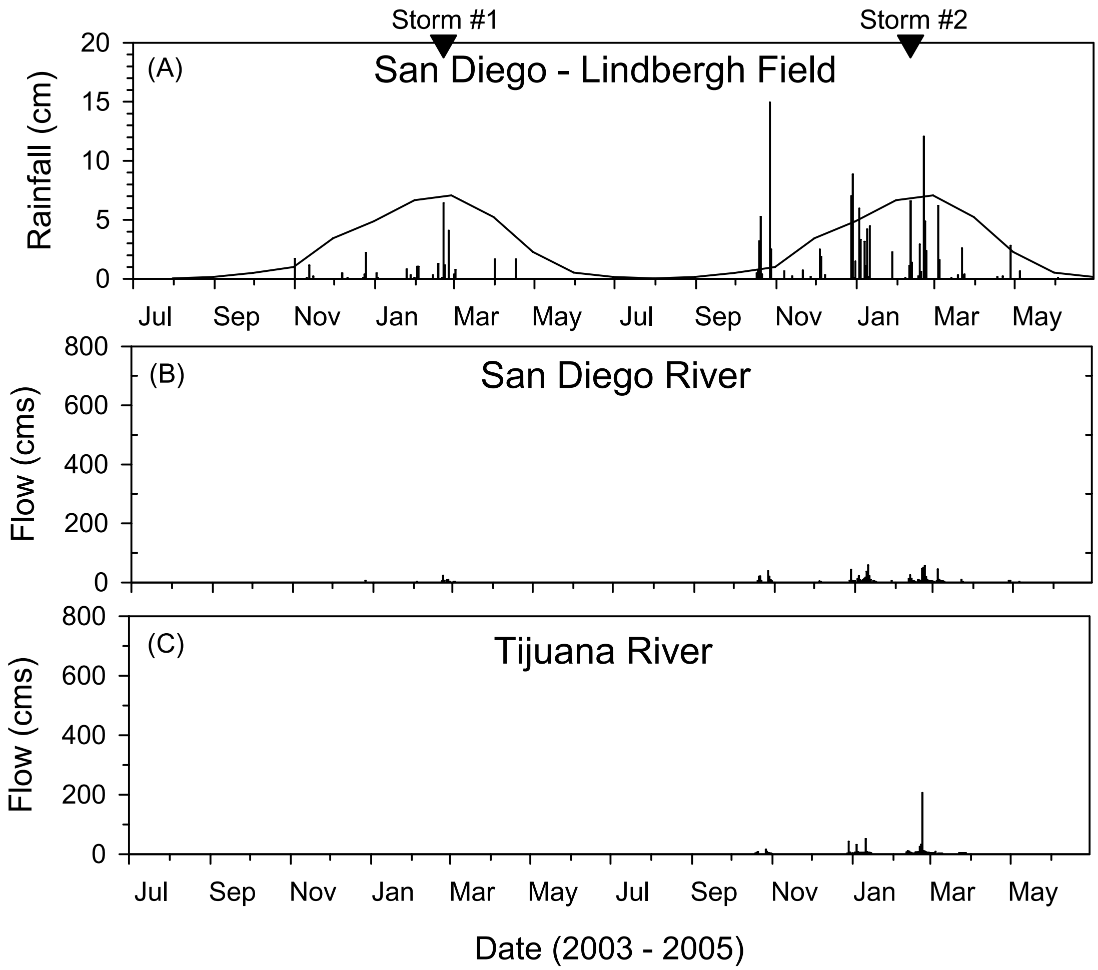

Figure II-7. Rainfall and stream flow conditions for the southern portion of the SCB over two water year (July 1 to June 30) period. Days of the month are located between the tick marks. (A) Daily, beginning at midnight, rainfall accumulations at the San Diego airport (Lindbergh Field) with a historical average curve from Table II-3 of monthly accumulations in the background. (B) Mean daily flow from USGS gage #11023000 on the San Diego River. (C) Mean daily flow from the IBWC gage at the international border on the Tijuana River.

San Diego region

Sampling event # 1 was initiated on February 22, 2004. The rain gage at San Diego airport (Lindbergh Field, Figure II-7) recorded a 3-day storm beginning February 21 (Figures II-7 through II-8). The precipitation rate on February 21 totaled 0.05 cm. The storm totaled 7.7006 cm, the bulk of water precipitated during the afternoon of February 22 (Figure II-8). Two days earlier, a 1-day storm totaled 1.2742 cm. Three days before that storm, another 1-day storm totaled 0.3324 cm. There was a 10-day dry period prior to that 1-day storm. After sampling was initiated, another 2-day storm, 4.1550 cm, began on February 24. Two days later another 2-day storm, 1.1634 cm, passed the area. After which an extended dry period began. The largest storm of the season was targeted during the 2003–2004 rainy season.

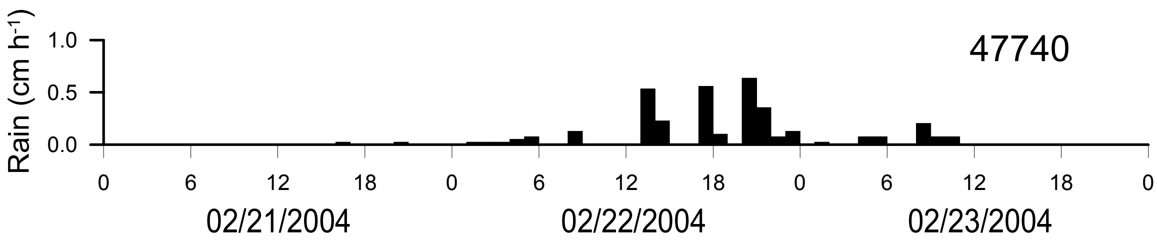

Figure II-8. Rainfall at San Diego airport (Lindbergh Field, gage station # 47740; Table II-5) during February 21-23, 2004. X-axis is local time (PST).

Stormwater flow for event # 1 on the San Diego River peaked one day after peak rainfall. The Tijuana River peaked the day of peak rainfall. Peak flows for the San Diego River and Tijuana River were 24 and 2 $m^3\ s^{-1}$, respectively (Figure II-7). The San Diego River took 3 to 4 days to approach background levels or until another storm passed the area. The Tijuana River took one day to respond. The Tijuana River did not respond to any subsequent storm until on March 1 2004, recorded the highest flow the following day and continued until March 9. Note the international treatment plant may influence the discharge rate on the river. Sampling event # 1 captured the largest storm in regards to runoff for the 2003–2004 winter season.

Sampling event # 2 initiated on February 11, 2005. The Lindbergh Field rain gage recorded a 3-day storm starting on the afternoon of February 10 (Figure II-9). The storm totaled 9.0856 cm. Two days earlier, a 1-day storm totaled 0.1108 cm. There was a 9-day dry period prior to that 1-day storm. After the trigger storm ended, a 4-dry period ensued before two nearly back-to-back storms passed the area, the second of which produced the second largest daily rainfall total for the 2004–2005 wet season.

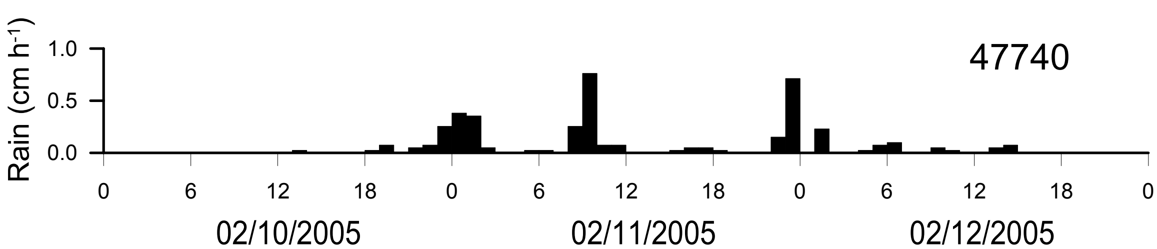

Figure II-9. Rainfall at San Diego airport (Lindbergh Field, gage station # 47740; Table II-5) during February 10-12, 2005. X-axis is local time (PST).

Stormwater flow response for event # 2 was different then in event # 1. Both watersheds had peak flow the day after peak rainfall. Peak flows for San Diego River and Tijuana River were 25 and 11 $m^3\ s^{-1}$, respectively (Figure II-7). Measured flows in both systems fell on subsequent days but not to the levels observed during the 2003–2004 wet season. Only after the heavy rains subsided did levels return to background conditions.

Hourly Rainfall Analysis

North/Central Sampling Group

In both 2004 and 2005, the rain zone propagated from the northwest to the southeast, which is evident from the analysis of hourly precipitation measured at five gage stations from Santa Barbara County to San Diego County (Table II-5). In 2004, at Santa Barbara the rainstorm started at noon February 25 (Figure II-10), achieved maximum (1.5 – 2 cm h^{-1}) between 3 p.m. and 6 p.m. and ceased at 7 p.m. At Ventura the storm started the same day four hours later, at 4 p.m., reached maximum at 8 p.m. and ceased at 2 a.m. February 26, 2004. Further to the south, at LA International Airport (LAX), the rainstorm started at 5 p.m. February 25, 2004, achieved maximum (0.5 – 0.8 cm h^{-1}) from 8 p.m. till 10 p.m., and ceased at 4 a.m. the next day. The LA Civic Center recorded measurable rain (0.0254 cm) on the third day from scattered showers passing the area. Further south and inland, Orange County, maximum rain (~1 cm h^{-1}) was observed from 9 p.m. February 25 till midnight; after that the rain ~0.5 cm h^{-1} lasted until 6 a.m. February 26. In San Diego (Lindbergh airport), the storm started as late as 4 a.m., achieved maximum (~0.5 cm h^{-1}) at 6 a.m. and almost finished at 9 a.m. February 26, 2004.

Table II-5. Rain gage stations used for hourly rainfall analysis.

#	NCDC identifier	County	Latitude	Longitude	Elevation (m)
1	47859 (San Marcos Pass)	Santa Barbara	34º31'	119º49'	213.7
2	48261 (Simi Valley Sanitation Plant)	Ventura	34º17'	118º49'	61.3
3	45114 (Los Angeles International Airport)	Los Angeles	34º03'	118º15'	9.3
4	41057 (Brea Dam)	Orange	33º53'	117º56'	25.5
5	47740 (San Diego-Lindbergh Field Airport)	San Diego	32º44'	117º10'	1.2

In 2005, the rainstorm started in Santa Barbara County (gage station 47859) at 8 a.m. March 22 (Figure II-11). During the next few hours the rain magnitude gradually increased and achieved maximum (~1.8 cm h^{-1}) at noon. After that, the precipitation rate decreased and the storm ceased at 8 p.m. In Ventura County (gage station 48261) the rainstorm (~0.8 cm h^{-1}) started at 2 p.m., then its magnitude decreased, and the rain was over at 7 p.m. March 22. At LAX (gage station 45114), the rain started at 3 p.m. of March 22, achieved maximum (~1.3 cm h^{-1}) at 5 p.m., and ceased at 8 p.m. In Orange County (gage station 41057) the rain started one hour later (at 4 p.m.), increased by 1.2 cm h^{-1} at 6 p.m., and almost stopped in next two hours. In San Diego (gage station 47740) the storm started the same day at 7 p.m., achieved maximum (~0.9 cm h^{-1}) at 9 p.m., and ceased at 1 a.m. next day, March 23, 2005.

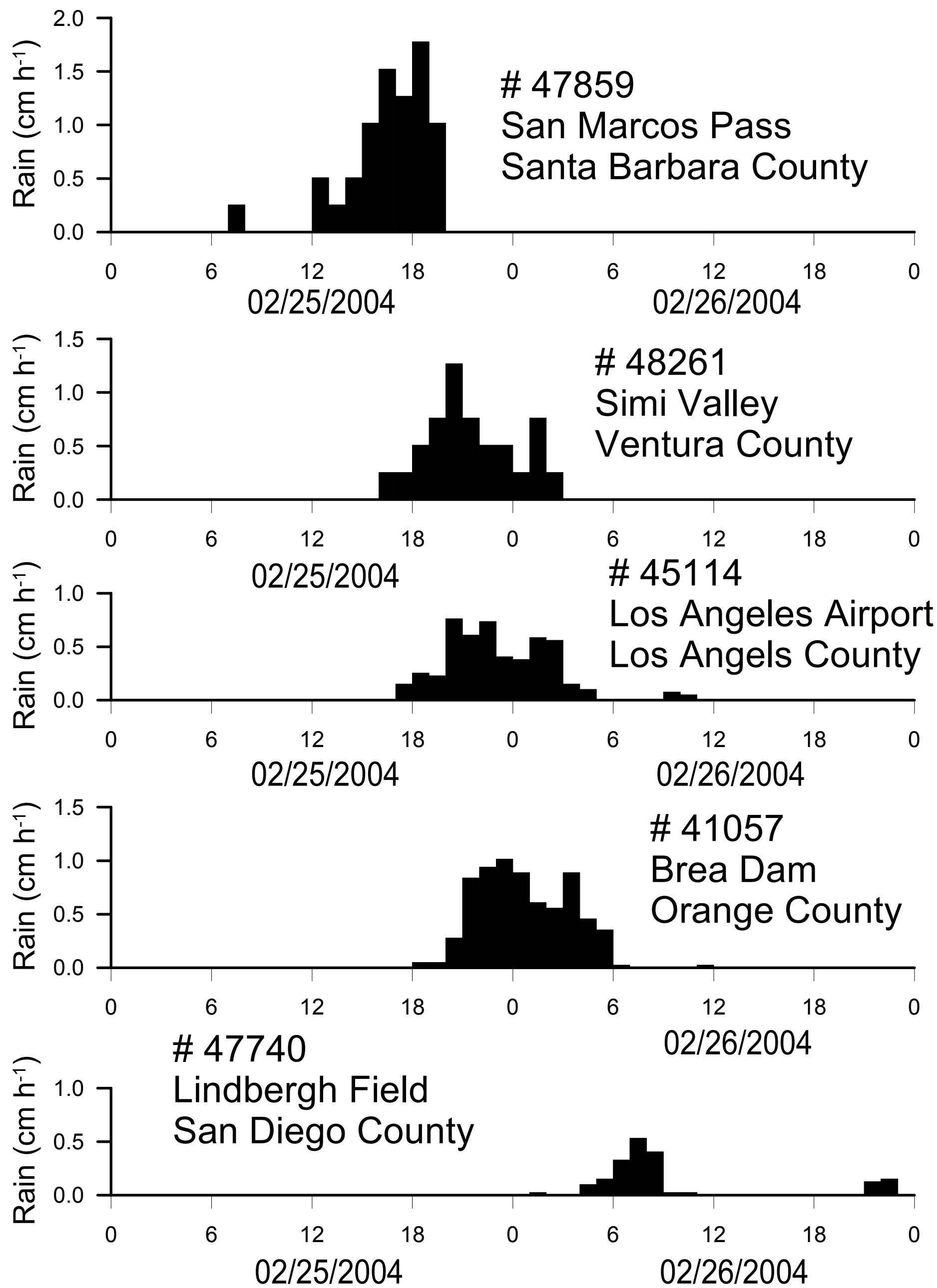

Figure II-10. Rainfall at five stations in SC (Figure II-1; Table II-5) during February 25-26, 2004. X-axis is local time (PST).

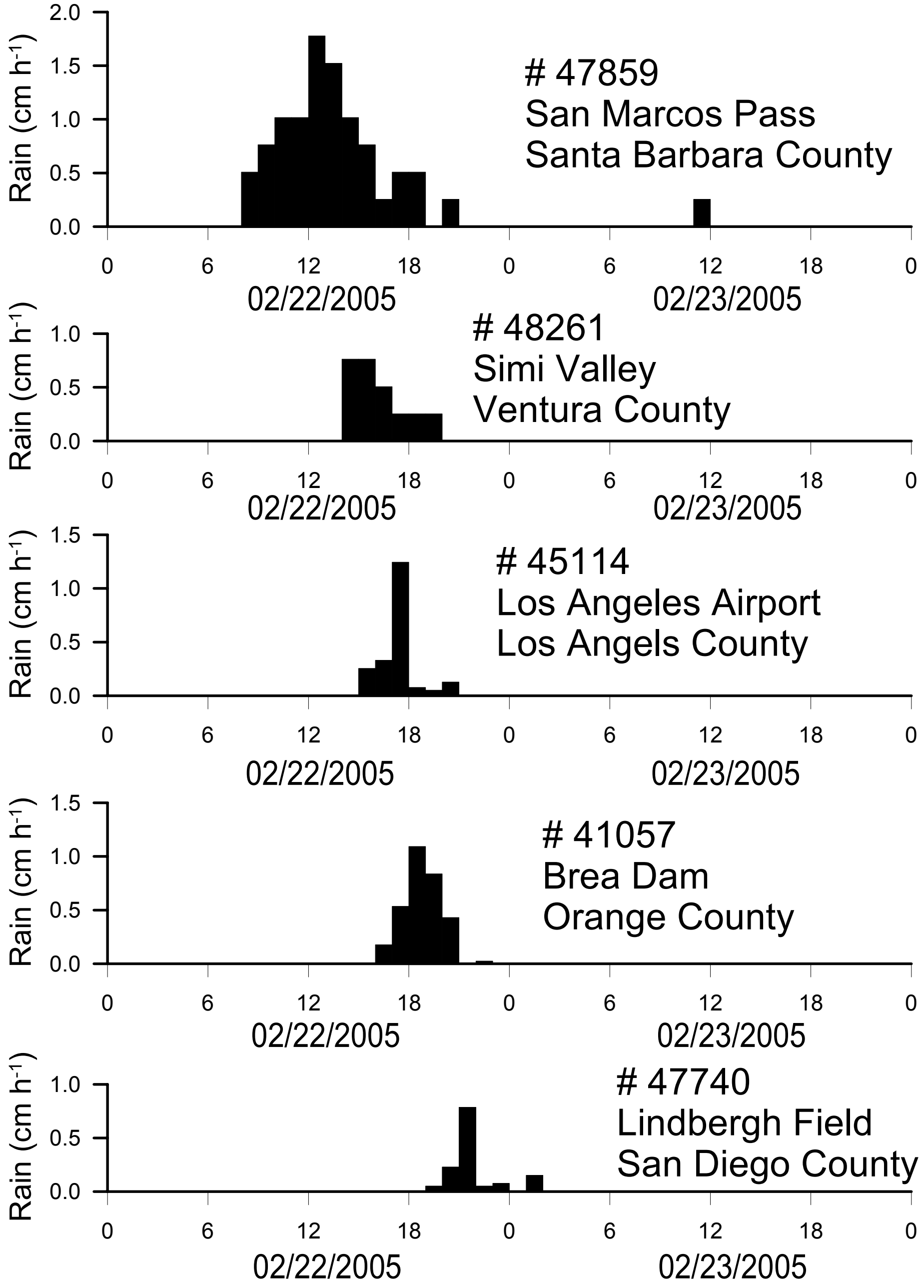

Figure II-11. Rainfall at five stations in SC (Figure II-1; Table II-5) during March 22–23, 2005. X-axis is local time (PST).

Southern Sampling Group

San Diego experienced scattered rainfall during the two sampled storm events. The 2004 rainstorm (Figure II-8) started at 5 p.m. on February 21. With intermittent showers, rain gradually increased and achieved maximum (~0.7 cm h^{-1}) at 8 p.m. on the following day. After that, the precipitation rate decreased and the storm ceased at 11 a.m. on February 23. Storm # 2

(Figure II-9) started at 1 p.m. on February 10, 2005. Again rainfall magnitude slowly increased with two peaks (~0.7 cm h^{-1}) occurring approximately 13 hours apart on the following day. Then precipitation rate decreased and the storm ceased at 3 p.m. on February 12. The sampled storm events for the northward section of the Bight appeared as solid blocks of rain versus the scattered appearance of storm # 1 and 2 in the San Diego region.

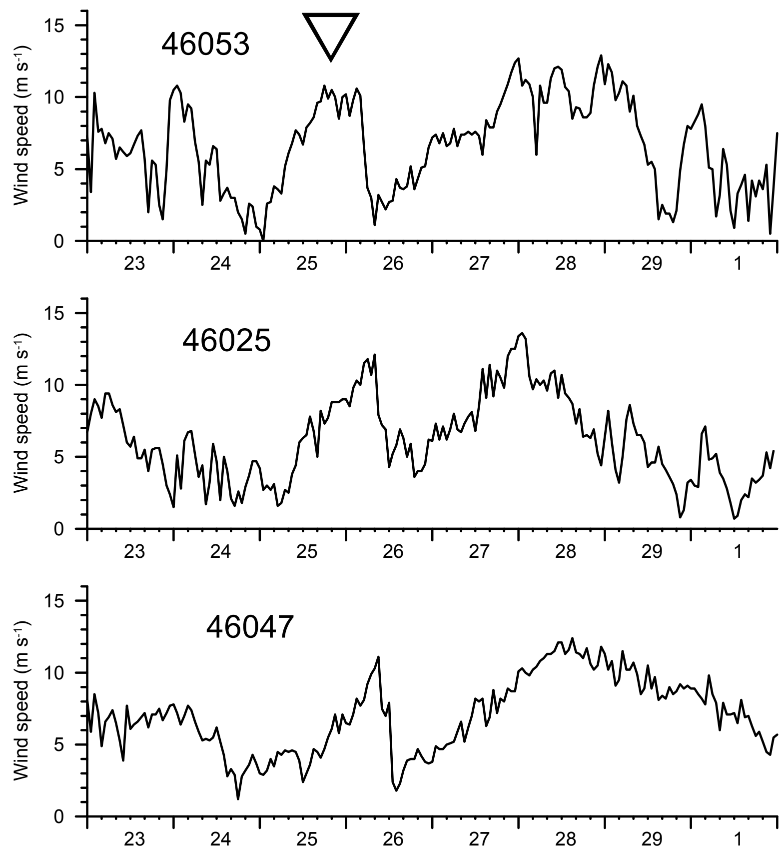

Figure II-12. Wind speed measured by three buoys in the SCB during February 23 – March 1, 2004. X-axis is UTM time. Triangle indicates the start of the rainstorm in the northern part of study area.

Wind and waves

<u>North/Central Sampling Group</u>

In February 2004, the start of the rainstorm was accompanied by an increase of wind speed (Figure II-12) and a change of wind direction from alongshore northwesterly to onshore southerly (Figure II-13). During the next day the wind direction changed back to northwesterly, its speed weakened and during the next two days increased again.

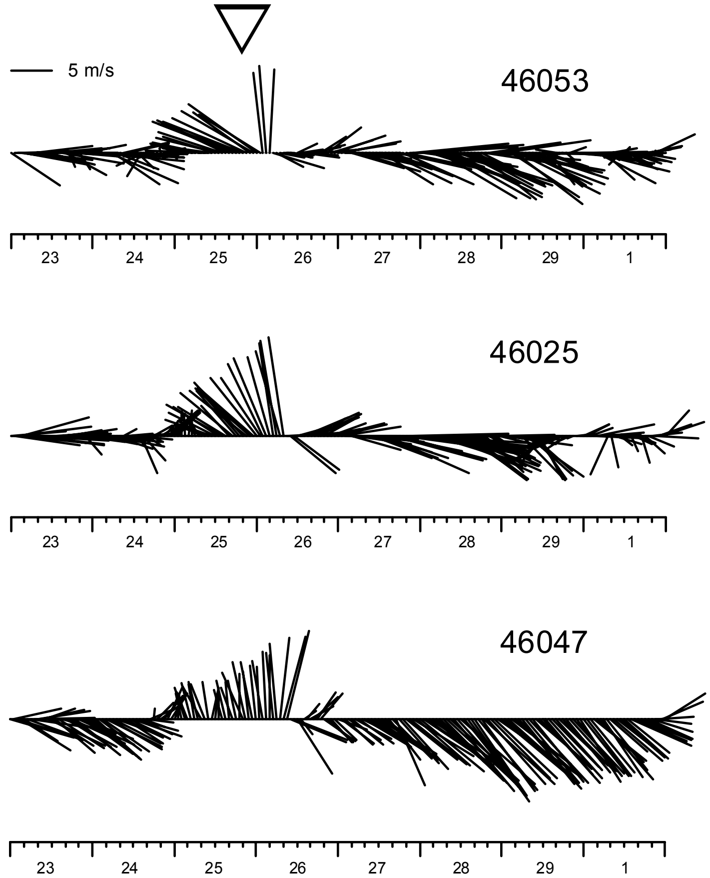

Figure II-13. Wind direction measured by three buoys in the SCB during February 23–March 1, 2004. X-axis is UTM time. Triangle indicates the start of the rainstorm in the northern part of study area.

During the day when the rainstorm started (i.e., February 25), the wave height was not higher than normal (Figure II-14). A significant increase of wave height happened the next day, February 26. This increase was especially pronounced in the Santa Barbara Channel (NDBC buoy 46053) and the open part of SCB (NDBC buoy 46047), where the wave height exceeded 5 m. In more sheltered Santa Monica Bay (NDBC buoys 46025 and 46221) the increase of wave height was not so great, but also substantial. The increase of wave height on February 26 coincided with the change of wave direction from southwesterly to southerly (Figure II-15). The SCB is open to wind and waves from the southwest and even a short-period southerly wind observed on February 25 – 26 resulted in higher waves than typical to that area from northwesterly wind.

In March 2005, during the major rainstorm wind speed also increased and changed the direction from northwesterly to southerly (Figures II-16 through II-17). These changes were less pronounced and did not last as long as in February 2004. As a result, wave height increased insignificantly (Figure II-18), in spite of an evident short-time change of the wave direction in San Pedro Basin from typical westerly to southerly (Figure II-19).

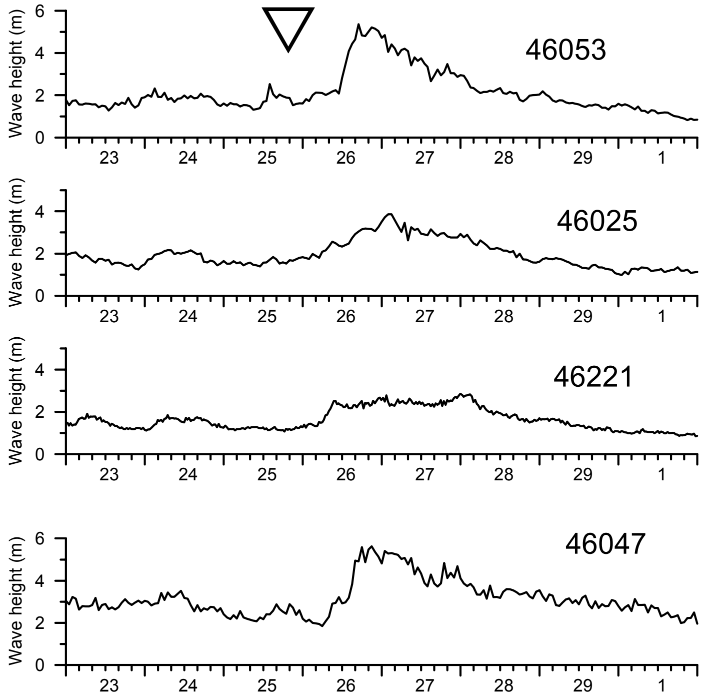

Figure II-14. Wave height measured by four buoys in the SCB during February 23 - March 1, 2004. X-axis is UTM time. Triangle indicates the start of the rainstorm in the northern part of study area.

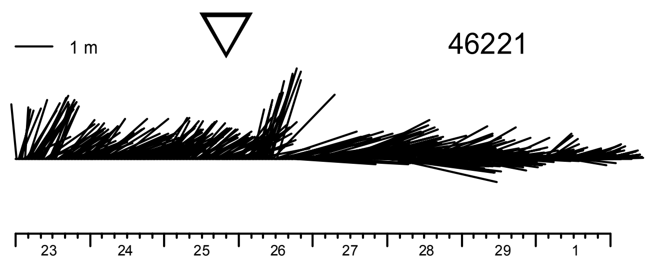

Figure II-15. Wave direction measured by NDBC buoy 46221 in Santa Monica Bay during February 23 - March 1, 2004. X-axis is UTM time. Triangle indicates the start of the rainstorm in the northern part of study area.

San Diego region

In the southern part of the SCB, wind speed was much lower and wind direction more variable than in the northern and central parts of the SCB (Figures II-20 through II-21). During the rain event # 1 on February 22, 2004, the wind speed increased and wind direction changed to southeasterly. Wave height did not increase after the rainstorm (Figure II-22), on the contrary, before the rainstorm the wave height decreased, which can be explained with the change of wind direction. The San Diego area is open to the ocean from the west; hence, southeasterly wind cannot produce high waves in that coastal zone.

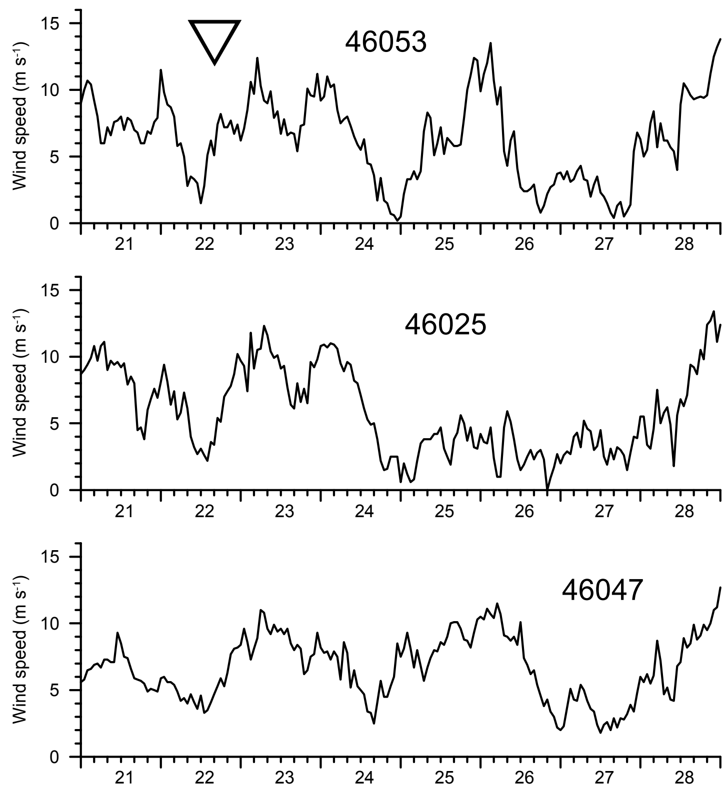

Figure II-16. Wind speed measured by three buoys in the SCB during March 21 – 28, 2005. X-axis is UTM time. Triangle indicates the start of the rainstorm in the northern part of study area.

In February 2005, wind speed increased significantly on February 11, soon after the start of rainstorm (Figure II-23). By the beginning of the next day, February 12, wind direction was south-southeasterly, and then gradually changed to southerly and south-westerly (Figure II-24). This change resulted in a significant increase of wave height, which evidently increased on February 12, one day after the rainstorm, and decreased to normal height during the next day (Figure II-25). Indeed, in this coastal area open to the ocean from the west, easterly winds cannot produce high waves, in contrast to westerly winds.

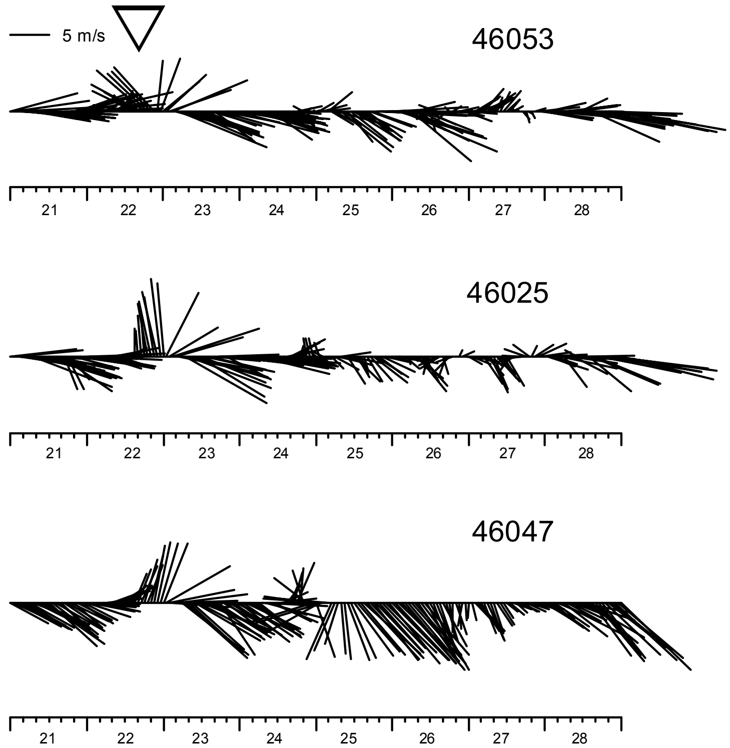

Figure II-17. Wind direction measured by three buoys in the SCB during March 21 – 28, 2005. X-axis is UTM time. Triangle indicates the start of the rainstorm in the northern part of study area.

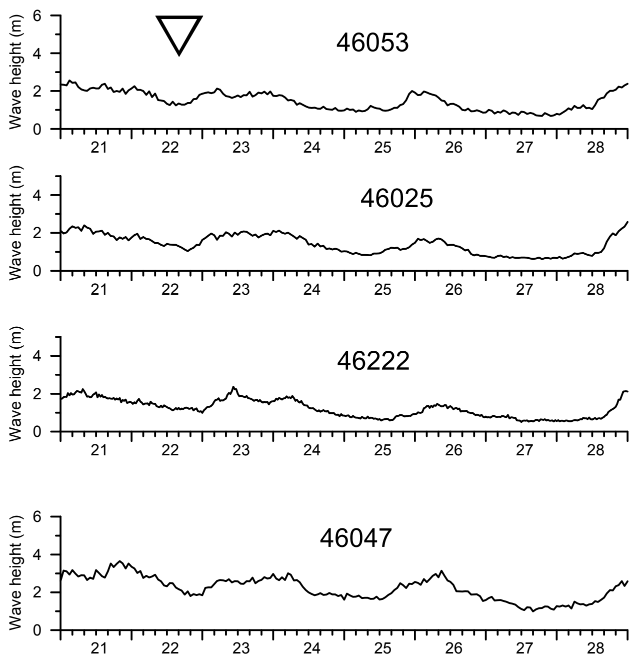

Figure II-18. Wave height measured by four buoys in the SCB during March 21 – 28, 2005. X-axis is UTM time. Triangle indicates the start of the rainstorm in the northern part of study area.

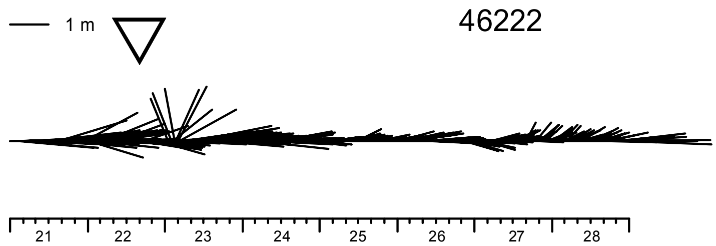

Figure II-19. Wave direction measured by NDBC buoy 46221 in the San Pedro Basin during March 21 – 28, 2005. X-axis is UTM time. Triangle indicates the start of the rainstorm in the northern part of study area.

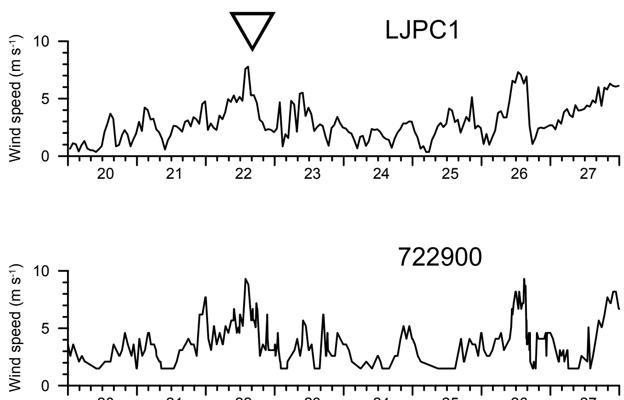

Figure II-20. Wind speed near San Diego measured by LJPC1 buoy and at meteorological station 722900 at San Diego airport (Lindbergh Field) during February 20 – 27, 2004. X-axis is UTM time. Triangle indicates the start of the rainstorm.

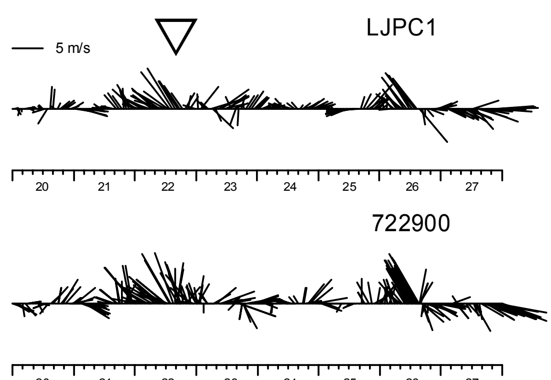

Figure II-21. Wind direction near San Diego measured by LJPC1 buoy and at meteorological station 722900 at San Diego airport (Lindbergh Field) during February 20 – 27, 2004. X-axis is UTM time. Triangle indicates the start of the rainstorm.

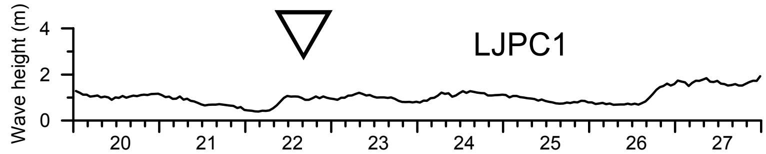

Figure II-22. Wave height measured by LJPC1 buoy near San Diego during February 20 – 27, 2004.

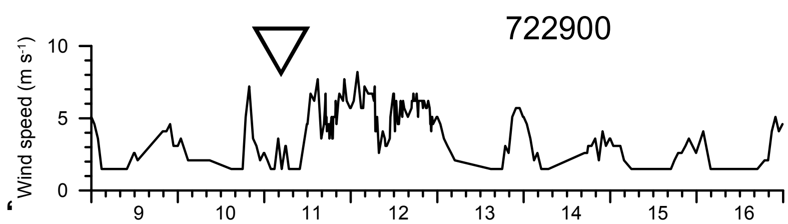

Figure II-23. Wind speed near San Diego measured at meteorological station 722900 at San Diego airport (Lindbergh Field) during February 9 – 16, 2005. X-axis is UTM time. Triangle indicates the start of the rainstorm.

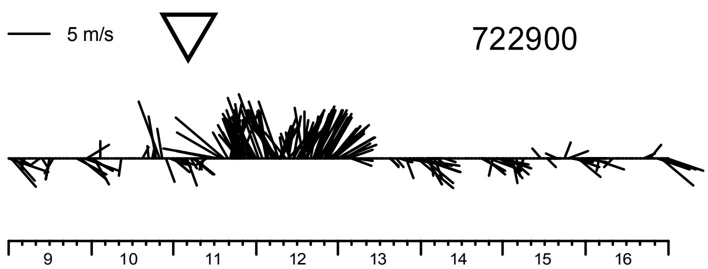

Figure II-24. Wind direction near San Diego measured at meteorological station 722900 at San Diego airport (Lindbergh Field) during February 9 – 16, 2005. X-axis is UTM time. Triangle indicates the start of rainstorm.

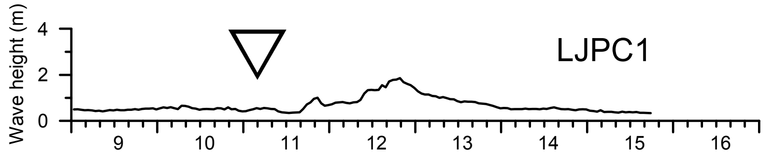

Figure II-25. Wave height measured by LJPC1 buoy near San Diego during February 9 – 16, 2005. X-axis is UTM time. Triangle indicates the start of the rainstorm.

Conclusion

It is important to note that while storm runoff was the target of the study, other issues influenced sampling and logistical decision making during the project. Questions such as: Were there going to be clear days after the storm passed? Was there enough rainfall during the storm to start sampling? Were wind and sea conditions acceptable to safely sample using boats? Logistically, the study had to deal with multiple jurisdictional agencies trying to collect field samples during two major storms. Scheduling personnel for unpredictable "major" storms was difficult. Rain events often occurred during nights, weekends and holidays. Coordinating field sampling with satellite imagery to capture the storm runoff event complicated logistics. Since field sampling involved boats, weather (wind and sea conditions) introduced another layer of complexity.

The decision to sample these rainstorms triggered other issues and concerns. What runoff characteristics would sampling teams expect from their selected watershed? Given the general ocean current circulation within the SCB, would runoff plumes be wind influenced on a regional scale or local? Would ocean water properties be obvious enough to relate to stormwater runoff and be visible on the spatial scales need for satellite imagery? Many of these issues are dealt with directly in other sections of this report. This section provided some general, as well as detailed information useful to understanding the bigger picture of the study.

Summary

This section has presented background information and context on meteorological related variability within SC, as well as relevant oceanographic and watershed characteristics and conditions. The information was a mixture of historical, as well as, current conditions experienced during the study. The reader should bear in mind that this study involved other aspects not mentioned in the section: bacteriology, toxicology, and water quality. Parameters such as colored dissolved organic material (CDOM), chlorophyll, and suspended particulate material are mentioned in subsequent sections and are used to relate satellite imagery to *in situ* measurements. The following summarizes the main points and relates them to the present study.

1) Southern California has a well-defined rainy season with highest precipitation occurring between December and March. This provides a narrow window of finite sampling opportunities, which can be further limited by the criteria set in terms of only sampling storm events that exceed a certain precipitation threshold (see next section).

2) Location and geographic setting influence land-based as well as ocean-based wind conditions. SC weather data (inland or nearshore) has a dominant diurnal wind pattern. Winds may be

difficult to characterize on a regional scale, but at site-specific locations can reveal important information and patterns. Rainstorms change surface wave patterns, through wind, to atypical conditions for 2–4 days after an event.

3) The SCB has a dominant, well-characterized ocean circulation pattern. Current patterns may change from site to site due to local wind, swell, tide and basin flows but their fluctuations are short term.

4) Runoff varies by drainage area between watersheds. Natural lined rivers are more permeable to rain, take larger and more frequent storms to produce runoff, and contain higher sediment loads then concrete lined channels. Dams influence stormwater runoff on watersheds.

5) Study participants sampled the largest storm in 2004. In 2005, a smaller storm was sampled. The 2004–2005 wet season had unusually high rainfall accumulations. Runoff from these heavy storms sometimes blended with smaller storms, complicating and at times preventing sampling because differentiating the impacts of one storm versus another in the ocean (e.g., runoff and plumes) would be difficult if not impossible.

6) The rain zone of a storm typically propagates from northwest to southeast in SC. The intensity and duration of the rain also tends to decrease as it moves toward San Diego. The San Diego area sometimes receives added tropical moisture to produce rain not recorded in other SC locations. As such, decoupling the two areas in terms of the storms selected and attendant sampling efforts was both appropriate and necessary.

7) The wind zone of the two sampled storms exhibited similar latitudinal trends as the rain zone (decrease as it moves south). As the storm arrives, wind intensity increases and direction turns southerly. As the front passes, the wind returns to normal. The residual wave effects usually don't arrive until after the storm front passes and can linger for days. High swells were recorded in Santa Barbara Channel during the February 2004 storm that closed Ventura Harbor for days. The San Diego area was open to the west so storm winds usually don't produce high waves but conditions can still be rough due to mixed seas.

8) Southern California typically has suitable weather and oceanographic conditions to test the relationship between satellite observations and coastal *in situ* water quality measurements, albeit with a few complicating factors as noted in subsequent sections.

III. METHODS

A detailed description of methods is available in the Bight '03 Water Quality Workplan. Following is a brief overview summary accompanied by additional specific details germane to this report's technical sections and associated findings.

Meteorological observations

Absolute wave height (m) was measured at six buoys (Figure II-1); wave direction at two buoys, and wind speed ($m\ s^{-1}$) and direction at four buoys (Table II-2). The data were obtained from the National Data Buoy Center (NDBC) website (http://www.ndbc.noaa.gov). The time-series of wave height and direction (the angle to north) were converted into zonal (U) and meridional (V) components; wind speed and direction were processed similarly. All six time series (i.e., absolute value and U and V components of wind speed and wave height) were averaged over 1-hour or 3-hour time intervals and attributed to rainstorm events. Hourly averaged wind speed and direction were used to evaluate the wind stress forcing on the river plumes, where wind stress was computed by the iterative quadratic formulation of Large and Pond (1981) for each hourly measurement.

River discharge observations were obtained from U.S. Geological Survey (USGS) gauging stations, stations operated by Los Angeles County Department of Public Works (LACDPW), and a daily discharge gage for the Tijuana River operated by the International Boundary and Water Commission. USGS sites provided discharge rates at 15-minute intervals and included the following sites: the Ventura River (USGS station 11118500), the Santa Clara River (sum of USGS 11113000 and 11109000), the Santa Ana River (USGS 11078000), and the San Diego River (USGS 11023000). LACDPW stations provided discharge rates at 1-hour intervals and included Ballona Creek (station F38C), the Los Angeles River (F319), and the San Gabriel River (sum of F354 and F42B).

Ship-based water quality observations

The study involved sampling four geographic regions that represent the river mouths of the largest southern California watersheds (see Figure II-1). These regions included (from the north): the eastern Santa Barbara Channel (Santa Clara and Ventura Rivers); Santa Monica Bay (Ballona Creek); the San Pedro Shelf (Los Angeles, San Gabriel, Santa Ana Rivers, and Newport Harbor); and the southern Bight (San Diego and Tijuana Rivers; Figure III-1). These regions and river systems were chosen because they represented a broad distribution of watershed land use and river types (open space, agricultural and urban) and because they covered a broad geographic extent of southern California.

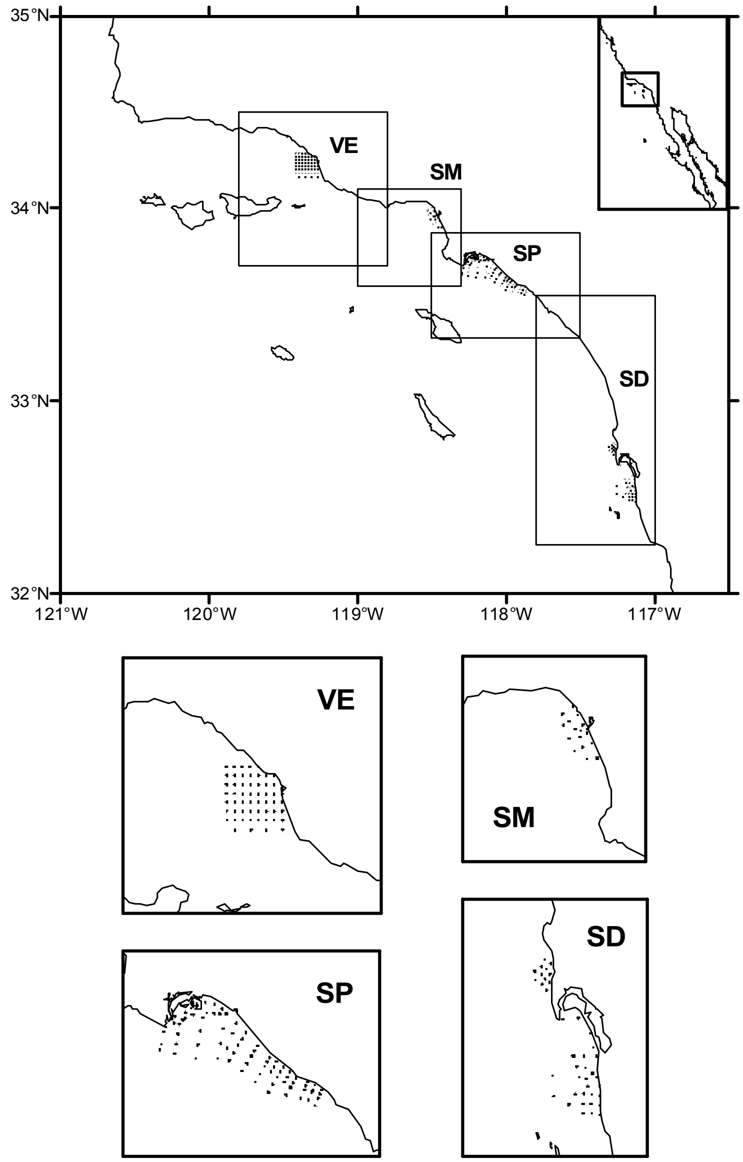

Figure III-1. Regions in Southern California Bight and stations of ship-based sampling during Bight '03 Program: Ventura (VE); Santa Monica Bay (SM); San Pedro shelf (SP); San Diego (SD).

The primary method of investigation was shipboard profiling of the plumes with an enhanced CTD system (conductivity, temperature, depth, dissolved oxygen, pH, transmissometer, chlorophyll fluorometer, and CDOM fluorometer), hereafter referred to as CTD+. Water turbidity was computed from transmissometer observations as the beam attenuation coefficient at 660 nm (hereafter referred to as beam-c). CDOM fluorescence was linearly calibrated with up to 100 ppb of quinine sulfate dehydrate (QSD). Water samples were also obtained by triggered 5-liter Niskin bottles attached to the CTD+ carousel and triggered remotely. Sampling occurred on regularly spaced grids for each region, with some local instances of adaptive sampling and stations being relocated based on near-real time satellite imagery of plume locations. The primary intent of the grids was to sample the nearshore discharge areas and assess water quality there, not necessarily to track plumes as they advected away from the river mouth regions. Some stations were positioned further offshore so that they provided "non-plume" profiles for comparative purposes. Profiles were obtained to within 2 m of the seabed or to a depth of 60 m for sites deeper than 60 m. Water samples were taken at 1-m water depth for most sites and at a sub-surface depth(s) below the buoyant plume for a limited number of sites.

Among other parameters, vertical profiles of temperature (T, ºC), salinity (S, psu), CDOM (mg m^{-3}), TSS (mg L^{-1}), beam attenuation coefficients (beam-C, m^{-1}), chlorophyll concentration (CHL, mg m^{-3}), and discrete samples for chlorophyll (CHL, mg m^{-3}), NO_2, NO_3, PO_4, SiO_4, NH_4 (µM), and total coliforms, fecal coliforms, and *Enterococcus* bacterial counts (CFU 100 ml^{-1}) were measured.

To analyze the correlations between optical properties of ocean surface and CDOM concentration, "remotely sensed" CDOM ($CDOM_{rs}$) values were calculated for each station as a weighted average of *CDOM(z)* vertical profile from the surface to maximum sampled depth *Zmax*, taking into account the contribution of each sampled layer to the resulting surface color (c.f. Gordon and Clark 1980):

$$CDOM_{rs} = \frac{\int_0^{Z\max} CDOM(z) * K(z) * dz}{\int_0^{Z\max} K(z) * dz} . \qquad \text{[III-1]}$$

For each depth, the weight coefficient *K(z)* was estimated by integrating the beam-c [*C(z)*] attenuation from the surface down to that depth, using the equation

$$K(z) = \int_0^Z \exp[-C(z) * dz] . \qquad \text{[III-2]}$$

The resulting "remotely sensed" $CDOM_{rs}$ was very close to surface CDOM ($R^2 = 0.986$; linear regression equation with zero intercept and the slope close to unity), which can be explained by low water column transparency in the study area.

The sampling plan called for sampling two events across each region, and three days of sampling during each event as conditions permitted (to be nominally conducted on days 1, 3 and 5 following the discharge peak). One ship was dedicated to each region, except for the San Pedro Shelf where three monitoring vessels were utilized coincidentally and the Tijuana River where two ships were used. However, not all sites were sampled in the proposed fashion largely due to limitations from weather and sea-state (Figures III-2 through III-3). Further, sampling of the Tijuana River plume was conducted during an event not sampled at the remaining sites (Figure III-3), due to a storm that was directed largely toward the southern portion of the study area. The resulting sampling effort consisted of 574 CTD+ stations and 705 water samples during a total of 36 ship-days.

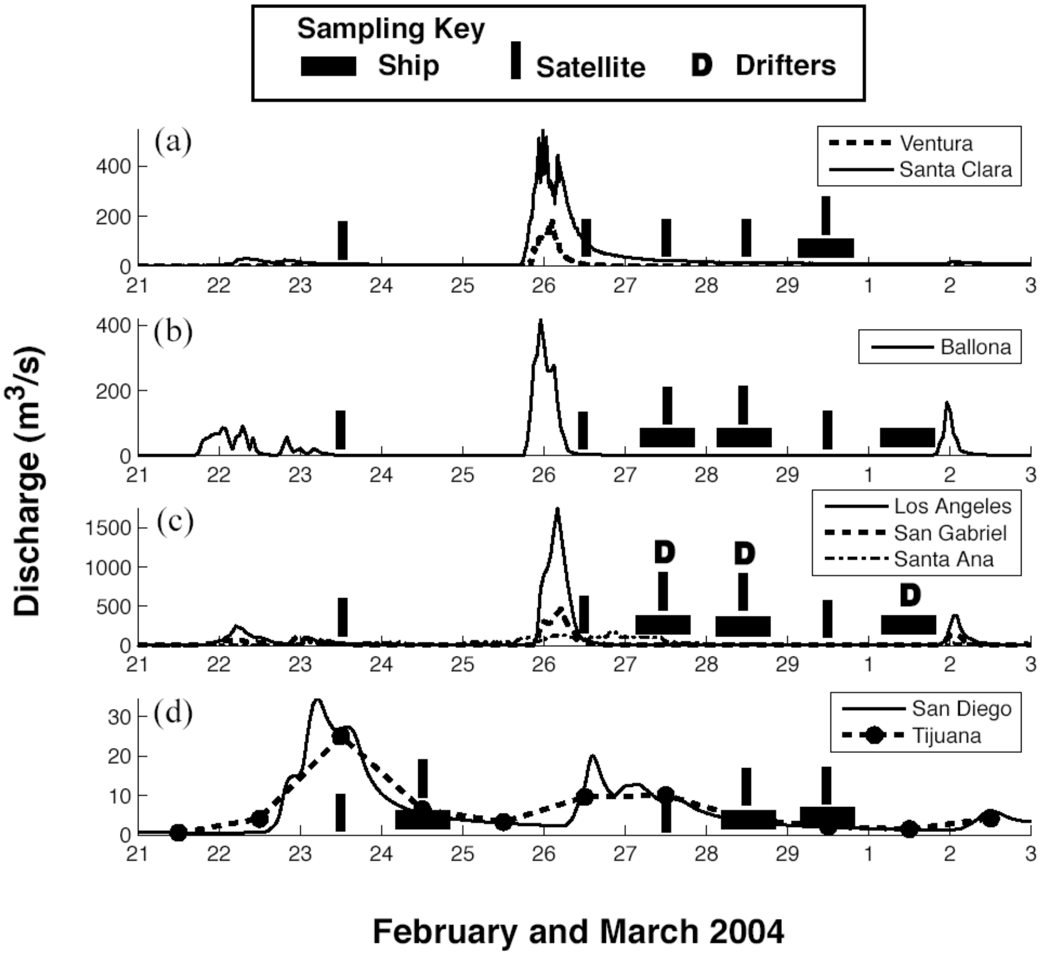

Figure III-2. Discharge and sample timing for the first event sampled.

Sampling Logistics

The sampling effort for the Bight '03 water quality program consisted of two separate sampling efforts. The original goal was to sample two separate storms during the winter of 2004. However, the timing of rain events in 2004 was such that it was not possible to sample two separate storms with sufficient rainfall to meet the minimum criteria of 0.5 inches measured rainfall for a discrete storm event during the available sampling window. The decision was made to continue the project during the winter of 2005 in order to sample a second storm. During the 2004 sampling, the sampling effort was 378 stations divided among eight sampling area's of responsibility. During the 2005 sampling, the sampling effort was 345 stations divided among seven sampling area's of responsibility.

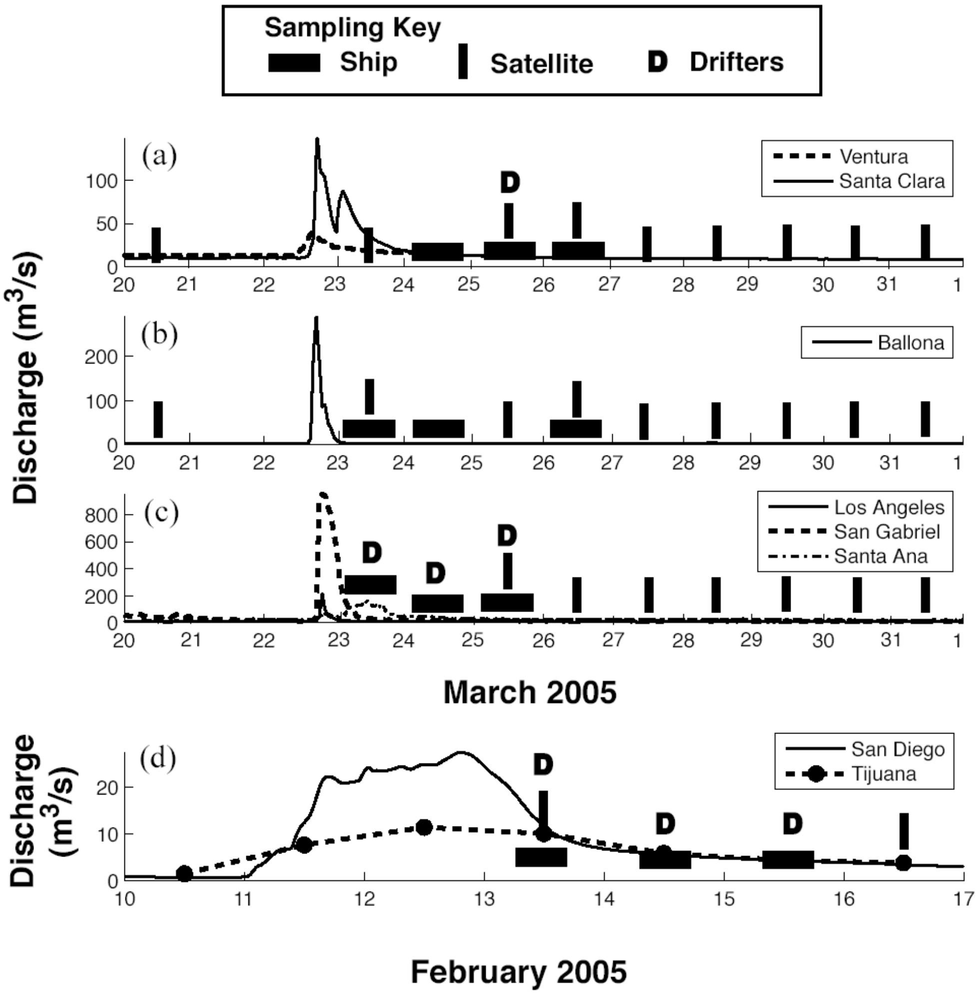

Figure III-3. Discharge and sample timing for the second event sampled. Note that the Tijuana River (d) was sampled on a different schedule than the other systems (a-c).

Site Selection

Sampling sites for the CTD surveys were allocated to a series of transects perpendicular to shore. Nominal distance between transects was 2 to 4 km. Sampling was focused near river mouths, with transects located at the mouth and then at 1 km and 2 km in either direction. Sampling extended offshore from four to eleven kilometers, depending on the watershed. These distances were selected to capture the areas of maximum response gradient based on historical data records.

Each transect was sampled cross-shelf at distances of 0, 1, and 2 km from shore and then at 2 – 3 km intervals (the 0 km station was assigned to the 10 meter isobath because that was the minimum sampling depth for many of the vessels used in the survey). Transect length was generally 6 – 8 km, though longer transects were placed at some sites in order to get outside the runoff plume. While site selection generally followed these criteria (Table III-1), a strong effort was also made to incorporate existing survey sites if they occurred close (e.g., <0.5 km) to the desired transect locations. The primary benefit of this effort to incorporate existing sites was to make it easier and faster to occupy stations with known positions and bottom depths during adverse sea conditions

Table III-1. Site selection criteria for the CTD survey.

Vertical	Bottom depth □ 100 m: Surface to near bottom (2 m) Bottom depth >100 m: Surface to 100 m
Cross-shelf	
Transect Orientation:	Cross-shelf
Between station spacing:	First 2 km – 1 km (i.e. 0, 1, 2 km) Beyond 2 km - 2-3 km
Maximum offshore distance:	10 km
Relative to POTWs:	One station on each transect will be on 60 m isobath
Along-shelf	
Near POTW (Over ZID):	
Large discharge (>100 mgd):	2 km
Small discharge (<50 mgd):	0.5 km
Near river sources:	1 km for first 2 km
Away from river source:	4-6 km for distances >2 km from source
Open Areas:	4-6 km

Sampling Effort

Each organization sampled the following number of stations per day (Table III-2):

<u>*Storm 1*</u>

1) Mexico 12 stations south of the international border;
2) City of San Diego – 12 from the Mexican border to Point Loma;
3) MEC (South) – 12 around the mouth of the San Diego River;
4) OCSD – 21 from south of Newport Harbor to the Santa Ana River;
5) MEC (North) – 21 from the Santa Ana River to the San Gabriel River;
6) LACSD – 19 from the San Gabriel River to Palos Verdes;
7) City of Los Angeles – 17 from Redondo Beach to Santa Monica; and
8) ABC Labs – 12 around the mouth of the Santa Clara River.

<u>*Storm 2*</u>

1) Mexico 12 stations south of the international border;
2) City of San Diego – 12 from the Mexican border to Point Loma;
3) OCSD – 22 from south of Newport Harbor to the Santa Ana River;
4) MEC (North) – 20 from the Santa Ana River to the San Gabriel River;
5) LACSD – 20 from the San Gabriel River to Palos Verdes;
6) City of Los Angeles – 17 from Redondo Beach to Santa Monica; and

7) ABC Labs – 12 around the mouth of the Santa Clara River.

Table III-2. Stations sampled by the agencies participating in Bight '03 Water Quality Program.

Responsible Agency	Storm 1 Station Commitment	Storm 2 Station Commitment
Mexico	12 x 3 = 36	12 x 3 = 36
City of San Diego	12 x 3 = 36	12 x 3 = 36
MEC-South	12 x 3 = 36	NA
OCSD	21 x 3 = 63	22 x 3 = 66
MEC-North	21 x 3 = 63	20 x 3 = 60
LACSD	19 x 3 = 57	20 x 3 = 60
City of Los Angeles	17 x 3 = 51	17 x 3 = 51
City of Oxnard/ABC Labs	12 x 3 = 36	12 x 3 = 36
TOTAL	126 x 3 = 378	115 x 3 = 345

Sampling Schedule

<u>*Storm 1*</u>

The field sampling was storm-dependant, with sampling scheduled to begin December 3, 2003 and end March 31, 2004. Sampling was blacked-out from December 23, 2003 to January 4, 2004. Sampling began on the first day after the storm that vessels could safely collect offshore samples. Sampling occurred on three days over a 5 – 6 day stretch, nominally on Days 1, 3 and 5. However, depending on sampling conditions and vessel/crew availability, these days were shifted forward or back a day, depending on the agency involved.

<u>*Storm 2*</u>

The field sampling was storm-dependant, with sampling scheduled to begin January 4, 2005 and end April 1, 2005. Sampling began on the first day after the storm that vessels could safely collect offshore samples. Sampling occurred on two or three days over a four-day stretch, nominally on Days 1, 2, and 3. However, depending on sampling conditions and vessel/crew availability, these days were shifted forward or back a day, depending on the agency involved.

Site Acceptability Criteria

The location of each station was designated in advance as a set of coordinates (latitude and longitude). Upon initial arrival at the site, the depth at the station depth was determined by fathometer. This was regarded as the nominal station depth for all subsequent sampling at the station during the survey and was used for calculating station acceptability if the station was moved.

Sampling was sometimes not possible at some stations for a variety of reasons (e.g., falling outside depth range, shoals, etc.). The fathometer reading at a station was examined to determine whether the bottom was unsuitable for sampling. If the station could not be sampled, the following rules were followed:

The station was moved no more than 100 m (.054 nautical miles) from any assigned coordinate site and ± 10% of the nominal depth.

CTD Surveys

At each site, vertical profiles measured the distribution of temperature, salinity, density, dissolved oxygen, pH, turbidity, chlorophyll-a, and color dissolved organic matter (CDOM). Profiles extended from the surface to within two meters of the bottom, except in water depths greater than 60 meters, where only the upper 60 meters of the water column were profiled. CTD profiles were supported by surface batch measurements of chlorophyll concentration, total suspended solids (TSS), nitrite (NO_2), nitrate (NO_3), phosphate (PO_4), silicate (SiO_4), bacteria (total coliforms, fecal coliforms, and *Enterococcus*), and toxicity.

Equipment

A Sea-Bird SBE 9/11 or SBE 25 was used to provide a continuous water-column profile of temperature, salinity, dissolved oxygen, pH, transmissivity, chlorophyll, and CDOM with depth (Table III-3). If a SBE 9 was used, it was interfaced with either a SBE 17 RAM unit or SBE 11 deck box. The interfacing software was Seasave Win32 V 5.29b or greater. In the event of equipment failure, other CTD users in the area had spare sensors or instrument packages available.

Navigation

Accurate location of sampling sites was crucial to the success of the Bight '03 water quality surveys. Station charts and coordinates (latitude and longitude) are located in Appendix B. Vessel positioning was determined by means of a Differential Global Positioning System (DGPS). If, during the course of field sampling, the differential signal was interrupted or lost, sampling continued using standard GPS.

Table III-3. The equipment used in Bight '03 Water Quality Program.

Agency	ABC LABS	CLAEMD	LACSD	OCSD	MEC	City of San Diego	Mexico
Units	SBE 25	SBE 25	SBE 9/11	SBE9/11	SBE 25 SBE9/11	SBE 9/11	Idronaut 316
Real Time	No	Yes	Yes	Yes	Yes	Yes	Yes
Chl. Sensor	Wetlabs	Wetlabs	Wetlabs	Wetlabs	Wetlabs	Wetlabs	Turner
Transmissometer	Wetlabs	Wetlabs	Wetlabs	Wetlabs	Sea Tech	Wetlabs	Sea Tech
D.O.	SBE	SBE	SBE	SBE	Beckman	Beckman	Beckman
pH	SBE	SBE	SBE	SBE	SBE	SBE	SBE
CDOM	Wetlabs	Wetlabs	Wetlabs	Wetlabs	None	None	None

CTD deployment

Positioning on station proceeded according to protocols described above. At each station the required information was recorded on the CTD data sheets. A new file name was created for each cast. This name was the station name. The file name had the following format: B03WNNN.DAT, where NNN was the three-digit station number.

The CTD was deployed using either a SBE 11 deck unit or with a SBE 17 RAM unit. In the configuration file, the scan rate was set at 24 scans/second for SBE 9/11 or 8 scans/second for SBE 25. All data was averaged to 1 scans/bin (i.e. number of scans to average (NAVG =1).

The CTD descent rate was approximately 1 m s^{-1}, which is the optimum descent rate. When deploying real-time, this rate was monitored by displaying and viewing the descent rate variable. If RAM was used during deployment, the rate was determined with a meter wheel and a timer.

Before beginning a cast, the CTD sensors were brought to thermal equilibrium with the ambient seawater. The pump was activated and bubbles purged from the tubing. This was accomplished by lowering the CTD a few meters and monitoring salinity and dissolved oxygen values to ensure their stabilization. However, deployment with the SBE 17 RAM unit precluded monitoring these values. In either case, 90 seconds was the minimum soak time for thermal equilibrium and sensor stabilization. After sensor stabilization and at least 90 seconds, the CTD was raised so the top of the cage is at the water surface and profiling began. Only downcast data was be used for data processing; however, data was logged throughout the entire cast. The CTD was deployed to within 2 meters of the bottom or to a maximum of 60 meters if the station is deeper than this depth.

Safety

Collection of samples during field surveys is inherently hazardous and this danger is greatly compounded in bad weather. Thus, the safety of the crews and equipment was of paramount importance throughout the project. Many accidents at sea are preventable. Safety awareness by the Boat Captain and all crewmembers was the greatest single factor that reduced accidents at sea. Each survey crew followed established rules and provisions within their respective agency's safety program. Sampling was canceled or postponed during hazardous weather conditions. The final decision was made by the Boat Captain, who was responsible for the safety of everyone on board. As with any field program, the first priority was the safety of the people on board, followed by the safety of the equipment, and the recovery of the data. As such not all storms were sampled to the same level of effort in all regions.

Cruise Documentation

Cruise Log

The Chief Scientist was responsible for maintaining a Cruise Log, which recorded the basic vessel, crew, and tide information along with all relevant activities conducted throughout the sampling day.

Discrete Sample Labels/Tracking
Each sample was identified and tracked by the station, date sampled, and parameter. Individual log numbers were used at the discretion of the sampling organization.

Labels
Labels were printed by the agency responsible for field sampling prior to the survey and included, at a minimum, the station number, date, and parameter. Dates were reported as day/month/year. External labels were covered with clear postal tape to prevent them from falling off the container if they would not stick on some surfaces.

Field Data Sheets
Data sheets and cruise logs were retained by the sampling organization until sampling was completed. Upon completion of sampling, original field data sheets were sent to SCCWRP with copies retained by the sampling organization.

Shipping of Samples
All discrete were shipped to SCCWRP. Most samples did not have to be delivered on the day of collection but could held for a few days and shipped once a week. All shipment of samples was the responsibility of the field sampling organizations.

Chain of Custody Forms
Chain of custody forms were filled out at the end of each sampling day detailing the transfer of samples from the vessel crew to the laboratory, or to delivery personnel. A form was filled out for each set of samples that were transferred. The sample and container type was included on the form to identify the samples being transferred. This form was signed by the crewmember transferring the samples and the laboratory staff member receiving them. A copy of the form was kept and the original form with signatures accompanied the samples. If samples were shipped by carrier, a copy of the chain of custody form was faxed to SCCWRP for tracking purposes.

Field Data Base Management
A field computer system was developed for the Bight '98 project that was used for Bight '03, which included the forms for all of the field data sheets. This system employed laptop computers and had an instruction manual for training and reference. Use of the field computer system was optional during the Bight '03 survey.

The data entry screens were identical to the field data sheets. Data was either entered into the computer while at sea, or it could be taken from the data forms at a later time. Although hard copies of all field data sheets were mandatory, these could either be hand-written or hard copy printouts from the computer.

The data entered into each field of the electronic forms was checked automatically by the software and provided a warning when the data did not fall within an expected range. After entering the data into the field computer system, it was be printed out to hard copy and checked by the Chief Scientist against the original handwritten data sheets. Once the data was checked, corrected (if necessary), and accepted by the Chief Scientist, the crew was not granted access to the data any further.

Data Analysis Methods

Data Processing

Seven or eight different CTD's were used for this project. Data was captured at the highest rate possible with the various instruments. At the high end, this meant that data was recorded at 24 scans per second. At the low end, this meant that data was recorded at 8 scans per second. Initially, this data was processed using the software provided by the CTD manufacturer to apply small time offsets between different sensors due to delays in water reaching sensors through pumping systems, or to adjust for certain sensors with a response delay. Manufacturers' software was also used to apply calibration/conversion functions to produce final engineering units from raw sensor signals. Data was processed according to a standard procedure. At this point ASCII data files containing all recorded data at each unique sampling location were generated. These files included the equilibration period while sensors adjusted to ambient conditions in surface waters. This period also included the period before the CTD package was placed in the water, and possibly a pre-cast submergence of the package down to about 5 m in order to prime the water pump and flush any trapped air bubbles from the system. Following the equilibration period, the instrument package was brought to the surface in preparation for the actual downcast. During the cast, the CTD was lowered at a relatively constant rate to just above the seafloor, then lowered gently to the bottom. Upon reaching maximum depth, the CTD was raised to the surface and recovered. The "upcast" data is also recorded in the preliminary file.

To eliminate all non-representative data, reduce what was a tremendous amount of data to a more manageable level, and to prepare a data set amenable to graphical and statistical analysis, a further data reduction process was completed in post-processing. This downcast portion initially includes all data; at up to 24 scans per second, which at typical descent rates of 1 meter per second could mean discrete readings at close as 5 centimeters vertically.

Data post-processing was accomplished by loading ASCII data into the Interactive Graphical Ocean Data Systems (IGODS) software created by A. Steele. The process involves retaining a site's downcast data for the water column and identifying possible outliers based upon the difference between the downcast standard deviation and a five point (midpoint is the evaluated datum) running average standard deviation. Datum was flagged if it exceeded the criteria limit for a measured parameter: temperature (0.5), salinity (0.3), dissolved oxygen (0.5), and transmissivity (0.5). The vertical profiles for each parameter were graphically and statistically evaluated looking for outlier points. Outliers are points that for some reason are not representative of real conditions. They may be due to electrical noise, physical interruptions of sensors (e.g. by bubbles), or by tiny time offsets between measurements that are combined to produce some parameters (e.g., salinity). Data points were removed if considered an artifact of equipment behavior rather than an actual oceanographic event. An offset of more than a certain fraction of the standard deviation of the entire profile's data was utilized to assign a point potential outlier status. In addition to points statistically determined to be outliers, a small number of additional points were identified as outliers based on visual examination of the entire downcast. These points were removed from the raw downcast data and documented in a text file that listed the points removed from each station. Upon removal, the cast was re-evaluated until all outliers were removed and the site's data was accepted. All removed data were written to an outlier file. The outlier criteria were only guidelines, so points exceeding the limits were not automatically discarded and points below the limits were not automatically retained.

The next data-reduction step was to produce one-meter depth values. This step was accomplished using the downcast data remaining after outlier removal. The process of producing a value at each integer one-meter depth interval was simple. For each parameter, the data were scanned to find the nearest data point in depth immediately above and below the integer depth. After one-meter depth averaging was completed, missing data were recovered by examining the upcast data and using the appropriate depth value for any missing data. The final step was a review of the graphical representations of each parameter to determine whether further outlier removal was necessary. A minimal number of points were removed during this review.

Graphics Production

The two and three-dimensional views of the results of water column sampling during each survey were produced using simple linear interpolation and color filling. As part of the data processing, data at all CTD stations was interpolated to fixed one-meter depth intervals. At every CTD station there is a latitude, longitude, and a depth (X, Y and Z coordinate) associated with each discrete sample of each parameter (e.g. temperature, salinity, beam attenuation, etc). To construct the three-dimensional views, a viewer position and distance are first selected by specifying a tip (angle above horizon), a spin (angle towards which the view is directed), and a zoom (effectively the distance of the viewpoint from the study area). Any view that shows vertical cross-sections of the water column is constructed by establishing the point in space of the same depth at two adjacent stations. Then values were linearly interpolated on a straight line between these points, with each intermediate point assigned a color value based on the specified scale and palette selected.

To produce constant depth views, two pairs of points at the same depth, which have been pre-selected to best represent the local area using all of the available data, are used. A linear interpolation of values is made between the endpoints of real data at the same depth for each pair. In addition to interpolating the parameter values, the latitude and longitude are also interpolated for each intermediate point, and these two sets of interpolated points then form the basis for a second series of interpolations that fill in the color used to represent values of the parameter being represented

Surface Currents Measurements by Drifters and HF Radars

Surface currents were obtained from the tracks of high resolution drifting buoys drogued at 1 m depth (Ohlmann *et al.* 2005). The drifters, with known water following capabilities, record their position every 10 minutes using GPS. Individual drifter tracks give an indication of how river plume water moves in the coastal ocean. The relative motion of drifter pairs allows for quantification of plume dispersion. Sets of up to 21 drifters were released within the river plumes just beyond the surf zone at the Santa Clara River (1 day), Santa Ana River (6 days) and the Tijuana River (3 days). The drifters were typically released in the morning and retrieved before sunset. If a drifter was clearly about to enter the surf zone, thus being subject to damage, it was retrieved and re-deployed offshore of the river mouth. The individual drifter tracks along with flow information determined from the position data can be viewed on the web at (www.drifterdata.com).

High-frequency (HF) radar was used for the Santa Clara/Ventura and Tijuana River systems to track surface currents during the sampled events. The northern HF radar array is part of the UCSB Ocean Surface Currents Mapping Project, which consists of 4 sites to characterize surface currents in the Santa Barbara Channel (http://www.icess.ucsb.edu/iog/realtime/index.php). The Tijuana River region is included in the San Diego Coastal Ocean Observing System (SDCOOS) administered by Scripps Institution of Oceanography (SIO; http://sdcoos.ucsd.edu/).

Satellite observations

The satellite data and images used in this study were primarily collected by NASA's Moderate-Resolution Imaging Spectroradiometer (MODIS) instruments (Esaias *et al.* 1998). MODIS sensors operate onboard two near-polar sun-synchronous satellite platforms orbiting at 705-km altitude: Terra (since February 24, 2000) and Aqua (since June 24, 2002). Terra passes across the equator from north to south at ~10:30 local time, while Aqua passes the equator south to north at ~13:30 local time. As such, all the images were acquired within 2 h before or after local noon (18:00–22:00 UTC). MODIS sensors provided daily or better coverage of the SCB study area, although clear-sky images were obtained for only about half of the days of interest and largely on days following river discharge peaks (Figures III-3 through III-4). Nearly all of the images and data utilized for this study were ultimately from MODIS-Aqua given that significant problems exist with MODIS-Terra observations that preclude accurate product generation.

The MODIS sensors collect data in 36 spectral bands, from 400 to 14000 nm; only some of these are useful for ocean applications. The radiances measured by the satellite sensors were converted into normalized water-leaving radiances (nLw) using standard SeaDAS 5.0 software and utilized for the analyses described below. The nLw parameter is defined to be the upwelling radiance just above the sea surface, in the absence of an atmosphere, and with the sun directly overhead. The nLw radiances were estimated at seven visible wavelengths: 412, 443, 488, 531, 551, 667, and 678 nm. MODIS pixel size is ~1 km. Pixels that did not pass the cloud screening test were eliminated from the analysis. Cloud detection in MODIS imagery is more accurate as compared with other satellite sensors of similar resolution; seventeen (of total 36) MODIS bands are used for cloud discrimination, including bands of 250-m to 500-m spatial resolution, which provide reflectances and reflectance ratios at a finer resolution than infrared and ocean color bands.

The basics of the atmospheric correction algorithm were described by Gordon and Morel (1983). The goal of the atmospheric correction is to remove the influence of the atmosphere and sun angle on the measurements to make the radiances from different images comparable. For atmospheric correction (Gordon and Wang 1994b, Gordon 1997), a multi-scattering aerosol model option with 2-band model selection and near-infrared (NIR) correction were used. The atmospheric contamination of the signal was estimated from two NIR wavebands (748 and 869 nm), where ocean surface was assumed to be black. In coastal regions with high concentrations of chlorophyll, TSS, and CDOM, this assumption often does not work, resulting in an overcorrection of atmospheric effects (Siegel *et al.* 2000). The overestimation of atmospheric signal can result in erroneously low (sometimes negative) nLw. Newly emerging techniques (Wang and Shi 2005, Wang 2007, Wang *et al.* 2007) focus on the use of the MODIS shortwave infrared (SWIR) bands to improve atmospheric corrections in turbid coastal waters; these approaches will be evaluated in subsequent regional analyses and studies.

Inherent Optical Properties (IOPs), including detritus and CDOM (Gelbstoff) absorption at 412 nm ($a_{dg}412$) and total backscattering at 551 nm (b_b551) were estimated from MODIS imagery using the Quasi-Analytical Algorithm (QAA; Lee *et al.* 2002); note the absorption of CDOM can not presently be easily separated from that of colored detrital matter using satellite observations because they have similar spectral shapes. These wavelengths were selected from the available MODIS channels (412–678 nm) because CDOM absorption is highest on the shortest wavelengths of the visible domain (i.e., at ~400 nm) (Bricaud *et al.* 1981) and backscattering at medium TSS concentrations (20–50 mg L^{-1}) is highest at ~550 nm where optical absorption is often minimal (Toole and Siegel 2001, Otero and Siegel 2004, Warrick *et al.* 2004a). To qualitatively track the combined sediment, CDOM and phytoplankton signatures of the buoyant plume, "true-color" MODIS imagery was frequently utilized. Standard MODIS chlorophyll products were also generated and examined but are not part of the principal analyses and findings described here; phytoplankton variability and dynamics associated with stormwater runoff will be examined in greater detail as part of the Bight '08 Water Quality Component, as well as in an associated NASA-funded investigation of the Santa Monica and San Pedro Bay/Basin regions currently underway through 2008.

Synthetic aperture radar (SAR) imaging data (Radarsat-1 *et al.*) were also acquired for this project, but given limited data acquisitions, less than optimal temporal match-ups with the storm events, and frequently high winds, these data did not provide conclusive observations of the stormwater runoff plumes under investigation and as such were not utilized in the subsequent analyses and assessments.

IV. QUALITY ASSURANCE AND QUALITY CONTROL (QA/QC)

Introduction

The 2003 Southern California Bight Regional Survey (Bight '03) was the third Bight-wide coordinated survey by multiple local agencies within the southern California area. The goal of the water quality element of Bight'03 was to assess the fate and transport of stormwater runoff and correlate the data synoptically with satellite imagery across the Bight. Because of the large number of participating organizations, it was important to implement appropriate quality assurance and quality control (QA/QC) measures to ensure quality data. This section describes QA/QC procedures and results from the Bight '03 survey, expanding upon the initial descriptions provided in the Bight '03 Water Quality Workplan. The goal of the section is primarily to assess data comparability among agencies.

Procedures

The QA/QC program for Bight '03 consisted of two distinct but related activities: quality assurance and quality control. Quality assurance (QA) included design, planning, and management activities conducted prior to the study to ensure that the appropriate kind, quantity, and quality of data were collected. Quality control (QC) activities were implemented during the project to evaluate the effectiveness of the QA activities in controlling measurement bias and error.

There were two types of QA activities conducted prior to the implementation of the program. Participants ascribed to common guidelines regarding field sampling, calibration, and data handling. Standard methods were used to reduce inconsistencies between the many field crews involved in the survey. An inter-comparison exercise assessed and controlled the variability introduced into the survey by multiple instruments. Instrument sensors were required to meet the performance criteria in Table IV-1.

QC procedures consisted of CTD sensor drift analysis, in-survey chlorophyll-*a* samples, and reference standards during laboratory analysis. Temperature and conductivity sensors were only checked for disparate readings because of known stability. Laboratory nutrient chemistry analyses were calibrated from standards made with nutrient standards listed in Table IV-2. These standards were run prior to and after each set of batch samples. Extracted particulate chlorophyll measurements were measured on a laboratory fluorometer or spectrophotometer calibrated to pure chlorophyll-*a* obtained from Sigma Scientific.

Table IV-1. Listed are the performance criteria goals for agencies participating in the inter-comparison exercise and regional survey. The equilibrium data for each probe had to be within the specified range for the group mean or reference standard. One decibar approximates a meter depth in seawater, usually correct within 3% for almost all combinations of salinity, temperature, depth, and gravitational constant.

Parameter	Units	Acceptable Range
Pressure	decibars (dbar)	+/- 0.5
Temperature	°C	+/- 0.03
Salinity	Practical salinity unit (psu)	+/- 0.03
Beam transmission (660 nm)	%	+/- 5.0
Dissolved Oxygen	mg L^{-1}	+/- 0.5
pH		+/- 0.3
Chlorophyll-*a* fluorescence	µg L^{-1}	+/- 2.0
Pressure	decibars (dbar)	+/- 0.5

Table IV-2. Standards used for nutrient analysis runs.

Nutrient	Standard Compound	Standard Concentrations
Nitrate (NO_3)	$NaNO_3$	0, 10, 20, and 40
Nitrite (NO_2)	$NaNO_2$	0, 1, 2, and 4 µM
Phosphate (PO_4)	KH_2PO_4	0, 1, 2, and 4 µM
Silicate (SiO_4)	Na_2SiF_6	0, 20, 40, and 80 µM
Ammonium (NH_4)	NH_4CL	0, 1, 2, and 4 µM

QA Inter-comparison Exercise

Prior to the survey, each instrument had to be evaluated for inter-comparability through a pre-survey comparison exercise. Seven organizations, seven instruments, and three different manufacturer models participated in the Bight '03 regional survey (Table IV-3). A prerequisite for participation was that each instrument had their temperature and conductivity sensor factory calibrated within six months of the survey. All organizations pre-calibrated their CTDs prior to the comparison day as if each were preparing to deploy the instrument in the field. The comparison was done on December 2, 2003.

A common seawater tank was placed within a temperature-controlled room (16°C). The water temperature was controlled with a chiller to 10°C. The water was aerated for several days prior to the exercise to achieve oxygen saturation. After logistical setup and adequate thermal equilibration of CTDs, each agency was asked to collect a series of three-minute data sets simultaneously. During each data series, water was analyzed by reference probe or collected for later laboratory analysis (salinity).

Table IV-3. Conductivity-Temperature-Depth profilers (CTD) used in the Bight '03 regional survey. Internal sampling rate represents the number of scans recorded into memory. Effective sampling rates represent the maximum effective data output downloaded from the instrument.

	CTDs*		
Model Types	Idr 316	SBE 25	SBE 911 plus
Internal Sampling Rate (Hz)	4	8	24
Effective Sampling Rate (Hz)	4	8	24
Number of Instruments	1	3	3
Organizations with Instrument	1	4	2

*CTD Manufactures: Idr = Idronant, SBE = SeaBird Electronics

QC Post-Survey Analyses

Sensor drift was assessed using data from pre-calibration and post-calibration work sheets. All organizations were asked to calibrate their instrument prior to survey sampling. After the survey, all agencies post-calibrated their instrument to assess sensor drift during the survey.

CTD data post-processing involved a two-step approach. The first step eliminated outlier data points from the high frequency, downcast, raw data set. The second step interpolated the remaining raw data into comparable one-meter increments. The QC evaluation involved the outlier removal step. This step utilized both an objective criteria method and a subjective removal process. The objective method flagged any datum using the difference between the downcast standard deviation (all together) and a downcast five point (midpoint is the evaluated datum) running average standard deviation. Following this process, data points were subjectively removed if considered an artifact of equipment behavior rather than an actual oceanographic event. The subjective step relied on an experienced CTD technician to make the judgment. A CTD cast at any site could have been evaluated multiple times until the data were deemed acceptable. The QC objective was to ensure that excessive outlier removal did not significantly influence the interpolation process and that a representative data set was produced.

Discrete in-survey chlorophyll samples were analyzed for comparison and possible adjustments to CTD values derived from sensor fluorescence voltages. Surface water samples were collected from at least 10% of the survey sites for laboratory analysis.

Results

Pre-Survey

Inter-comparison Assessment

Over a one-hour period, five 3-minute data collection periods, 69002 data lines were recorded. Sensors measured some variables (temperature, conductivity, pressure, pH, beam transmission, and fluorescence) and software derived (depth, salinity, dissolved oxygen, oxygen saturation, sigma-t) various parameters from voltage and measured variables. Starting time delays from CTD water pumps or air bubbles caused missing data files or data removal from two organization's cast series. In addition, one organization's pressure sensor and transmissometer was above water during the inter-comparison exercise. Their data was not included in the results.

All organizations generally performed within acceptable limits for the inter-comparison exercise (Table IV-4). Some probes did not meet the quality assurance criteria's presented in Table IV-1. A color dissolved organic material (CDOM) fluorescence sensor was added to most CTD instrument packages for this survey, with the CDOM fluorometers assessed using a quinine sulfate dehydrate solution as a standard. Agencies were undergoing calibration method development during the comparison exercise.

Suggested Remedial Action

A suggested remedial action involves post-survey data corrections of sensor data outside the expected range. Table IV-5 shows the agency CTD and sensors out of range and the suggested correction factor to apply to their post-survey data. Chlorophyll was not included in the table because scaling factor corrections from discrete in-survey water samples improve data values better then offset corrections. Since this survey was a multi-agency cooperative study, each agency has ownership to their data. Agencies with problematic sensors can choose to apply the correction factor. Other factors involved in their decision could be probe replacement or data offset corrections in the CTD configuration files after the inter-comparison exercise.

In-Survey

Sampling Success

Field sampling occurred mostly as planned, with little deviation from required protocols. All four management zones (Ventura, Santa Monica Bay, San Pedro Bay, and San Diego plus Mexico) sampled two wet weather events. Due to atmospheric irregularities, one storm was sampled during the winter of 2003–2004 and the other during the winter of 2004–2005. The region experienced heavy swell and surf conditions during the first storm that closed Ventura Harbor to all vessel traffic for several days. All groups experienced some lost sampling hours/days or schedule changes because of weather. Cumulatively, the groups occupied 574 stations with 306 occurring during Storm #1 and 268 during storm #2. Discrete water samples were taken at the surface from most stations with a subset of sites having mid-depth, within the stormwater plume, and below the plume samples. Discrete water samples were analyzed from 574 offshore stations, 829 depths, and 29 rivers during the Bight '03 regional water quality survey.

Table IV-4. The December 2, 2003 inter-comparison exercise results for the Bight '03 survey. Measured parameters were conductivity, temperature, adjusted pressure (m), salinity, transmissivity (Xmiss), dissolved oxygen (mg L^{-1}), hydrogen ion concentration (pH), and chlorophyll fluorescence (µg L^{-1}). The expected ranges (Table IV-1) were bracketed around the group mean or a reference value.

	Mean Measured Values by Parameter								
CTD Number	Cond (S m^{-1})	Temp (°C)	Adj Pres (m)	Sal (psu)	Xmiss (%)	DO (mg L^{-1})	pH	Chloro (µg L^{-1})	CDOM (mg m^{-3})
1	3.668	10.259	0.24	33.319	80.92	9.02	7.78	1.52	0.74
2	3.667	10.260	0.33	33.313	80.87	8.98	7.86	0.36	5.11
3	3.664	10.259	1.21*	33.284*	83.13	9.15	7.93	1.14	1.56
4	3.678	10.377*	OW	33.318	OW	8.68	7.73	3.85*	4.71
5	3.669	10.260	0.08	33.325	81.99	8.67	7.93	0.80	5.18
6	3.668	10.258	-0.02	33.320	85.93	8.38	7.88	1.24	NA
7	3.671	10.271	0.05	33.339	NA	7.33*	VO	VO	NA
QA/QC expected ranges:									
Minimum	NA	10.220	-0.36	33.296	77.57	8.31	7.55	-0.99	NA
Maximum	NA	10.280	0.64	33.356	87.57	9.31	8.15	3.01	NA
Mean	3.669	10.261	0.14	33.322	82.57	8.81	7.85	1.01	3.46
Ref Value		10.250	0.00	33.326					

Note: * indicates mean was either below or above the expected range. OW means sensor was out of water. NA means sensor not available during inter-comparison. VO means voltage only submitted without proper conversion formula to engineering units. Dissolved oxygen for CTD 7 was originally presented as 5.13 ppm or ml L^{-1} and converted to mg L^{-1} by multiplying with 1.42903 (Seabird).

Drift Assessment

Pre and post calibration procedures showed some parameters drifted, but the drift was within acceptable range for individual agencies (Table IV-6). The largest transmissometer (Xmiss) drift was 7% at the upper end of storm # 1 values. The largest pH drift was 0.30 units but within the acceptable criteria found in Table IV-3. The largest dissolved oxygen drift was associated with an old style probe. Only one agency utilized the older less stable probe. All agencies calibrated the probes using the oxygen saturation method. Agencies using this method have shown good comparability among instruments from previous inter-comparison exercises (unpublished data). No surveys were re-done or post-processed data changed due to sensor drift.

Table IV-5. Suggested correction factors to post-survey data for sensors outside expected range from inter-comparison exercise on December 2, 2003. These are considered offset values to every record.

CTD Number	Sensor	Correction Factor	Units
3	Pressure	-1.206	meters
3	Salinity	+0.042	psu
4	Temperature	-0.1274	°C
7	Dissolved Oxygen	+1.482	mg L^{-1}

In general, most established electronic sensors are relatively stable. Typical sensors are engineered to measure a voltage, 0 – 5 VDC, and convert it to engineering units through linear regression and specialized formulas. Two important features of sensor drift are span (slope of the line) and offset voltage (related to intercept). Proper drift assessment requires voltage values on both ends of the sensor scale. Most manufactures recommend single point calibration checks on stable sensors with possible offset adjustments and two point adjustments on less stable sensors. The observed survey drift may reflect imbalances during pre-survey calibrations or improper lens cleaning. The pH sensors are generally the least stable sensors for the group. For dissolved oxygen, the new style probes generally exhibit lower drift when compared to the older sensors. Drift in any sensor may also be affected by calibration tank water conditions, atmospheric temperature/pressure, reference standard analysis, and methodology variability from pre to post calibration within and among the different agencies. Many agencies utilize a two-phase approach with part of the calibration done in air while the other performed in a tank of water.

Discrete Chlorophyll Samples Versus CTD measurements

The relationship between laboratory-measured chlorophyll-*a* samples and CTD derived fluorometric measures were better during storm 2 than storm 1. Figures IV-1 and IV-2 show the trend between expected versus observed. Further analysis showed dissimilar trends among the participating agencies. Because of system variability with the CTD and fluorescence sensor, scaling factors were different among the agencies. Consider the scaling factor as the slope of a regression line or multiplicative value. Applying a common scaling factor or an offset to all the data would not solve the discrepancies. Developing a new scaling factor for each agency during each cruise or day and applying it to the senor voltage output would mitigate the disparities and bring the data closer to acceptable variability. Acceptable chlorophyll-*a* variability includes changes in phytoplankton species, time of day differences, and age of the species. Stormwater runoff contributes to the fluorescence signal. The laboratory analysis technique also has an associated measurement error.

Table IV-6. Summary of sensor drift information compiled from pre- and post-survey calibration data. Org represents the agency involved in the sampling effort. The lower and upper range change shows hypothetical results if each agency experienced the minimum and maximum values observed during each storm. Days indicate the time it took to reach the hypothetical results.

		Storm 1			Storm 2		
	Org	Days between Calibration	Lower Range Change & Direction	Upper Range Change & Direction	Days between Calibration	Lower Range Change & Direction	Upper Range Change & Direction
Xmiss	1	2	0.00	-0.06	5	0.00	0.16
Storm 1 range	2	15	0.04	-0.79	8	-0.02	-0.67
0.2 - 91.33 %	3	69	0.00	-0.11	235	0.00	0.12
Storm 2 range	4	6	0.00	0.40	10	0.00	0.00
0.01 - 94.55 %	5	6	0.02	7.19	4	0.00	-2.85
	6	7	-0.02	0.02	3	-0.04	-0.06
	7	NA*	NA*	NA*	NA*	NA*	NA*
pH	1	2	-0.03	-0.02	5	-0.10	-0.10
Storm 1 range	2	15	-0.14	-0.15	8	0.06	0.06
7.56 - 8.44 units	3	69	0.16	0.14	235	-0.07	-0.08
Storm 2 range	4	6	-0.04	0.04	10	-0.30	-0.27
7.64 - 8.40 units	5	6	0.01	-0.01	4	-0.01	-0.04
	6	7	0.06*	0.06*	3	-0.02	-0.03
	7	NA*	NA*	NA*	NA*	NA*	NA*
				Total Drift Winkler - CTD			Total Drift Winkler - CTD
Dissolved Oxygen	1	2		0.00	5		0.10
Storm 1 range	2	15		NA*	8		NA*
4.60 - 12.48 mg L^{-1}	3	69		NA*	235		NA*
Storm 2 range	4	6		-0.07	10		-0.02
6.34 - 7.80 mg L^{-1}	5	6		-0.45	4		-0.11
**	6	7		-0.01	32		0.00
	7	NA*	NA*	NA*	NA*	NA*	NA*

*NA means information was not provided or missing. * means drift represents 3 days because probe was calibrated 4 days earlier, during the survey, with a drift of -0.08 pH units. ** Means dissolved oxygen change was not derived from Winkler/CTD values but rather from the change in slope used to convert voltage to concentration.

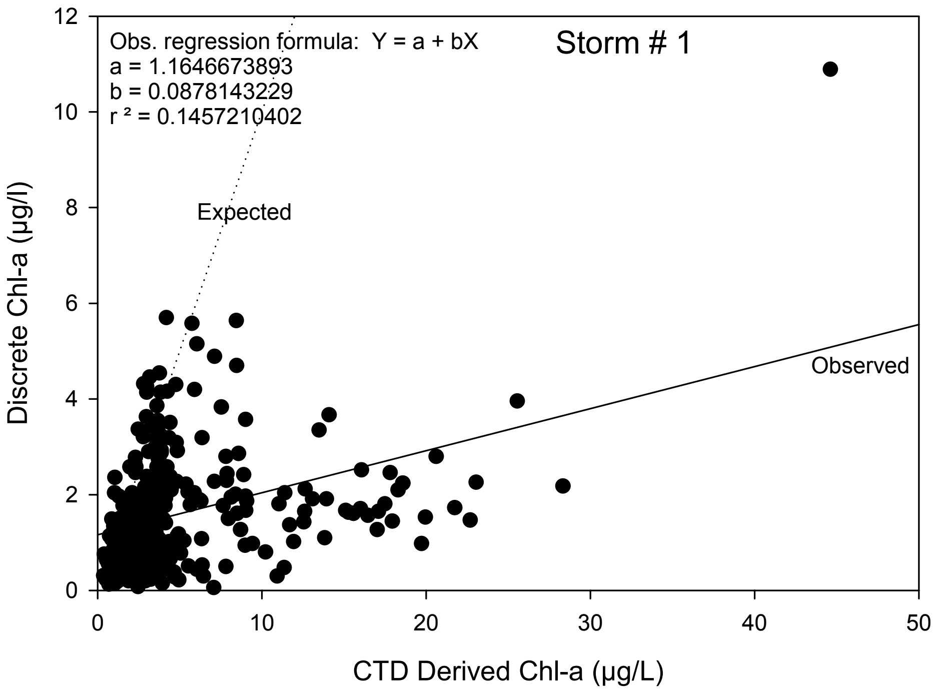

Figure IV-1. Chlorophyll-*a* comparison between CTD derived values and laboratory measured values from discrete water samples taken during storm #1 for the Bight '03 regional water quality survey.

Post-Survey

Data corrections

No data corrections were made as a result of the inter-comparison exercise or chlorophyll-a analysis of in-survey discrete water samples.

Outlier Analysis

The outliers removed by the data processing group usually represent a small fraction of the total used for data interpolation. The analysis was done on available data files. Three agencies from storm 1 and four from storm 2 did not submit files. These represent 48% of the expected outlier files. Outlier removal was parameter specific. For example, salinity removed at depth 5.63 m would not affect the temperature or dissolved oxygen value for the same depth. A total of 33452 downcast data points (scans) were removed from 210 stations. Each station has a matrix of depth collected at 4, 8, or 24 Hz (scans per second) and 11 parameters. Depths ranged from 5 to 60 meters and decent rate goals were 1 m s^{-1}. The largest categories of outliers were salinity, 34%, density, 23%, and temperature, 13%. The outlier points were removed from the raw downcast data prior to reduction into one-meter increments.

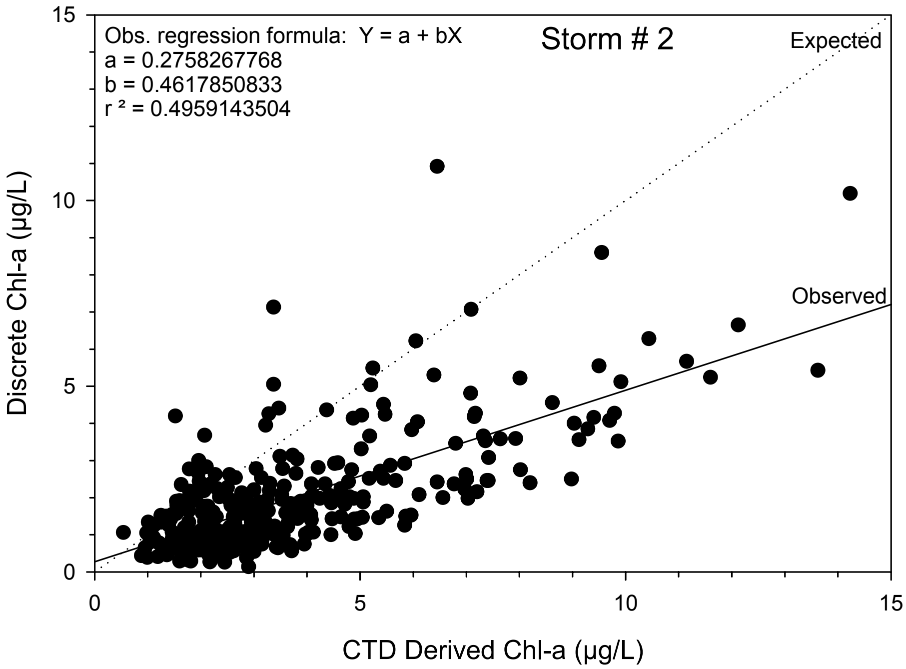

Figure IV-2. Chlorophyll-*a* comparison between CTD derived values and laboratory measured values from discrete water samples taken during storm #2 for the Bight '03 regional water quality survey.

The data processing group was not able to determine the total downcast data points prior to any data removal or any subsequent outlier removal. Labor constraints influenced the decision. The group may revisit this issue in future surveys.

Outliers were not flagged or separated into objective or subjective categories. Objective data removal was from two iterations of a computer data processing program. Subjective was termed for further data point removal based on interpretation of mechanical verses natural water column events.

<u>*Chemistry Analysis*</u>

Two laboratories did the analysis on discrete water samples. The U.S. participants used Laboratory 1. Laboratory 2 analyzed samples collected by the Mexican scientists participating in the project. No split samples or reference samples were exchanged between the laboratories but both followed established analysis procedures. Specific methods were referenced in the database. Holding times (Table IV-7) varied between laboratories but nutrient (NO_2, NO_3, PO_4, SiO_4, NH_4) and chlorophyll samples were frozen until analysis, while total suspended solid (TSS) samples were kept in the dark at 4°C until analysis. Analysis took longer than expected due to the high volume of samples. The common parameters measured by both laboratories during the survey were chlorophyll-a, NO_2, NO_3, PO_4, SiO_4, and TSS with associated detection limits presented in Table IV-8. Detection limits varied between laboratories because of methodology differences. QA/QC on any microbiology data can be found in a separate report presented by the Bight '03 Shoreline Microbiology Working Group. QA/QC on any toxicity data can be found in a separate report presented by the Bight '03 Toxicology Working Group.

Table IV-7. Sample holding time for laboratories analyzing discrete water samples collected during the Bight'03 Water Quality survey. S1 and S2 represent the first and second storm.

		Samples (N)		Hold Time (days)	
Lab Num	Parameter	S1	S2	S1	S2
1	Nitrate (NO_2)	193	144	19 - 27	25 - 31
1	Nitrite (NO_3)	193	144	19 - 27	25 - 31
1	Phosphate (PO_4)	193	144	19 - 27	25 - 31
1	Silicate (SiO_4)	193	144	19 - 27	25 - 31
1	Chlorophyll-*a*	195	142	1 - 13	1 - 11
1	Total Suspended Solids	198	172	2 - 15	1 - 13
1	Particulate Domoic Acid	27	26	176 - 177	173
1	Pseudo-nitzschia abundance	31		189 - 192	
2	Ammonium (NH_4)	22	42	7 - 10	6 - 7
2	Nitrate (NO_2)	22	42	7 - 10	6 - 7
2	Nitrite (NO_3)	22	42	7 - 10	6 - 7
2	Phosphate (PO_4)	22	42	7 - 10	7 - 8
2	Silicate (SiO_4)	22	42	7 - 10	7 - 8
2	Chlorophyll-*a*		42		12 - 13
2	TOC	22		9 - 12	
2	Organic Suspended Solids	22	42	12 - 15	8 - 9
2	Inorganic Suspended Solids	22	42	12 - 15	8 - 9
2	Total Suspended Solids	22	42	12 - 15	8 - 9

Table IV-8. Detection limits for laboratories analyzing discrete water samples collected during the Bight'03 Water Quality survey. S1 and S2 represent the first and second storm.

Lab Num	Parameter Code	MDL	Units
1	Chlorophyll-*a*	0.01	µg L^{-1}
1	NO2	0.01	µM
1	NO3	0.05	µM
1	PO4	0.01	µM
1	SiO4	0.1	Cells/ml
1	Total Suspended Solids	0.1	µM
1	Particulate Domoic Acid	0.01	µg L^{-1}
1	Pseudo-nitzschia abundance	10	cells L^{-1}
2	Chlorophyll-*a*	0.01	µg L^{-1}
2	NH4	0.02 - 0.2	µM
2	NO2	0.01 - 0.1	µM
2	NO3	0.1	µM
2	PO4	0.03	µM
2	SiO4	0.05 - 0.1	µM
2	Total Suspended Solids	0.005 - 0.01	µg L^{-1}
2	Inorganic Suspended Solids	0.005	µg L^{-1}
2	Organic Suspended Solids	0.005 - 0.01	µg L^{-1}
2	TOC	0.005	µg L^{-1}

Field Replicates

There were 23 discrete water sample field replicates measured during the regional survey. The breakdown was 1 sample during storm #1 and 22 from storm #2. Laboratory 2 analyzed 87% of the replicates. The relative percent difference (RPD) for chlorophyll-*a* ranged from 0 to 111% (Figure IV-3). The larger differences occurred between 0.03 and 0.59 µg L^{-1}. Any data pairs with non-detectable measurements were eliminated from the graph. Measurement variability increased as values approach the limits of the analytical method or instrumentation. Only one field replicate was taken for total suspended solids, RPD = 5.11%. Two replicates represent nutrient parameters for nitrite (NO_2), nitrate (NO_3), phosphate (PO_4), and silicate (SiO_4). Their mean RPD were 12.23%, 46.48%, 3.47%, and 1.35%, respectively.

Lab Duplicates

The average method variability was low for most measured parameters (Table IV-9). Duplicates were done on 5.4 to 13.8% of the 889 sampled locations. Laboratory 2 provided most of the data to calculated RPD. The within lab variability was assumed to be similar to Laboratory 1.

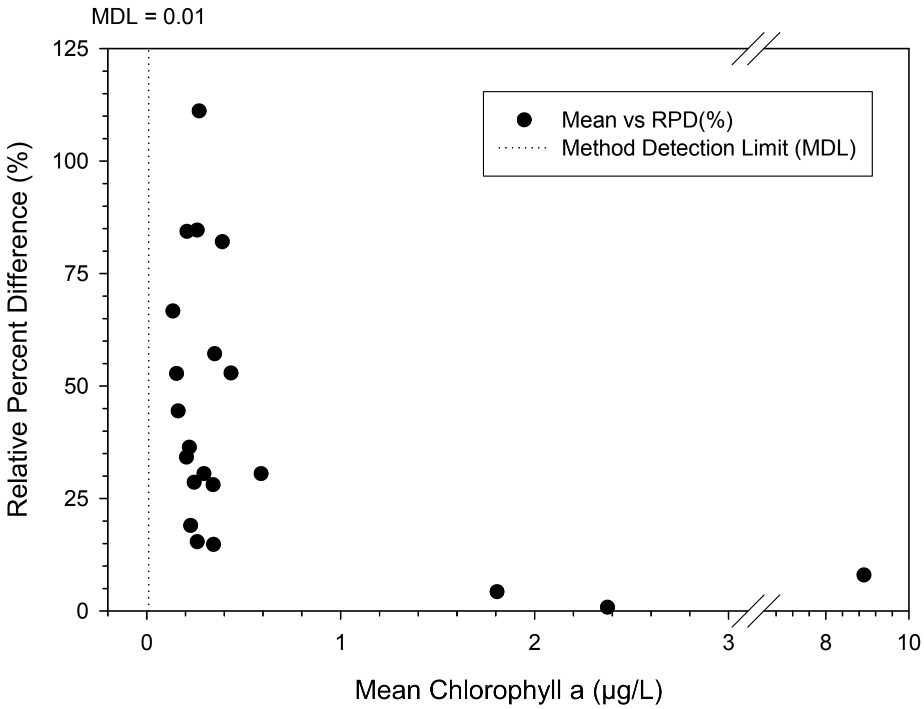

Figure IV-3. Field replicates measured during the Bight'03 regional survey. The relative percent difference (RPD) between the original and the replicate was plotted against their mean value. The zero value means below detection limit. The method detection limit (MDL) line for the chlorophyll-*a* appears near zero.

Table IV-9. Overall average method variability among laboratory duplicates analyzed on discrete water samples collected during two storms for the Bight'03 water quality survey.

Parameter	Locations (N)	Overall (%)
Chlorophyll-*a*	48	29
NO_2	82	15
NO_3	122	14
PO_4	123	11
SiO_4	123	11
NH_4	123	10
Total Suspended Solids	122	7
Inorganic Suspended Solids	98	46
Organic Suspended Solids	123	20
Total Organic Carbon	53	9

Discussion

Data comparability becomes an important component to the Bight '03 regional water quality survey. Data from 7 agencies and 2 laboratories were incorporated into synoptic results and discussion found in this report. Table IV-10 shows the interpretive limits of any CTD point when viewing the results from the regional context. These low limits are based on only December 3rd comparison and do not extend beyond the survey. Time, funding, and commitments to other projects preclude regular inter-comparison surveys and method development on instruments among the group. Further analysis with discrete water samples showed CTD derived chlorophyll-*a* values to be problematic. Any interpretations should be done on laboratory-measured chlorophyll-*a* values or CTD measured voltages. The CDOM fluorescence sensor has similar characteristics to the chlorophyll sensor. No discrete water samples were done for CDOM so CTD derived results should be interpreted with caution or make voltage comparisons only. Table IV-11 presents the variability associated with a given discrete water sample value measured by a laboratory. The relative percent difference with lab parameters was low compared to pesticide and trace metal duplicate data found in other Bight '03 reports.

Table IV-10. CTD comparability among measured parameters for participating agencies during the Bight '03 regional water quality survey.

Parameter	95% Confidence Limit	
Temperature	±	0.0326 °C
Conductivity	±	0.0033 S m^{-1}
Pressure	±	0.3641 m
Salinity	±	0.0033 psu
Dissolved Oxygen	±	0.46 mg L^{-1}
Ph	±	0.07
Transmissivity	±	1.83%
Chlorophyll	±	NA
CDOM	±	NA

Table IV-11. Laboratory comparability among measured parameters for participating agencies during the Bight '03 regional water quality survey. Percentages are discrete water samples only.

Lab Parameter	N	Average RPD (%)
Chlorophyll *a* (Chl-a)	48	29
Nitrate (NO_2)	84	15
Nitrite (NO_3)	124	15
Phosphate (PO_4)	125	11
Silicate (SiO_4)	125	11
Total Suspended Solids (TSS)	123	8

Conclusion

The group was confident that the data results accurately reflect true environmental conditions experienced in the field. The survey successfully sampled stormwater runoff during rough seas and sub-optimal conditions. Spatial and temporal variability of rainfall within the southern California region made a regional snapshot difficult to obtain. Incorporating scientists from Mexico into the regional survey enhanced water quality knowledge from Ensenada, Mexico, to the Ventura River, USA.

Logistical Recommendations

Improvements for the next regional survey should include:

1) Additional CDOM laboratory measures on discrete water samples.

2) Laboratories should include lab duplicates in their data reporting. Field crews should include a percentage of field replicates as part of their standard QA practice.

3) Sensor voltage output should be incorporated into the data management scheme of the agencies. Post-survey data corrections should be part of every agencies routine.

4) Post-processing schemes utilized by the agencies should be modified to incorporate some statistics on outlier data removal. Statistics should include downcast data points before modification and a quality assurance flag to indicate if the outlier was objectively or subjectively removed. The data from the output file should be easily extractable by common programs or spreadsheets.

V. PLUME PATTERNS AND DYNAMICS

Introduction

Southern California's coastal watersheds (Figure II-1) drain a highly modified landscape with 54% of the watershed area dammed and many of the channels straightened, leveed or channelized (Willis and Griggs 2003). These modifications, combined with the Mediterranean climate, lead to episodic river discharges, with large winter storms contributing the majority of annual water and sediment budgets (Inman and Jenkins 1999). These river systems also provide large loadings of pollutants and pathogens to the coastal ocean, surpassing loadings from municipal wastewater discharges for most constituents and as such merit detailed investigation (Schiff *et al.* 2000, Dojiri *et al.* 2003, Ahn *et al.* 2005, Warrick *et al.* 2005, Stein *et al.* 2006).

The plumes from these river discharge events can extend 10's km from the shoreline (Mertes and Warrick 2001, DiGiacomo *et al.* 2004, Nezlin and DiGiacomo 2005, Nezlin *et al.* 2005). Nezlin *et al.* (2005) found that plume areas defined by SeaWiFS radiometer-data were strongly correlated to antecedent precipitation. The maximum extent of these plumes occurs one to three days following precipitation, and multiple day plume persistence was found for all of the major river plumes (Nezlin *et al.* 2005). However, significant plume size variability is found across the California watersheds in both time and space (Mertes and Warrick 2001, Warrick and Fong 2004, Nezlin and DiGiacomo 2005, Nezlin *et al.* 2005).

Jones and Washburn (1997), Washburn *et al*. (2003) and Warrick *et al*. (2004b) have shown that the freshwater from southern California rivers quickly stratifies into a buoyant plume when it reaches the ocean. Warrick *et al*. (2004c) suggest that the movement of Santa Clara River plume near the river mouth is strongly influenced by the river discharge inertia, i.e., the momentum induced by the mass flux from the river. These river plumes are also likely subject to buoyancy, wind and tidal forcing, which will dictate dispersal patterns and dynamics (Stumpf *et al.* 1993, Garvine 1995, Pinones *et al.* 2005, Whitney and Garvine 2005). Better understanding of plumes in the Southern California Bight is needed to track and understand the potential health and ecological implications of the discharged pollutants.

Finally, satellite-derived ocean color products have been valuable tools to investigate the lateral movement of southern California river plumes, and most of these investigations utilize turbidity or suspended-sediment products as proxies to track plumes (e.g., Mertes and Warrick 2001, Nezlin *et al.* 2005). Although these river plumes are commonly quite turbid, sediment mass balances suggest that little of the discharged sediment resides in the buoyant plume due to rapid settling near the river mouth (Warrick *et al.* 2004b). It is necessary and valuable, then, to evaluate which satellite-based measurements may best track the freshwater plumes.

Here we present the results of the Bight '03 Water Quality program to describe post-storm runoff plumes from the eight largest river systems in southern California. Each of these systems was assessed for up to five days following each of two storms during 2004 and 2005. We combine *in situ* and remotely sensed data to evaluate plume dispersal patterns and rates and the forcing function(s) responsible for these transformations. Emphasis is placed on identifying transport and transformations processes that could be generalized across systems and discharge events.

Results

General Plume Patterns

Two events were sampled for each river mouth region during the winters of 2004 and 2005 (Figures III-2 through III-3). The 2004 event resulted in approximately twice the discharge rates and volumes of the 2005 events. Both events were modest sized, however, as the peak discharges were equivalent to approximately 2-year and 1.5-year recurrence interval events based on longer discharge records. Therefore, the sampled events were slightly smaller than the "annual" recurrence events (i.e., the 2.3-year recurrence event) for each river.

Ship-based sampling occurred within 1-5 days of the discharge events (Figures III-2 through III-3). However, the 2004 event was generally more difficult to sample due to sea-state. Sampling for the Santa Clara River during 2004 was only possible on the fourth day following peak discharge (Figure III-2a). Sampling of Ballona Creek was very limited on February 27, 2004 due to sea-state and only 4 stations were sampled. The 2005 efforts resulted in sampling immediately following discharge and for three full days of sampling for each region (Figure III-3).

Two representative profiles of salinity and beam-c from the Tijuana River plume are shown in Figure V-1. Both profiles were obtained approximately 4-km from the river mouth on February 14, 2005, and both show a freshened buoyant plume in the upper 3–5 m of the water column. Similar plume observations were obtained throughout the other study areas. These buoyant surface plumes also had elevated beam-c compared to waters immediately underneath the plume (Figure V-1). The waters immediately above the seabed differ considerably, however: the shallower station (Figure V-1b) reveals an ~5 m nephloid layer above the seabed, which was a common characteristic of many of the shallow profiles, while the deeper profile did not (Figure V-1a). It is instructive, however, to also contrast the buoyant plumes: the deeper station (Figure V-1a) had lower salinity (i.e., more freshwater) while having lower suspended sediment (i.e., beam-c and TSS) than the shallow station (Figure V-1b). This suggests that the river water and sediment were not mixing in a simple conservative manner with respect to a single river endmember water type. Below we show that this one observation from the Tijuana River plume was typical of a generally poor relationship between salinity and sediment concentration in stormwater plumes over the entire Southern California Bight.

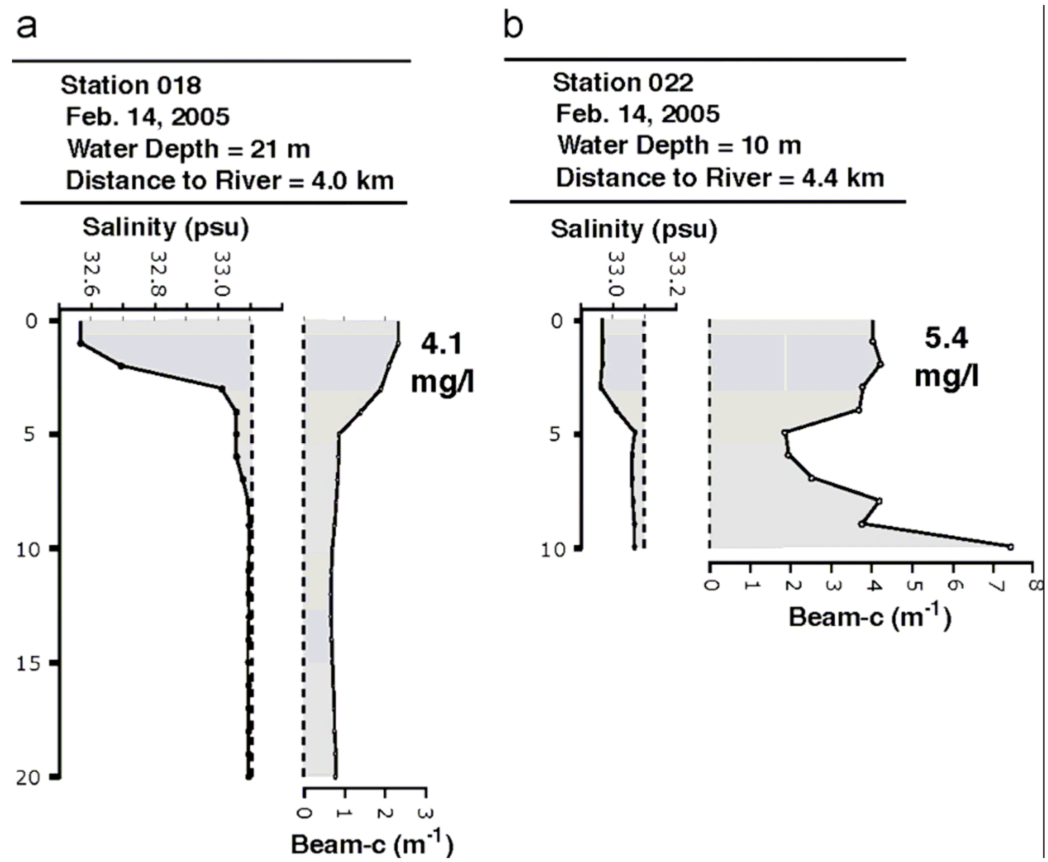

Figure V-1. Example salinity, beam-c and TSS data from CTD casts taken on February 14, 2005 offshore of the Tijuana River. TSS concentrations are shown for 1 m water depth samples. Dashed lines represent reference levels of 33.1 psu salinity and 0 m^{-1} beam-c.

Spatial mapping of the salinity and beam-c data from each site revealed synoptic characteristics of the buoyant plume properties. For example, data from Ballona Creek on February 28, 2004 show a buoyant plume with lowest salinities immediately offshore of the river mouth, and these low salinities continue to the southern side of the river mouth, which is in the opposite direction of Coriolis influence (Figure V-2a). In contrast, the highest beam-c on the same day was measured close to shore and away from the river mouth (Figure V-2b). The three-ship monitoring effort along the San Pedro Shelf on March 25, 2005 revealed that low salinity/high beam-c waters extended 10's of km along- and across-shore from the river mouths (Figure V-3). Further, it appears that a portion of this broad plume was detached from the coastline, because two regions of low salinity and high turbidity on this date were observed ~5 km offshore of the coast and laterally offset from the river mouths (Figure V-3).

These two synoptic examples of plume salinity and turbidity (Figures V-2 and V-3) reveal another pattern consistent with all of the remaining sampling dates: although the sampling grids extended many km's along- and across-shore, low salinity plumes always extended beyond the geographical limits of the surveys. Thus, none of the surveys captured the "entire" extent of the river plume, as was anticipated.

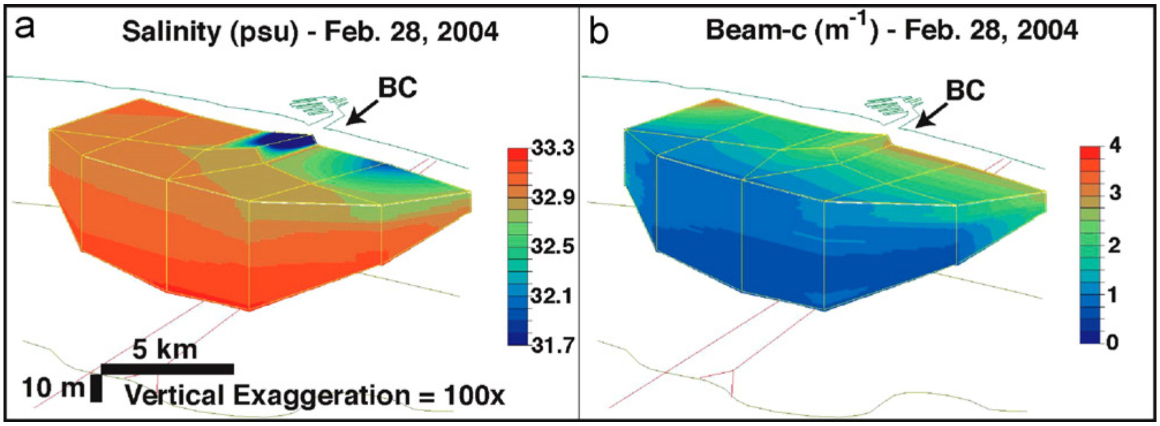

Figure V-2. Three-dimensional presentation of salinity and beam-c data offshore of Ballona Creek (BC) showing the freshened and turbid river plume waters along the sea-surface. Linear interpolation has been used to estimate parameter values between stations, which are shown with vertical yellow lines and line intersections along the water surface.

Plume Freshwater Volume Calculations

The volume of freshwater residing in the plumes each day can be estimated by spatially integrating the reduced salinity measurements across the sampling grid (Gilbert *et al.* 1996). For each profile a freshwater fraction (F_{fw}, in m of freshwater) was calculated by:

$$F_{fw} = \int_z \{[S_0 - S(z)] / S_0\}\, dz \qquad \text{[V-1]}$$

where S_0 is a reference salinity (in psu), S is the measured salinity (in psu) at depth z (in m). We selected S_0 from the profiles outside of the influence of the plumes either laterally or from the waters underlying the plumes. Unique values of S_0 were calculated for each event within each of the four regions; however similar values of 33.0 psu during 2004 and 33.1 psu during 2005 were obtained for all of the sites. Uncertainty in these values of S_0 was approximately 0.1 psu, which induced less than 10% error across the freshwater volumetric calculations. To compute freshwater volumes we assumed that F_{fw} changed linearly between each station. Further, if $S(z)$ was greater than S_0 for any depth, we set the quantity $[S_0 - S(z)]$ equal to zero.

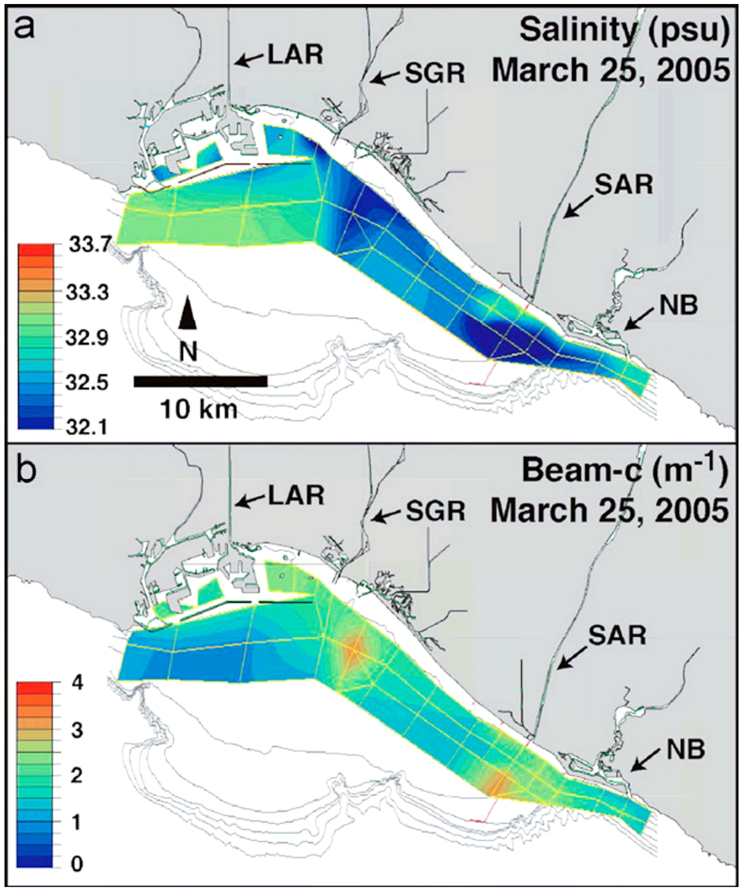

Figure V-3. Surface measurements of salinity and beam-c data from the San Pedro Bay on March 25, 2005. Linear interpolation has been used to estimate parameter values between stations, which are located at the intersections of the yellow lines. The three main river mouths and a bay are also identified (LAR - Los Angeles River, SGR - San Gabriel River, SAR - Santa Ana River, NB - Newport Bay).

Results of the volumetric calculations reveal that 10's of millions of cubic meters of freshwater could be accounted for within the survey limits (Tables V-1 and V-2). The greatest amounts of freshwater were consistently observed along the San Pedro Shelf portion of the study, which not only had the largest river discharge inputs (Figures III-2 and III-3) but also had a sampling area 2–20 times larger than the other sites (Tables V-1 and V-2). The volume of freshwater observed within the survey areas generally decreased with sample date, which suggests that plume waters moved outside of the sampling grids, rather than simply mixing down into the water column.

A couple of exceptions to this multiple-day pattern exist, and they can largely be accounted for by changes in the sampling grids. For example, only a limited sampling effort was possible on the San Pedro Shelf on March 24, 2005 (31.4 km^2 versus the typical ~230 km^2), which resulted in much less freshwater observed (Table V-2). The 2005 data from the Tijuana River plume suggested that freshwater volume in the plume doubled on the last day of sampling (Table V-2); however, the sampling grid was significantly altered on this date in an attempt to capture the presumably northward transporting plume. This modified sampling plan also resulted in capturing another reduced salinity plume from Mission Bay. Lastly, sampling of the Santa Clara River suggested increases in the freshwater plume volume with time (Table V-2). Although this is correct, we note below that the portion of the river discharge flux actually observed in this plume was insignificant on all days.

Table V-1. Integrated CTD survey results for the 2004 surveys.

	Santa Clara River	Ballona Creek	San Pedro Shelf	San Diego River	Tijuana River
Area Surveyed (km^2)					
24-Feb-2004	--	--	--	10.2	35.9
27-Feb-2004	--	*(1)*	155.9	--	--
28-Feb-2004	--	35.2	291.0	--	114.5
29-Feb-2004	76.8	--	--	--	114.5
1-Mar-2004	--	35.2	291.0	--	--
Integrated Fresh Water (m^3)					
24-Feb-2004	--	--	--	79,501	1,362,000
27-Feb-2004	--	*(1)*	27,512,000	--	--
28-Feb-2004	--	1,264,700	21,003,000	--	411,680
29-Feb-2004	34,570		--	--	88,899
1-Mar-2004	--	321,870	16,503,000	--	--
Surface Plume Sediment Mass (t)					
24-Feb-2004	--	--	--	42	1,577
27-Feb-2004	--	*(1)*	31,709	--	--
28-Feb-2004	--	1,027	4,744	--	1,076
29-Feb-2004	1,740	--	--	--	1,171
1-Mar-2004	--	864	2,114	--	--
Ratio of Fresh Water to Sediment ($kg\ m^{-3}$)					
24-Feb-2004	--	--	--	0.53	1.16
27-Feb-2004	--	(1)	1.15	--	--
28-Feb-2004	--	0.81	0.23	--	2.61
29-Feb-2004	50.33	--	--	--	13.17
1-Mar-2004	--	2.68	0.13	--	--

Notes: *(1)* data collection not adequate to spatially integrate.

The ratios between the observed plume freshwater volume and the river discharge volume were computed and are shown in Figure V-4. We included an additional amount of river discharge for the third day of the 2005 Tijuana River observations equal to the San Diego River discharge because the ungaged watershed area discharging into San Diego Bay is approximately equivalent to the watershed area of the San Diego River.

Table V-2. Integrated CTD survey results for the 2005 surveys.

	Santa Clara River	Ballona Creek	San Pedro Shelf	Tijuana River
Area Surveyed (km^2)				
13-Feb-2005	--	--	--	81.0
14-Feb-2005	--	--	--	81.0
15-Feb-2005	--	--	--	83.1
23-Mar-2005	--	--	226.5	--
24-Mar-2005	28.9	35.2	31.4	--
25-Mar-2005	28.9	--	228.5	--
26-Mar-2005	28.9	35.2	--	--
Integrated Fresh Water (m^3)				
13-Feb-2005	--	--	--	1,918,000
14-Feb-2005	--	--	--	1,645,400
15-Feb-2005	--	--	--	3,536,000
23-Mar-2005	--	--	23,270,000	--
24-Mar-2005	21,800	2,805,000	1,322,000	--
25-Mar-2005	35,190	--	11,754,000	--
26-Mar-2005	51,440	1,661,000	--	--
Surface Plume Sediment Mass (t)				
13-Feb-2005	--	--	--	960
14-Feb-2005	--	--	--	602
15-Feb-2005	--	--	--	1,539
23-Mar-2005	--	--	5,894	--
24-Mar-2005	4,133	273	575	--
25-Mar-2005	1,014	--	2,207	--
26-Mar-2005	939	60	--	--
Ratio of Fresh Water to Sediment ($kg\ m^{-3}$)				
13-Feb-2005	--	--	--	0.50
14-Feb-2005	--	--	--	0.37
15-Feb-2005	--	--	--	0.44
23-Mar-2005	--	--	0.25	--
24-Mar-2005	189.59	0.10	0.43	--
25-Mar-2005	28.82	--	0.19	--
26-Mar-2005	18.25	0.04	--	--

A substantial portion of the river discharge volume was observed during most cruise dates, although these values typically decrease with sample date (Figure V-4). Significant variability also exists across the study regions. As alluded to above, there was consistently negligible river water observed offshore of the Santa Clara River mouth (Figure V-4). We suggest below that this river water was transported to the south of the sampling grid due to wind-dominated alongshore currents as discussed below. For Ballona Creek, San Pedro Shelf and Tijuana River, between 35 and 65% of the river water could be accounted for during the first day following a peak discharge date (Figure V-4). Although these ratios appear relatively high compared to the remaining observations, they also suggest that roughly half of the river water had advected away from the sampling grids in the first day of plume formation. The rate of removal of freshwater from the sampling grids on subsequent days ranged 12% of the remaining water per day (San Pedro Shelf) to 80% per day (Tijuana River) for these three sites (mean ± st.dev. = 37 ± 23% per day).

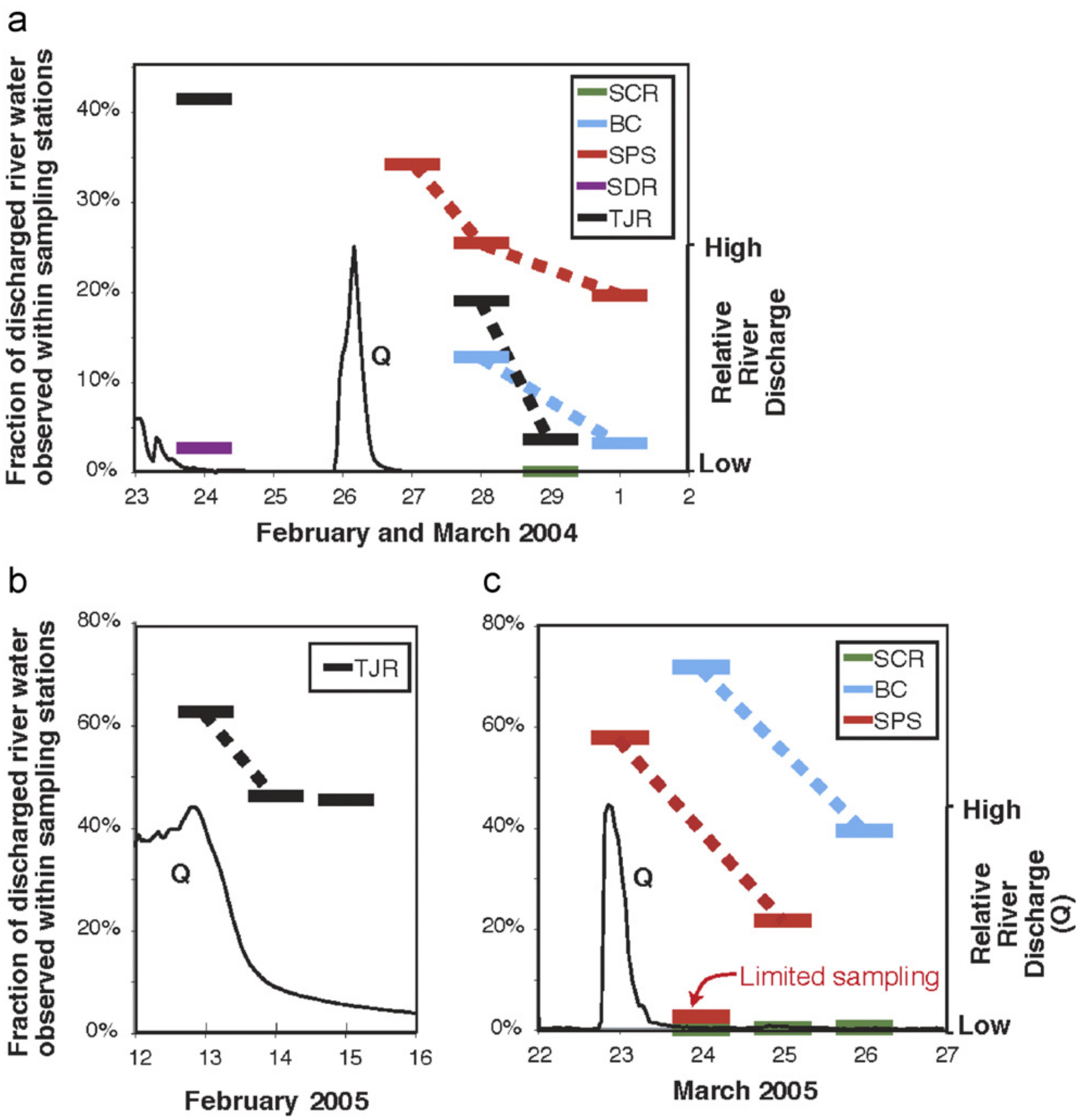

Figure V-4. Integrated plume fresh water observed during the surveys as a proportion of the total event river discharge. Sites include the Santa Clara River (SCR), Ballona Creek (BC), the San Pedro Shelf (SPS), the San Diego River (SDR), and the Tijuana River (TJR). A discharge (Q) curve is also presented based upon the mean discharge shown in Figures III-2 and III-3. Note the difference in scale between (a), (b) and (c).

Plume Sediment and CDOM Relationships

As noted above, patterns of salinity and sediment generally did not correlate well. A compilation of all total suspended-solids (TSS) and salinity samples shows that salinity explained very little of the variance in the TSS data across the region during the surveys (R^2 = 0.02; data not shown). In fact, the three highest measured concentrations of TSS (45–80 mg L^{-1}) occurred in waters with negligible freshwater. Salinity and beam-c also correlated poorly, and very little of the beam-c variance could be explained by salinity (R^2 = 0.15; data not shown). These poor relationships did not exist only for the data when considered in bulk, but also existed when individual sample days were considered for each river system (Figure V-5). Although one sample date had excellent salinity-TSS correlation (R^2 = 0.94; Figure V-5), we note that this was for the Santa Clara River during the 2004 sample date when little of the river water was observed (*cf.* Figure V-4).

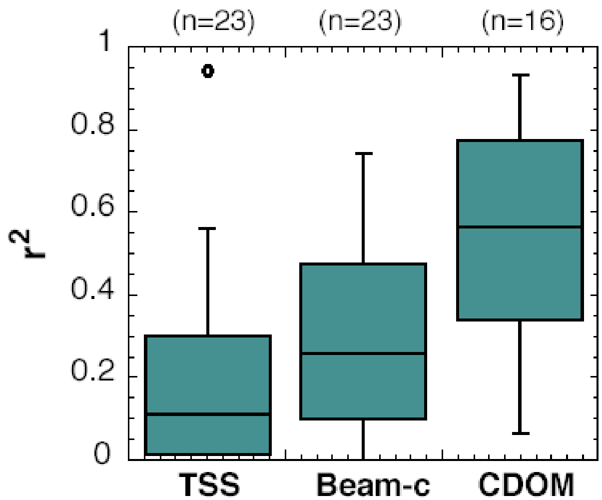

Figure V-5. Box-plots of the correlation coefficients from site-specific linear regressions of TSS, beam-c and CDOM with salinity during each sampling date. Total number of regressions (n) differs because the Tijuana River plume was not sampled for CDOM. Boxes are defined by quartiles, lines show the limits of the data within 1.5 times the interquartile distance from the quartiles, and outliers are shown with circles.

The fluorometer-derived CDOM concentrations correlated much better with salinity than did either TSS or beam-c (overall R^2 = 0.58; Figure V-5). No significant ($p<0.05$) relationships between sample date and CDOM correlation coefficients were found, although slight decreases in linear regression slope with sample date was observed in most data. The CDOM correlations were consistently poor for the Santa Clara River data (R^2 = 0.32 ± 0.14), and this may be due to either the limited river water observed or actual variability in the river water characteristics. Much better CDOM correlations existed for Ballona Creek (R^2 = 0.65 ± 0.28) and the San Pedro Shelf (R^2 = 0.54 ± 0.28), while CDOM fluorescence was not measured for the Tijuana River system. We discuss the implications of these observations to remote sensing of these river plumes in the Discussion section below.

Although the relations between salinity and sediment concentrations were poor, the TSS and beam-c data were adequate to estimate the mass of sediment in the buoyant river plumes. To estimate sediment mass we used a similar spatial integration method as used in the freshwater volume calculations above. For each CTD+ station we computed the plume sediment mass (*Sed,* in g m^{-2}) by:

$$Sed = \int_z \alpha \, [C_p(z) - C_O] \, dz \qquad \text{[V-2]}$$

where C_p is the measured beam-c profile (in m^{-1}) with respect to depth (*z,* in m) within the buoyant plume, C_O is the ambient ocean water beam-c defined from our data to be 1 m^{-1} (cf. Figures V-1 through V-3), and α is a coefficient (in mg-m L^{-1}) converting beam-c to suspended-sediment concentration. As noted, calculations were limited to the surface buoyant plume by limiting the *Sed* calculations to portions of the profiles with salinities less than the plume thresholds discussed above (33.0 and 33.1 psu). Further, if $C_p(z)$ was less than C_O we set $[C_p(z) - C_O]$ equal to zero.

To calculate α we compared the TSS and beam-c data from the surface water samples. A significant linear relationship forced through the origin was found between these variables, and beam-c explained almost half the variability in TSS. This relationship was much better during 2004 than 2005 (R^2 of 0.61 and 0.39, respectively), although the slopes during these two periods were not significantly different ($p < 0.05$). The correlation differences between TSS and beam-c may be a result of: (1) differences in sampling technique – bottle samples versus *in situ* optical samples, and/or (2) grain-size variability in the sediment, which is known to induce significant variability in α (Baker and Lavelle 1984). Although it is difficult to assess the causes of the variability in the data, we note that the value of α derived from this data (1.65 mg-m L^{-1}) is both near the suggested value of 1.4 mg-m L^{-1} for clay and fine silt particles by Baker and Lavelle (1984) and consistent with data from the Santa Clara River plume reported by Warrick *et al*. (2004b). Lastly, we note that relationship between F_{fw} and *Sed* was also very poor ($R^2 = 0.01$; data not shown), which is consistent with other results discussed above.

The calculated mass of sediment contained within the buoyant plumes ranged from O(10) to O(10,000) t on the various sampled dates, and sediment mass within each sampled plume generally decreased with sampling date (Tables V-1 and V-2). The river suspended-sediment concentration, if sediment mixed conservatively, was estimated by the ratio of observed plume sediment to plume fresh water (Tables V-1 and V-2). This sediment:water ratio was 0.1 to 1.2 kg m^{-3} for the first day of sampling from the all systems but the Santa Clara (the Santa Clara had very little water sampled and the first day ratios in excess of 50 kg m^{-3}). We note that actual river suspended-sediment concentrations during these events were likely ~10 times higher than these ratios (Brownlie and Taylor 1981, Warrick and Milliman 2003). Further, although thousands of tonnes of sediment were estimated in the plumes (Tables V-1 and V-2), these amounts were consistent to other measurements of southern California river plumes (Mertes and Warrick 2001) and were considerably less than the hypothetical amounts of sediment flux from such events on the rivers (Brownlie and Taylor 1981). Thus, we suggest that at least 90% of the river suspended-sediment was not observed on the first day of sampling, likely due to high rates of particle settling (cf. Warrick *et al.* 2004b).

During the subsequent days, both increases and decreases were observed in the sediment:water ratios (Tables V-1 and V-2), which suggests that both losses and gains of sediment occurred in the sampled plumes. Gains were especially apparent in the Tijuana River system (Table V-1).

Observations of Plume Transport

Results presented above suggest that plume freshwater was transported significantly beyond the sampled stations. Here we examine measurements of this transport from drifters, HF radar and satellite remote sensing. Ten drifter deployments within plumes revealed many different patterns of plume movement. For example, two contrasting observations from the Santa Ana River plume are shown in Figure V-6. The majority of drifter observations were dominated by alongshore transport, which could exceed 30 cm s^{-1} (Figure V-7). Across-shore currents were strongly correlated with alongshore currents but were consistently smaller in magnitude (Figure V-7). Rivers did not appear to influence the across-shore velocity as drifter trajectories were not deflected offshore immediately seaward of the river mouths, which was likely related to low river discharge rates on the drifter deployment days (cf. Figures III-2 and III-3).

Surface currents were also measured by HF radar arrays in two of the study regions. We spatially subsampled the surface current data into areas relevant to plume movement (Figure V-8). For the Santa Clara River only a region immediately offshore of the river was sampled, while four regions were subsampled for the Tijuana River to evaluate the variability of circulation of this region ((cf. Roughan *et al.* 2005); Figure V-8). The variance of the hourly current measurements within each subsampled region was generally low, and mean hourly standard deviations were 12 cm s^{-1} for the Santa Clara, <6 cm s^{-1} for all nearshore Tijuana (I, II and III) and 9 cm s^{-1} for offshore Tijuana (IV). For all subregions, we calculated mean daily currents centered on local midnight to best represent total circulation between satellite imagery (obtained approximately at local noon) and to approximate the subtidal portions of the currents.

Compilations of some of the available HF radar, drifters, and satellite imagery are shown in Figures V-9 through V-11. During and following the 2004 event, strong equatorward currents (>30 cm s^{-1}) were measured in both the Santa Clara River plume and the San Pedro Shelf regions (Figure V-9). Satellite imagery obtained during this period revealed plume fronts from the Santa Clara River and San Pedro Shelf regions moving offshore and equatorward at rates (>30 km d^{-1}) consistent with the measured current directions (Figure V-9).

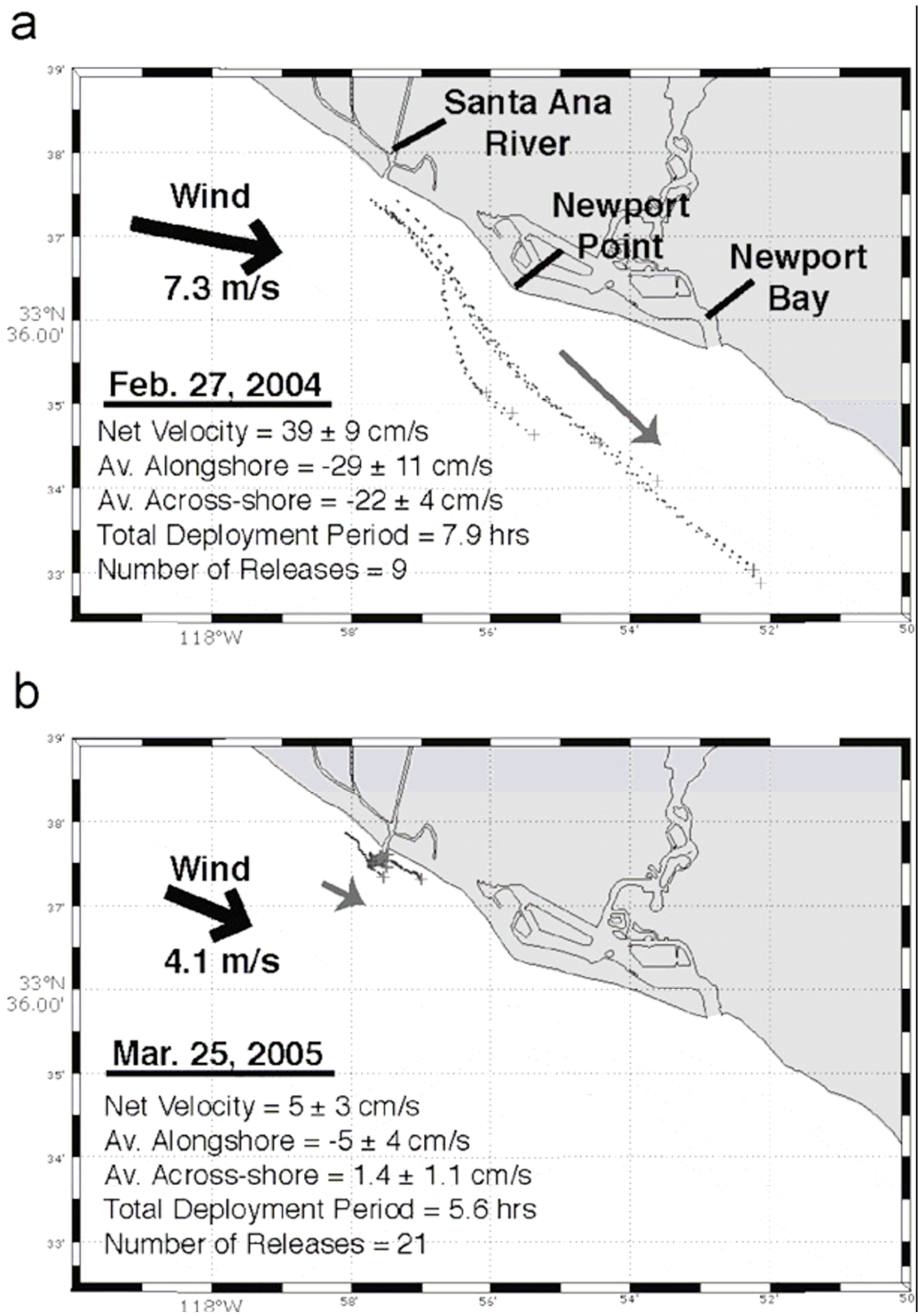

Figure V-6. Drifter results from the Santa Ana River plume during contrasting advection conditions. Positions of each drifter are shown at 10-minute increments. Summary statistics for the releases shown in the lower left of each subfigure. Mean wind speed vectors shown for a 6-hr period of time prior to the middle of the observations from NDBC 46025.

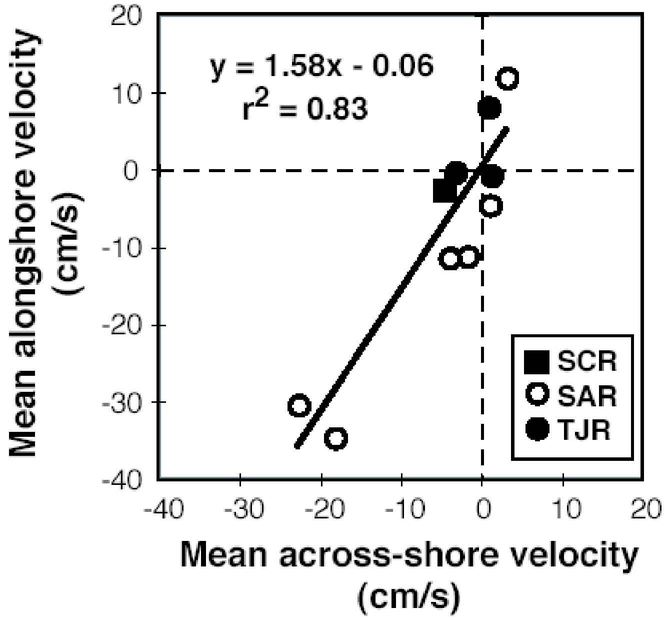

Figure V-7. Mean alongshore and across-shore current velocities from the river plume drifter deployments. Alongshore defined as poleward (positive) and equatorward (negative), and across-shore defined as onshore (positive) and offshore (negative). Rivers plumes monitored include the Santa Clara River (SCR), Santa Ana River (SAR), and Tijuana River (TJR).

During 2005 similar equatorward currents existed and persisted near the Santa Clara River mouth for at least 10 days as shown by HF radar data (Figure V-10). For both events mean currents on the Santa Pedro Shelf were strongest (>30 cm s^{-1}) during the first day following river discharge (Figures V-9 and V-10). The equatorward currents offshore of the Santa Clara River mouth were clearly responsible for transporting the Santa Clara River plume toward Santa Monica Bay for a period of at least a week (Figure V-10). During this time, long (~50 km) filaments of turbidity, CDOM and perhaps phytoplankton were observed originating near the Santa Clara River and extending into the outside of both Santa Monica and San Pedro Bays (Figure V-10). Both HF radar and satellite data suggest that advection of this plume averaged 15 – 45 cm $s\text{-}^{1}$ each day (mean = 26 cm s^{-1}), which is fast enough to transport Santa Clara River water into the center of Santa Monica Bay in 2 – 6 days (mean = 3.5 days).

We note that plumes from Ballona Creek during both events were much more difficult to identify with the satellite imagery than from either the Santa Clara River or San Pedro Bay regions (Figures V-9 and V-10), which may be due to the small size and/or quick dispersal of this plume.

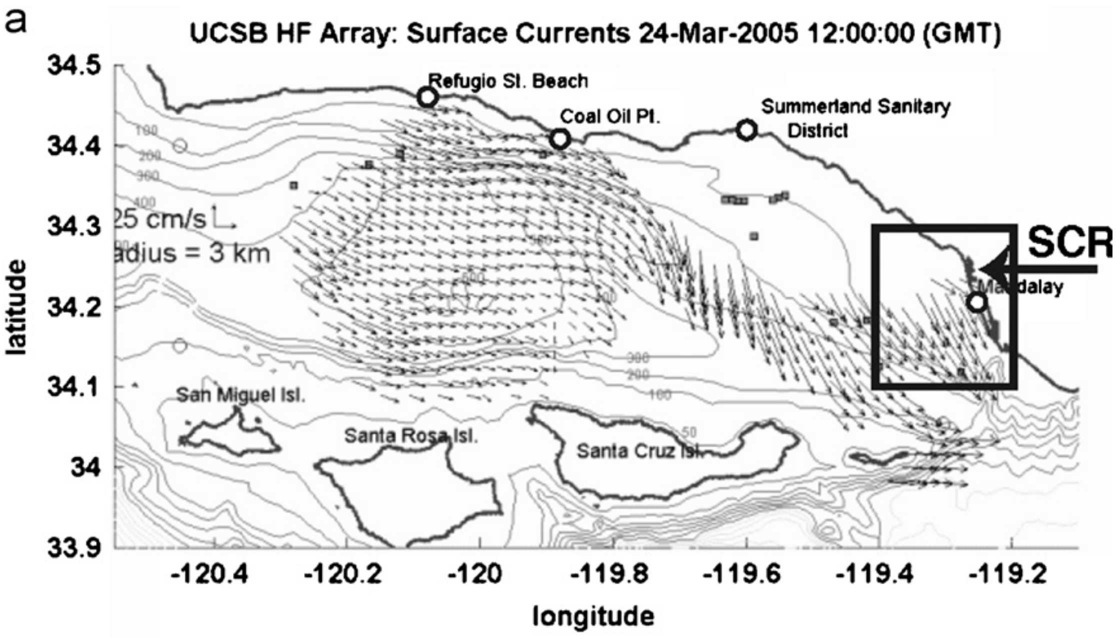

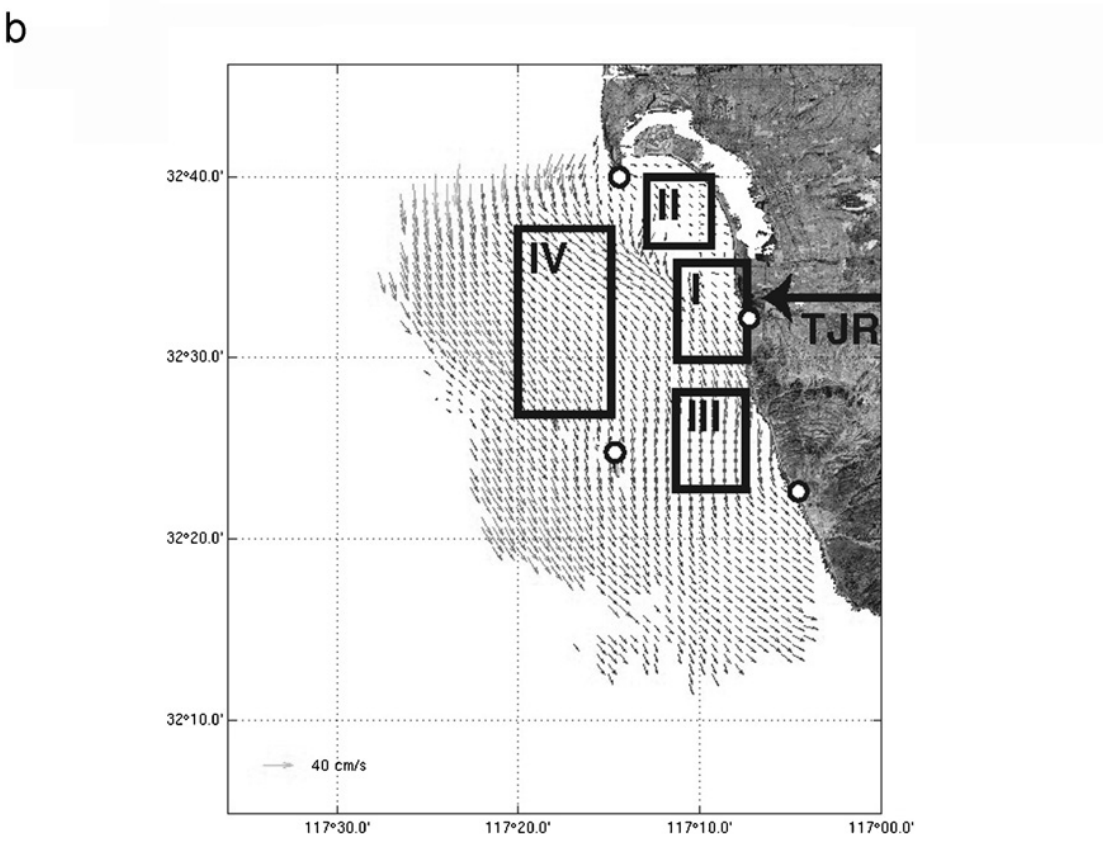

Figure V-8. Example mean daily surface currents from the two HF Radar surface current arrays. Inset boxes show the regions directly offshore of the river mouths for which mean currents were calculated (see text). (a) Surface currents near the Santa Clara River mouth (SCR) from the UCSB HF Radar array. (b) Surface currents near the Tijuana River mouth (TJR) from the SIO HF Radar array.

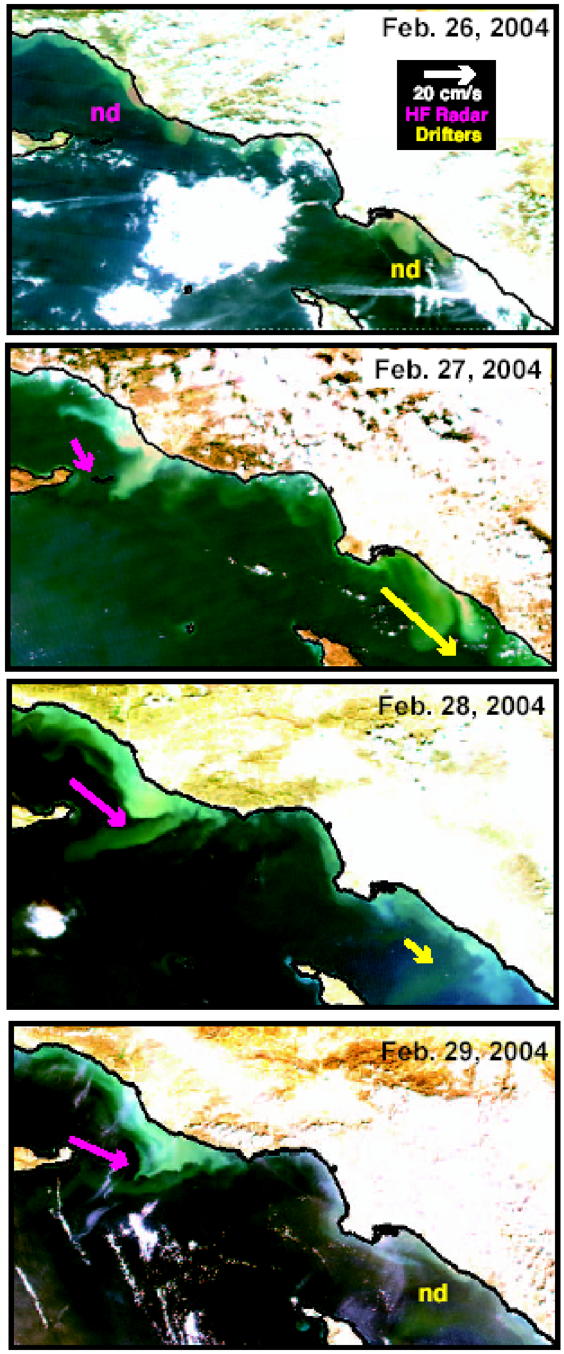

Figure V-9. Four-day time series of true-color satellite imagery from MODIS Aqua and Terra of the northern portion of the study area during the 2004 sampling period. Velocity vectors are shown from the HF Radar observations of the Santa Clara River plume area (pink) and drifter releases offshore of the Santa Ana River (yellow). Days without velocity observations are denoted with "nd".

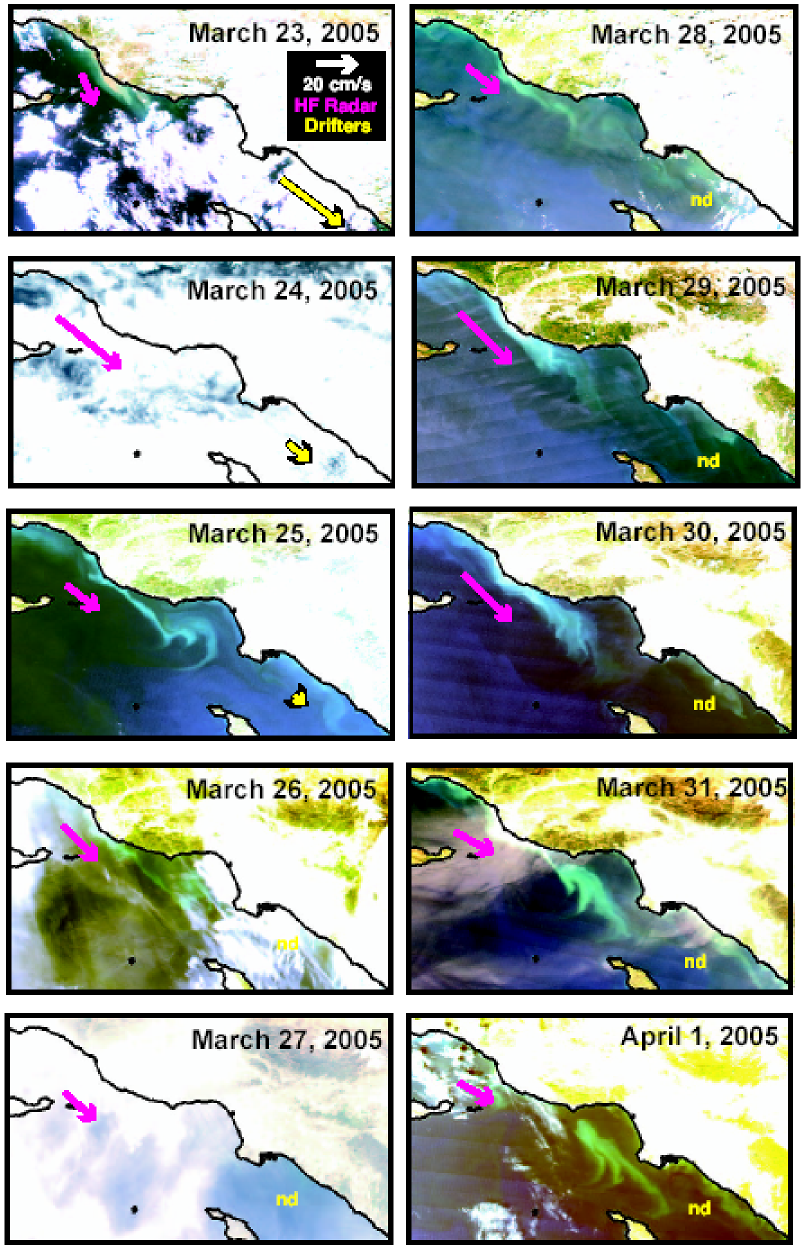

Figure V-10. Ten-day time series of true-color satellite imagery from MODIS Aqua and Terra of the northern portion of the study area during the 2005 sampling period. Velocity vectors are also shown from the HF Radar observations of the Santa Clara River plume area (pink) and drifter releases offshore of the Santa Ana River (yellow). Days without velocity observations are denoted with "nd".

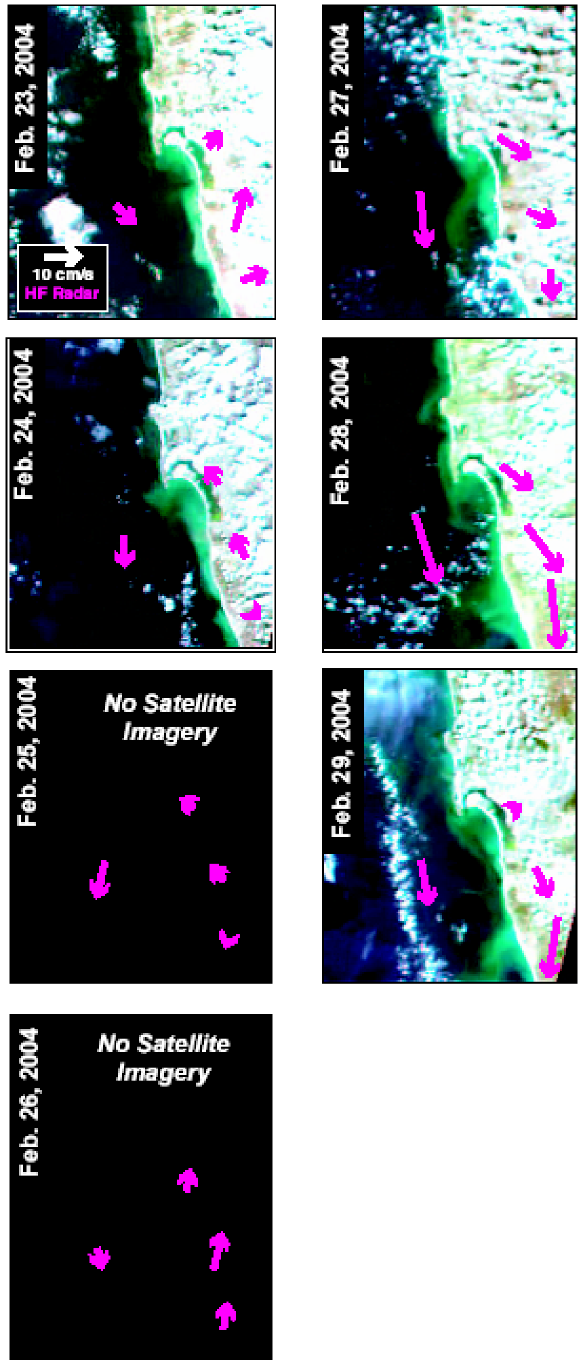

Figure V-11. True-color satellite imagery from MODIS Aqua and Terra of the southern portion of the study area during the 2004 sampling period. Mean daily velocity vectors are also shown from the HF radar observations of the Tijuana River plume area (pink). Vectors have been placed on land immediately adjacent to the sampled regions so that the coastal plumes are not obscured.

Satellite and HF radar observations for the Tijuana River plume show that circulation in the Tijuana River plume region was complex during the events (Figure V-11). A counterclockwise eddy was observed south of Pt. Loma during February 23–26, 2004, which changed to southerly flow conditions on February 27–29, 2004. We note that the mean daily alongshore currents furthest offshore of the Tijuana River (region IV, Figure V-8b) explained 60%, 51% and 76% of the alongshore mean current variance in three inshore regions (I – river mouth, II – north of mouth, III – south of mouth), respectively during the 2004 and 2005 events. Thus, although there is spatial variability in the currents, there was relatively strong coherence in the current patterns during the events sampled.

Transport Forcing

In this section we examined a number of plume transport forcing parameters to evaluate why the plumes transported in they manner they did. Our techniques closely follow those of Garvine (1995), Geyer *et al*. (2000), Fong and Geyer (2002), and Whitney and Garvine (2005). A synthesis of these results is included in the Discussion section.

First, the baroclinic height anomaly (h_f) was calculated assuming hydrostatic pressure with the baroclinic pressure anomaly (P_f), such that,

$$h_f = P_f / g \rho_0 \qquad \text{[V-3a] , where}$$

$$P_f = g \int_h [\rho_0 - \rho(z)]\, dz \qquad \text{[V-3b]}$$

and g is the gravitational constant, ρ_0 is the ambient seawater density, $\rho(z)$ is the density at depth z, and h is the total water depth. The maximum h_f for each cruise was consistently measured on the first day of sampling and ranged between 0.0 and 1.7 cm across the sites (Table V-3). Values of h_f were consistently lower for the Santa Clara River plume than for the remaining sites.

Secondly, the baroclinic velocity anomaly (u_f) provides an estimate for the initial plume velocity associated with buoyancy forcing at the river mouth and was computed using Bernoulli's equation and h_f,

$$u_f = (2\, g\, h_f)^{0.5} \qquad \text{[V-4]}$$

The maximum values of this baroclinic velocity were generally 20 – 55 cm s^{-1} during each cruise (Table V-3).

Table V-3. Plume forcing statistics from the CTD+ casts during 2004 and 2005. Days without velocity observations are denoted with "nd".

	Santa Clara River	Ballona Creek	San Pedro Shelf	San Diego River	Tijuana River
Maximum Salinity Anomaly (cm)					
2004 cruise	1	26	58	5	7
2005 cruise	7	27	32	nd	14
Maximum Baroclinic Height Anomaly (cm)					
2004 cruise	0.01	0.73	1.67	0.25	0.27
2005 cruise	0.18	1.16	1.22	nd	1.57
Maximum Baroclinic Velocity Anomaly (cm s^{-1})					
2004 cruise	4.8	37.9	57.3	21.9	23.1
2005 cruise	18.6	47.6	48.8	nd	55.5
Geostrophic Velocity (cm s^{-1})					
2004 cruise	0.1	5.7	13.1	1.9	2.1
2005 cruise	1.4	9.0	9.5	nd	12.3
Wind Stress Index (|Ws|)					
peak discharge	0.3-0.8	0.4-0.6	0.4-0.5	0.4-0.6	0.4-0.6
peak wind	1.8	>2	1.5	1.6	1.6
Linear Slope of Wind-Current Correlation					
mean	0.039	nd	0.033	nd	0.027
95% confidence interval	0.013	nd	0.016	nd	0.006

If the plumes resulted in geostrophic momentum balances, Fong and Geyer (2002) suggest that the alongshore velocity of this transport can be approximated by:

$$v = g' h_0 / f L \qquad \text{[V-5]}$$

where g' is the reduced gravitational constant resulting from the plume (equivalent to $g\Delta\rho/\rho_0$), h_0 is the thickness of the plume nearest the coast, f is the Coriolis parameter (~8.2 x 10^{-5} s^{-1}) and L is the plume width offshore of the coastline. Using maximum values for g' and h_0 for each cruise and assuming L was O(10) km, geostrophic velocities were computed to be O(10) cm/s (Table V-3). We note that these velocities would be directed poleward, which is both smaller and in the opposite direction of the majority of observations presented here (Figures V-9–V-11).

We next looked into the effects of winds on the buoyant river following a number of previous studies (e.g., Chao 1988, Munchow and Garvine 1993, Kourafalou *et al.* 1996, Geyer *et al.* 2000, Whitney and Garvine 2005). We examined both wind speed and wind stress, and wind speed provided the best correlations with plume velocity observations, consistent with the theory and observations presented by Garvine (1991) and Whitney and Garvine (2005). Mean alongshore currents measured by the drifters were significantly correlated to local alongshore wind speed ($R^2 = 0.66$, $p < 0.01$; Figure V-12). Maximum correlation was found for the mean winds occurring during the 6-hours prior to the middle of the drifter release period.

Stronger correlations were found between mean daily wind stress and mean daily plume velocity immediately offshore of the river mouths from the HF radar data (Figure V-13). High correlations were found at zero lag for 24-hr averages (R^2 = 0.68 to 0.71), but peak correlations occurred for mean 24-hr winds that were lagged by 3 hours compared to currents (R^2 = 0.71 to 0.74; Figure V-13). This observation is consistent with a multiple hour lag for maximum correlation in wind-plume response by Munchow and Garvine (1993) and Geyer *et al*. (2000). For the regions immediately offshore of the Santa Clara and Tijuana river mouths, mean daily wind stress explained 71–74% of the alongshore surface current variance and captured most of the temporal shifts in these currents (Figure V-13). Across-shore surface currents were somewhat poorly correlated with wind speed (maximum R^2 = 0.28–0.44, data not shown).

Further evaluation of the influence of wind can be provided by a framework suggested by Whitney and Garvine (2005). They propose that the wind stress index (W_s) can determine whether a plume's along-shelf flow is wind- or buoyancy-driven, where W_s is the ratio of buoyancy-driven velocity (u_{dis}) and the wind-driven alongshore velocity (u_{wind}). The first variable can be evaluated by either considering a two-layer system in geostrophic balance, which may be reduced to:

$$u_{dis} = K^{-1} (2\, g'_r\, Q f)^{1/4} \qquad \text{[V-6]}$$

where K is the dimensionless current width (or Kelvin number), which is ~1 for southern California plumes (Warrick *et al.* 2004c), g'_r is the reduced gravity of the river water (~0.24 m s^{-2} assuming 32 psu ambient seawater and 0 psu river water both at 10ºC), Q is the volumetric river discharge rate, and f is the Coriolis parameter, or by using Equation V-4 to solve for u_f if the plume is not geostrophic. Assuming a barotropic wind response, a steady state momentum balance between wind stress and bottom stress, and quadratic drag laws, Whitney and Garvine (2005) suggest that u_{wind} can be estimated by:

$$u_{wind} = \{(\rho_{air}/\rho)\, (C_{10}/C_{Da})\}^{1/2}\; U \qquad \text{[V-7]}$$

where ρ_{air} and ρ are the density of air and seawater, C_{10} and C_{Da} are the drag coefficients for the air-sea boundary and the seabed, and U is the alongshore component of the wind speed. It can be shown that u_{wind} is equal to ~$0.0265U$ under the assumptions given above (Whitney and Garvine 2005). When the absolute value of W_s is less than one, a river-induced buoyancy current should dominate. However when W_s is greater than one, the plume should be dominated by wind-driven flow. Upwelling-favorable winds will arrest or, perhaps, reverse a buoyant geostrophic coastal current, whereas downwelling-favorable winds will enhance the current.

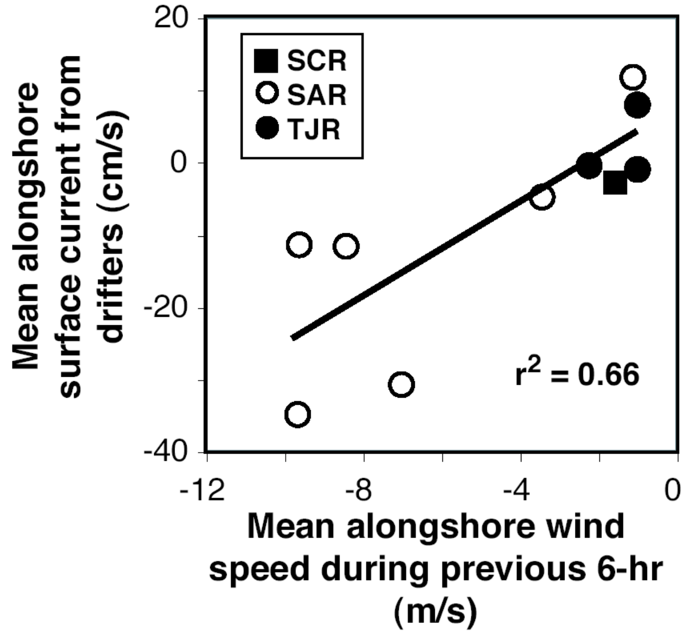

Figure V-12. The relation between alongshore wind speed and mean alongshore surface currents measured for drifters. Maximum correlation occurs for the mean wind stress during the 6-hours prior to the deployment. Alongshore defined as poleward (positive) and equatorward (negative). Rivers plumes monitored include the Santa Clara River (SCR), Santa Ana River (SAR) and Tijuana River (TJR).

Using this framework, we computed W_s for the time series of daily mean discharge and wind records surround the sampled events. On peak days of river discharge $|W_s|$ ranged between 0.3 and 0.8 (Table V-3). Peak winds often occurred within one to three days after the peak discharge, during which $|W_s|$ ranged from 1.5 to over 2, suggesting wind-driven flow (Whitney and Garvine 2005). If the assumptions made above hold, then the linear slope between U and u_{wind} should be approximately 0.0265. Using data presented in Figures V-12 and V-13, we computed linear slopes between winds and currents that were somewhat higher but statistically indistinguishable from this theoretical value (Table V-3).

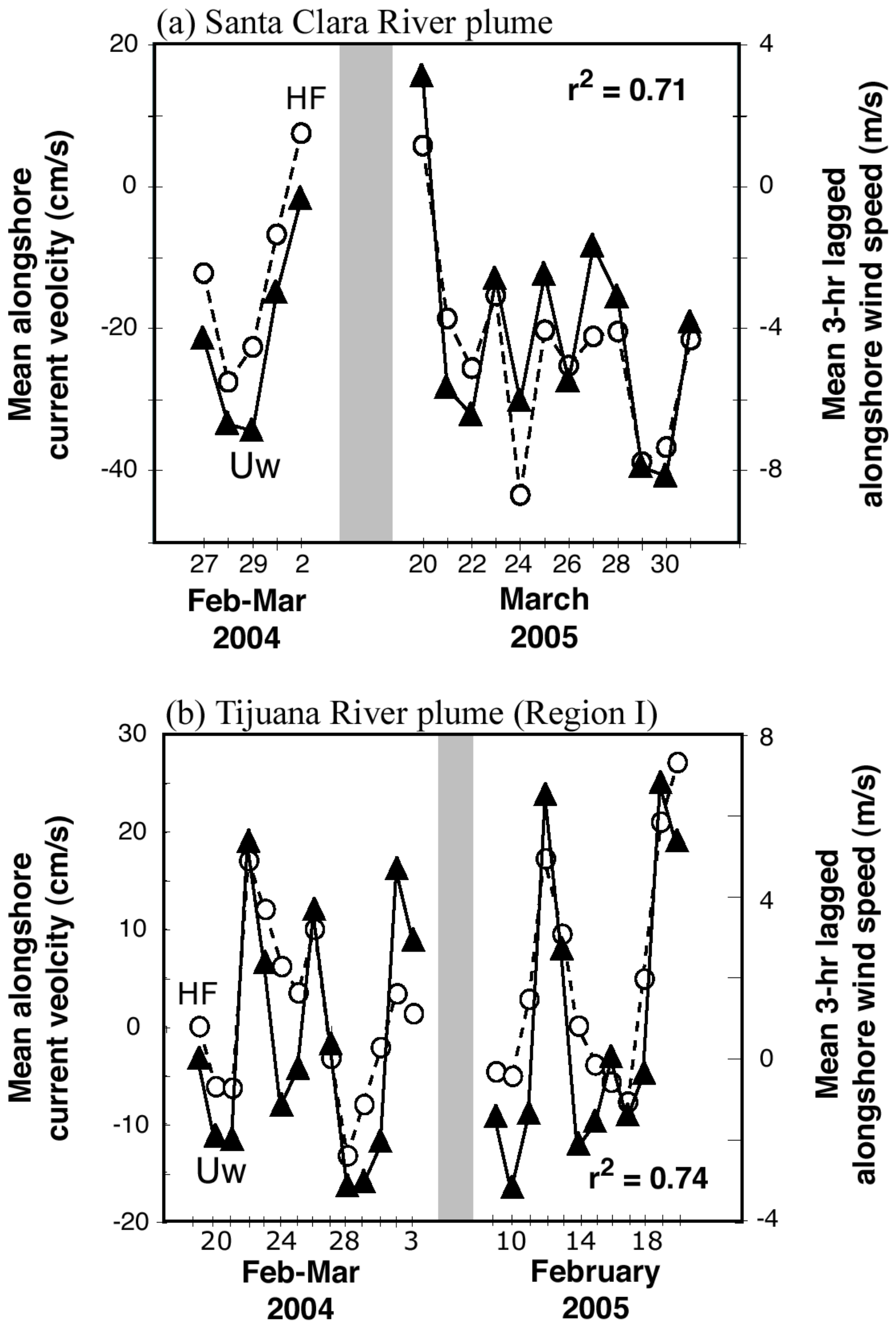

Figure V-13. The relationship between mean daily alongshore wind speed (filled triangles) and mean daily surface currents of river plumes from HF radar (unfilled circles) during sampled events. (a) Santa Clara River plume with 24-hr mean wind stress from the NDBC East Santa Barbara Channel buoy (46053) lagged by a 3-hr preceding period. (b) Tijuana River plume (region I in Figure V-8b) with 24-hr mean wind stress from the NDBC San Clemente Basin buoy (46086) lagged by 3-hr. Correlation coefficients given for the linear regression between currents and winds. Alongshore defined as poleward (positive) and equatorward (negative).

Finally, we computed the wind strain timescale (t_{tilt}), which is defined by the time is takes for Ekman transport to either compress a plume toward the shoreline during downwelling winds or expand a plume offshore by upwelling winds by a scale of 2 (Whitney and Garvine 2005), and can be approximated by:

$$t_{tilt} = (K R h_1 \rho f) / (16 |\tau_{sx}|) \qquad \text{[V-8]}$$

where K is approximately 1 (Warrick *et al.* 2004c), the internal Rossby radius (R) is approximately 10^4, the plume thickness (h_1) is ~3 m, ρ is ~1024 kg m^{-3}, and the alongshore wind stress (τ_{sx}) is calculated with the quadratic drag laws described above. Using equation V-8, t_{tilt} values for wind speeds of 2, 4 and 8 m s^{-1} were computed to be 8, 2 and 0.5 hours, respectively. Thus, for the wind speeds typically observed during and immediately following river discharge events (*cf.* Figures V-13 and V-14), the effect of wind occurs on time-scales much shorter than a day.

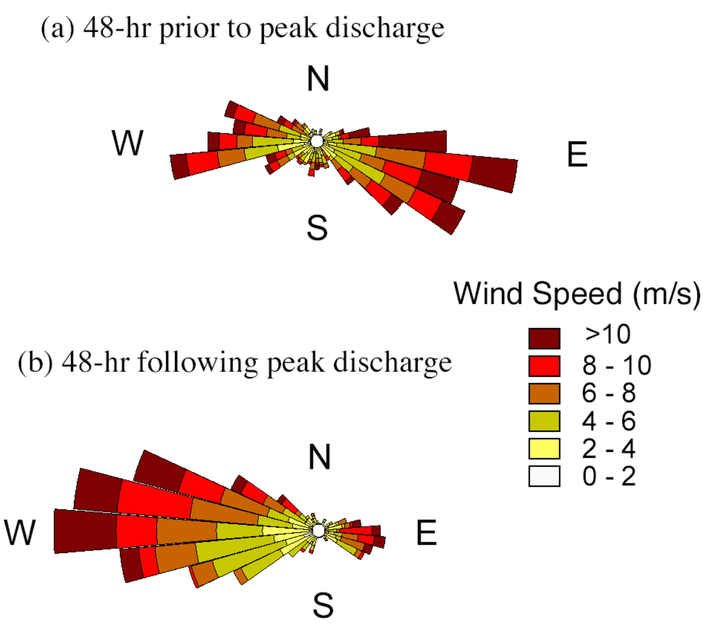

Figure V-14. Wind rosettes from the East Santa Barbara Channel (NDBC 46053) during the 48-hr prior to and following peak discharge in the Santa Clara River from 15-minute discharge data. Wind is oriented to the direction from which the wind originated and was compiled for the 18 events in excess of 25 m^3 s^{-1} during the period overlapping records (1994–2004).

Discussion

Previous studies have established, primarily through the use of satellite imagery, that southern California river plumes are transported far offshore. Our study indicates that alongshore movement of these plumes can be more prevalent than across-shore movement. Mean daily alongshore plume advection, as measured by drifters, HF radar and satellite was as high as 50 cm s^{-1}, suggesting that contaminants discharged from a river system can be quickly transported to coastal waters offshore of adjacent basins. This was especially apparent for the Santa Clara

River plume, which was observed to extend toward Santa Monica Bay during all of our observations.

The plumes were also found to retain their integrity as they advected along the coast. While the salinity signature of the river discharge changed dramatically within the first kilometer of mixing with ocean water (i.e., inshore of our ship measurements), the plumes were clearly distinguishable as a water mass for at least five days following a storm. This distinction was apparent in both lateral and vertical dimensions, extending 10's of km and several meters, respectively. Unfortunately we could not calculate rates of vertical mixing with the CTD+ data, largely because of the strong lateral movements that prevented resampling of water masses.

Although there is widespread consensus that local wind stress explains little of the current variability within the Southern California Bight (e.g., Lentz and Winant 1986, Noble *et al.* 2002, Hickey *et al.* 2003), we found that wind was an important, and often the dominant, forcing function for transport of the river plumes. We note that although wind explained only 66% of the alongshore current variability as measured by the drifters, we did not attempt to remove tidal effects from these data, which would likely improve correlations.

Because winter storms are related to broad atmospheric low-pressure systems moving across southern California, wind patterns are commonly poleward (downwelling) prior to river discharge and equatorward (upwelling) following discharge (Winant and Dorman 1997, Nezlin and Stein 2005). An example of this can be seen in the winds of the Santa Barbara Channel during the 48-hr before and after river discharge events (Figure V-14). During the 48-hr following a discharge event, winds are 4-times more likely to be upwelling (from the west) than downwelling, and ~80% of these winds are greater than 4 m s^{-1}. Post-storm variability in wind stress will be related to broad atmospheric conditions across the eastern Pacific and western North America. The 11-day period of upwelling winds following the March 2005 event (Figure V-13a) was related to a transition to spring conditions of upwelling-dominated wind and appears to be uncommonly long. Post-storm upwelling winds appear to more commonly last only 1 – 5 days following an event.

We note here that wind explained more of the surface current variance immediately offshore of the Tijuana River mouth than for any of the adjacent coastal subregions measured with HF radar (Figure V-15). Hydrographic surveys of this broad region show that freshwater-induced stratification was consistently strongest immediately offshore of the river during the time considered. These combined results are consistent with observations that shallow stratification increases the response of surface currents to wind stress (e.g., Chao 1988, Kourafalou *et al.* 1996). The poor-relationship ($R^2 = 0.36$) in the offshore region was consistent both with lower measured levels of stratification in this region and with the observation by Lentz and Winant (1986) that wind stress becomes less important in the momentum balance with depth on the southern California shelf.

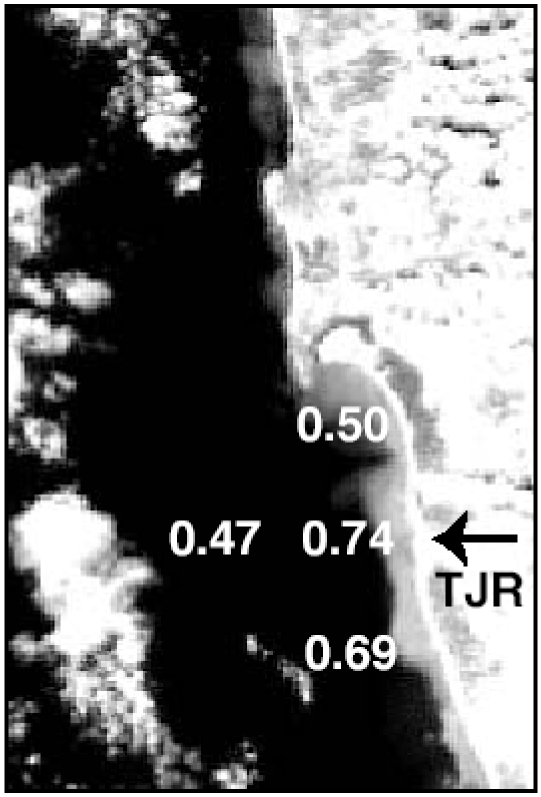

Figure V-15. Maximum correlation coefficient (R^2) for linear regression between lagged mean daily alongshore wind speed at NDBC 46086 and mean daily alongshore HF radar surface currents within the four regions identified in Figure V-8b.

Thus, wind stress explained a majority of the plume transport variance over temporal scales of days. Due to the temporal coherence of winds and river discharge (e.g., Figure V-14), river plumes are commonly observed to flow to the left after leaving the river mouths, which is opposite of the expected direction due to Coriolis (Yankovsky and Chapman 1997). Although wind-dominance is observed in a number of river plume systems throughout the world (e.g., Hickey *et al.* 2005, Pinones *et al.* 2005, Whitney and Garvine 2005), we note that the southern California plumes are distinctive in that the discharge events occur over time scales of hours and the winds are temporally coherent with discharge and have time scales of days. Thus, the upwelling wind-dominance of southern California river plumes is a common condition. Other river plumes have much longer discharge events, which may or may not be coherent with winds, resulting in less regular wind-dominance or alternating direction of wind-dominance (Hickey *et al.* 2005, Pinones *et al.* 2005, Whitney and Garvine 2005).

We fully expect that other factors, such as river discharge inertia, buoyancy-related currents, tidal currents, and non-wind generated subtidal currents, also have significant effects on plume advection within specific scales of space and time. For example, tidal currents were observed in the hourly HF radar data with magnitudes of 5 – 15 cm s-^{1}, and although these currents are important to instantaneous plume advection, they generally induced no net current over daily time scales. Further, we computed values of plume-induced baroclinic velocities of up to 20 – 55 cm s-^{1} (Table V-3), which suggests that initial advection of the plumes from the river mouths was quite rapid in response to this buoyancy. The initial advection was also likely influenced by river discharge inertia from the velocity of the river flux (~50 cm s-^{1}; (cf. Warrick *et al.* 2004c)). The jet-like plume shapes observed by satellite on February 26, 2004 (Figure V-9) likely result from these high initial velocities (cf. Garvine 1995). We calculate that the four visible plume fronts in this image advected ~20 km from the river mouths, which is equivalent to a mean velocity of ~45 cm s-^{1} since the peak discharge of the rivers (cf. Figure III-2). We note that these initial (i.e., 12-hour) velocities appear to be strongly across-shore in direction, which differs from the alongshore-dominated transport measured later during the events. Lastly, geostrophic velocities were computed to be small compared to actual observed velocities and also directed in the opposite direction of the majority of observations. Thus, we suggest that geostrophic flows were generally much weaker than wind-induced flows, which is consistent with calculations of W_s and t_{tilt} above and Santa Monica Bay observations of Washburn *et al*. (2003). Summarizing, plume advection appears to be dominated by river inertia and buoyancy within a few hours and kilometers of the river mouth, while winds dominate plume advection during the following days.

Accurately describing these storm-induced river plumes required a combination of assessment tools. Ships provided the best information, but the rapidity of plume evolution outpaced ship movement while sampling. Even with the large number of ships that were mustered for this study, we found that almost half of the plume water volume occurred outside of the area able to be sampled within the first study day. In addition we found that ships were unable to sample on several of the days most critical to plume evolution, as the high winds that typically follow a storm event led to an unsafe sea state (cf. Nezlin *et al.* 2007).

Satellites provided a valuable synoptic view, but once or twice per day (at best) frequency of the moderate-resolution polar orbiting satellites is temporally insufficient to describe the rapidly evolving plume. Moreover, these images are often obscured by cloud cover (Nezlin *et al.* 2007), further reducing their temporal resolution. High frequency radar provided a continuous synoptic view but only provided surface currents, without definition of plume edge. Drifters provided a Lagrangian perspective of surface currents that could be utilized real-time to track plume advection or in retrospective analyses of current forcing. Although not utilized here, we suggest that autonomous underwater vehicles (AUVs) would fill important information gaps on the movement and mixing of water properties when ships are not able to sail and cloud-cover prevents satellite observations. When combined altogether we found that these techniques provided essential information to track plumes and better understand the transport of watershed-derived pollutants and pathogens in the coastal ocean.

Future identification of discharged river water and its water quality impacts throughout the Southern California Bight will require tracers of the discharged water and pollutants. Although salinity is surely the best plume tracer, it can only be readily measured *in situ* with conductivity/temperature sensors, which limits the timing and locations of observations. Measurements of salinity from remote platforms have great potential and would provide a valuable synoptic overview, but these observations are presently limited to an experimental basis using airborne sensors. Further, it is not clear how well these emerging capabilities will be able to adequately resolve and characterize the small-scale variability and narrow ranges of salinity often observed in these coastal regions. Our results suggest that the optical properties of CDOM may be effectively exploited to track plumes in southern California and could serve as better tracers than suspended sediment or turbidity observations. This is especially relevant for future identification and tracking of plumes with remotely sensed imagery (e.g., Mertes and Warrick 2001, Nezlin *et al.* 2005), and we suggest further investigation of the use of CDOM absorption and other satellite ocean-color derived products to monitor the distribution of plumes and assess their ecological impacts. This is assessed further in the subsequent sections.

Conclusions

The combined use of ship-based sampling and remotely sensed ocean imagery provided new insights into the patterns and dynamics of river plumes offshore of the largest southern California watersheds. Plumes were observed to quickly move from the river mouths and to respond strongly and quickly to winds. The combined measurements clearly show how plume waters were transported to adjacent portions of the Southern California Bight within days of discharge. This suggests that water quality and ecological impacts from outflow of a watershed may be exhibited in portions of the coastal ocean far from this source watershed. Considering that these plumes are important vectors for land-based pollutants, pathogens and nutrients, better understanding is needed of the water quality and ecological implications and impacts of these plumes.

VI. IMPACT OF STORMWATER RUNOFF CONTAMINANTS IN THE SOUTHERN CALIFORNIA BIGHT: RELATIONSHIPS AMONG PLUME CONSTITUENTS

Introduction

The improvement of water quality is a major issue for local, state, and federal agencies. Coastal waters provide numerous beneficial uses including recreation, fishing, marine habitat, navigation, and aesthetic enjoyment. In southern California, approximately $9 billion of the economies of coastal communities comes from ocean-dependent activities. A broad range of chemical and biological contaminants is discharged into coastal waters of the Southern California Bight (SCB) including pesticides, fertilizers, trace metals, synthetic organic compounds, suspended sediments, inorganic nutrients, and human pathogens (National Research Council 1990). Reductions in water quality due to these discharges can greatly affect the beneficial uses of the receiving waters and can affect the local coastal economies.

Flood events due to rain/storm events contribute more than 95% of the total runoff volume annually to the coastal zone. Surface runoff, which receives no treatment prior to discharge into ocean waters, is one of the largest sources of contaminants to the SCB (Schiff *et al.* 2000). Many studies of stormwater runoff conducted in southern California have focused on public health issues such as human pathogens and contaminants (Schiff *et al.* 2002). Beach closures due to high levels of fecal indicator bacteria (FIBs) and other indicators of human pathogens are common during and immediately following rain events (Geesey 1993). Evidence of high levels of toxicity associated with urban runoff, especially stormwater runoff, has also been noted in several southern California watersheds (Bay *et al.* 2003, Gersberg *et al.* 2004). In addition to pathogens, stormwater supplies large amounts of "new" nutrients to coastal areas contributing to coastal productivity and eutrophication. Coastal runoff plumes are buoyant and contain high nutrient concentrations, creating ideal conditions for phytoplankton growth, and these conditions have been correlated with harmful algal blooms (Horner *et al.* 1997, Smayda 1997). Even the high levels of sediment themselves can cause environmental damage through several mechanisms such as smothering of benthic organisms, reduction of visual clarity, irritation of fish gills, and reduction of light available for photosynthesis (Davies-Colley and Smith 2001). Proper management of these parameters is important for restoring and maintaining healthy beaches, marinas, bays, and coastal areas.

Both *in situ* and satellite remote sensing studies of stormwater plumes in the SCB have shown that plumes created from pulses of stormwater runoff can affect large areas, can penetrate up to 10 m into the water column, and can persist for days to weeks (Washburn *et al.* 2003, Nezlin *et al.* 2005). Although the spatial and temporal extents of stormwater plumes have begun to be examined through satellite imagery, the extent of impact from human pathogens, nutrients, and toxicants is not known. Runoff plumes have the potential, however, to disperse these constituents over large distances, especially small particles and dissolved materials that remain in the surface waters.

The California Ocean Plan (COP) defines the current standards required by the state of California for beach monitoring (State Water Resources Control Board 2005). Beach posting is recommended when single FIB samples exceed these standards. The accepted monitoring protocols require collection of water samples that are evaluated for FIBs using assays that require 24 to 48 hours to complete, thus limiting the number of samples that can be practically analyzed. It is impossible to adequately and routinely sample plumes by collecting water samples from a few locations limited by sampling capabilities and resources. Remotely sensed ocean color could be used as a way to track stormwater plumes over large spatial scales with high temporal coverage (e.g., Nezlin and DiGiacomo 2005, Nezlin *et al.* 2005, Nezlin *et al.* 2007). The understanding and accuracy of the information on the fate of contaminants within the plumes is still questionable and is a focus of this study.

Remote sensing studies of stormwater plumes have used reflectance from the nearsurface layer, typically measured as normalized water-leaving radiance in the range of 551–555 nm (nLw551 for MODIS and nLw555 for SeaWiFS), as a tracer of plumes in the coastal area (see Section VII). Remote sensing reflectance at this wavelength is primarily a function of light backscattering from small particles, and is therefore related to turbidity. By analyzing Sea-viewing Wide Field-of-view Sensor (SeaWiFS) imagery, Nezlin and DiGiacomo (2005) concluded that measurements of nLw555 greater than 1.3 mW cm^{-2} μm^{-1} sr^{-1} distinguished stormwater plumes from ambient water on the San Pedro shelf. As turbidity is associated with sediment particles, the majority of which quickly sink from surface waters, turbidity can only be used as a short-term, non-conservative tracer of the particulate components of stormwater plumes. Colored or chromophoric dissolved organic matter (CDOM), defined as the light-absorbing fraction of dissolved organic matter, is a more conservative tracer. CDOM is not subject to sedimentation. Decreases in its concentration occur through the process of photodegradation, a process that takes weeks to months to occur (Vodacek *et al.* 1997, Opsahl and Benner 1998). Rivers constitute a major source of CDOM in the coastal ocean (Siegel *et al.* 2002, Del Castillo 2005). CDOM concentration is therefore useful in tracking freshwater plumes and can be used to assess the impact of river-borne components such as nutrients and pollutants in the coastal ocean (Coble *et al.* 2004). Like turbidity, CDOM can also be estimated from ocean color but is more likely to be associated with the dissolved constituents of the plumes rather than the particulate fractions.

In this section, we address two aspects of the impact of plumes on the continental shelf of the SCB. The first aspect that will be addressed is the magnitude and area of impact of contaminants on the shelves based on ship-based sampling during the Bight '03 study of two rain events (2004 and 2005). The second aspect evaluates the utility of variables that can be derived from remotely sensed ocean color to evaluate the impacts of runoff plumes on the shelves. We will address the correlation between known contaminants and components that can be readily measured from ocean color measurements, to assess and evaluate the extent to which remotely sensed ocean color can be used to infer the magnitude and spatial extent of plume impacts.

Spatial and correlation analyses

Areas of contaminant (FIBs, nutrients, and toxicity) impacts offshore each major river system in the SCB were assessed by contouring concentrations exceeding the COP standards using the Interactive Graphical Ocean Data Systems (IGODS) water quality contouring program. The impacted areas were then measured using the Google Earth area measuring tool. This method provides a conservative estimate of the area impacted by bacteria since the concentrations measured at a given site were extrapolated across up to 4 km. It is not possible to know where on this continuum the bacterial concentrations drop below the recreational standards.

To examine the fate of various contaminants in relation to stormwater plumes, relationships of contaminants to salinity and total suspended solids (TSS) were explored. The contaminants measured include nitrate (NO_3^-), nitrite (NO_2^-), phosphate (PO_4^{3-}), silicate (SiO_4), FIBs (total coliforms, fecal coliforms, and *Enterococcus*), and toxicity (measured as percent fertilization in the sea urchin fertilization assay (US EPA 1995)). For each relationship, regression analyses were first performed on all data. Individual regressions were then performed on data separated by storm event (2004 and 2005), by watershed, and by sampling date within each storm event. Only data from the top 5 m were included as the majority of stormwater is found within this depth (Washburn *et al.* 2003). Stations were separated into watershed groupings based on their proximity to major sources of inflow (Figure III-1; see Appendix B for the latitudes and longitudes of each sampling station). For the three watersheds in the San Pedro Shelf region (Los Angeles/San Gabriel Rivers, Santa Ana River, and Newport Harbor), stations were grouped by examining nearshore salinity data. Note that these watersheds were not analyzed individually in the spatial analyses but were grouped as the San Pedro Shelf. Contaminant data were also examined by grouping the data into salinity and TSS ranges and calculating the summary statistics for each group. Statistical analyses were done using SYSTAT™ v. 11.0 (SSI 2004). Censored box plots and summary statistics of FIB data were created using the NADA package for R (see below).

Approximately 28%, 56%, and 59% of the total coliform, fecal coliform, and *Enterococcus* data, respectively, were recorded as being below one of 3 detection limits (10 and 100 most probable number (MPN)/100 ml for total and fecal coliforms; 10 and 20 MPN/100 ml for *Enterococcus*). An additional 7 total coliform values (approximately 1%) were reported as >80,000 MPN/100 ml. Censored data is defined as data that falls either below the minimum detection level or above the maximum detection range of an analytical method. These data cannot be analyzed using standard statistical methods. Instead, the data were analyzed using the methods of Helsel (2005) through the S-language software package NADA, an add-on package for the R environment for statistical computing (R Development Core Team 2006). These methods can be used to analyze multiple-censored data sets (data sets with multiple detection limits) with up to 80% censored data. The program, however, only supports left-censored data. Therefore, the 7 total coliform data points reported as >80,000 MPN/100 ml were replaced with the value 80,000 MPN/100 ml. Though this will introduce some error, these values represent such a small proportion of the data set that this error is expected to be small. Summary statistics and box plots were done using the censored regression on order statistics (ROS) method (Lee and Helsel 2005). Correlations of large data sets (>40 observations) were done using censored maximum likelihood estimation (MLE). MLE has been shown to perform poorly with small data sets (less than 25 to 50 observations). Therefore, correlations with the small data sets were estimated using Theil-Sen nonparametric regression (Helsel 2005). In NADA, this method calculates Kendalls τ, a nonparametric correlation coefficient similar to R^2, the Akritas-Theil-Sen slope, and the Turnbull estimate of the intercept. Note that values of Kendall's τ will generally be lower than values of the traditional R^2 for linear associations of the same strength (Helsel and Hirsch 2002).

In addition, we explored the relationship between *in situ* tracers of plume water and variables that can be estimated using ocean color data from satellite imagery. The best *in situ* tracer of freshwater plumes is salinity. Since evaporation will have a minimal effect over the time spans of storm events, surface salinity acts as a conservative tracer of freshwater runoff. High concentrations of CDOM are also present in stormwater. Salinity is not currently measured using satellite imagery; however, CDOM concentrations can be assessed using satellite-derived ocean color. We therefore explored the *in situ* relationship between salinity and CDOM to determine whether salinity could ultimately be approximated from CDOM in satellite imagery (Monahan and Pybus 1978, D'Sa *et al.* 2002, Miller and McKee 2004). A second tracer of stormwater plumes is turbidity. Turbidity can be measured *in situ* by measuring the concentration of TSS or with a transmissometer that measures the attenuation of a beam of light at a wavelength of 660 nm (referred to as beam-c). Whereas salinity and CDOM represent the dissolved components of the plume, TSS and beam-c represent the particulate components; the latter can also be estimated from ocean color images as a turbidity assessment. Regression analyses were done using CDOM and beam-c as the independent variables because we ultimately want to predict salinity and TSS from CDOM and beam-c, respectively. Because low salinity water was never sampled in the Santa Clara River watershed, these data were not included in the bulk regressions. All regressions were done using SYSTAT™ v. 11.0 (SSI 2004).

Results

This section will be presented in three parts. The first part presents the results of *in situ* mapping of specific contaminants present in stormwater: FIBs, toxic effects, and nutrients. The spatial area and temporal extent of impacts is evaluated. The second part examines relationships between the contaminants and readily measured water quality parameters that are considered tracers of stormwater plumes. It addresses the question of the extent to which these parameters can be used as a proxy for contaminants of concern. In the third part, the use of remotely sensed ocean color is considered for the evaluation of plume impacts based on the ability to estimate water quality variables from imagery using the proxy relationships to infer spatial and temporal scales of stormwater impacts.

Spatial and Temporal Extents of Impact

The two sets of contaminants for which either a receiving water standard or environmental impact threshold exists are FIBs and toxicity as measured by the sea urchin fertilization test. Tables VI-1 and VI-2 summarize the number of samples and exceedances of these thresholds that occurred for each of the five major river discharges that were studied during the Bight '03 study (Santa Clara River, Ballona Creek, San Pedro Shelf, San Diego River, and Tijuana River). Nutrient distributions are also examined, but regulatory standards do not currently exist for these runoff constituents.

Fecal Indicator Bacteria

Over 2000 water samples were analyzed for FIBs from all surveys and river systems combined. While bacterial exceedances were associated with each of the major river discharges, the overall percentage of samples that exceeded the COP standards was mostly less than 10%. Elevated concentrations of FIBs were found offshore of each of the major river systems following both storm events in 2004 and 2005 (Figures VI-1 and VI-2). In 2004, less than 10% of the samples exceeded the single sample COP standards offshore each of the river systems (Table VI-1). Single sample exceedances tended to be highest during the first day after the storm. Of the three FIBs, the *Enterococcus* threshold was most often exceeded, with high numbers of exceedances in the San Pedro Shelf and Tijuana River areas. The greatest number of samples exceeding the standards occurred offshore of the Tijuana River (10%). During 2005, the total number of exceedances across all river systems increased (14%). However, this was the result of a large increase in exceedances of all FIBs offshore of the Tijuana River where the single sample standard was exceeded in 54% of the samples. During the 2005 storm event, the river discharged at a rate of over 10 $m^3 s^{-1}$ (228 mgd) for nearly 48 hours (Figure III-3). Sampling commenced on March 13th, as the discharge from the Tijuana River was waning. Exceedances offshore of the Santa Clara River, Ballona Creek, and San Pedro Shelf were similar to 2004.

In most cases, the exceedances were constrained to the very nearfield region of the discharge. For instance, following the February 2004 storm, elevated levels of bacteria for Ballona Creek and the Los Angeles River were found only directly in front of the river mouths, but not away from the river mouths (Figure VI-1). The one significant caveat in these results is that the major discharge from these systems occurred early on February 26, but field sampling did not occur until March 1 and February 28, respectively, two to three days after the core discharge event because of adverse conditions immediately following the storm.

Table VI-1. Summary of the number of single sample exceedances for each day for the first (February 2004) and second (February and March 2005) storm events. Day indicates the number of days after each storm (for Storm 1, day 0 occurred on 23 February 2004 for the San Diego and Tijuana Rivers and on 26 February 2004 for the rest of the sampling areas; for Storm 2, day 0 occurred on 12 February 2005 for the Tijuana River and on 22 March 2005 for the rest of the sampling areas). The number of stations sampled during each time period is indicated in parentheses.

	Santa Clara River	Ballona Creek	San Pedro Shelf	San Diego River	Tijuana River	Total
Storm 1 - 2004						
Total Coliform[1]						
Day 1	-	2 (8)	4 (38)	0 (18)	7 (18)	13 (82)
Day 2	-	0 (23)	4 (74)	-	0 (16)	4 (113)
Day 3	0 (18)	-	-	0 (18)	1 (37)	1 (73)
Day 4	-	0 (23)	0 (78)	0 (18)	2 (35)	2 (154)
Fecal Coliform[2]						
Day 1	-	2 (8)	1 (14)	0 (18)	1 (18)	5 (58)
Day 2	-	0 (23)	1 (50)	-	1 (16)	2 (89)
Day 3	1 (18)	-	-	0 (18)	0 (37)	0 (73)
Day 4	-	0 (23)	0 (54)	0 (18)	1 (35)	1 (130)
Enterococcus[3]						
Day 1	-	2 (8)	10 (38)	0 (18)	10 (18)	24 (82)
Day 2	-	3 (23)	6 (74)	-	6 (16)	16 (113)
Day 3	2 (18)	-	-	1 (18)	2 (37)	9 (73)
Day 4	-	0 (23)	2 (78)	5 (18)	2 (35)	2 (154)
TOTAL	3 (54)	9 (162)	28 (498)	6 (162)	33 (318)	79 (1194)
% of samples	5.6%	5.6%	5.6%	3.7%	10%	6.6%
Storm 2 – 2005						
Total Coliform[1]						
Day 1	-	3 (10)	0 (26)	-	16 (18)	19 (54)
Day 2	0 (20)	0 (23)	1 (28)	-	11 (18)	12 (89)
Day 3	0 (20)	0 (23)	0 (80)	-	4 (18)	4 (141)
Day 4	0 (20)	-	-	-	-	0 (20)
Fecal Coliform[2]						
Day 1	-	3 (10)	-	-	20 (30)	23 (40)
Day 2	0 (20)	0 (23)	0 (28)	-	16 (30)	16 (101)
Day 3	0 (20)	0 (23)	0 (54)	-	1 (18)	1 (115)
Day 4	0 (20)	-	-	-	-	0 (20)
Enterococcus[3]						
Day 1	-	3 (10)	3 (26)	-	21 (30)	27 (66)
Day 2	0 (20)	0 (23)	0 (28)	-	14 (30)	14 (101)
Day 3	1 (20)	0 (23)	1 (80)	-	11 (18)	13 (141)
Day 4	1 (20)	-	-	-	-	1 (20)
TOTAL	2 (180)	9 (168)	5 (350)	-	114 (210)	130 (908)
% of samples	1.1%	5.4%	1.4%	-	54%	14%

[1]Total coliform REC 1 standards = single sample 10,000
[2]Fecal coliform REC 1 standards = single sample 400
[3]*Enterococcus* REC 1 standards = single sample 104

Table VI-2. Summary of toxicity (% of fertilization) evaluations for each of the sampling regions for both storm events.

	Santa Clara River			Ballona Creek			San Pedro Shelf			San Diego			Tijuana River		
	>84%	84=x=50%	<50%	>84%	84=x=50%	<50%	>84%	84=x=50%	<50%	>84%	84=x=50%	<50%	>84%	84=x=50%	<50%
Storm 1-2004															
Day 1	-	-	-	8	0	0	37	1	0	15	2	1	5	13	0
Day 2	-	-	-	22	1	0	72	2	1	-	-	-	-	-	-
Day 3	18	0	0	-	-	-	-	-	-	18	0	0	18	0	0
Day 4	-	-	-	21	2	0	74	4	0	18	0	0	17	1	0
TOTAL	18	0	0	51	3	0	183	7	1	51	2	1	40	14	0
% of samples	100	0	0	94	6	0	96	4	1	94	4	2	74	26	0
n =		18			54			191			54			54	
Storm 2 - 2005															
Day 1	-	-	-	11	0	0	52	2	0	-	-	-	18	0	0
Day 2	20	0	0	23	0	0	28	0	0	-	-	-	18	0	0
Day 3	20	0	0	23	0	0	80	0	0	-	-	-	18	0	0
Day 4	20	0	0	-	-	-	-	-	-	-	-	-	-	-	-
TOTAL	60	0	0	57	0	0	160	2	0	-	-	-	54	0	0
% of samples	100	0	0	100	0	0	99	1	0	-	-	-	100	0	0
n =		60			57			162			-			54	

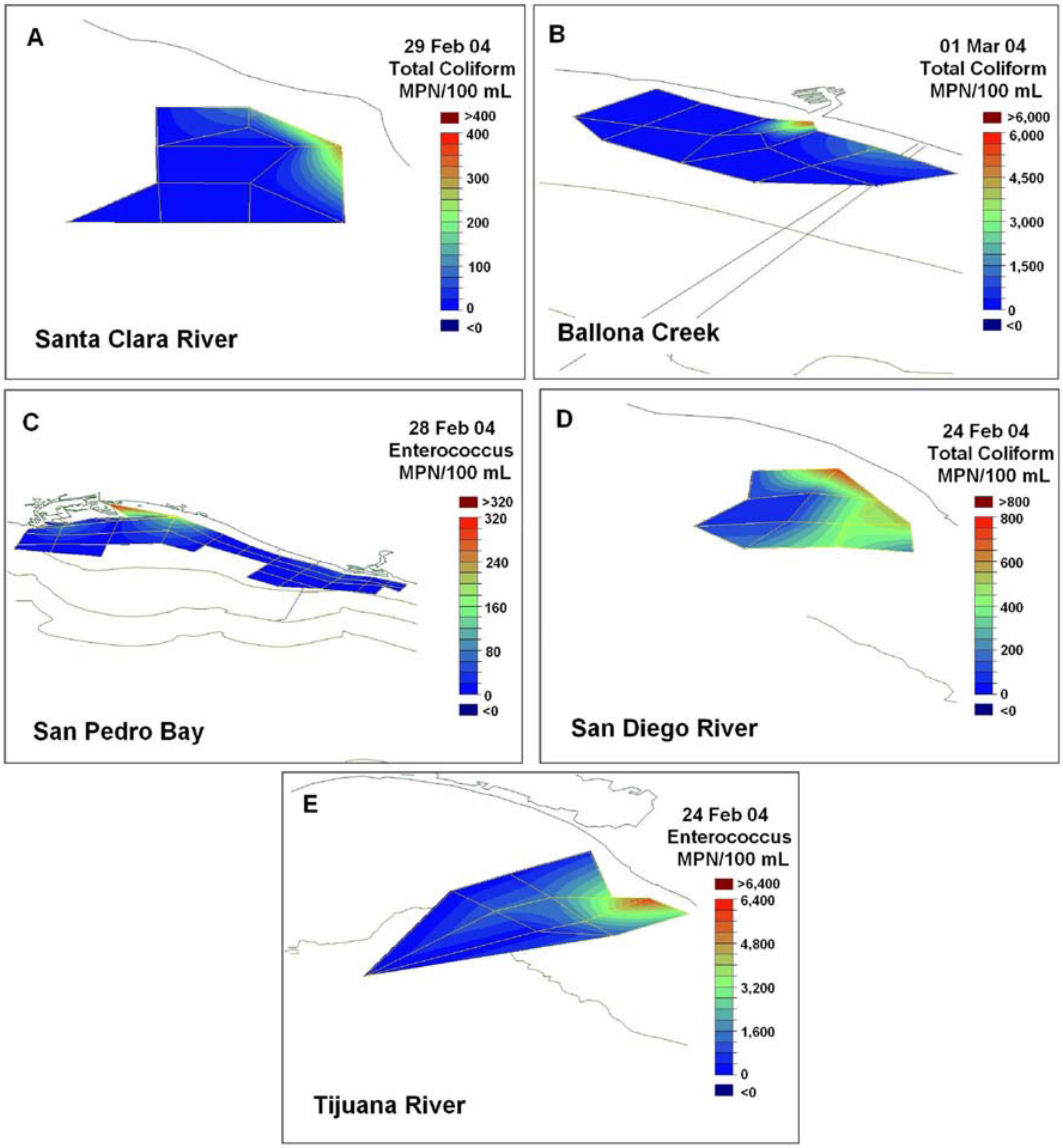

Figure VI-1. Surface distributions of FIBs showing elevated concentrations for each of the five major watersheds following the February 2004 storms. The maps are for one of the FIBs for A) Santa Clara River – total coliforms, B) Ballona Creek – total coliforms, C) San Pedro Bay – *Enterococcus,* D) San Diego River – total coliforms, and E) Tijuana River – *Enterococcus.* Note that the color scales have different ranges for each plot.

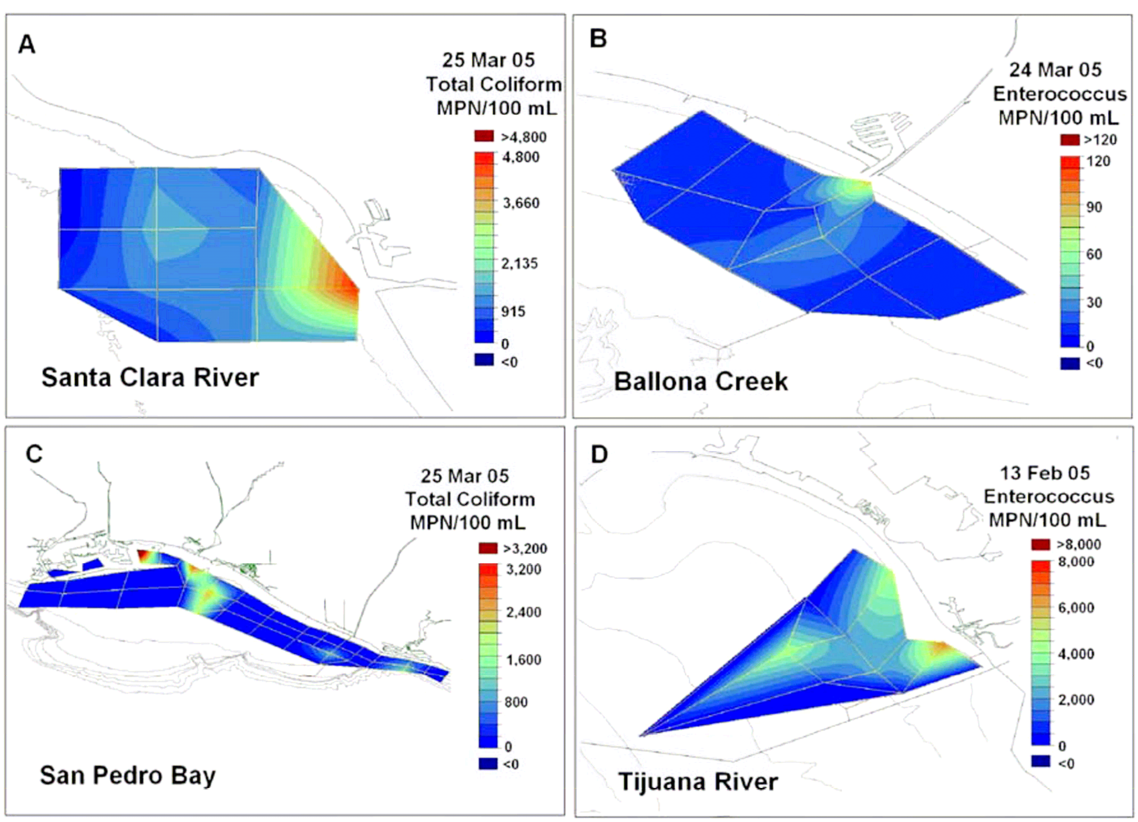

Figure VI-2. Surface distributions of FIBs showing elevated concentrations for each of the four major watersheds following the February 2005 storms. The maps are for one of the FIBs for A) Santa Clara River – total coliforms, B) Ballona Creek – *Enterococcus,* C) San Pedro Bay – total coliforms, and D) Tijuana River – *Enterococcus*. Note that the color scales have different ranges for each plot.

To assess the surface area impacted by FIBs offshore of each river system, bacteria concentrations were contoured onto maps where concentrations exceeding the single sample standard could be easily delineated. The effected spatial area, as well as the area of the sampling grid, was then measured. Summaries of affected spatial areas for the 2004 and 2005 events are shown in Figures VI-3 and VI-4, respectively. Note that each histogram bar height represents the total area sampled for each day during the survey. These figures should be treated with caution, because sampling areas differed due to sea state conditions and the ability of the ship crews to collect samples. Also, the areas sampled for each river system were different and depended on sampling resources and the time required to return the bacteria samples to the laboratory to meet holding time requirements.

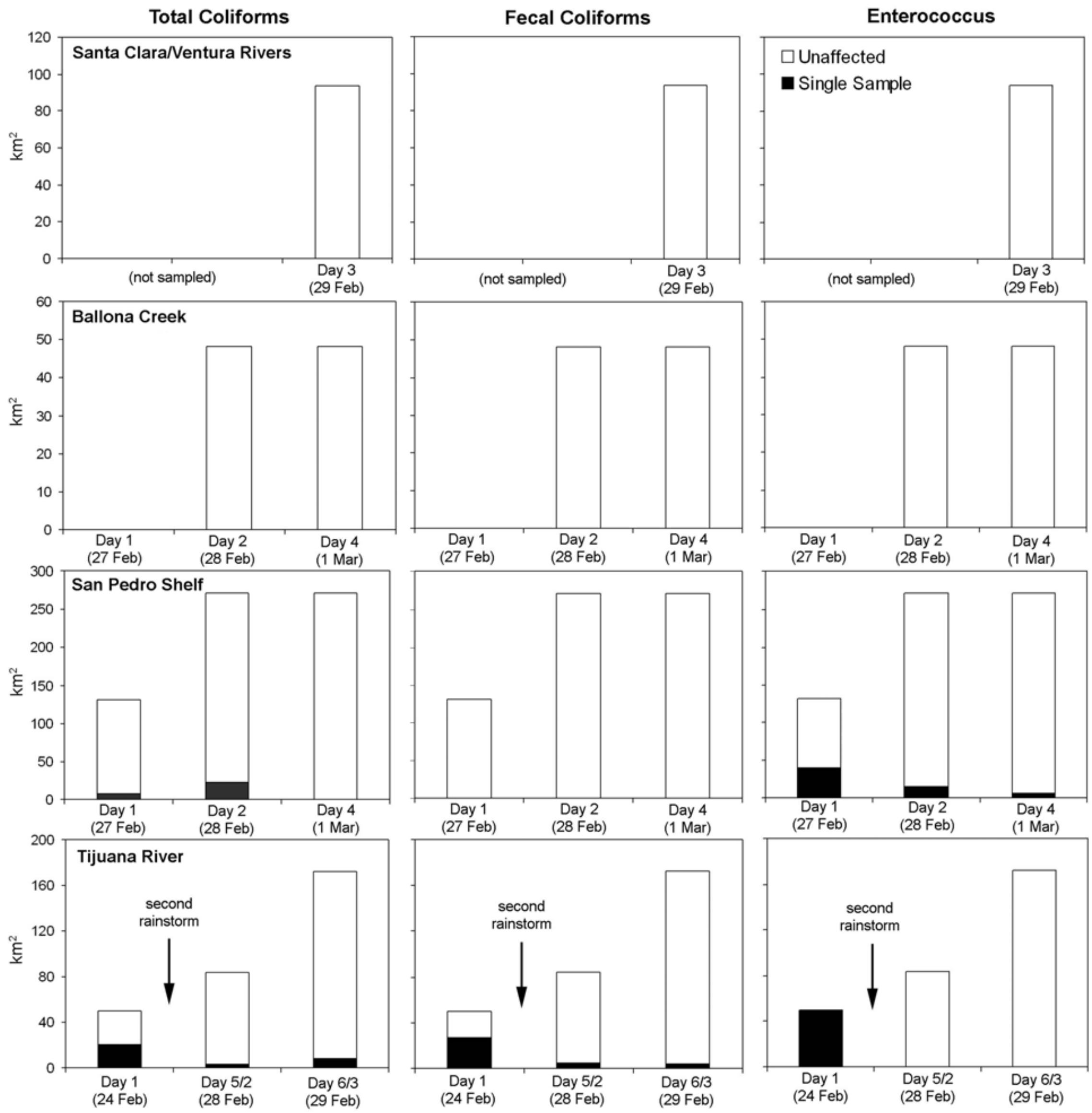

Figure VI-3. Summary bar chart of spatial impacts of the three fecal indicator bacteria groups for the February 2004 storm event. The white portion of the bars indicates the areas that did not exceed the California Ocean Plan single-day standards, and black indicates the area that exceeded the single day standards for each of the indicator bacteria. Day indicates the number of days after each storm (day 0 occurred on 23 February for the San Diego and Tijuana Rivers and on 26 February for the rest of the sampling areas). Note that a second rainstorm occurred in the Tijuana River region during the sampling period.

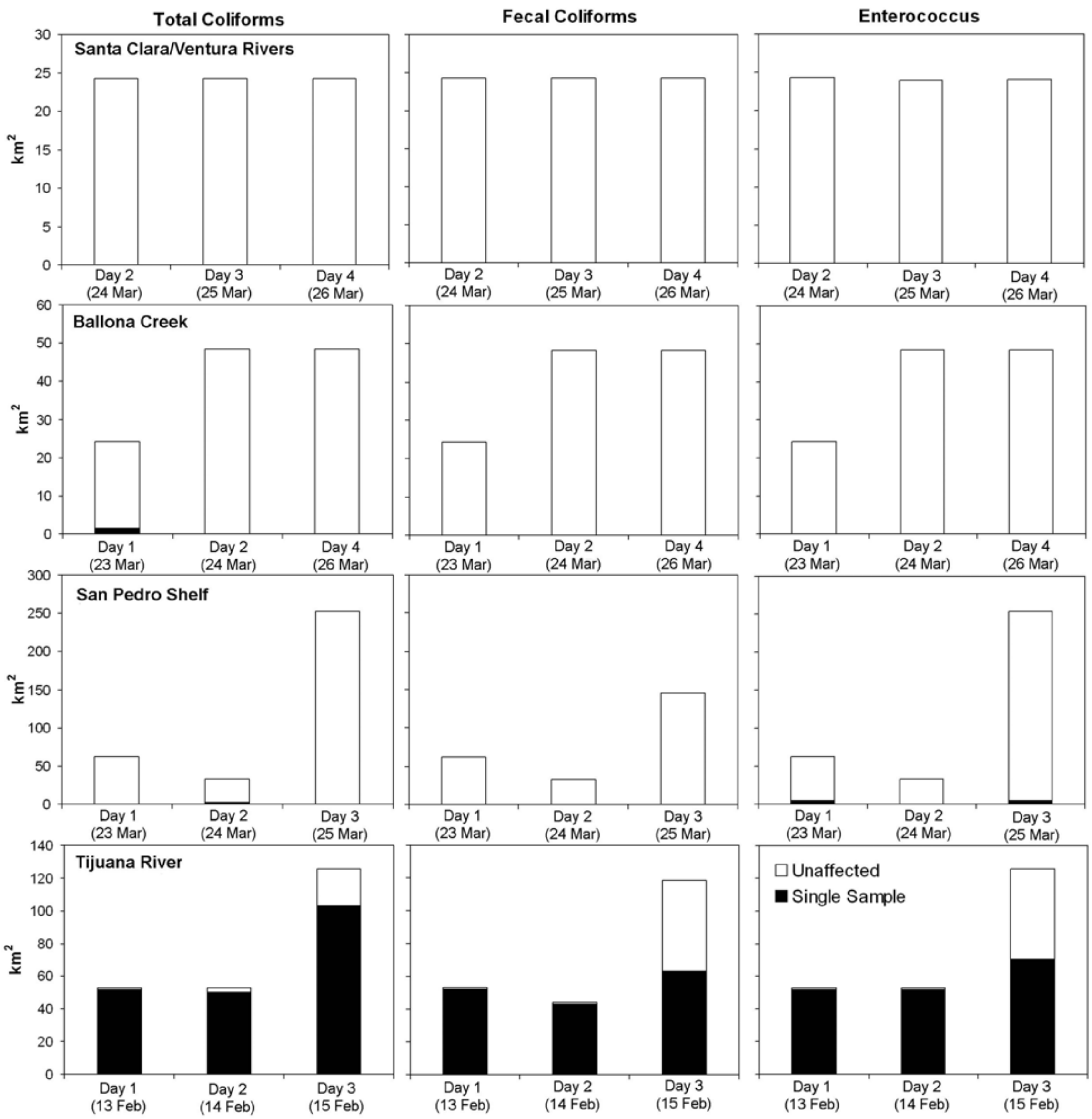

Figure VI-4. Summary bar chart of spatial impacts of the three fecal indicator bacteria groups for the February-March 2005 storm event. Day indicates the number of days after each storm (day 0 occurred on 12 February for the San Diego and Tijuana Rivers and on 22 March for the rest of the sampling areas).

The areas of exceedance for the Santa Clara River and Ballona Creek were relatively small. During both storms, no part of the sampled area from the Santa Clara region exceeded the single-day standard. In 2004, the first day of sampling offshore of the Santa Clara River occurred three days after the discharge event (Figure III-2). It is conceivable that by the time of sampling, the plume had advected away from the river mouth (*c.f.* Section V). Ballona Creek showed a similar pattern with no exceedances in 2004 and a relatively small area of exceedance (<25 km^2) in 2005. In 2004, Ballona Creek was not sampled until the second day after the storm.

The two systems that showed the largest areas of impact were the San Pedro Bay region and the Tijuana River plume just north of the Mexican border. The area of impact for San Pedro Bay rose to a maximum of about 50 km^2 during the 2004 sampling event for total coliforms and *Enterococcus*. The area of impact was much smaller in 2005 (up to 5 km^2). No samples collected in this region exceeded the single-day sample criterion for fecal coliforms. The Tijuana River plume impact for all three indicators reached 96 km^2 in 2004 and 237 km^2 in 2005. The fact that in both 2004 and 2005, nearly the entire sampled area exceeded the single sample standard on at least one day for each FIB group shows that the sampling area was not large enough to encompass the entire affected area.

The temporal evolution of the impacted areas is also demonstrated in Figures VI-3 and VI-4. In all but one of the cases, the areal extent of FIB impact was greatly reduced or absent by the third or fourth day of sampling. The one exception is the Tijuana River plume in February 2005, when high concentrations of each of the FIBs persisted through the entire survey (Figure VI-4). Note that the areal increase on the third sampling day was the result of an increased sampling area, not necessarily an increased plume impact area. The Tijuana River does not have a large flow volume compared to the Los Angeles or San Gabriel River systems (Figures III-2 through III-3), with a discharge rate of 5–10 $m^3 s^{-1}$ (114–228 mgd). This implies that FIBs in the Tijuana River are highly concentrated and are not rapidly diluted or advected from the region in the three days following the storm.

<u>*Nutrients*</u>

Nutrient distributions were also measured in the surface layer during each of the storm samplings (Figures VI-5 and VI-6). We have displayed only nitrate in these plots because it is generally representative of the trends in all of the nutrients. In late February 2004, the highest nutrient concentrations were typically found near the river mouths (Figure VI-5), consistent with the distribution of bacteria (Figure VI-1). Maximal nitrate concentrations (~40 micromolar [µM], 1 µM NO_3 = 2.48 mg NO_3 L^{-1}) were found in Los Angeles/Long Beach Harbor at the mouth of the Los Angeles River. Concentrations of 10–15 µM were also observed off the mouths of Ballona Creek and the Santa Clara River. In the San Diego region concentrations were elevated, but were less than 10 µM.

The temporal response of the systems showed both spreading and decreased concentrations with time following a discharge event (Figure VI-6). Figure VI-6 shows two systems, Ballona Creek and San Pedro Bay offshore of Orange County from late March 2005.

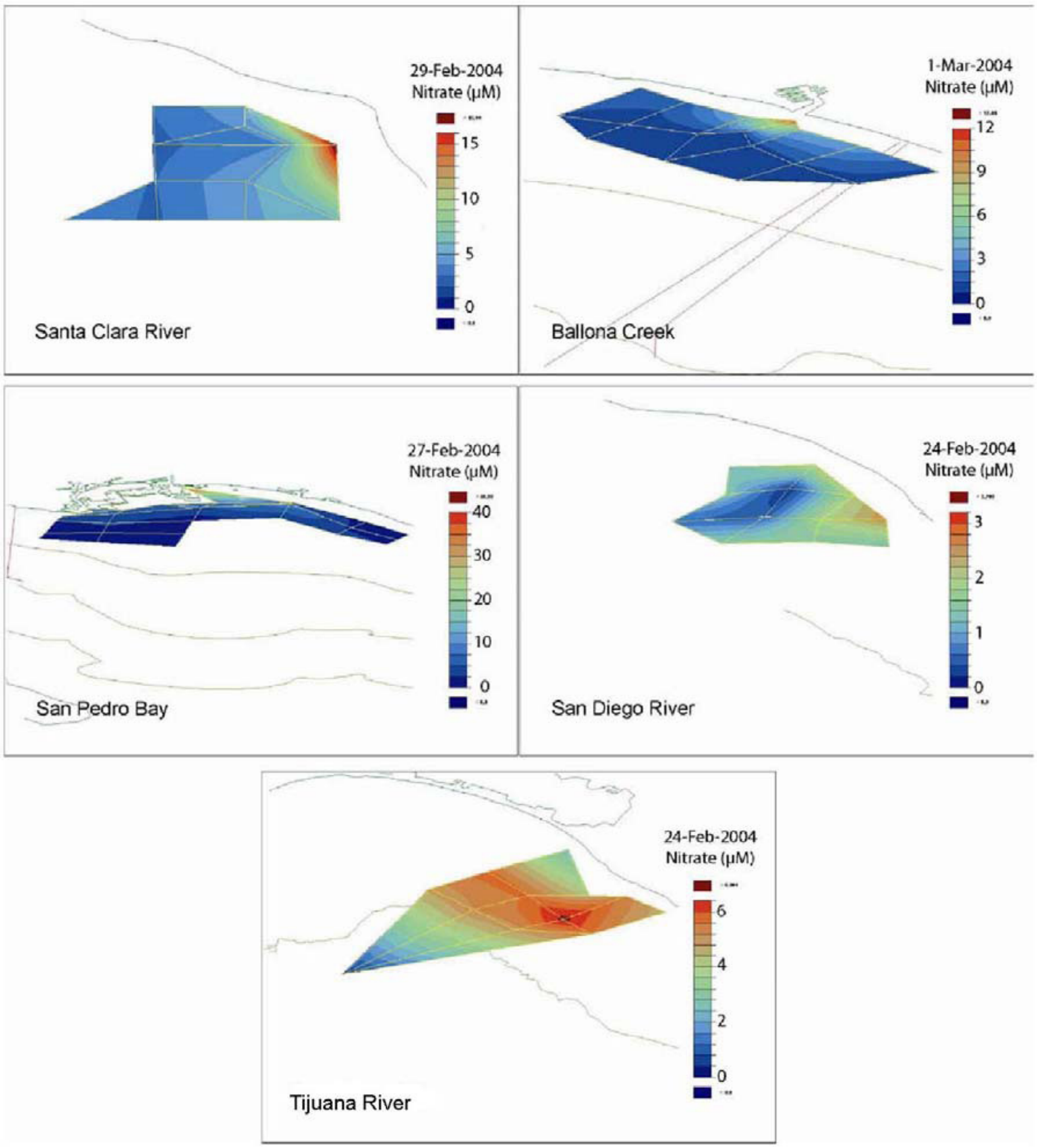

Figure VI-5. Surface distributions of nitrate for each of the five major watersheds sampled following the February 2004 storm event. Note that the color scales have different ranges for each plot.

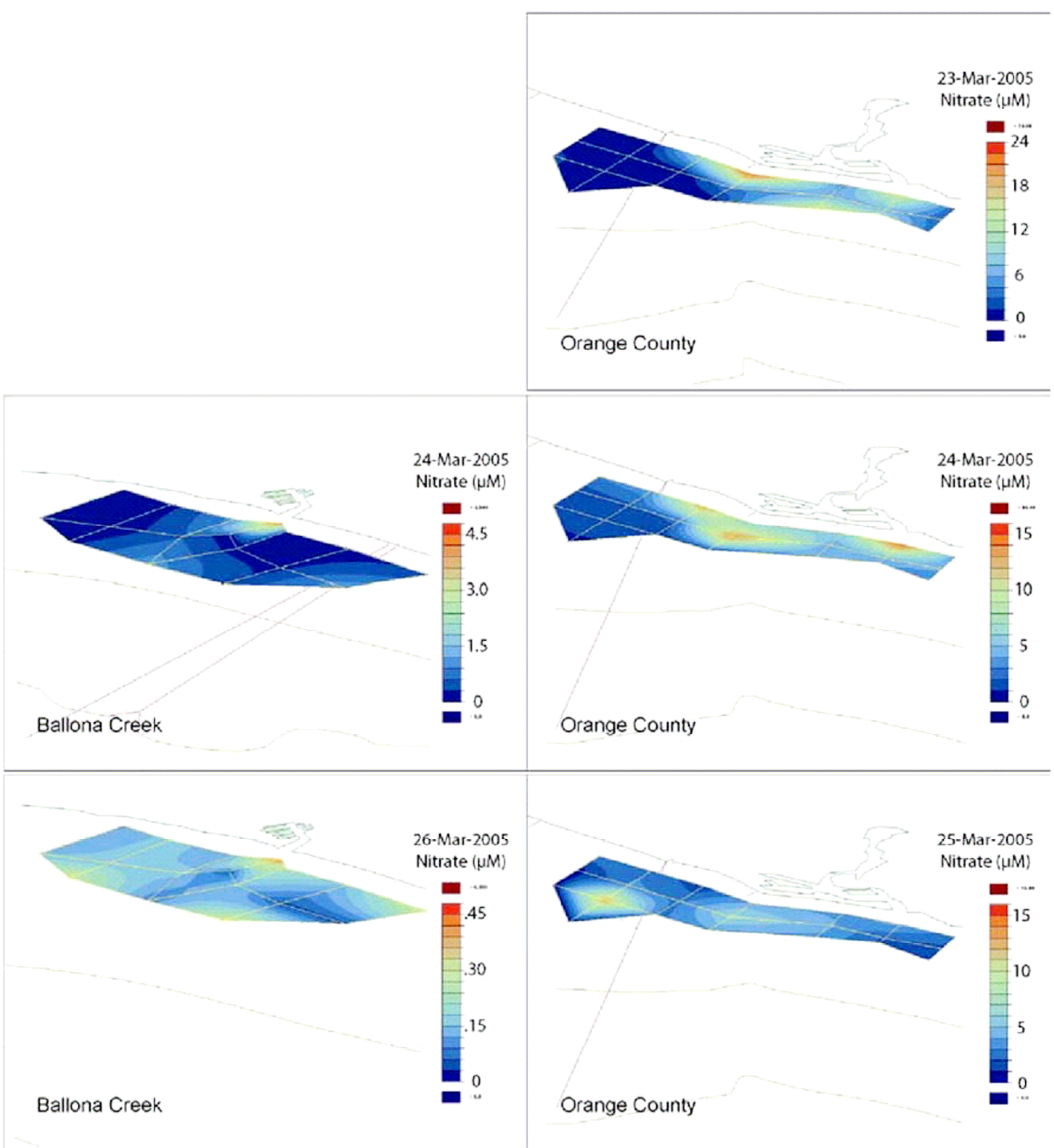

Figure VI-6. Surface maps of nitrate for Ballona Creek and Orange County (including the Santa Ana River and Newport Harbor) for the March 2005 storm. Both regions were sampled on multiple days. These maps provide an indication of the temporal evolution of the nitrate distribution for their respective regions. Note that the color scales have different ranges for each plot.

Toxicity

Of the over 700 water samples that were analyzed for toxicity by sea urchin fertilization from all surveys and river systems combined, very few exhibited toxicity (Table VI-2). Significant toxicity was chosen to be those values where sea urchin fertilization success is less than 84% (Bay *et al.* 2003). Only 41 samples exhibited toxicity considered to be of environmental significance (< 84% fertilization) and even fewer (3) exhibited highly toxic effects (<50% fertilization). The greatest number of toxic samples was observed in the Tijuana River plume on the first day of sampling during the February 2004 event when the fertilization rate for 13 out of 18 samples (72%) was less than 84%. In contrast, during February 2005 when high bacteria concentrations were observed in the Tijuana River plume, no toxicity values less than 84% fertilization were observed in the plume.

Vertical Distributions

The vertical distributions of salinity, FIBs, nutrients, and toxicity (shown as percent fertilization) conform to the expected patterns of a buoyant runoff plume (Figures VI-7–VI-8). The significant pattern in these profiles is that the stormwater plumes in these events were confined to the upper 5–10 m of the water column, consistent with the distributions described by Washburn *et al*. (2003). Nearly all of the FIB samples that exceeded the single sample limit occurred in the top 10 m of the water column during both years. This was also the case for toxicity, where sea urchin fertilization <85% only occurred above 10 m depth. We should note, however, that sampling was sometimes limited to the upper 10 m of the water column, and only a small proportion of discrete water samples came from deeper than 10 m.

In 2004, the maximum near-surface nutrient concentrations were significantly greater than in 2005. For example the maximum measured nitrate in 2004 was >53 μM, but in 2005 the maximum was about 22 μM. The high concentration in 2004 was found at the mouth of the Los Angeles River. Storm sampling in 2004 occurred one month earlier than in 2005. It is possible that many watersheds had been flushed out prior to sampling in 2005 resulting in an overall decrease in nutrient loading from that storm. Another apparent difference between the two years is the higher concentrations of nutrients below 10 meters in 2005. It is likely that these higher concentrations may be due to upwelling occurring along the coast. Upwelling typically begins to occur along the southern California coast in mid to late March.

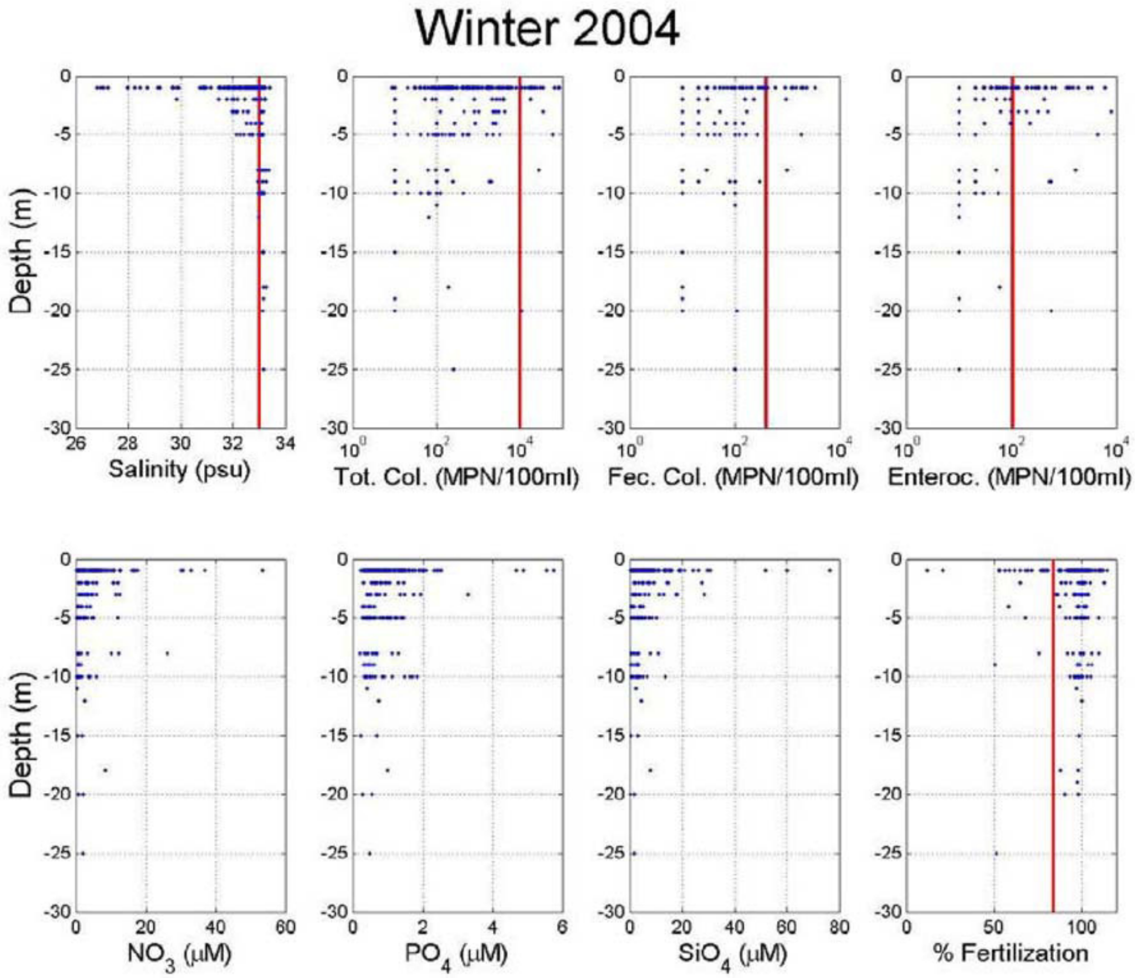

Figure VI-7. Vertical profiles of salinity and contaminants for the 2004 storm. These plots include data from all stations sampled. In the salinity plot, the red line indicates a salinity of 33 psu, a nominal threshold below which is indicative of measurable levels of freshwater. The red lines in the bacteria plots indicate the single standard thresholds from the California Ocean Plan (total coliforms – 10,000 MPN/100 ml; fecal coliforms – 400 MPN/100 ml; *Enterococcus* – 104 MPN/100 ml). The red line in the percent fertilization plot indicates 84% fertilization. No standards currently exist for nutrient concentrations.

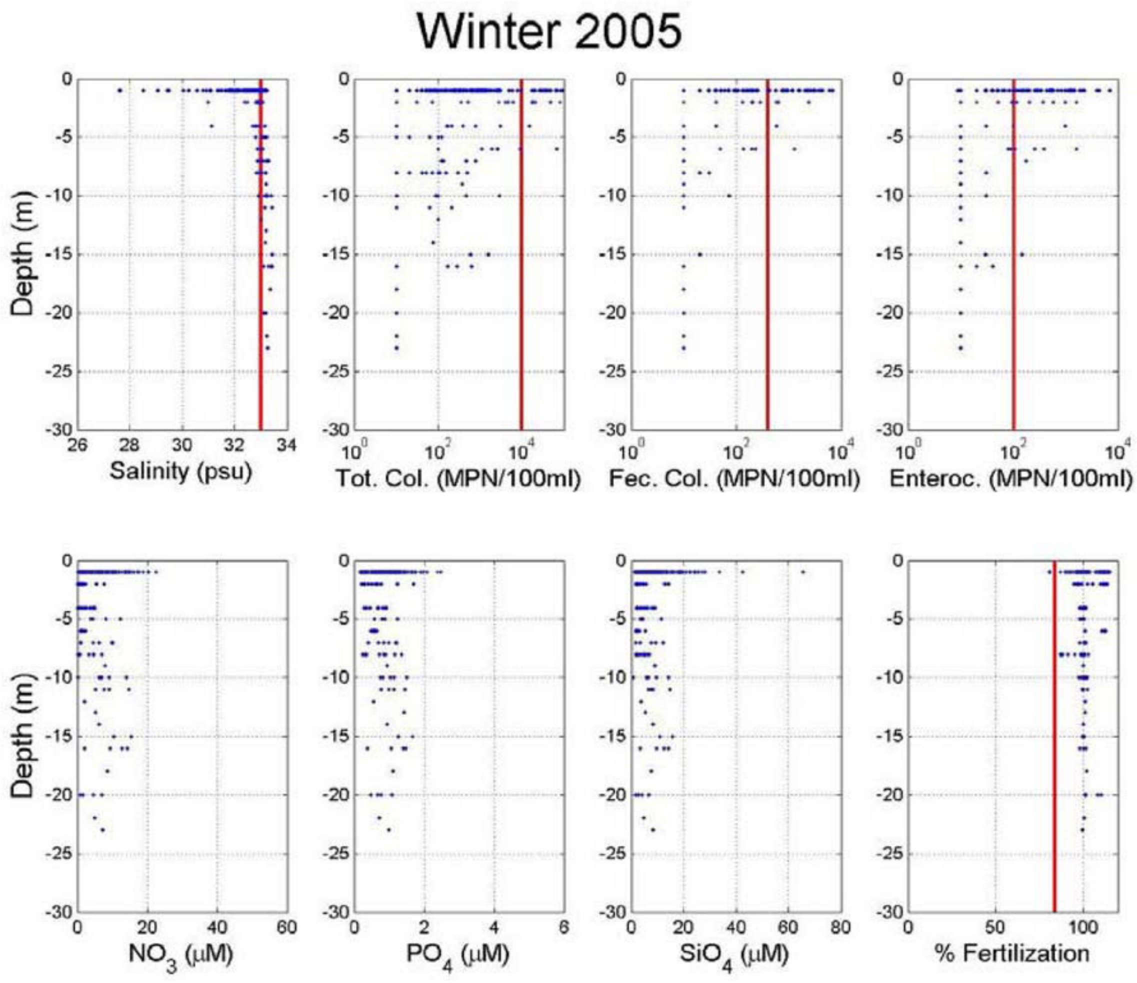

Figure VI-8. Vertical profiles of salinity and contaminants for the 2005 storm. These plots include data from all stations sampled. In the salinity plot, the red line indicates a salinity of 33 psu, a nominal threshold below which is indicative of measurable levels of freshwater. The red lines in the bacteria plots indicate the single standard thresholds from the California Ocean Plan (total coliforms – 10,000 MPN/100 ml; fecal coliforms – 400 MPN/100 ml; *Enterococcus* – 104 MPN/100 ml). The red line in the percent fertilization plot indicates 84% fertilization. No standards currently exist for nutrient concentrations.

In situ contaminant relationships with salinity and TSS

As a first step in understanding the relationships between the freshwater plumes and the contaminant variables, the relationships of the contaminants with salinity, an indicator of the dissolved components of the plume, and TSS, the mass concentration of suspended particulate material, were evaluated. Linear regressions of nutrients and salinity were variable but generally showed negative relationships, i.e., increasing nutrient concentrations with decreasing salinity. For example, two nitrate vs. salinity relationships within the Ballona Creek plume had very different slopes for subsequent sampling days even though both were strong negative relationships (Figure VI-9). The regression for February 28, is nearly identical to the regression that Ragan (2003) obtained for the Ballona plume in December 1996. A total of 33 individual regressions were run corresponding to each sampling date within each watershed. Where the R^2 were greater than 0.5, the median intercept for the nitrate/salinity regression was 96, indicating that a nominal concentration for nitrate in the runoff water for most watersheds is on the order of 100 µM, or ~6.2 mg L^{-1}. A more detailed summary of the individual nutrient/salinity relationships for each watershed and each sampling date are compiled in Appendix C. When all of the nutrient/salinity relationships are considered for the two Bight '03 sampling events, the general conclusion is that nutrient concentrations increase as the fraction of freshwater increases (Figure VI-10 A–D). The largest decrease in all nutrients occurred in the 32–33 psu (<1–4% stormwater) salinity range where median nutrient concentrations were 2–3 times less than in the next higher salinity range (30–32 psu; 4-10% stormwater).

Not surprisingly, the relationships between nutrients and TSS, an index of turbidity, were not as strong as the nutrient vs. salinity relationships. The fact that these relationships are not as strong is expected since nutrients are dissolved components and therefore are expected to be dispersed more like salinity, whereas particulate components will have a sinking component that make them a non-conservative tracer of the plume. When grouped into TSS ranges, however, higher nutrient concentrations did tend to occur at very high concentrations of TSS (>30 mg L^{-1}; Figure VI-10 E-H). See Appendix D for a detailed summary of the individual nutrient/TSS relationships for each watershed and sampling date.

Relationships between salinity and FIBs were also variable but were generally negative. The overall distribution of FIB concentrations vs. salinity is shown in Figure VI-11 A–D. The highest concentrations occurred in the freshest water, but the linear relationships between salinity and FIBs were not strong (see Appendix E for detailed analyses of these relationships). The median FIB concentration dropped below COP standards in the 32–33 psu salinity range (<4% stormwater) for total coliforms and *Enterococcus* and in the 28–30 psu salinity range (<16% stormwater) for fecal coliforms. When salinity values indicated that >10% stormwater was present (<28 psu and 28–30 psu ranges), the standards were often exceeded. FIBs were generally at very low concentrations in water where the salinity was >32–33 psu. Median FIB concentrations in the >33 psu salinity range were 7–16 times lower than those in the next lower salinity range (32–33 psu).

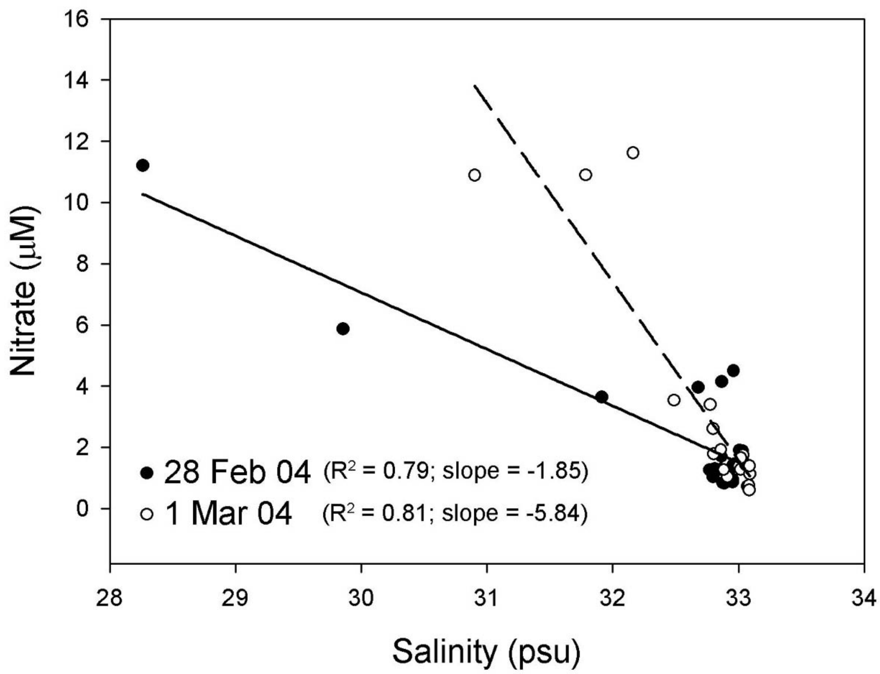

Figure VI-9. Nitrate vs. salinity relationships from the Ballona Creek watershed on two sampling dates following the 2004 storm event.

The relationships between FIBs and TSS were generally positive, but also highly variable. In Figure VI-11 E–H, the bulk relationships indicate that FIBs were characteristically higher in waters with higher TSS loadings (>30 mg L^{-1}) similar to what was observed in the nutrient concentrations. This result is somewhat surprising as we generally find that human pathogenic bacteria are associated with smallest size fractions, not with larger particulate size fractions (i.e., <1 micron, J. Fuhrman, personal communication; (Ahn *et al.* 2005)). At lower TSS concentrations, FIBs were generally below COP standards, and for fecal coliforms and *Enterococcus*, were often below detection limits. Detailed summaries of the FIB/TSS relationships are found in Appendix F.

Toxicity showed no patterns with salinity or with TSS (Figure VI-11). The median percent fertilization was around 100% for all salinity and TSS ranges and never fell below 84%.

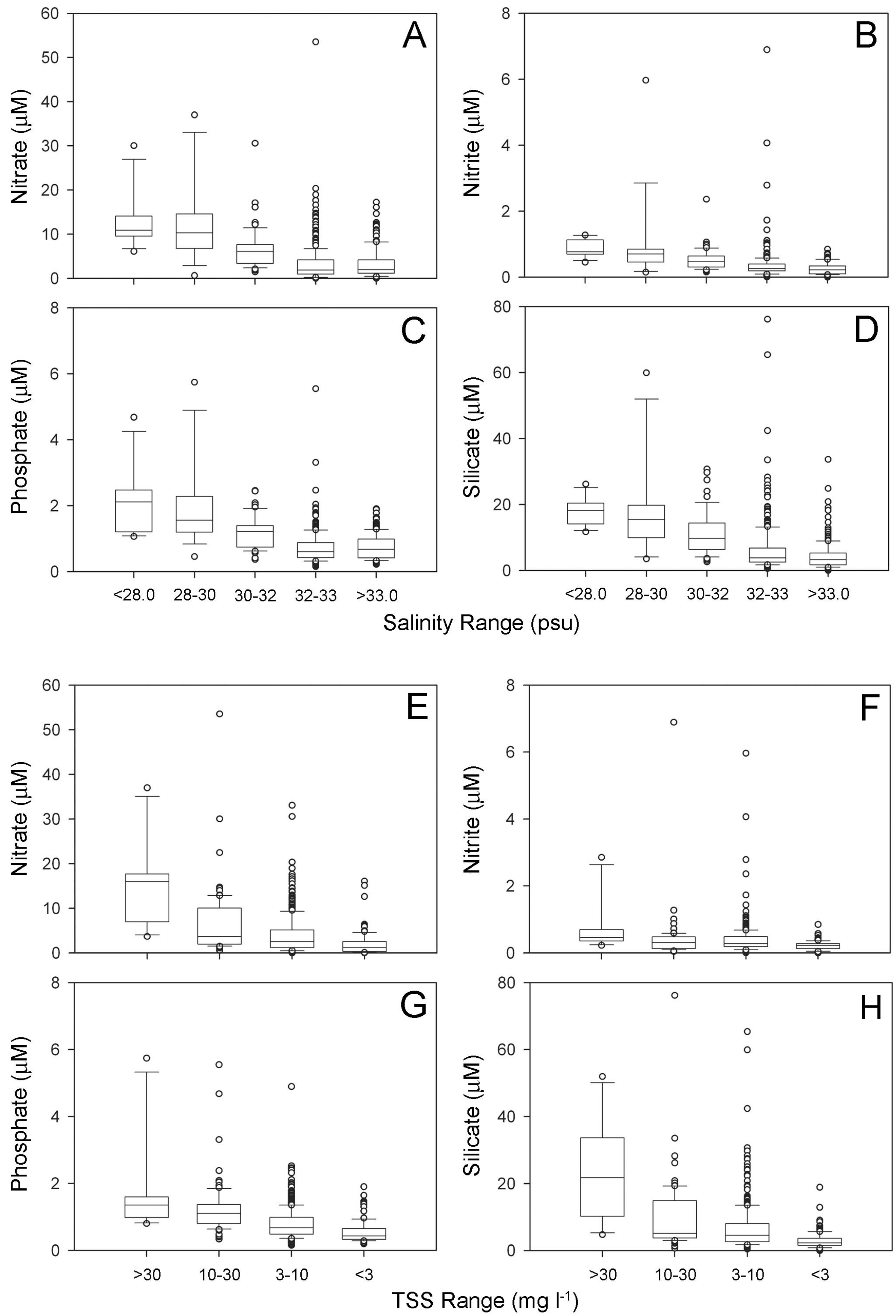

Figure VI-10. Box plots showing the medians and quantiles of nutrient concentrations in five salinity ranges (A–D) and four ranges of total suspended solids (E–H).

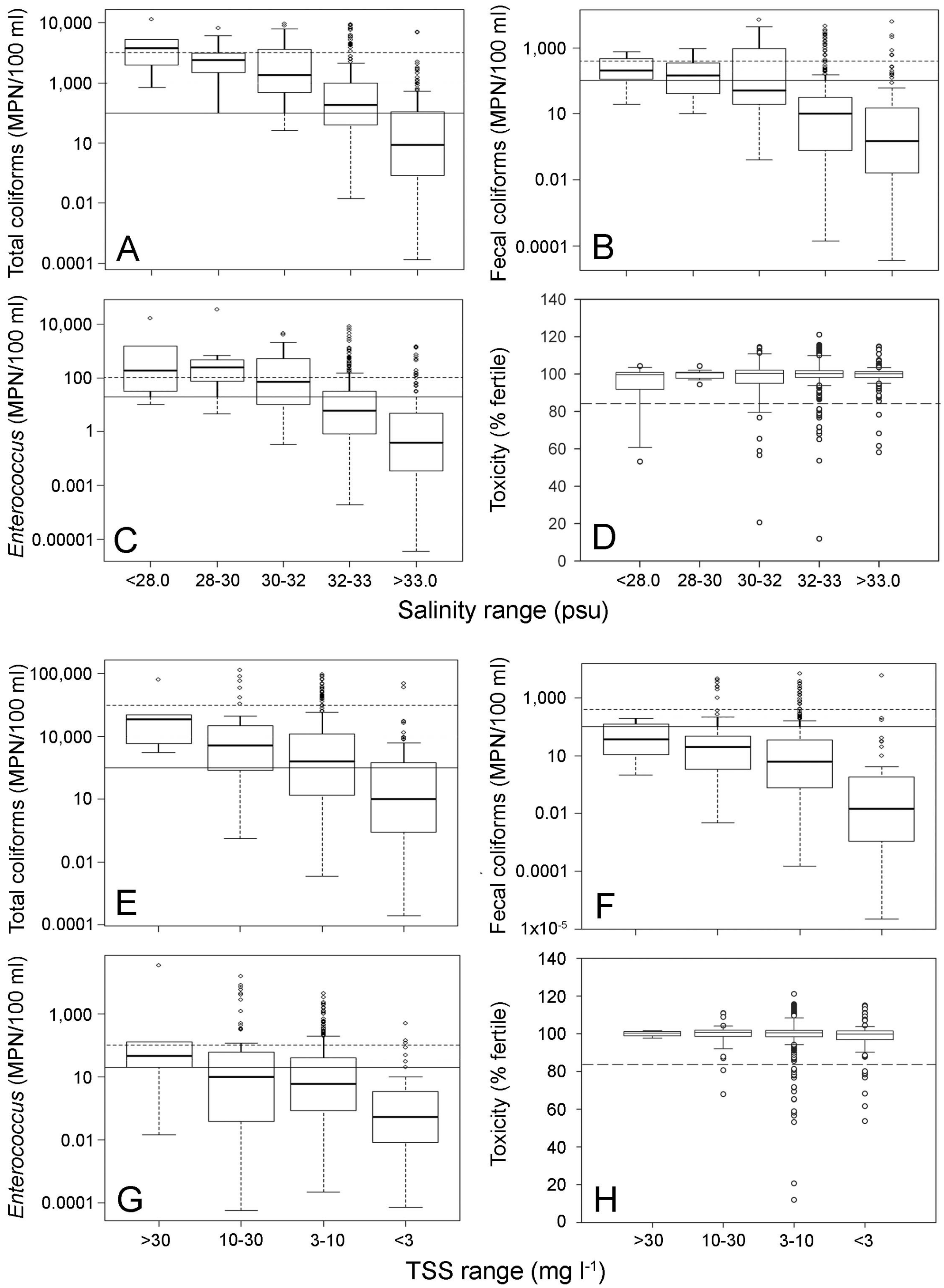

Figure VI-11. Box plots showing the medians and quantiles of concentrations of fecal indicator bacteria and toxicity in five salinity ranges (A–D) and four ranges of total suspended solids (E–H). The solid horizontal lines indicate the maximum detection limit. Below this level, the distributions are approximate (i.e. estimated). The dashed lines indicate the single sample California Ocean Plan standards. The dashed line in the toxicity plots indicates 84% toxicity.

In situ relationships: CDOM vs. salinity and Beam-c vs. TSS

In general, the CDOM vs. salinity relationships were quite good (Figure VI-12). CDOM concentration generally increased linearly with decreasing salinity, or increased freshwater content. Two significant conclusions are apparent in this data. First, when all of the samples from all of the watersheds are lumped together, for the most part, they demonstrate a reasonably consistent relationship that is watershed independent throughout the SCB. The second conclusion is that these relationships are not temporally dependent. The relationships for CDOM vs. salinity were very similar if not indistinguishable between the 2004 and 2005 sampling events (see Appendix G for detailed regression results).

In analyzing the CDOM vs. salinity relationship, a subset of the samples demonstrated increased CDOM fluorescence in the absence of any significant decrease in salinity (Figure VI-12 A). This subset came from three stations in the Los Angeles/San Gabriel River watershed and three stations in the Newport Harbor watershed during the 2004 storm event. These stations are located either just inside or just outside major river mouths. The increases in CDOM fluorescence may have been due to the presence of particles with similar fluorescence properties as CDOM. Chen & Bada (1992) noticed that in samples collected from Scripps Pier (San Diego, California), CDOM fluorescence decreased by about 20% after filtration, a phenomenon not observed in samples collected further offshore. Further research is needed to determine whether particulate fluorescence can interfere with the CDOM fluorescence signal and, if so, when and where this occurs.

The beam-c vs. TSS relationship was also good, although not as strong as the CDOM vs. salinity relationship. The bulk regressions for each storm event are shown in Figure VI-13. In addition, 30 individual regression analyses were run corresponding to each sampling date within each watershed for each storm event (see Appendix F for details of the regression results). In approximately half of these relationships, R^2 was 0.5 or greater, and nine had an R^2 greater than 0.8. The overall relationship was stronger for the 2004 storm event (R^2=0.51 and 0.32 for 2004 and 2005, respectively). A possible explanation of higher TSS/beam-c correlation in 2004 is that the analyzed storm event in 2005 (end of March) occurred one month later than in 2004 (end of February), i.e., at the end of the wet season, when more sediments had already been swept from watersheds by antecedent rain events. For individual regressions with R^2>0.5, the slope ranged between 0.87 and 2.78 with the majority falling below 2.0. The y-intercept for these relationships ranged between -0.43 and 3.15.

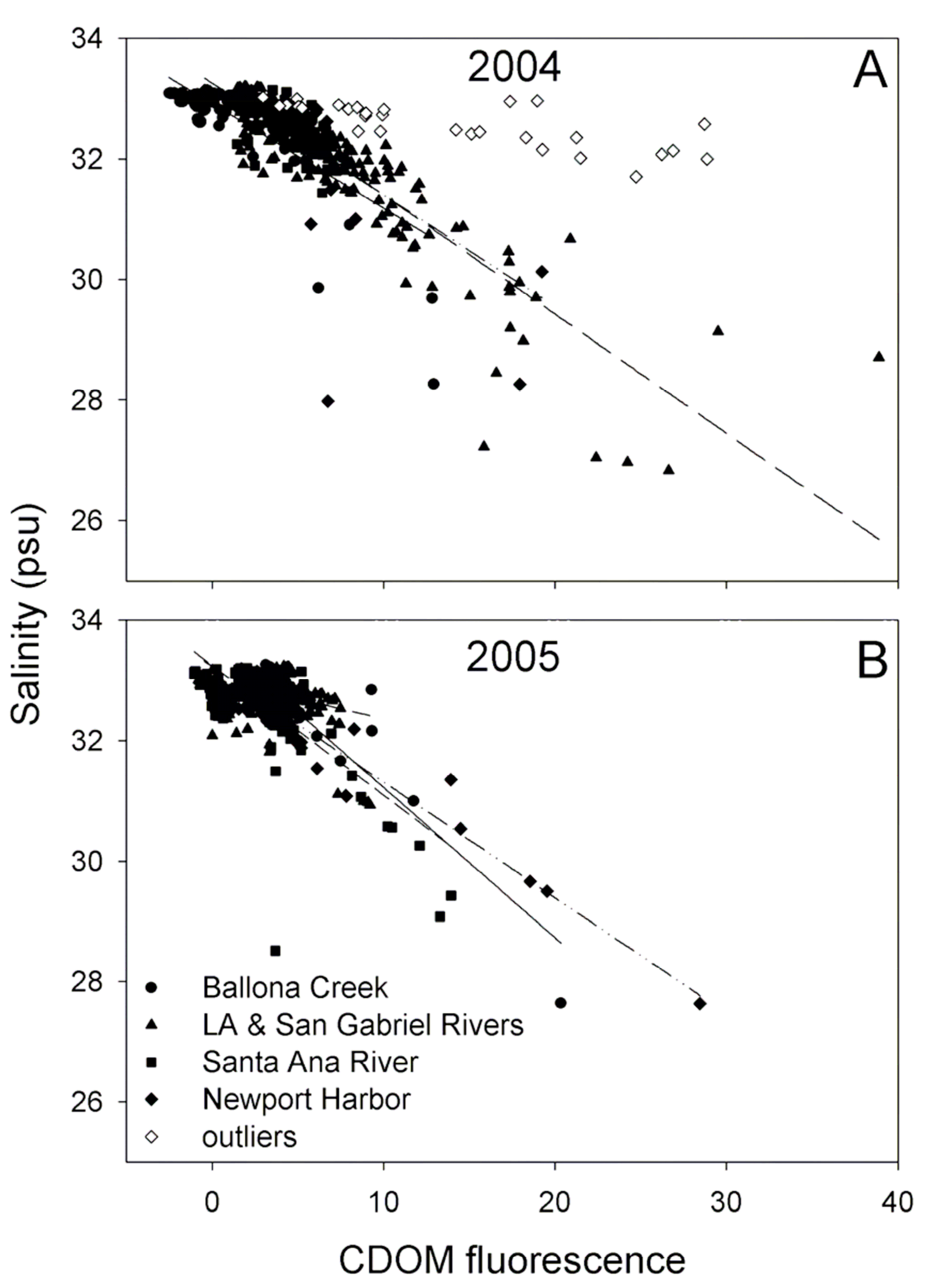

Figure VI-12. CDOM vs. salinity separated by watershed for the 2004 (A) and 2005 (B) storm events. Linear regressions are plotted for Ballona Creek (solid line), Los Angeles/San Gabriel Rivers (long dashed line), Santa Ana River (short dashed line), and Newport Harbor (dot-dashed line).

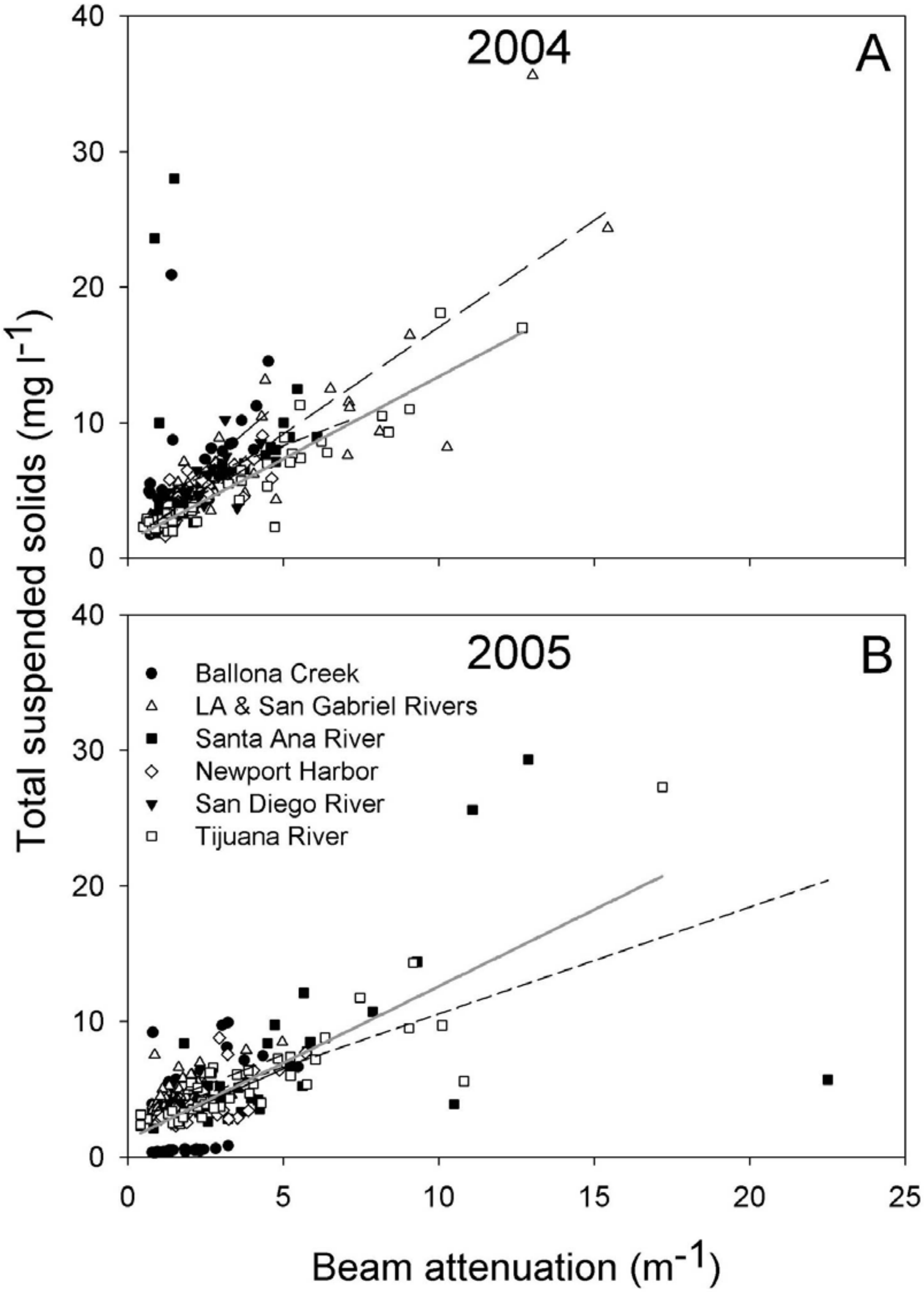

Figure VI-13. Beam attenuation coefficient vs. total suspended particulate matter separated by watershed for the 2004 (A) and 2005 (B) storm events. Linear regressions are plotted for Ballona Creek (solid line), Los Angeles/San Gabriel Rivers (long dashed line), Santa Ana River (short dashed line), and Newport Harbor (dot-dashed line), San Diego River (dotted line), and Tijuana River (thick grey line).

Beam-c and TSS represent two different ways to examine the particulate component of seawater. TSS is a measurement of the concentration, by weight, of particles whereas beam-c is an optical measurement related to the size and concentration of particles. Because of the dependence of light attenuation on particle size, beam-c depends on the geometrical cross-section of particles per unit volume, not necessarily on TSS (Davies-Colley and Smith 2001). Therefore, changes in particle size and composition (i.e., inorganic vs. organic) can result in a change in beam-c without a corresponding change in TSS. The variability in both the strength of the beam-c/TSS relationship and in its parameters is likely due to variability in the characteristics of the particles in the study area, both in space and time. This is not true for salinity and CDOM, which both represent concentrations of dissolved constituents. If runoff is a major source of both CDOM and low-salinity water, we would expect similar changes in the concentrations of both parameters as a result of simple mixing with coastal waters. In theory, salinity and CDOM could be used interchangeably as tracers of the dissolved portion of a runoff plume. Beam-c and TSS, however, are not always interchangeable and actually measure slightly different aspects of the particulate portion of a plume.

Discussion

The *in-situ* measurement of contaminants requires significant effort to both acquire and analyze the samples, limiting the ability to make frequent offshore measurements for FIBs, water column toxicity, and nutrients. The results presented above indicate that impacts from contaminants such as nutrients and FIBs after storm events are generally brief and occur only near the major sources of stormwater. However, important exceptions to this, such as stormwater from the Tijuana River, do occur. Use of ocean color remote sensing provides both spatial synopticity and the ability to build a time series (days) of observations so that the temporal evolution of a given region of the ocean can be examined.

How problematic is stormwater?

The lack of a strong linear relationship between contaminants and *in situ* tracers of stormwater plumes (salinity and TSS) indicates that factors other than simple mixing/dilution are involved in determining spatial and temporal patterns of these parameters. Other sources of nutrients may be present in the coastal ocean, especially in late winter/early spring when upwelling usually commences in the SCB. FIBs cannot survive for long periods of time in the surface ocean, and mortality is increased by exposure to ultraviolet radiation (Fujioka *et al.* 1981, Davies and Evison 1991, Noble *et al.* 2004). Their concentrations, therefore, will depend on the environment to which they have been exposed, not simply on loading and dilution rates. Some studies have found relationships between salinity and various contaminants such as nutrients or toxicity (Bay *et al.* 2003, Ragan 2003); however, others have found no consistent relationship between FIBs and plume tracers similar to what was found in our study (Ahn *et al.* 2005). Concentrations of contaminants seem to be highly variable, especially when the proportion of stormwater is ~1–4% (see Figures VI-10 and VI-11). Although median values of contaminants do show trends with salinity and TSS, this variability masks any linear relationships that might be present. We can, however, determine when and where contaminants are likely to exceed COP standards through quick and easy measurements such as salinity and TSS concentration by using the median values as a guideline.

In past studies of the SCB, high concentrations of FIBs and/or toxicity were found in stormwater itself, near sewage outfalls and stormdrains/river outlets, and at sites very nearshore (e.g. beaches and surfzone areas) (Geesey 1993, Bay *et al.* 2003, Gersberg *et al.* 2004). The few studies that have attempted to examine FIBs in offshore waters have found that they tend to occur in low concentrations but can exceed California standards offshore of major rivers after storm events (ZoBell 1941, Ahn *et al.* 2005). During the Bight '03 project, exceedances of COP standards generally occurred near areas of stormwater discharge during the first day or two after the storm event similar to what was found in these past studies. However, several major exceptions are worth noting.

Waters offshore of the Tijuana River consistently exceeded COP standards for multiple FIBs, and in 2005 the area of exceedance was even larger than what could be mapped based on the fixed sampling grid. Gersberg *et al*. (2004) also found marked increases in toxicity in the Tijuana River during storm events. The Tijuana River, with a discharge rate of 5–10 $m^3 s^{-1}$ (114–228 mgd), does not have a large flow volume compared to the Los Angeles or San Gabriel River systems whose storm discharge rates often exceed 1,000 $m^3 s^{-1}$ (Figures III-2 through III-3). This implies that FIBs in the Tijuana River are highly concentrated and are not rapidly diluted or advected from the region in the three to four days following the storm.

Contrary to prior studies, very few samples collected during the Bight '03 survey showed high levels of toxicity, and toxicity was not related to the variables used to track plume location (salinity and TSS). Bay *et al*. (2003) detected toxicity in samples collected in the Ballona Creek discharge plume when the proportion of stormwater exceeded 10%. Samples outside the Ballona Creek plume were not toxic. In that study, the authors did not use a fixed grid of samples but adapted their stations based on salinity levels always collecting samples both inside and outside the plume. The Bight '03 study was designed to monitor specific locations around major river discharges. This design likely missed much of the plumes as evidenced by the small proportion of sites located in low salinity water. Coastal currents can advect plumes at speeds that typically range from 5 – 20 cm s^{-1} (~5–20 km day^{-1}). Therefore, runoff plumes can be advected through the area of a given sampling grid in as little as a day. This transport is discussed in Section V, demonstrating that plumes generated in one location can impact adjacent regions along the coast. Because the plume is moving and the sampling grid is stationary, it is likely that even though the sampling was distributed over several days, it did not accurately sample the evolution of the discharge plume. Additional adaptive sampling is recommended for future efforts.

Differences between the results from Bight '03 and other past studies may also be due to differences in the time spans over which sampling took place. In a project of this type, it is difficult to obtain a good time series of observations that span the time from initial discharge to thorough dilution and/or dispersion in the coastal receiving waters. First, the exact timing of the storms is not known in advance, and it is difficult to schedule the boat and crew to guarantee availability during the event. Secondly, even if available, the sea state often prevents operations by the vessels typically used for this type of sampling (Nezlin *et al.* 2007). Because of the commitments of the scientific crews and vessels to other sampling and/or monitoring, it is difficult to maintain a sufficiently long time series to follow the evolution of these systems. During Bight '03, no sampling occurred during the runoff events, so the effects of the initial mixing of the stormwater into the coastal ocean were missed. Bay *et al* (2003) were able to sample during as well as immediately after storms which may also explain the differences in their findings.

Feasibility of using CDOM and beam-c to map plumes

Beam-c and TSS represent two different ways to examine the particulate component of seawater. TSS is a measurement of the concentration, by weight, of particles whereas beam-c is an optical measurement related to the size and concentration of particles. Because of the dependence of light attenuation on particle size, beam-c depends on the geometrical cross-section of particles per unit volume, not necessarily on TSS (Davies-Colley and Smith 2001). Therefore, changes in particle size and composition (i.e., inorganic vs. organic) can result in a change in beam-c without a corresponding change in TSS. Beam-c and TSS are not always interchangeable and actually measure slightly different aspects of the particulate portion of a plume. The variability in both the strength of the observed beam-c/TSS relationship and in its parameters is likely due to variability in the characteristics of the particles in the study area both in space and time.

This is not true for salinity and CDOM, which both represent concentrations of dissolved constituents. River and runoff systems typically have elevated levels of CDOM that can correlate with salinity, such that CDOM concentration increases with decreasing salinity (D'Sa *et al.* 2002). In theory, salinity and CDOM could be used interchangeably as tracers of the dissolved portion of a runoff plume. This is of particular note given that CDOM has a characteristic absorption spectrum and can therefore also be detected with satellite ocean color sensors (Lee *et al.* 2002). Through examining the *in situ* relationships between these parameters measured during Bight '03, CDOM seems to have a high potential for estimating stormwater plumes from ocean color (the CDOM/salinity relationship was strong). This finding is significant in that CDOM is indicative of the dissolved portion of the plume, and many contaminants (e.g., nutrients and FIBs) are either dissolved or can behave as dissolved material. Although a relationship between nLw551 and *in situ* salinity has been observed in this study (see Section VII), our data indicate that estimates of CDOM would better track the dissolved portion of stormwater plumes.

Conclusions

As part of the Bight '03 program, the effects of runoff from two storms, one in February 2004 and the other in March 2005, were studied. The overall ecological impact of the plumes was in most cases not large. The areal impact from bacterial contamination and from water column toxicity was constrained to small areas near the watershed mouths. The worst contamination occurred in the region off the Tijuana River where exceedances of the COP standards persisted for two to three days following the storm event. The effects from the rain events were confined primarily to the upper 5–10 meters of the water column for single storm events, and they tended to decrease below threshold levels of concern within two to three days. In addition, we found that the chance of exceeding the single COP standard decreased in areas containing <10% (~30 psu) stormwater, and dramatic decreases in all FIBs and nutrients were observed in water with <1% (>33 psu) stormwater.

In an effort to evaluate the use of proxy variables to describe and, if possible, quantify the impacts of microbial, toxicity, and nutrient effects, relationships were evaluated between these contaminant variables and easily-measured variables that characterize the dissolved and particulate fractions, i.e., salinity and turbidity. In general, FIB and nutrient concentrations increased with increasing freshwater content (decreasing salinity). When the bulk data set was considered, the FIBs also showed a relationship with turbidity, with higher FIB concentrations at higher concentrations of TSS.

Correlations between CDOM with salinity and beam-c with TSS indicate that remotely sensed ocean color can be used to infer salinity gradients and turbidity, respectively. CDOM and beam-c and their analogs can be derived from the inherent optical properties of the water column, which in turn can be derived from the remote sensing reflectance obtained by ocean color sensors on satellites. The semi-quantitative (QAA) algorithms developed for deriving inherent optical properties from remotely sensed ocean color provide one mechanism with which to do this (e.g., Lee *et al.* 2002). The CDOM/salinity relationship appears to be similar enough throughout the SCB that a single linear relationship can be used to characterize salinity as a function of CDOM. Although, preliminary analysis of ocean color data suggests regional variability (see Section VII for an analysis of satellite imagery), we expect that this could be corrected with additional regional tuning of the standard/global algorithms. The beam-c/TSS relationship also suggests that a single relationship might be used, but there is sufficient variability in the relationship between watersheds that it is uncertain how accurate this method will be.

Several things are needed to improve the capability of using ocean color to detect and quantify the impacts from coastal watersheds in southern California. First, better statistical characterization of the relationships between the measurable variables and contaminants is required. Secondly, regional tuning of the satellite processing algorithms is required for the local region to ensure the quality of the inherent optical properties from ocean color. Finally, improvements in atmospheric corrections would improve estimates of these inherent optical properties.

VII. MODIS IMAGERY AS A TOOL FOR SYNOPTIC WATER QUALITY ASSESSMENTS IN THE SOUTHERN CALIFORNIA BIGHT

Introduction

This section is focused on developing the ability to routinely detect, classify and characterize stormwater runoff plumes in the Southern California Bight (SCB) for the purposes of synoptic water quality assessments in this region. Stormwater runoff plumes are a main source of coastal pollution in the SCB, where concentrations of contaminants in plumes are related to salinity (Bay *et al.* 2003, see also Section VI). The plumes are identified as water masses with decreased salinity relative to ambient ocean water. Such gradients in salinity can only be presently measured through *in situ* measurements. Salinity can not yet be measured from space (nor in the near-future with necessary resolution for coastal applications), although a high correlation between salinity and "ocean color" parameters has been shown in many coastal regions (Monahan and Pybus 1978, Vasilkov *et al.* 1999, Siddorn *et al.* 2001, Miller and McKee 2004).

In this context, optical signatures that can be used to discriminate stormwater plumes result from high concentrations of suspended sediments (measured as Total Suspended Solids [TSS]) and Colored Dissolved Organic Matter (CDOM) in terrestrial runoff associated with coastal storm events. The temporal characteristics of TSS and CDOM, however, are very different. CDOM as a freshwater tracer is substantially more conservative than TSS, given that particles coagulate and settle out during a relatively short period after storm events (Ahn *et al.* 2005).

In Section VI we have shown that *in situ* measurements of CDOM collected during the Bight '03 Regional Water Quality Program strongly correlate with salinity throughout the SCB suggesting that CDOM could be used as an optical tracer of stormwater plumes. Relationships between two measures of turbidity (TSS and the beam attenuation coefficient) were not as strong and were more variable throughout the SCB but also show potential as tracers of the particulate components of plumes. Although strong linear correlations did not seem to exist between *in situ* measurements of contaminants (e.g., fecal indicator bacteria) and salinity or turbidity, several standards were often exceeded in waters with >10% stormwater (salinity of <30 psu) or with TSS concentrations >30 mg l^{-1} during Bight '03 (see Section VI). If salinity and TSS can be related to optically active parameters (e.g., CDOM and the beam attenuation coefficient), this suggests that ocean color satellite imagery could also be used to estimate when and where high concentrations of contaminants occur.

To determine if these results could be applied to ocean color satellite imagery, we explored correlations between CDOM and turbidity estimated from MODIS satellite imagery and *in situ* salinity and TSS concentrations collected during Bight '03. We also analyzed the remotely-sensed ocean color characteristics typical to plume waters and the persistence of these characteristics in different regions of the SCB. In addition to simply tracking the location and movement of stormwater plumes, we explored whether ocean color imagery could be used as a tool to track the fate of contaminants typically found in stormwater plumes. This information would be especially useful to coastal managers and governing agencies who are required to perform additional monitoring and close beaches if contaminants exceed various standards (State Water Resources Control Board 2005).

Previous regional satellite-based plume studies (e.g., Nezlin and DiGiacomo 2005, Nezlin *et al.* 2005) focused primarily on multi-year analysis of plume dynamics, whereas the present effort is geared toward developing an event detection, classification and impact assessment system for near-real time synoptic characterizations of water quality. The results of this study could be used to develop a cost-effective synoptic water quality monitoring strategy in the SCB and other urban coastal regions that would provide environmental managers with information on coastal water quality that is both faster and spatially more extensive than the exclusively *in situ*, shipboard sampling techniques currently in use.

MODIS imagery classification method

All ship-based stations were classified into plume (surface S<33.0 psu, ~>1% fresh water) or ocean water (S≥33.0 psu) stations assuming normal ocean salinity in the SCB as 33.6 psu (Hickey 1993). The remotely sensed optical properties from MODIS images (i.e., the seven aforementioned nLw values, $a_{dg}412$, and b_b551) were attributed to each station sampled during that day. From these, each Level 2 image (i.e., data in sensor coordinates) was converted into a Level 3 regular grid with a spatial resolution of 0.01 degrees latitude and longitude. Data were interpolated using a kriging method (Isaaks and Srivastava 1989, Oliver and Webster 1990). To avoid extrapolation to areas not covered by the observations, the "missing data" mask was applied to the pixels located over land and to the pixels located >2 km from the nearest pixel of a Level 2 MODIS image containing valid data (i.e., not eliminated by a cloud discrimination algorithm). All nLw were averaged separately for plume and ocean stations. The resulting mean nLw (optical spectra) were used as endmembers for supervised classification of all available MODIS images collected during the Bight '03 observations.

A minimum distance supervised classification technique (Richards 1999) used the mean vectors of each endmember (i.e., seven-nLw vectors of plume and ocean water, respectively) and calculated the Euclidean distance from each image pixel to the mean vector for each class. Each pixel from the MODIS image was classified to the nearest class (i.e., plume or ocean). The accuracy of classification (Congalton and Green 1999) was estimated comparing the pixels at all ship-based stations with the classes to which these stations were attributed based on surface salinity. Another method to evaluate the plume classification accuracy was to compare the stations attributed to plumes to the stations where bacterial contamination exceeded California State Water Board standards (*Enterococcus* counts >104 CFU 100 ml^{-1}). On the basis of a confusion (contingency) matrix (i.e., the table comparing classification results with ground truth information) we estimated the overall accuracy of the classification (i.e., the percentage of pixels classified correctly). Also, we estimated producer and user accuracies for each class (i.e., plume or ocean). Producer accuracy is the ratio (in %) between the number of stations correctly classified by satellite imagery (N) and the total number of stations of this class classified on the basis of ship-based measurements. Low producer accuracy represents high omission error, i.e., the chance for each pixel to be erroneously attributed to another class. User accuracy is the percentage of correctly classified stations in the total number of stations attributed to that class on the basis of satellite imagery. It is related to commission error, i.e., the chance for a certain class to be contaminated by pixels from other classes. These measures of accuracy are conventional in remotely-sensed mapping of terrestrial objects (Congalton and Green 1999). As a result of this classification, the plume areas were estimated in four regions corresponding to the regions where the Bight '03 surveys were conducted (Figure III-1). The boundaries of rectangles surrounding each region are given in Table VII-1.

Table VII-1. The boundaries of the ocean regions surrounding the Bight '03 survey areas and used for analysis of MODIS imagery.

Region	Region abbreviation	Latitude	Longitude
Ventura	VE	33.70° - 34.50° N	119.8° -118.8° W
Santa Monica Bay	SM	33.60°- 34.10° N	119.0° -118.3° W
San Pedro	SP	33.33°- 33.87° N	118.5° -117.5° W
San Diego	SD	32.25°- 33.55° N	117.8° -117.0° W

For purposes of this study we decided that plume discrimination from satellite images would be based on the entire optical spectra versus based on only one "significant" wavelength (e.g., 555 nm in SeaWiFS imagery with threshold 1.3 mW cm^{-2} μm^{-1} sr^{-1} (Otero and Siegel 2004, Nezlin and DiGiacomo 2005, Nezlin *et al.* 2005)). Using this approach we minimize the chance of improper wavelength selection, important for reasons described below. Our choice of a binary ("plume" or "ocean") classification scheme rather than a gradient (or fraction) of each endmember (see Warrick *et al.* 2004a) is based on 1) presumptive nonlinearity of the correlations between optical properties and water quality characteristics; 2) an opportunity to assess classification accuracy using methodology previously demonstrated and proven effective in land remote sensing; and 3) the management focus of this study, whereby the decision to close recreational beaches affected by stormwater plumes is also binary (i.e., either accepted or rejected).

Results

<u>*Plume discernment using nLw optical spectra*</u>

In the San Pedro (SP) and San Diego (SD) regions, the nLw spectra of plumes and ambient ocean waters were significantly different, especially on the next day after rainstorms (Figures VII-1a and VII-2c), when the nLw at wavelengths 531 – 551 nm in plume waters were significantly higher than in surrounding ocean waters. In the short (412 – 433 nm) and long (667 – 678 nm) parts of nLw spectra the differences were much less or absent. During the first two days after the storm the differences between nLw spectra decreased, became very low on the third (Figure VII-2b), and negligible on the fourth (Figure VII-1c) days.

In Ventura (VE) and Santa Monica Bay (SM), the differences between plume and ocean nLw spectra were insignificant during all surveys (Figure VII-3) and plume signatures could not be detected. The reasons for this similarity, however, seem quite different for the two regions. In the VE region, the non-plume baseline nLw at 531–551 nm were higher than in other regions, which can be explained by the relatively high concentrations of suspended sediments found in the less-episodic river discharge from the less urbanized watersheds relative to other regions. At the same time, the sampled area in VE was much smaller than the plume, resulting in a ship-sampled dataset that captured only a fraction of the plume. This was largely due to southward advection of the plume away from the river mouth (see Figure VII-4) (*cf.* Section 5). In SM, the nLw at 531–551 nm (Figure VII-3b) were lower than in other areas (Figures VII-1, VII-2 and VII-3a), which was caused by a low concentration of suspended sediments in the "urbanized" freshwater discharge inputs to SM.

To classify the pixels in all images collected simultaneously with ship-based sampling, the nLw spectra obtained from six MODIS-Aqua images with evident plume signatures (SD on February 28, 2004; February 29, 2004; February 13, 2005 and SP on February 27, 2004; February 28, 2004; March 01, 2004) were used as endmembers (training areas). Two general nLw spectra (characterizing plumes and ambient ocean waters) were obtained by averaging the nLw data for all stations with evident plume signatures with S≤33.0 psu (plume) and S>33.0 psu (ocean). Then each pixel of each image was attributed to one of the two groups (plume or ocean) using a minimum distance classification method. The results of the classification showed solid plume patterns located along the coast and originating from river mouths (Figures VII-4 through VII-7). The plume areas obtained from satellite imagery significantly exceeded the areas covered by ship-based surveys, whose station grids were not intended to capture the entire regional plumes given the time, expense, and logistical difficulty that would result from such an effort. In the VE region, the sampled area was restricted to the zone near the mouths of the Santa Clara and Ventura rivers, while the signature of turbid plume was extended downcoast, especially in March 2005 (Figure VII-4). Plume signatures in SM were small (Figure VII-5), but in March 2005 the tip of a large plume was transported from the VE region to the western part of the SM region. In the SP region in February 2004, the plume also propagated downcoast beyond the area of the ship-based surveys (Figure VII-6). In spring 2005, the plume signature was not observed after the rainstorm (March 23) due to cloud cover; two days later (March 25) the plume was very small. Several small plumes were observed in the SD sample region and along the coast of Orange and San Diego counties (Figure VII-7).

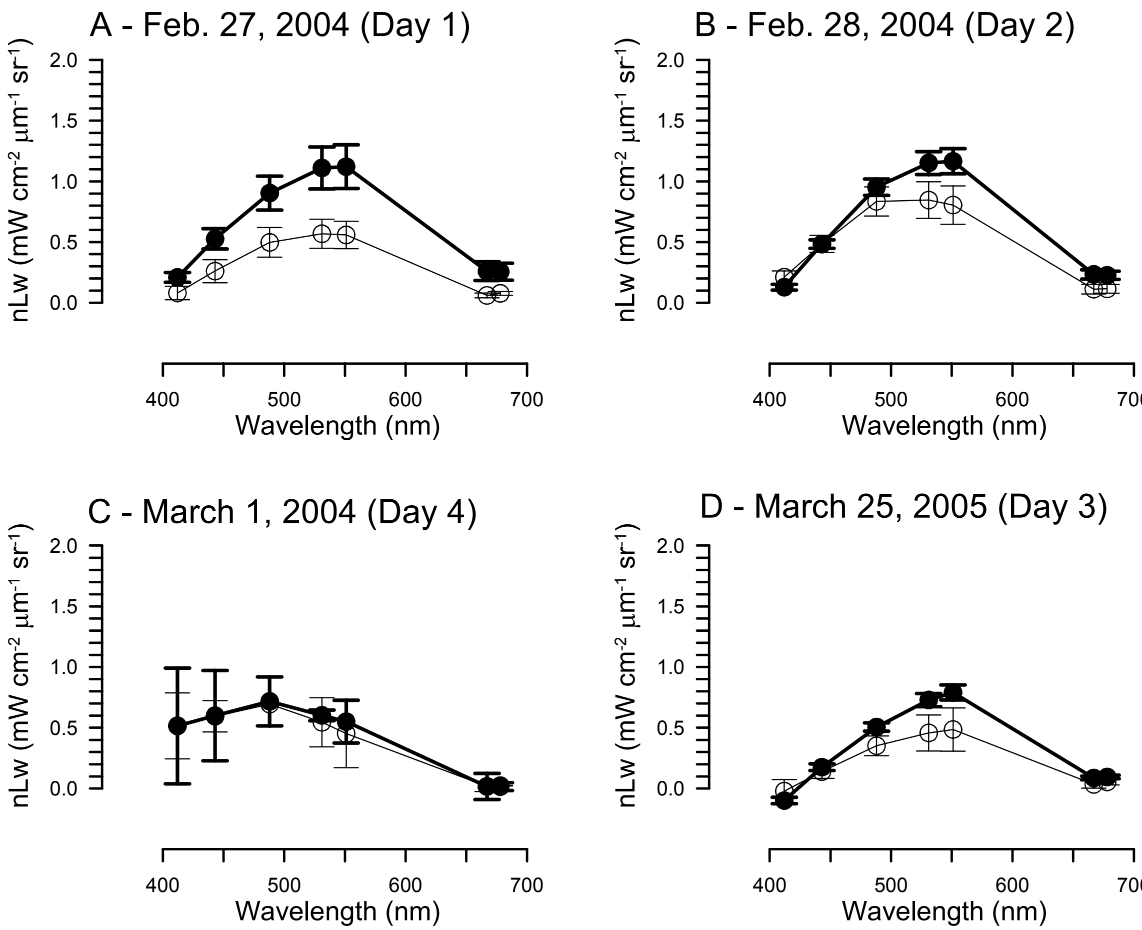

Figure VII-1. The optical signatures of plume waters (salinity <33.0 psu; solid circles and thick line) and ocean waters (salinity >33.0 psu; open circles and thin line) in San Pedro region. Number of days following the storm are indicated in parenthesis. Vertical bars indicate the standard errors at 95% confidence level.

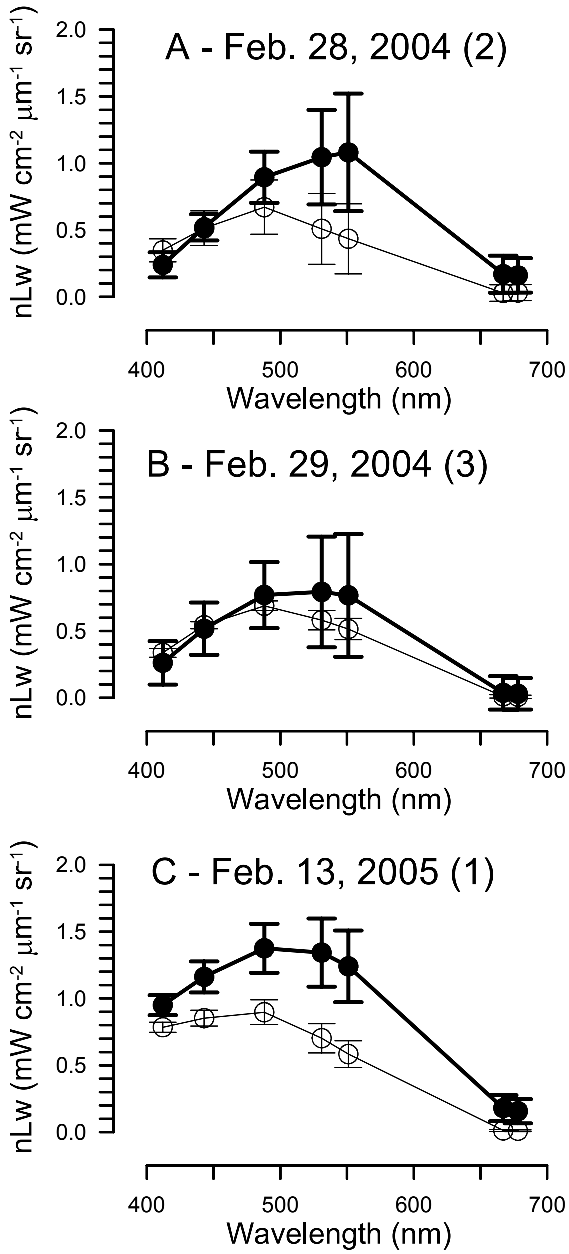

Figure VII-2. The optical signatures of plume waters (salinity <33.0 psu; solid circles and thick line) and ocean waters (salinity >33.0 psu; open circles and thin line) in San Diego region. Number of days following the storm are indicated in parenthesis. Vertical bars indicate the standard errors at 95% confidence level.

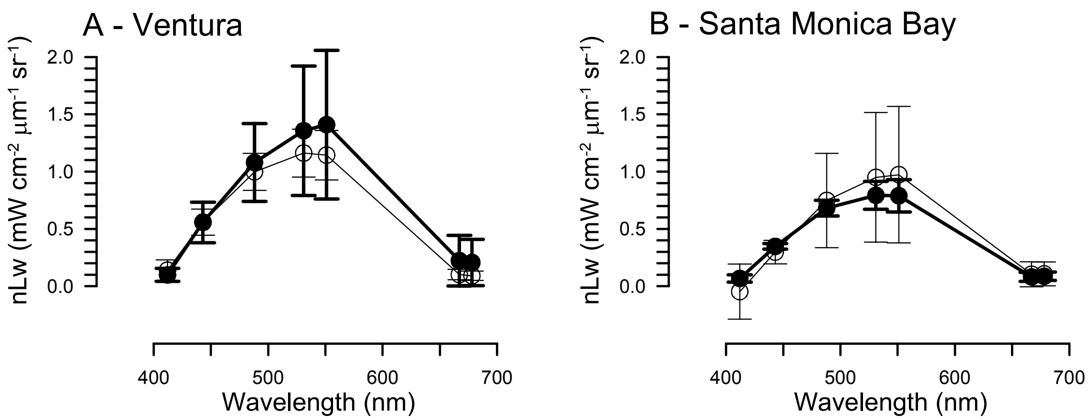

Figure VII-3. The optical signatures of plume waters (salinity <33.0 psu; solid circles and thick line) and ocean waters (salinity >33.0 psu; open circles and thin line) in Ventura (A) and Santa Monica Bay (B) regions averaged over all observed days of both 2004 and 2005 storms. Vertical bars indicate the standard errors at 95% confidence level.

The total accuracy of classification was 77% for the six images where plume optical signatures were evident (shaded cells in Table VII-2). For each separate region and date, the total accuracy varied within a range of 69–100%. The producer accuracy (i.e., the percent of properly classified pixels) was 50–91% for plume waters (average 74%) and 62–100% for ambient ocean waters (average 82%). The user accuracy (i.e., the chance of each pixel to be properly classified) was 67–100% for plume waters (average 86%) and 47–100% for ambient ocean waters (average 68%). Typically, user accuracy was higher than producer accuracy for plume waters and lower for ocean waters, indicating higher chance of commission error and lower chance of omission error for plume pixels.

When the endmember nLw spectra obtained from the six regions/dates with evident plume signatures were applied to other SCB regions/dates, the accuracy of classification was lower as compared with the observations where plume signatures were obtained. The overall accuracy for all dates and regions was 58% (Table VII-2). Nevertheless, the user accuracy of plume classification (i.e., the chance that the pixels coinciding with sample stations with S<33.0 psu were classified as plume at the satellite image) was as high as 80% on average. Only once (VE; February 29, 2004) was it low (13%); in all other cases it was 57–100%. We conclude that plume differentiation based on this method, even with endmembers based on only a small number of observations, provides promising results. In contrast, for ambient (non-plume) ocean waters, the chance to be properly classified was much lower (41%), indicating that ocean waters could often be erroneously classified as plume.

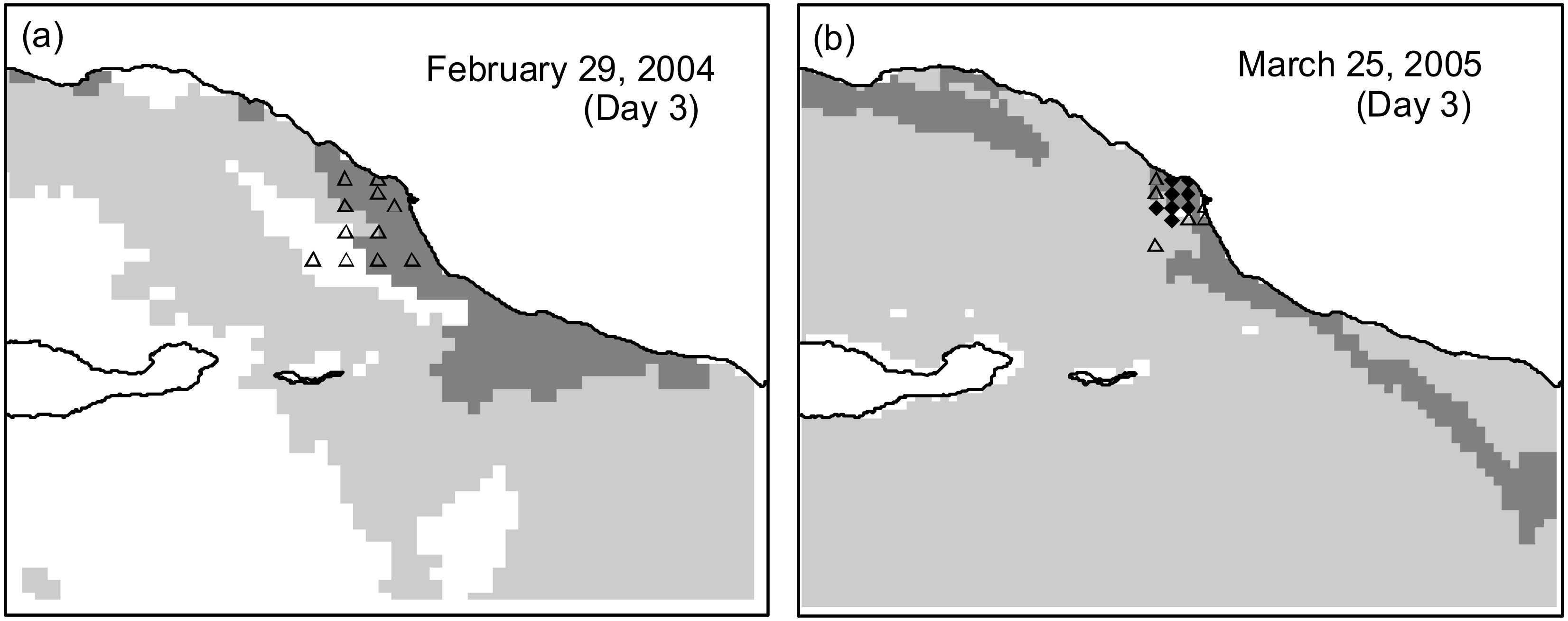

Figure VII-4. Plume areas (dark shaded) in the Ventura (VE) region resulting from classification of MODIS imagery and the Bight '03 stations. Light shading indicates ocean waters; white color the absence of MODIS imagery due to cloud cover. Black diamonds indicate the stations with surface salinity <33.0 psu (plume); triangles indicate the stations with surface salinity >33.0 (ocean).

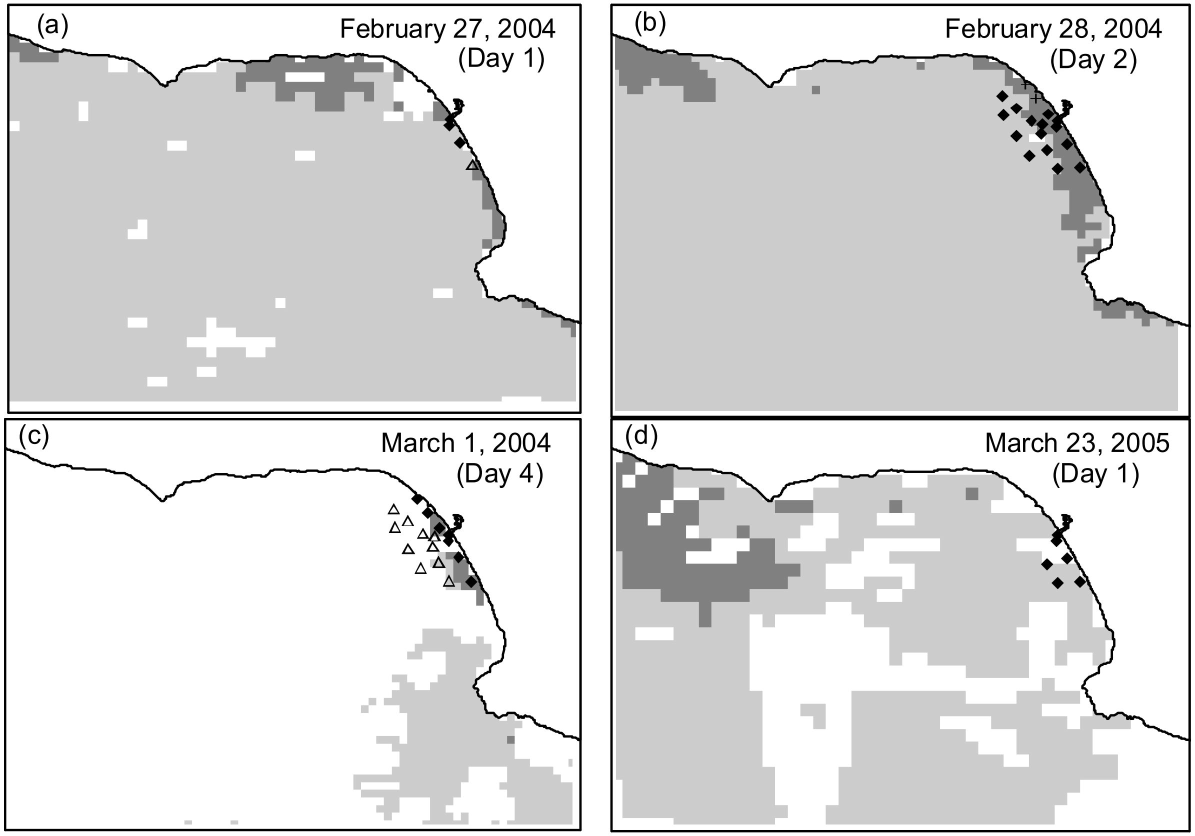

Figure VII-5. Plume areas (dark shaded) in Santa Monica Bay (SM) region resulting from classification of MODIS imagery and the Bight '03 stations. Light shading indicates ocean waters; white color the absence of MODIS imagery due to cloud cover. Black diamonds indicate the stations with surface salinity <33.0 psu (plume); triangles indicate the stations with surface salinity >33.0 (ocean).

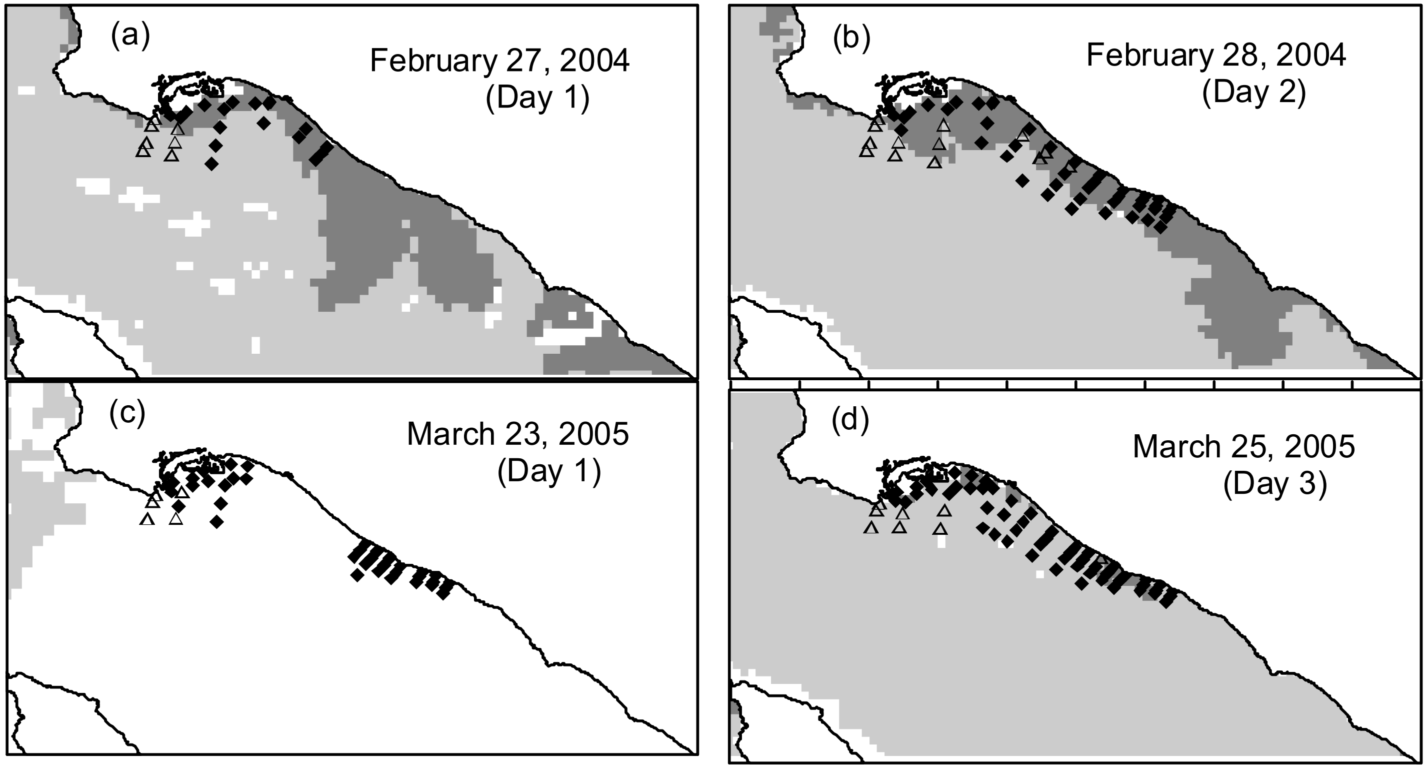

Figure VII-6. Plume areas (dark shaded) in the San Pedro (SP) region resulting from classification of MODIS imagery and the Bight '03 stations. Light shading indicates ocean waters; white color the absence of MODIS imagery due to cloud cover. Black diamonds indicate the stations with surface salinity <33.0 psu (plume); triangles indicate the stations with surface salinity >33.0 (ocean).

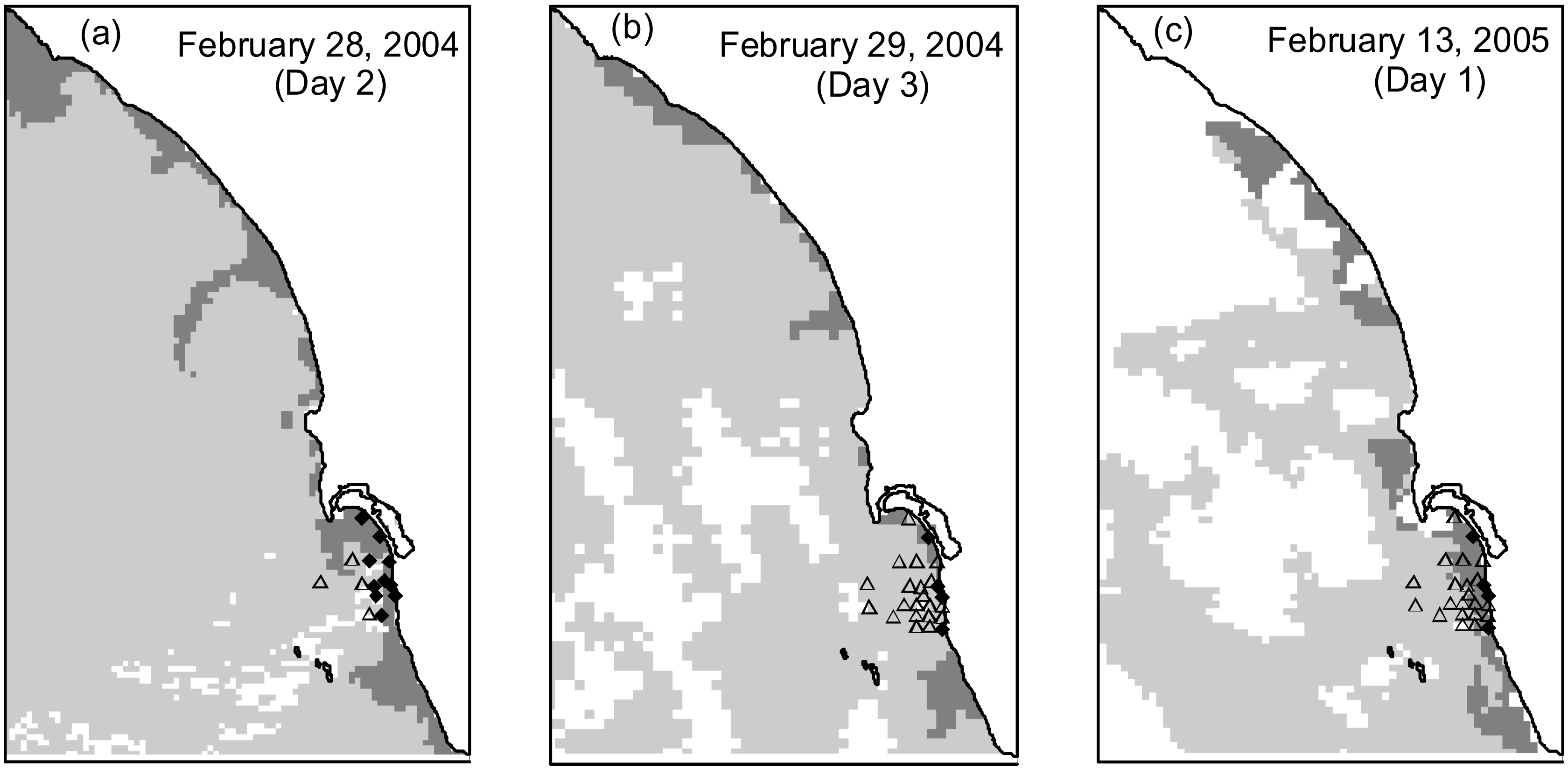

Figure VII-7. Plume areas (dark shaded) in the San Diego (SD) region resulting from classification of MODIS imagery and the Bight '03 stations. Light shading indicates ocean waters; white color the absence of MODIS imagery due to cloud cover. Black diamonds indicate the stations with surface salinity <33.0 psu (plume); triangles indicate the stations with surface salinity >33.0 (ocean).

Table VII-2. Accuracy (%) of plume classification in the SCB based on nLw (412 – 678 nm) obtained in the SP and SD regions. The days and regions, which plume optical signatures were used as endmember spectra are shaded and the numbers of matching/total stations are in brackets.

Region	Date	Overall accuracy	Plume		Ambient ocean	
			Producer accuracy	User accuracy	Producer accuracy	User accuracy
SD	02/24/2004	27% (4/15)	15% (2/13)	100% (2/2)	100% (2/2)	15% (2/13)
SD	02/28/2004	75% (9/12)	63% (5/8)	100% (5/5)	100% (4/4)	57% (4/7)
SD	02/29/2004	87% (20/23)	50% (2/4)	67% (2/3)	95% (18/19)	90% (18/20)
SD	02/13/2005	85% (17/20)	91% (10/11)	83% (10/12)	78% (7/9)	88% (7/8)
SM	02/27/2004	50% (2/4)	33% (1/3)	100% (1/1)	100% (1/1)	33% (1/3)
SM	02/28/2004	47% (8/17)	53% (8/15)	80% (8/10)	0% (0/2)	0% (0/7)
SM	03/01/2004	80% (4/5)	75% (3/4)	100% (3/3)	100% (1/1)	50% (1/2)
SM	03/23/2005	0% (0/3)	0% (0/3)	- (0/0)	- (0/0)	0% (0/3)
SP	02/27/2004	69% (18/26)	67% (12/18)	86% (12/14)	75% (6/8)	50% (6/12)
SP	02/28/2004	74% (40/54)	78% (32/41)	86% (32/37)	62% (8/13)	47% (8/17)
SP	03/01/2004	100% (2/2)	- (0/0)	- (0/0)	100% (2/2)	100% (2/2)
SP	03/25/2005	31% (17/54)	22% (10/46)	91% (10/11)	88% (7/8)	16% (7/43)
VE	02/29/2004	22% (2/9)	100% (1/1)	13% (1/8)	13% (1/8)	100% (1/1)
VE	03/25/2005	50% (6/12)	57% (4/7)	57% (4/7)	40% (2/5)	40% (2/5)
Images which nLw spectra were used as endmembers		77% (105/137)	74% (61/82)	86% (61/71)	82% (45/55)	68% (45/66)
All regions		58% (149/256)	52% (90/174)	80% (90/113)	72% (59/82)	41% (59/143)

Plumes frequently extended upward of 10 km offshore (e.g., Figure VII-6). Overall, the largest plume area size (976 km^2) was observed in the VE region on February 28, 2004 (Table VII-3). During other days when the sky was clear and a significant part of the VE region was observed by satellite, the plumes in VE were also large (602 – 783 km^2), especially when the part of the VE plume transported into the SM region (i.e., VE to SM rectangle at Figure III-1) was also taken into account (Table VII-4). Plumes of comparable size were observed in SP in February 2004 one to two days after the storm (606–689 km^2); on the next day, however, the plume size substantially decreased (310 km^2). Plumes in the SD region in February 2004 were also large (393–739 km^2). The smallest plumes (94–171 km^2) were observed in the SM region; one observation (March 25, 2005) when the plume area was higher (427 km^2) can be attributed to the plume transported from the VE region.

The plume areas estimated on the basis of ocean surface color were significantly larger than the areas of impact calculated on the basis of FIB exceedances by interpolating over *in situ* sampling grid (Table VII-5). No impact in terms of FIB was estimated for Ventura and Santa Monica. For San Pedro Shelf, the largest area of FIB impact was < 40 km^2 (on the first day after storm), which was ~ 6% of the plume area estimated from ocean color. In San Diego area, the impact of Tijuana river was ~ 50 km^2 in 2004 and 50–100 km^2 in 2005. The plume area estimated from ocean color in San Diego region included the plumes of small rivers located to the north of Tijuana; the size of these plumes were comparable (see Figure VII-7). The plume of Tijuana River estimated from ocean color was 150–250 km^2; as such, the area of FIB impact was as large as 30–70% of the plume observed by satellite.

Table VII-3. The size of plume areas (km^2) and the portion of the ocean area in each region visible at MODIS-Aqua imagery (%) during different days after rainstorms.

Date	Day after storm	Ventura		Santa Monica		San Pedro		San Diego	
		(km^2)	%	(km^2)	%	(km^2)	%	(km^2)	%
24-Feb-2004	1*	0	16	0	29	0	18	70	55
27-Feb-2004	1	602	98	137	97	689	98	421	90
28-Feb-2004	2	976	100	171	100	606	99	739	99
29-Feb-2004	3	548	62	94	97	310	95	393	83
01-Mar-2004	4	0.9	0.1	20	12	0.9	18	13	5
13-Feb-2005	1*	0	3	0	0	35	2	496	56
23-Mar-2005	1	627	78	234	70	0	7	0	12
25-Mar-2005	3	487	99	427	98	56	100	115	100
26-Mar-2005	4	0	0	0	2	0	28	0	5

*Storm was in San Diego area only

Table VII-4. The size of plume areas (km^2) and the portion of the ocean area visible at MODIS-Aqua imagery (%) during different days after rainstorm in the region including Ventura and Santa Monica Bay.

Date	Day after storm	(km^2)	%
23-Mar-2005	1	647	68
25-Mar-2005	3	783	100
26-Mar-2005	4	0	0.7

Table VII-5. The size of the areas of impact (A; km^2) calculated on the basis of FIB exceedances by interpolating over *in situ* sampling grid, and the size of total area sampled (T; km^2).

Storm	Day after storm	FIB	Ventura		Santa Monica		San Pedro		San Diego	
			A	T	A	T	A	T	A	T
2004	1	Total coliforms	0	93.8	-	-	7.8	131	20.3	50
		Fecal coliforms	0	93.8	-	-	0	131	26.8	50
		Enterococcus	0	93.8	-	-	39.4	131	48.7	50
	2	Total coliforms	-	-	0	48.2	22.3	272	3	84
		Fecal coliforms	-	-	0	48.2	0	272	4.7	84
		Enterococcus	-	-	0	48.2	15.2	272	0	84
	3	Total coliforms	-	-	-	-	-	-	8.5	172
	3	Fecal coliforms	-	-	-	-	-	-	3.8	172
	3	*Enterococcus*	-	-	-	-	-	-	0	172
	4	Total coliforms	-	-	0	48.2	0	272	-	-
	4	Fecal coliforms	-	-	0	48.2	0	272	-	-
	4	*Enterococcus*	-	-	0	48.2	5.7	272	-	-
2005	1	Total coliforms	-		1.53	24.3	0	62	51.9	53
		Fecal coliforms	-		0.05	24.3	0	62	51.9	53
		Enterococcus	-		0	24.3	5	62	51.9	53
	2	Total coliforms	0	24.3	0.02	48.4	2.13	33	50.3	53
		Fecal coliforms	0	24.3	0	48.4	0	33	42.9	53
		Enterococcus	0	24.3	0	48.4	0	33	51.9	53
	3	Total coliforms	0	24.3	-	-	0	253	103	126
		Fecal coliforms	0	24.3	-	-	0	146	63	126
		Enterococcus	0	24.3	-	-	4.4	253	70.5	126
	4	Total coliforms	0	24.3	0	48.4	-	-	-	-
		Fecal coliforms	0	24.3	0	48	-	-	-	-
		Enterococcus	0	24.3	0	48	-	-	-	-

Backscattering and absorption in stormwater plumes

The quantitative relationships between $a_{dg}412$, b_b551, TSS, CDOM and S were analyzed using correlations between linear and log-transformed values. Analyzing the correlations, we took into account the spatial location of each station. For this, we interpolated the ship-based data collected during each day, to a regular grid similar to a remotely sensed data grid, removing the data from the grid nodes located >3 km from the nearest station. The correlations between the data taken from the corresponding nodes of both grids were analyzed. This transformation increased the number of data used in the correlation analysis and improved its statistical significance. The coefficients of linear regression equation between S and $a_{dg}412$ were used for reconstruction of salinity fields from MODIS imagery.

The correlation between *in situ* measured TSS and the remotely sensed backscattering proxy b_b551 varied from one observation to another and depended on the time lag between the rainstorm and the observation date. The total coefficient of determination (R^2) of the correlation between TSS and b_b551 calculated by QAA algorithm, both log-transformed, was as low as 0.014 (Table VII-6). At the same time, during some days of observations the TSS/b_b551 correlations were high. In the SD, SM, and SP regions, the TSS/b_b551 correlations were highest during the first and second days after the rainstorm and decreased thereafter. We can explain this decrease with rapid TSS sedimentation during a short post-storm period as well as perhaps high variability within the 1-km resolution provided by the satellite imagery. In the VE region, where TSS concentration in stormwater runoff is typically higher than in other regions, the TSS/b_b551 correlation was estimated only three days after the storm (sampling occurred February 29, 2004; poor sea conditions prevented any earlier field sampling) and had a negative slope, which can be explained by having too small of an area where both ship-based samples and MODIS imagery were available (see Figure VII-4a). For a different event on March 25, 2005 (3rd day after storm), the correlation was high (R^2 = 0.540) and comparable with TSS/b_b551 correlations in other regions obtained during the first day after the storm. This provides evidence that in the VE region the TSS concentration in freshwater discharge was higher and the plume optical signature was more persistent than in other SCB regions.

The total correlation between *in situ* CDOM concentration and obtained from MODIS data log-transformed $a_{dg}412$ was low (R^2=0.100) and varied between different days and regions (Table VII-6). In contrast to the TSS/b_b551 correlation, the CDOM/$a_{dg}412$ correlation was independent of the time lag between the rainstorm and the observation day. For example, in the SP region, the CDOM/$a_{dg}412$ correlation observed two and four days after the rainstorm was higher than the correlation observed the next day after the rainstorm (0.449–0.624 vs. 0.345). This is not surprising because the CDOM signal in coastal water is more persistent compared with TSS for reasons discussed earlier.

According to ship-based measurements, CDOM was highly correlated with salinity (R^2=0.464–0.997; Table VII-6) at all stations excluding the SP region on March 25, 2005, when CHL concentration exceeded 4 mg m^{-3}, indicating a phytoplankton bloom. High phytoplankton biomass can potentially have an impact on these CDOM relationships, particularly as a source of CDOM, independent of freshwater discharge, potentially resulting in a low correlation between S and CDOM as observed on March 25, 2005 (R^2=0.059 for the SP region).

Table VII-6. Coefficients of determination (R^2) of linear regression between salinity (S) and CDOM; log-transformed TSS and log-transformed b_b551; CDOM and log-transformed $a_{dg}412$; S and log-transformed $a_{dg}412$; mean chlorophyll *a* (CHL) concentration (mean ± 95% standard error).

Region	Date	Day after storm	R^2 (S/CDOM)	R^2 (TSS/bb551)	R^2 (CDOM/a412dg)	R^2 (S/a412dg)	CHL (mg m^{-3})
San Diego	02/24/2004	1*	-	0.353	-	0.000	1.70 ± 0.46
	02/28/2004	2	-	0.000	-	0.689	1.62 ± 0.73
	02/29/2004	3	-	0.008	-	0.397	1.28 ± 0.46
	02/13/2005	1*	=	0.216	-	0.632	1.75 ± 0.36
San Pedro	02/27/2004	1	0.705	0.568	0.345	0.226	2.16 ± 0.55
	02/28/2004	2	0.642	0.513	0.624	0.488	1.23 ± 0.21
	03/01/2004	4	0.678	0.428	0.449	0.575	1.70 ± 0.36
	03/25/2005	3	0.059	0.0289	0.000	0.161	4.23 ± 0.58
Santa Monica	02/27/2004	1	0.931	0.691	0.375	0.334	1.22 ± 1.26
	02/28/2004	2	0.824	0.802	0.191	0.342	1.88 ± 0.52
	03/01/2004	4	0.777	0.147	0.349	0.401	1.93 ± 0.88
	03/23/2005	1	0.997	0.772	0.623	0.606	2.44 ± 2.43
Ventura	02/29/2004	3	0.503	0.361**	0.005	0.151	0.82 ± 0.22
	03/25/2005	3	0.464	0.540	0.338	0.059	2.59 ± 0.47
Total			0.703	0.014	0.100	0.233	-
SP and SM (02/27/2004; 02/28/2004;03/01/2004); SM (03/23/2005); VE (03/25/2005)			0.719	0.463	0.241	0.066	-
SP and SM (02/27/2004; 02/28/2004); SM (03/23/2005); VE (03/25/2005)			0.727	-	0.258	0.045	-
SP and SM (03/01/2004)			0.686	-	0.318	0.239	-

*Storm was in San Diego area only
**The slope of regression was negative

On March 25, 2005, during the same phytoplankton bloom in the SP region as described above (Table VII-6), CDOM in seawater was uncorrelated not only with S, but also with the values derived from MODIS data: QAA phytoplankton absorption coefficient $a_{ph}412$ and the sum of phytoplankton, detritus, and CDOM absorption ($a_{dg}412+a_{ph}412$); the R^2 were 0.044 and 0.056, respectively. A seemingly strong optical signal produced by phytoplankton chlorophyll potentially affected the estimation of the absorption and backscattering coefficients by the QAA algorithm. Another observation when both CDOM/$a_{dg}412$ and TSS/b_b551 correlations were extremely low was on February 29, 2004 in the VE region, when the area covered by both ship-based sampling and MODIS imagery was very small (see Figure VII-4a). A similar explanation can be applied to low TSS/b_b551 correlations in the SD region (Table VII-6).

After the above described observations with low TSS/b_b551 and CDOM/$a_{dg}412$ correlations were excluded from the dataset, the resulting correlation between TSS and b_b551 became satisfactorily high ($R^2 = 0.463$; Table VII-6; Figure VII-8a). At the same time, the correlation between CDOM and $a_{dg}412$ was not as good ($R^2=0.241$). Such a low correlation can be partly explained by the bias between $a_{dg}412$ coefficients obtained during different days. This bias was especially evident between $a_{dg}412$ on March 1, 2004 (in both SP and SM) and the rest of data (Figure VII-8b). This is not surprising because March 1, 2004 was very cloudy and the ocean surface area actually observed by MODIS was small (Figure VII-5c). Exclusion of the March 1, 2004 data made the CDOM/$a_{dg}412$ correlation slightly higher ($R^2 = 0.258$).

Surface salinity (S) was also correlated with the remotely-sensed CDOM absorption coefficients $a_{dg}412$, but the parameters of linear regression varied between observations. The R^2 were within the range 0.000 – 0.689 (Table VII-6), but explanations can be found for low correlations: in SD on February 24, 2004 nLw were extremely low, potentially due to poor atmospheric correction; in SP on March 25, 2005 a phytoplankton bloom affected estimation of the absorption coefficients by the QAA algorithm; in VE all correlations were low as a result of too small of a sampling area. However, even the data from the observations when the S/$a_{dg}412$ correlations were high could not be combined into one dataset, because the coefficients of linear regressions were different (Figure VII-9). Different slopes of linear regressions can be attributed to different CDOM concentrations in discharged freshwater in watersheds characterized by different land use: in the urbanized SP and SM watersheds more CDOM was discharged as compared with the more natural SD watershed, resulting in a more intensive $a_{dg}412$ signal, especially at high S. Both in SM and SP, the correlation scatterplots looked like the result of two merged datasets with different slopes of S/$a_{dg}412$ regression (Figure VII-9). The dataset with the steeper slope included very low S collected in the vicinities of river mouths.

Salinity fields reconstructed from $a_{dg}412$ using regression equations (Figure VII-9) resulted in plume patterns (Figure VII-10) that exceed in size the plumes estimated by classification methods based on nLw (Figures VII-4 through VII-7), a result that is not entirely surprising. The accuracy of these estimations (Table VII-7), which are estimated on the basis of surface salinity from ship-based samples, was comparable with the accuracy obtained by nLw classification (Table VII-2). High user accuracy for ambient ocean water indicates low chance for plume pixels to be erroneously classified as ocean and shows the advantage of the approach based on $a_{dg}412$/S correlation. Using the $a_{dg}412$/S relationship as a management tool for synoptic water quality assessments and monitoring would mean that potential contaminant impacts due to storm plumes might be spatially overestimated, but might more conservatively protect public health (although not factoring in economic impacts).

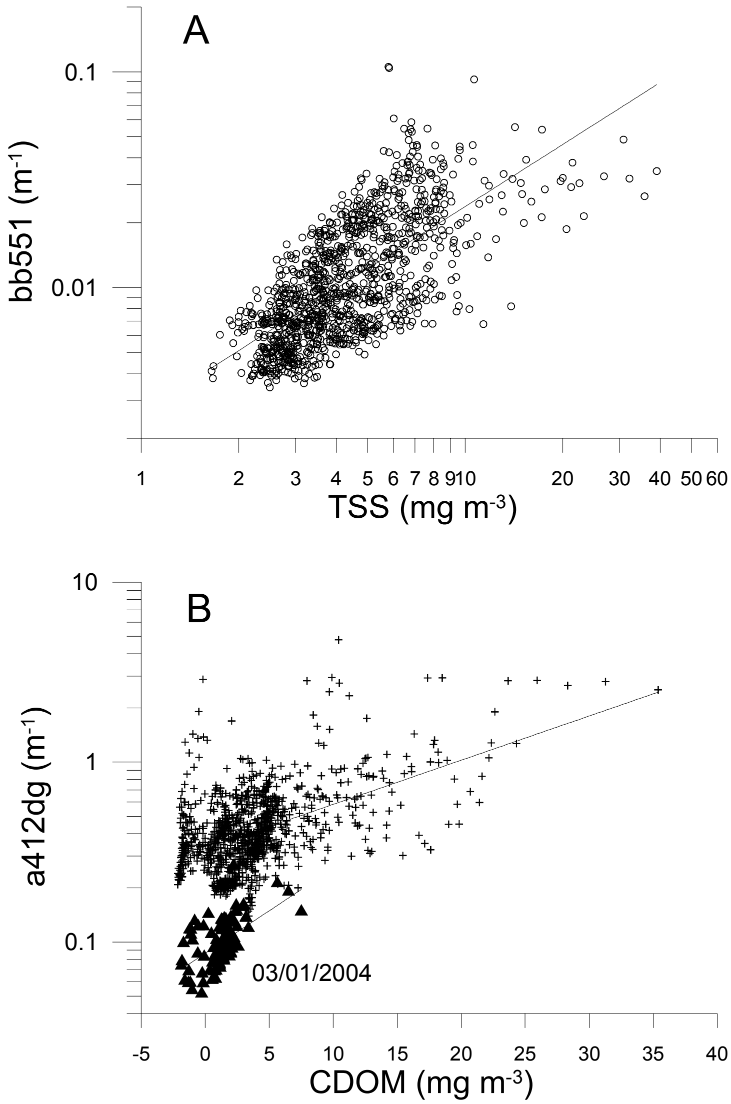

Figure VII-8. Correlations between TSS and b_b551 (A) and CDOM and $a_{dg}412$ (B). Triangles indicate MODIS image on March 1, 2004.

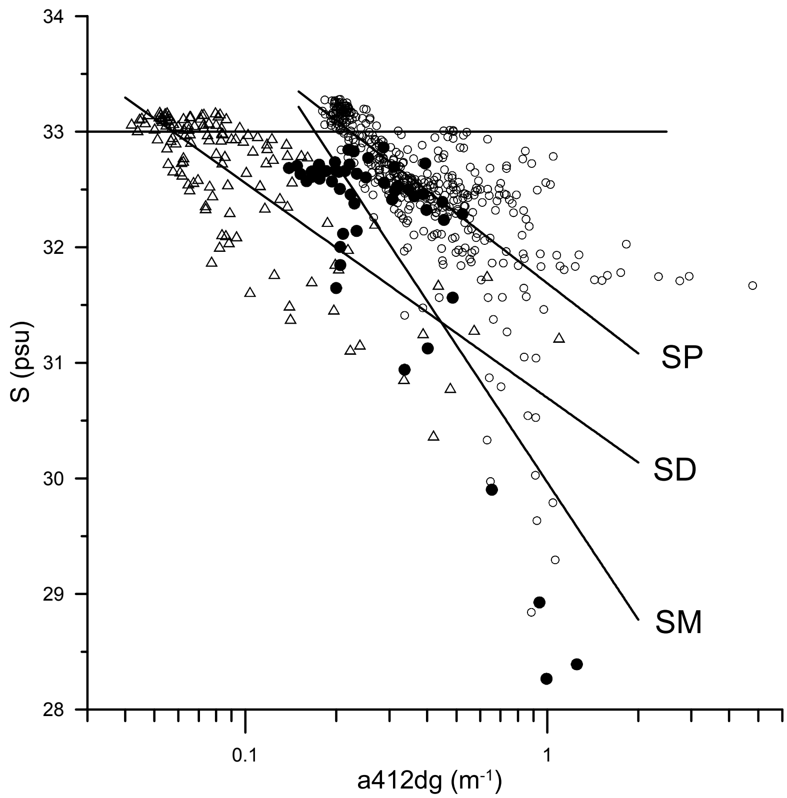

Figure VII-9. Correlation between *in situ* salinity (S) and remotely-sensed CDOM absorption (a_{dg}412) in SM region February 23 2005 (closed circles); in SP region February 28, 2004 (open circles); and in SD region February 13, 2005 (triangles). Horizontal line indicates the boundary between plume and ambient ocean water salinity.

Table VII-7. Accuracy (%) of plume classification in the SCB based on correlations between a_{dg}412 and S (Figure VII-9). Numbers of matching/total stations are in brackets.

Region	Date	Overall accuracy	Plume		Ambient ocean	
			Producer accuracy	User accuracy	Producer accuracy	User accuracy
SD	13-Feb-2005	71% (17/24)	100% (14/14)	67% (14/21)	30% (3/10)	100% (3/3)
SM	23-Mar-2005	75% (3/4)	75% (3/4)	100% (3/3)	- (0/0)	0% (0/1)
SP	28-Feb-2004	85% (46/54)	100% (41/41)	84% (41/49)	38% (5/13)	100% (5/5)

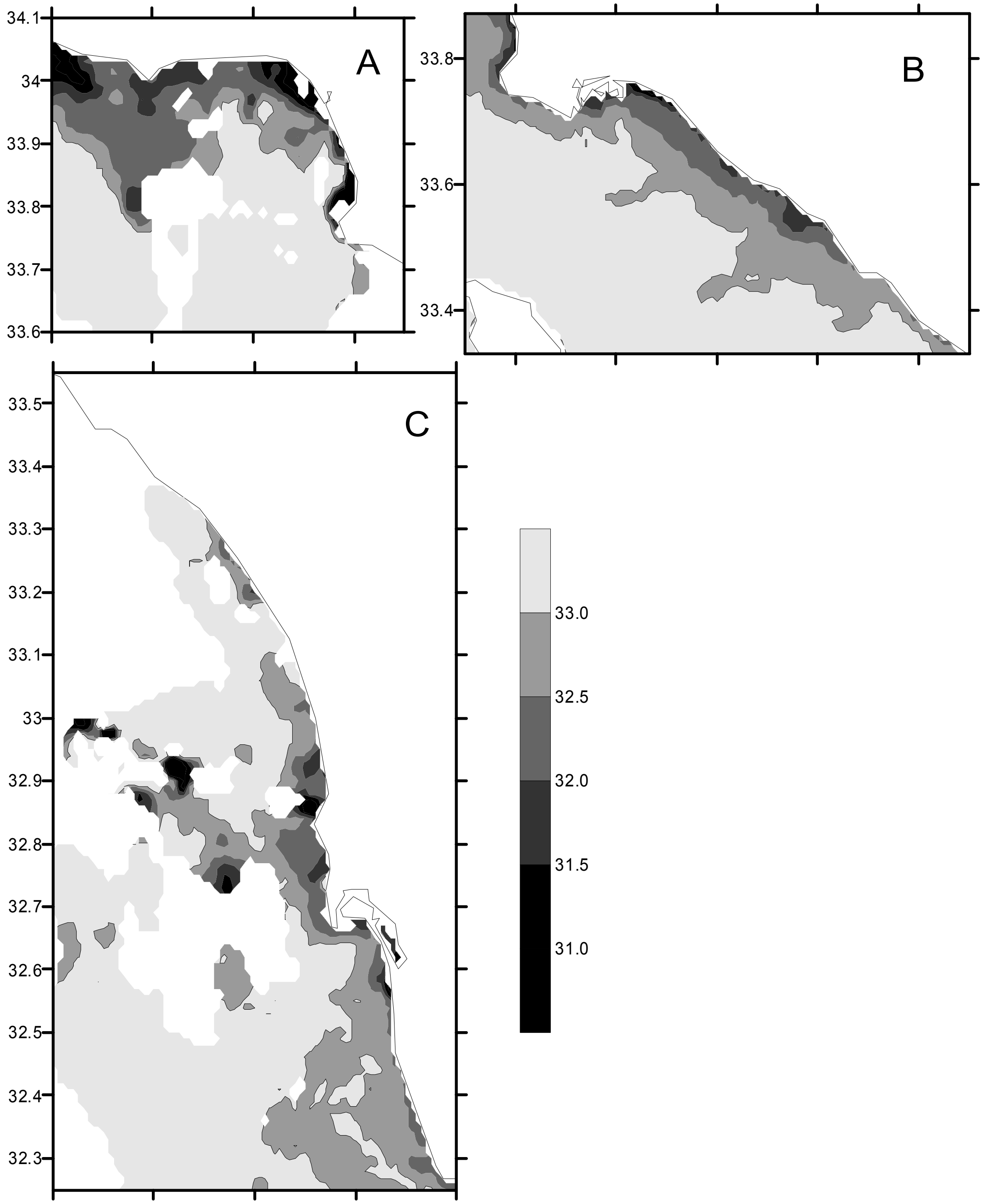

Figure VII-10. Plumes (S<33.0 psu) in SM March 23, 2005; (A), SP February 28, 2004 (B) and SD February 13, 2005 (C) regions reconstructed from $a_{dg}412$ remotely sensed CDOM absorption.

Discussion

This study shows that the data collected by "ocean color" satellites (e.g., MODIS) are a useful tool for detection of stormwater plumes. This is true even in areas like the SCB, where plume size is much smaller as compared with the plumes of large rivers like the Mississippi (Walker 1996, DelCastillo *et al.* 2001, D'Sa and Miller 2003), Amazon (Curtin and Legeckis 1986, Mertes *et al.* 1993, Del Vecchio and Subramaniam 2004), Orinoco (Muller-Karger *et al.* 1989), and Columbia (Fiedler and Laurs 1990). Ship-based data alone cannot show the plume boundaries or provide a synoptic view on the direction of propagation and offshore/alongshore extension of a plume. In all of the SCB regions, the areas covered by Bight '03 ship-based sampling were smaller than the areas of stormwater plumes detected by satellite sensors (*cf.* Section V), largely by design given the expense and logistical difficulties in sampling such large regions. It was especially evident in the VE region, where plumes are typically larger than in the rest of the SCB (Nezlin *et al.* 2005), which can be explained by large watershed area and high discharge volumes, high concentration of discharged sediments (Otero and Siegel 2004, Warrick *et al.* 2004a), and by dynamic circulation patterns typical to that region (Harms and Winant 1998, Bray *et al.* 1999). As a result, ship-based data collected near the mouths of the Ventura and Santa Clara rivers were insufficient to represent the entire spectrum of plume/ocean conditions.

The best model currently of plume detection from MODIS imagery in the SCB is based on nLw rather than TSS backscattering or CDOM absorption. The plume endmembers based on nLw are consistent in time and across the river systems and storms. This approach, confirmed by extended number of observations, can be used consistently for future monitoring and analysis of stormwater plumes and their impacts.

The nLw of 531–551 nm wavelengths was the most informative parameter for plume detection. These nLw depend mostly on backscattering of suspended sediments (Otero and Siegel 2004), dominated by lithogenic silica (Toole and Siegel 2001, Warrick *et al.* 2004b). Our previous studies of freshwater plumes in the SCB were based on similar remotely-sensed properties, i.e., SeaWiFS nLw of 555 nm wavelength (Nezlin and DiGiacomo 2005, Nezlin *et al.* 2005). Other wavelengths are useful, however, in classifying plume waters, especially in the first days following river discharge. Thus, multiple wavelength analyses are also useful in plume identification (Warrick *et al.* 2004b). The general plume characteristics revealed from SeaWiFS observations in 1997–2003 (Nezlin and DiGiacomo 2005, Nezlin *et al.* 2005) are in accordance with the results of this study: the largest plumes were observed in the VE region and the smallest in the SM region; maximum plume size occurred 1–2 days after a rainstorm.

The overall accuracy of MODIS plume detection based on nLw (77%) was not as high as the general accuracy level (85%) typically recommended for remotely-sensed data (Congalton and Green 1999). The user accuracy for plumes was higher as compared with ambient ocean waters, i.e., for plumes, the chance to be correctly classified exceeded a similar chance for non-plume areas. The accuracy of plume classification in terms of salinity, however, was not directly transferable to water quality (i.e., bacterial counts). The concentrations of total coliforms, fecal coliforms and *Enterococcus* in plume waters were typically higher in low salinity waters than in ambient ocean waters (see Section VI), but the stations where bacterial counts exceeded the California State Water Board standard often occurred beyond the plume limits. We also estimated the accuracy of plume detection, based on a salinity threshold of 33.0 psu and nLw endmembers, using as a criterion *Enterococcus* counts exceeding the California State Water Board standard of 104 CFU 100 ml^{-1}. This accuracy was as low as 45–56% (Table VII-8). At some stations, this accuracy was even lower. In performing this analysis, we assume that *Enterococcus* is present in stormwater and that it mixes in the same manner as salinity. *Enterococcus*, however, has a high mortality rate in sunlight (Davies and Evison 1991, Davies-Colley *et al.* 1994, Noble *et al.* 2004) and may therefore decrease at a much faster rate than that due to mixing alone. Furthermore, bacteria concentrations are typically quite patchily distributed (e.g., Boehm and Weisberg 2005, Rosenfeld *et al.* 2006). Meanwhile, an important assessment in terms of human health risk is the user accuracy for ambient ocean water, i.e., the chance that areas classified as non-plume (~non-contaminated) waters, do not exceed the bacterial contamination standard. This accuracy was 88% for plumes contoured by S and 77% for plumes contoured by remotely sensed nLw optical signatures. For plumes, the user accuracy was much lower than a similar statistic for ambient ocean waters. This means that of two types of errors (erroneous plume detection resulting in unjustified beach closures vs. undetected pathogen-laden plumes resulting in human health risk), the first error type looks more probable in remotely-sensed plume monitoring and assessments. This is also true in the SD and SP regions when we contoured the plumes using the correlation between CDOM in seawater and remotely sensed CDOM absorption (user accuracy for ocean waters was as high as 100%). The latter method, however, does not always provide accurate results, which reasons are discussed below.

In theory, CDOM absorption is perhaps the best proxy of plume water (other than salinity). In coastal regions freshwater discharge is a primary source of CDOM (Siegel *et al.* 2002, D'Sa and Miller 2003, Del Castillo 2005), which originates mostly from organic materials leached from soils into freshwater (Coble *et al.* 2004). CDOM concentration is more conservative than suspended sediments, for which concentrations are high in emerging plumes but rapidly decrease with time due to gravitational sedimentation (Warrick *et al.* 2004b, Ahn *et al.* 2005). Decreases in CDOM can occur due to photodegradation, but this process takes weeks to months (Vodacek *et al.* 1997, Opsahl and Benner 1998). However, in about one-half of the Bight '03 observations no significant correlation was found between *in situ* fluorometric CDOM measurements in the remotely sensed portion of the upper ocean layer and CDOM absorption ($a_{dg}412$) derived from satellite imagery, processed using current capabilities and the methodologies described above. The reasons can include 1) discrepancies resulting from plume instability during the time lag between satellite and ship-based observations; 2) inaccurate atmospheric correction; and 3) incorrect estimation of total absorption coefficients from water-leaving radiances and uncertain decomposition of total absorption coefficients into phytoplankton and detritus/CDOM absorption coefficients, among other potential factors (e.g. accurate calibration of *in situ* fluorometric CDOM measurements).

Table VII-8. Accuracy (%) of plume classification in the SCB in terms of matching between stations attributed to plume on the basis of S<33.0 psu or nLw endmembers and bacterial contamination exceeding California State Water Board standard (*Enterococcus* >104 CFU ml^{-1}).

Reg.	Date		Overall accuracy	Plume		Ambient ocean	
				Producer accuracy	User accuracy	Producer accuracy	User accuracy
SD	24-Feb-04	S	92% (11/12)	92% (11/12)	100% (11/11)	- (0/0)	0% (0/1)
		nLw	18% (2/11)	18% (2/11)	100% (2/2)	- (0/0)	0% (0/9)
SD	28-Feb-04	S	73% (8/11)	78% (7/9)	88% (7/8)	50% (1/2)	33% (1/3)
		nLw	55% (16/29)	20% (2/10)	29% (2/7)	74% (14/19)	64% (14/22)
SD	29-Feb-04	S	62% (13/21)	22% (2/9)	67% (2/3)	92% (11/12)	61% (11/18)
		nLw	69% (24/35)	17% (2/12)	67% (2/3)	96% (22/23)	69% (22/32)
SD	13-Feb-05	S	88% (21/24)	82% (14/17)	100% (14/14)	100% (7/7)	70% (7/10)
		nLw	80% (16/20)	79% (11/14)	92% (11/12)	83% (5/6)	63% (5/8)
SM	27-Feb-04	S	50% (2/4)	100% (1/1)	33% (1/3)	33% (1/3)	100% (1/1)
		nLw	100% (4/4)	100% (1/1)	100% (1/1)	100% (3/3)	100% (3/3)
SM	28-Feb-04	S	29% (5/17)	100% (3/3)	20% (3/15)	14% (2/14)	100% (2/2)
		nLw	47% (8/17)	67% (2/3)	20% (2/10)	43% (6/14)	86% (6/7)
SM	01-Mar-04	S	65% (11/17)	100% (1/1)	14% (1/7)	63% (10/16)	100% (10/10)
		nLw	50% (2/4)	- (0/0)	0% (0/2)	50% (2/4)	100% (2/2)
SM	23-Mar-05	S	17% (1/6)	100% (1/1)	17% (1/6)	0% (0/5)	- (0/0)
		nLw	100% (3/3)	- (0/0)	- (0/0)	100% (3/3)	100% (3/3)
SP	27-Feb-04	S	57% (16/28)	100% (9/9)	43% (9/21)	37% (7/19)	100% (7/7)
		nLw	54% (14/26)	56% (5/9)	38% (5/13)	53% (9/17)	69% (9/13)
SP	28-Feb-04	S	32% (18/57)	100% (5/5)	11% (5/44)	25% (13/52)	100% (13/13)
		nLw	34% (18/53)	60% (3/5)	8% (3/36)	31% (15/48)	88% (15/17)
SP	01-Mar-04	S	38% (23/61)	100% (1/1)	% (1/39)	37% (22/60)	100% (22/22)
		nLw	100% (2/2)	- (0/0)	- (0/0)	100% (2/2)	100% (2/2)
SP	25-Mar-05	S	15% (9/62)	100% (1/1)	2% (1/54)	13% (8/61)	100% (8/8)
		nLw	78% (42/54)	0% (0/1)	0% (0/11)	79% (42/53)	98% (42/43)
VE	29-Feb-04	S	92% (11/12)	- (0/0)	0% (0/1)	92% (11/12)	100% (11/11)
		nLw	11% (1/9)	- (0/0)	0% (0/8)	11% (1/9)	100% (1/1)
VE	25-Mar-05	S	36% (5/14)	0% (0/1)	0% (0/8)	38% (5/13)	83% (5/6)
		nLw	42% (5/12)	- (0/0)	0% (0/7)	42% (5/12)	100% (5/5)
	Total	S	45% (154/346)	80% (56/70)	24% (56/234)	36% (98/276)	88% (98/112)
		nLw	56% (157/279)	42% (28/66)	25% (28/112)	61% (129/213)	77% (129/167)

The time lag between ship-based data collection (surveys typically were from 7 a.m. to 4 p.m. local time) and MODIS-Aqua imagery (taken about 1 – 2 p.m.) can partly explain the discrepancies between the *in situ* and remotely sensed data. A horizontal velocity of 50 cm s^{-1} (equal to ~1.8 km h^{-1}) such as observed in southern California river plumes (see Section V) can move the plume boundary as far as 5 – 10 km during a few hours. However, discrepancies based on time lag are equally applicable to all kinds of satellite data, including nLw, absorption and backscattering, and cannot explain why the correlation between *in situ* fluorometric CDOM measurements and remotely-sensed $a_{dg}412$ was lower than the patterns revealed from nLw. During calibration and validation of remotely-sensed data, the observations are considered a match (i.e., coming from a unique station) when all measurements were made within a 12-hour window and within 0.05 degrees in both latitude and longitude (Maritorena *et al.* 2006). The data analyzed in this study conform to these criteria.

Inaccurate atmospheric correction can be a reason of poor correlation between *in situ* CDOM fluorescence and remotely-sensed $a_{dg}412$. In coastal waters, atmospheric correction of satellite imagery requires more sophisticated approaches as compared with open ocean waters (Siegel *et al.* 2000). The main difficulty is that the "black pixel assumption", i.e., the assumption that water-leaving radiance in near-infrared (NIR) is negligible, is true for clean oligotrophic ocean waters but typically does not work in coastal areas, where significant NIR backscattering results from high concentrations of phytoplankton and suspended sediments. In the open ocean, aerosol radiative properties can be easily determined from NIR remotely-sensed reflectances, which contain a signal from the atmosphere and no signal from the ocean surface (Gordon and Wang 1994b, Gordon 1997). In coastal waters more complex algorithms based on other assumptions are being developed and utilized (see Hu *et al.* 2000, Ruddick *et al.* 2000, Siegel *et al.* 2000, Lavender *et al.* 2005, Wang and Shi 2005, 2006, Wang 2007, Wang *et al.* 2007). However, ocean color retrievals in turbid coastal waters are still imperfect, with significant errors in derived products often resulting from ocean contributions at the NIR bands (Wang 2007). Using MODIS short-wave infrared (SWIR) instead of near-infrared (NIR) wavelengths for atmospheric correction looks like a promising method (Wang and Shi 2005, 2006, Wang 2007, Wang *et al.* 2007), because in the SWIR the ocean is black even in coastal waters due to much stronger water absorption. However, use of SWIR bands for atmospheric correction is still an emerging capability with further research and development efforts and testing needed in this and other coastal regions; this will be a focus of our future regional research efforts.

Another source of error can be an improper estimation of sea surface roughness and whitecaps on the sea surface, which can significantly contribute to ocean color (Gordon 1997). The contamination of optical signal by whitecaps and sun glint is estimated on the basis of wind speed data (Gordon and Wang 1994a, Frouin *et al.* 1996, Moore *et al.* 2000). This approach, however, sometimes provides erroneous results. For example, on February 27, 2004 the coefficients b_b551 and especially $a_{dg}412$ were unrealistically high in the open SCB zone ($a_{dg}412$ by 5 m^{-1} and b_b551 by 0.3 m^{-1}). In the nearshore zone, these coefficients were more plausible, with significant correlations between TSS/b_b551 and CDOM/$a_{dg}412$. However, the attempt to contour stormwater plumes from $a_{dg}412$ or b_b551 resulted in unrealistic plume patterns including the central open part of the SCB (not shown). That day (February 27, 2004) was characterized by very high waves (>5 m in the Santa Barbara Channel and in the center of the SCB), which could bias ocean color properties, especially absorption and backscattering coefficients. Indeed, the absorption and backscattering coefficients are estimated from nLw spectral slope (Lee *et al.* 2002), which in turn depends on sea surface roughness (Wang 2002), including contamination of optical signal by sun glint (Wang and Bailey 2001), and to a less extent by whitecaps (Gordon and Wang 1994a). During MODIS data processing, the contribution of sea surface roughness is estimated from the wind speed provided by the National Center for Environmental Prediction (NCEP) (Kalnay *et al.* 1996) modeled data of 1^ox1^o spatial and 6-hour temporal resolution.

According to these coarse data, on February 27, 2004 the wind speed over the SCB was <10 m s^{-1}. At the same time, the wind speed measured by NDBC buoys was ~12 m s^{-1} and the significant wave height of >5 m (observed in the SCB) corresponded to a wind speed of >15 m s^{-1} (calculated from the Pierson-Moskowitz spectrum). As such, for the MODIS-Aqua image acquired February 27, 2004, the contribution of sea surface roughness was significantly underestimated, resulting in obscured spectral slope and incorrectly estimated $a_{dg}412$ and b_b551. This error could be corrected by using local meteorological data instead of coarse NCEP meteorology. This would require modifications of the SeaDAS ocean color processing software.

Although the QAA algorithm estimates CDOM and detritus absorption coefficients better than many other methods (*cf.* Lee 2006), accurate results from its initial, untuned application are not guaranteed. Incorrect CDOM/detritus absorption coefficients could result from the uncertainty in the decomposition of the total absorption coefficient into phytoplankton and CDOM absorption (Lee *et al.* 2006). The SeaDAS 5.0 QAA version uses a fixed $a_{dg}(\lambda)$ spectral slope (default value 0.015). In reality, this coefficient varies widely based on the nature of waters under study, including humic vs. fulvic acids (Carder *et al.* 1989) and the abundance of detritus (Roesler *et al.* 1989). The CDOM absorption spectral slope is different for riverine and marine CDOM (Del Castillo *et al.* 2000, Del Castillo 2005). In particular, terrestrial CDOM (which is expected to be a proxy of freshwater plume impact), when compared to marine CDOM (resulting from biochemical transformation of by-products of phytoplankton vital activity), is characterized by stronger absorption on longer wavelengths (red-shift) (Del Castillo 2005). Based on our results, it is clear that the $a_{dg}(\lambda)$ spectral slope and other coefficients used in the QAA algorithm should be estimated regionally, on the basis of hydrological and bio-optical observations in the study area.

Although phytoplankton biomass (CHL) is one of the sources of CDOM, the absence of correlation between CDOM absorption and CHL can be explained by a long and yet unspecified process of transformation of mostly colorless products of biological activities (exudation by organisms, viral lysis, and sloppy feeding by zooplankton) into CDOM (see Siegel *et al.* 2002, Del Castillo 2005). As a result, the variability in CDOM concentration is significantly smaller than that in CHL (Kahru and Mitchell 2001) and at small spatial and temporal scales CDOM and CHL are uncorrelated.

Many of the challenges of remote sensing in nearshore regions result from the fact that the focus of satellite observations has only recently shifted from open ocean regions to coastal waters. Open ocean (Case 1) satellite data are easier to analyze than “optically complex” (Case 2) coastal waters (Morel and Prieur 1977, Sathyendranath 2000). Widespread development and use of Case-II algorithms is a comparatively recent endeavor, and scientific studies and publications utilizing, testing, and regionally improving these algorithms are only now starting to become common in the literature (Lee 2006).

The results from our study indicate that satellite data (e.g., MODIS) can be a useful tool for event-scale monitoring and near-real time assessments of coastal water quality, building upon previous regional investigations that looked at different properties and approaches. Several methods explored in this study show promise in detecting both the dissolved and particulate portions of stormwater plumes in the SCB. Currently, the methods using particulate plume signals estimated from ocean color satellite imagery (nLw 531–551; b_b551) appear to most accurately track plumes, especially in the first few days after a storm. CDOM has been shown to be a good tracer of plumes in this region when measured *in situ* (see Sections V–VI); the result was not quite as robust in this initial effort using satellite ocean color-derived estimates of CDOM (a_{dg}412) in support of regional water quality assessments. As such, improved CDOM product development through greater understanding and correcting for the geophysical and biological factors that can impact these ocean color derived estimates is a crucial need. Further algorithm development and refinement is needed; the coefficients used in the general QAA algorithm used here can be locally tuned using *in situ* optical measurements, which are currently being made throughout the SCB. Improved methodologies for atmospheric correction need to be further developed and implemented regionally. Further work is needed to link in a statistically significant manner those bio-optical parameters that can be accurately characterized from ocean color sensors with those that are greatest interest to water quality managers (including bacteria and toxicity levels). Finally, overall system improvements in our ability to observe ocean color from satellites, especially increases in spatial, temporal and spectral resolution, will greatly enhance our ability to use these data as a tool for studying regional coastal processes and features such as stormwater runoff plumes, as well as harmful algal blooms (Schnetzer *et al.* 2007). Satellite data, even qualitative data, provide critical synoptic information (e.g. plume size and location) for coastal managers that they cannot get from ship-based sampling alone and its use needs to be promoted and facilitated wherever and whenever possible.

VIII. CONCLUSIONS

- Stormwater runoff turbidity plumes were found to be spatially extensive, covering up to 2500 km^2 within the Southern California Bight nearshore zone and persisting over the entire duration of the post-storm sampling period (at least three days).

  Plumes frequently extended >10 km offshore from several of the river systems measured. For example, the San Pedro Shelf runoff plume was observed at times to extend well into the San Pedro Channel, approaching Catalina Island. However, alongshore movement of plumes was found to be as or more prevalent than across-shore movement, suggesting that runoff and attendant loadings discharged from a river system can potentially be quickly transported to coastal waters offshore of adjacent river systems. This was especially apparent for the Santa Clara River plume, which was observed to extend toward Santa Monica Bay during all of our observations.

- The spatial and temporal extent of the portion of the plume with contaminants was far less than that of the turbidity plume.

  While turbidity plumes often extended more than 50 km from the mouth of individual river systems, the areal impact from bacterial contamination and from water column toxicity was in most cases constrained to the nearfield region of the river discharge. Elevated concentrations of fecal indicator bacteria (FIB) were found offshore of each of the major river systems, but exceedances were generally limited to the nearfield region of the discharge. As such, the contaminated portion of the extensive turbid plume was typically small, e.g., up to 6% area for the San Pedro Shelf, although for the Tijuana system the percentage was much greater, up to 30–70% on several sampling days. Of over 700 water samples analyzed for toxicity, only 5% exhibited toxicity, and three exhibited highly toxic effects. The vertical distributions of FIBs and toxicity plume were confined to the upper 5–10 m of the water column, consistent with the expected patterns of a buoyant runoff plume.

  The extent of these ecological effects was also generally temporally limited. FIBs typically decreased below threshold levels of concern within two days. The one exception was for the Tijuana River plume in February 2005, when high concentrations of FIB persisted through the entire survey. However, toxicity results were mixed in terms of a temporal trend, significantly declining by the third day of sampling in some cases (Tijuana River plume, 2004 storm event), but conversely increasing in others (Ballona Creek and San Pedro Shelf plumes, 2004 storm event). The greatest number of toxic samples (72 %) was observed in the Tijuana River plume on the first day of sampling during the February 2004 event.

- Accurately describing stormwater runoff plumes requires a combination of *in situ* and remote sensing assessment tools, with satellite data providing valuable synoptic information.

  Stormwater plumes evolved rapidly during the study, with mean daily alongshore plume advection as high as 50 cm s^{-1}. Ships provide the opportunity to measure parameters that can not be measured through remote sensing, but ships move slowly relative to the rate of plume dispersion observed in this study, and do not provide a comprehensive assessment on their own. The synoptic perspective provided by satellite remote sensing was valuable in characterizing the spatial and temporal extent of runoff plumes, and also in determining whether the outflow of a particular watershed was impacting water quality in other parts of the SCB coastal ocean far from the source watershed.

The best models currently of plume detection from MODIS ocean color imagery in the SCB were those related to turbidity, i.e., normalized water leaving (nLw) radiances (~531 – 551 nm) and backscattering coefficients (b_b551), rather than colored dissolved organic matter (CDOM) absorption. However, CDOM shows significant promise for future space-based water quality monitoring efforts as a better proxy for salinity based on *in situ* measurements, with future research and development activities needed to improve and regionally tune the satellite algorithm used to derive CDOM absorption estimates (e.g., a_{dg}412).

Future work is also required to improve the linkages that can be made between parameters that can be remotely sensed with those that are of ecological significance; initial attempts to identify plumes with contaminants were only partially successful (overall accuracy of 56% using nLw data). Regardless, satellite remote sensing alone will certainly not provide all of the information needed by managers, and as such is not a replacement for *in situ* measurements, but satellites observations can be a key part of an integrated coastal monitoring and decision-support system, identifying areas of plume location and potential contamination, as well as adaptively vectoring coincident *in situ* sampling efforts.

- *Pseudo-nitzschia*, a harmful algae that produces domoic acid, strongly impacts near-shore coastal waters of the SCB.

The presence of *Pseudo-nitzschia*, a diatom that produces the neurotoxin domoic acid, was only examined in a portion of the Bight '03 study area and a bloom that reached moderate levels of toxicity was observed in the San Pedro Channel area at the end of February/beginning of March 2004 following one of the runoff events. Maximal levels of domoic acid were detected south of the Palos Verdes Peninsula and the Newport Bay area. *Pseudo-nitzschia* abundances and toxin concentrations were associated with decreases in macronutrient concentrations (phosphate and silicate) as well as with changes in nutrient ratios. However, *Pseudo-nitzschia* growth and domoic acid production could not be tied to the river runoff based on field observations. Generally, highest domoic acid concentrations have repeatedly been observed close to the shoreline and inside the Los Angeles harbor, suggesting that near-shore processes play a major role in bloom dynamics.

IX. RECOMMENDATIONS AND FUTURE DIRECTIONS

The following water quality monitoring recommendations result from the Bight '03 regional water quality monitoring findings:

- Future studies designed to describe stormwater plumes should include a combination of ship- and remote sensing-based methods.

  Ship-based measurements allow quantification of the parameters of most direct ecological interest, but ship-based collections are expensive and slow. This study found that the size and condition of the plume is sufficiently large and dynamic such that it cannot be synoptically described without deploying multiple ships, further adding to the expense. Moreover, wave conditions are often unfavorable following rainstorms, as this study found when ships were unable to mobilize on the day following the storm. Other coastal observing tools, such as remote sensing (airborne, satellite and shore-based HF radar) and gliders/autonomous underwater vehicles (AUVs), as well as modeling (nowcasts and forecasts), provide a means for identifying areas of plume location in near real time to direct ship-based collections to the most appropriate locations and to assist in interpolating between such measurements in space and time. Use of airborne assets in particular for event-scale sampling would provide significantly improved spatial and temporal resolution for a discrete period of time.

- CDOM should be added as a standard measurement parameter on water quality instrument packages.

  The ability to integrate satellite imagery with ship-based measurements will be significantly enhanced with the widespread addition of colored dissolved organic matter (CDOM) fluorometric measurements as part of the standard, routine ship-based water quality sampling protocols (already standard in the Central Bight). CDOM absorption is a good proxy of salinity, and therefore stormwater, and can be derived from satellite ocean color measurements of inherent optical properties. Analysis of existing data and collection of additional CDOM and *in situ* bio-optical measurements in the SCB will support development of improved, regionally tuned satellite algorithms and better quantify the relationship between CDOM and other standard *in situ* measurements toward obtaining more accurate, synoptic estimations of key water quality parameters and conditions.

- Investigations are needed that assess on a local basis the spatial extent of ecological effects of stormwater plumes early in the storm.

Conclusions about the spatial extent of toxic effects in Bight '03 were mostly limited to effects that were observed on the second day following rainstorms because high seas allowed only limited ship deployment on the first day following storms. The limited data collected on the first day suggests that the storm influence was not much larger then, but additional studies targeted on the first day should be conducted to confirm this, perhaps through frequent (e.g., hourly) field sampling at selected nearshore locales, if possible accompanied by high-resolution airborne imagery.

- The next Bight regional monitoring program should focus on quantifying nutrient loadings and dynamics in association with stormwater runoff and other sources, and characterize their attendant ecosystem impacts such as phytoplankton blooms.

  Pseudo-nitzschia, a diatom that produces the neurotoxin domoic acid, was found to occur in high numbers in Los Angeles Harbor during the Bight '03 study, but its occurrence in other parts of the SCB is not well documented. The timing and location of the Bight '03-measured bloom suggests that it was associated in some manner with a runoff event, but there are numerous other sources of nutrients to that area, including those from treated wastewater outfalls and from natural upwelling. Moreover, blooms associated with runoff are likely to manifest in the days to weeks following runoff, whereas the Bight '03 sampling was targeted at microbiological and toxicological effects that occur only in the first few days following a storm. Regionally targeted, adaptive ecological sampling to address nutrient contributions from various sources, covering a slightly longer post-storm period (e.g., 1–2 weeks) than was addressed in Bight '03, would provide insight as to the prevalence and dynamics of blooms and assessment of whether they are associated with runoff events.

X. LITERATURE CITED

Ahn, J.H., S.B. Grant, C.Q. Surbeck, P.M. DiGiacomo, N.P. Nezlin and S. Jiang. 2005. Coastal water quality impact of stormwater runoff from an urban watershed in southern California. *Environmental Science & Technology* 39:5940-5953.

Baker, E.T. and J.W. Lavelle. 1984. The effect of particle size on the light attenuation coefficient of natural suspensions. *Journal of Geophysical Research-Oceans* 89:8197-8203.

Bay, S., B.H. Jones, K. Schiff and L. Washburn. 2003. Water quality impacts of stormwater discharges to Santa Monica Bay. *Marine Environmental Research* 56:205-223.

Boehm, A.B. and S.B. Weisberg. 2005. Tidal forcing of Enterococci at marine recreational beaches at fortnightly and semidiurnal frequencies. *Environmental Science & Technology* 39:5575-5583.

Bosart, L.F. 1983. Analysis of a California Catalina eddy event. *Monthly Weather Review* 111:1619-1633.

Bray, N.A., A. Keyes and W.M.L. Morawitz. 1999. The California Current system in the Southern California Bight and the Santa Barbara Channel. *Journal of Geophysical Research-Oceans* 104:7695-7714.

Bricaud, A., A. Morel and L. Prieur. 1981. Absorption by dissolved organic matter of the sea (yellow substance) in the UV and visible domains. *Limnology and Oceanography* 26:43-53.

Brownlie, W.R. and B.D. Taylor. 1981. Sediment management for Southern California mountains, coastal plains and shoreline; part C, coastal sediment delivery by major rivers in Southern California. Environmental Quality Laboratory Report No. 17-C. California Institute of Technology. Pasadena, CA.

Burkov, V.A. and Y.V. Pavlova. 1980. Description of the eddy field of the California Current. *Oceanology.English Translation* 20:272-278.

Carder, K.L., R.G. Steward, G.R. Harvey and P.B. Ortner. 1989. Marine humic and fulvic acids: their effects on remote sensing of ocean chlorophyll. *Limnology and Oceanography* 34:68-81.

Chao, S.-Y. 1988. Wind-driven motion of estuarine plumes. *Journal of Physical Oceanography* 18:1144-1166.

Chen, R.F. and J.L. Bada. 1992. The fluorescence of dissolved organic matter. *Marine Chemistry* 37:191-221.

Coble, P.G., C. Hu, R.W. Gould, G. Chang and A.M. Wood. 2004. Colored dissolved organic matter in the coastal ocean: An optical tool for coastal zone environmental assessment and management. *Oceanography* 17:51-59.

Congalton, R.G. and K. Green. 1999. Assessing the accuracy of remotely sensed data: Principles and practices. Lewis Publishers. Boca Raton.

Culliton, T.J., M.A. Warren, T.R. Goodspeed, D.G. Remer, C.M. Blackwell and J.J. McDonough. 1990. Fifty years of population change along the nation's coasts, 1960-2010. Coastal Trends Series, Report No. 2. NOAA Strategic Assessment Branch. Rockville, MD.

Curtin, T.B. and R.V. Legeckis. 1986. Physical observations in the plume region of the Amazon River during peak discharge. I. Surface variability. *Continental Shelf Research* 6:31-51.

Dailey, M.D., J.W. Anderson, D.J. Reish and D.S. Gorsline. 1993. The Southern California Bight: Background and setting. pp. 1-18 *in*: M. D. Dailey , D. J. Reish and J. W. Anderson (Eds.), Ecology of the Southern California Bight. University of California Press. Berkeley, CA.

Davies, C.M. and L.M. Evison. 1991. Sunlight and the survival of enteric bacteria in natural waters. *Journal of Applied Microbiology* 70:265-274.

Davies-Colley, R.J., R.G. Bell and A.M. Donnison. 1994. Sunlight inactivation of enterococci and fecal coliforms in sewage effluent diluted in seawater. *Applied and Environmental Microbiology* 60:2049-2058.

Davies-Colley, R.J. and D.G. Smith. 2001. Turbidity, suspended sediment, and water clarity: a review. *Journal of the American Water Resources Association* 37:1085-1101.

Del Castillo, C.E. 2005. Remote sensing of organic matter in coastal waters. pp. 157-180 *in*: R. L. Miller , C. E. Del Castillo and B. A. McKee (Eds.), Remote Sensing of Coastal Aquatic Environments. Technologies, Techniques and Applications. Springer. Dordrecht.

Del Castillo, C.E., F. Gilbes, P.G. Coble and F.E. Muller-Karger. 2000. On the dispersal of riverine colored dissolved organic matter over the West Florida Shelf. *Limnology and Oceanography* 45:1425-1432.

Del Vecchio, R. and A. Subramaniam. 2004. Influence of the Amazon River on the surface optical properties of the western tropical North Atlantic Ocean. *Journal of Geophysical Research-Oceans* 109:C11001.

DelCastillo, C.E., P.G. Coble, R.N. Conmy, F.E. Muller-Karger, L. Vanderbloemen and G.A. Vargo. 2001. Multispectral in situ measurements of organic matter and chlorophyll fluorescence in seawater: Documenting the intrusion of the Mississippi River plume in the West Florida Shelf. *Limnology and Oceanography* 46:1836-1843.

DiGiacomo, P.M., L. Washburn, B. Holt and B.H. Jones. 2004. Coastal pollution hazards in southern California observed by SAR imagery: stormwater plumes, wastewater plumes, and natural hydrocarbon seeps. *Marine Pollution Bulletin* 49:1013-1024.

Dojiri, M., M. Yamaguchi, S.B. Weisberg and H.J. Lee. 2003. Changing anthropogenic influence on the Santa Monica Bay watershed. *Marine Environmental Research* 56:1-14.

Dorman, C.E. and C.D. Winant. 1995. Buoy observations of the atmosphere along the west coast of the United States. *Journal of Geophysical Research-Oceans* 100:16029-16044.

D'Sa, E.J., C. Hu, F.E. Muller-Karger and K.L. Carder. 2002. Estimation of colored dissolved organic matter and salinity fields in case 2 waters using SeaWiFS: Examples from Florida Bay and Florida Shelf. *Proceedings of the Indian Academy of Sciences-Earth and Planetary Sciences* 111:197-207.

D'Sa, E.J. and R.L. Miller. 2003. Bio-optical properties in waters influenced by the Mississippi River during low flow conditions. *Remote Sensing of Environment* 84:538-549.

Emery, K.O. 1960. The Sea off Southern California. John Wiley and Sons, Inc. New York, NY.

Esaias, W.E., M.R. Abbott, I. Barton, O.B. Brown, J.W. Campbell, K.L. Carder, D.K. Clark, R.H. Evans, F.E. Hoge, H.R. Gordon, W.M. Balch, R.M. Leteller and P.J. Minnett. 1998. An overview of MODIS capabilities for ocean science observations. *IEEE Transactions on Geoscience and Remote Sensing* 36:1250-1265.

Fiedler, P.C. and R.M. Laurs. 1990. Variability of the Columbia River plume observed in visible and infrared satellite imagery. *International Journal of Remote Sensing* 11:999-1010.

Fong, D.A. and W.R. Geyer. 2002. The alongshore transport of freshwater in a surface-trapped river plume. *Journal of Physical Oceanography* 32:957-972.

Frouin, R., M. Schwindling and P.-Y. Deschamps. 1996. Spectral reflectance of sea foam in the visible and near-infrared: In situ measurements and remote sensing implications. *Journal of Geophysical Research-Oceans* 101:14361-14371.

Fujioka, R.S., H.H. Hashimoto, E.B. Siwak and R.H. Young. 1981. Effect of sunlight on survival of indicator bacteria in seawater. *Applied and Environmental Microbiology* 41:690-696.

Garvine, R.W. 1991. Subtidal frequency estuary-shelf interaction: Observations near Delaware Bay. *Journal of Geophysical Research-Oceans* 96:7049-7064.

Garvine, R.W. 1995. A dynamical system for classifying buoyant coastal discharges. *Continental Shelf Research* 15:1585-1596.

Geesey, G.G. 1993. Microbiology. pp. 190-232 *in*: M. D. Dailey , D. J. Reish and J. W. Anderson (Eds.), Ecology of the Southern California Bight. University of California Press. Los Angeles, CA.

Gersberg, R.M., D. Daft and D. Yorkey. 2004. Temporal pattern of toxicity in runoff from the Tijuana River Watershed. *Water Research* 38:559-568.

Geyer, W.R., P. Hill, T. Milligan and P. Traykovski. 2000. The structure of the Eel River plume during floods. *Continental Shelf Research* 20:2067-2093.

Gilbert, P.S., T.N. Lee and G.P. Podesta. 1996. Transport of anomalous low-salinity waters from the Mississippi River flood of 1993 to the Straits of Florida. *Continental Shelf Research* 16:1065-1085.

Gordon, H.R. 1997. Atmospheric correction of ocean color imagery in the Earth Observing System era. *Journal of Geophysical Research-Atmospheres* 102:17081-17106.

Gordon, H.R. and D.K. Clark. 1980. Remote sensing optical properties of a stratified ocean: an improved interpretation. *Applied Optics* 19:3428-3430.

Gordon, H.R. and A.Y. Morel. 1983. Remote Assessment of Ocean Color for Interpretation of Satellite Visible Imagery: A Review. Springer-Verlag. New York, NY.

Gordon, H.R. and M. Wang. 1994a. Influence of oceanic whitecaps on atmospheric correction of ocean-color sensors. *Applied Optics* 33:7754-7763.

Gordon, H.R. and M. Wang. 1994b. Retrieval of water-leaving radiance and aerosol optical thickness over the oceans with SeaWiFS: a preliminary algorithm. *Applied Optics* 33:443-452.

Gumprecht, B. 1999. The Los Angeles River. Its Life, Death, and Possible Rebirth. The Johns Hopkins University Press. Baltimore, MD.

Haney, R.L., R.A. Hale and D.E. Dietrich. 2001. Offshore propagation of eddy kinetic energy in the California Current. *Journal of Geophysical Research-Oceans* 106:11709-11717.

Harms, S. and C.D. Winant. 1998. Characteristic patterns of the circulation in the Santa Barbara Channel. *Journal of Geophysical Research-Oceans* 103:3041-3065.

Helsel, D.R. 2005. Nondetects and Data Analysis. Wiley. New York, NY.

Helsel, D.R. and R.M. Hirsch. 2002. Statistical Methods in Water Resources. pp. 510 *in*, Hydrologic Analysis and Interpretation, Vol. 4. U.S. Geological Survey. USGS. Santa Cruz, CA.

Hickey, B.M. 1979. The California Current system: Hypotheses and facts. *Progress in Oceanography* 8:191-279.

Hickey, B.M. 1992. Circulation over the Santa Monica-San Pedro basin and shelf. *Progress in Oceanography* 30:37-115.

Hickey, B.M. 1993. Physical oceanography. pp. 19-70 *in*: M.D. Dailey , D.J. Reish and J.W. Anderson (eds.), Ecology of the Southern California Bight. University of California Press. Berkeley, CA.

Hickey, B.M., E.L. Dobbins and S.E. Allen. 2003. Local and remote forcing of currents and temperature in the central Southern California Bight. *Journal of Geophysical Research-Oceans* 108:3081, doi:3010.1029/2000JC000313.

Hickey, B.M., S. Geier, N. Kachel and A. MacFadyen. 2005. A bi-directional river plume: The Columbia in summer. *Continental Shelf Research* 25:1631-1656.

Horner, R.A., D.L. Garrison and F.G. Plumley. 1997. Harmful algal blooms and red tide problems on the U.S. west coast. *Limnology and Oceanography* 42:1076-1088.

Hu, C., K.L. Carder and F.E. Muller-Karger. 2000. Atmospheric correction of SeaWiFS imagery over turbid coastal waters: a practical method. *Remote Sensing of Environment* 74:195-206.

Inman, D.L. and S.A. Jenkins. 1999. Climate change and the episodicity of sediment flux of small California rivers. *Journal of Geology* 107:251-270.

Isaaks, E.H. and R.M. Srivastava. 1989. Applied geostatistics. Oxford University Press. New York, NY.

Isla, E.M., S. Vanderburg, C. Medjber and D. Paschall. 2004. Climate of San Diego, California. Second Edition, December 2004. NWS WR-270. NOAA.

Johnson, R.W. and R.C. Harris. 1980. Remote sensing for water quality and biological measurements in coastal waters. *Photogrammetric Engineering and Remote Sensing* 46:77-85.

Jones, B.H. and L. Washburn. 1997. Stormwater runoff into Santa Monica Bay: identification, impact and dispersion. pp. *in*: O.T. Magoon , H. Converse , B. Baird and M. Miller-Henson (eds.), California and the World Ocean '97. American Society of Civil Engineers. Reston, VA.

Kahru, M. and B.G. Mitchell. 2001. Seasonal and nonseasonal variability of satellite-derived chlorophyll and colored dissolved organic matter concentration in the California Current. *Journal of Geophysical Research-Oceans* 106:2517-2529.

Kalnay, E., M. Kanamitsu, R. Kistler, W. Collins, D. Deaven, L. Gandin, M. Iredell, S. Saha, G. White, J. Woollen, Y. Zhu, M. Chelliah, W. Ebisuzaki, W. Higgins, J. Janowiak, K.C. Mo, C.F. Ropelewski, J. Wang, A. Leetmaa, R. Reynolds, R. Jenne and D. Joseph. 1996. The NCEP/NCAR 40-year Reanalysis Project. *Bulletin of the American Meteorological Society* 77:437-471.

Kourafalou, V.H., T.N. Lee, L.-Y. Oey and J.D. Wang. 1996. The fate of river discharge on the continental shelf 2. Transport of coastal low-salinity waters under realistic wind and tidal forcing. *Journal of Geophysical Research-Oceans* 101:3435-3455.

Large, W.G. and S. Pond. 1981. Open ocean momentum flux measurements in moderate to strong winds. *Journal of Physical Oceanography* 11:324-336.

Lavender, S.J., M.H. Pinkerton, G.F. Moore, J. Aiken and D. Blondeau-Patissier. 2005. Modification to the atmospheric correction of SeaWiFS ocean colour images over turbid waters. *Continental Shelf Research* 25:539-555.

Lee, L. and D.R. Helsel. 2005. Statistical analysis of water-quality data containing multiple detection limits: S-language software for regression on order statistics. *Computers and Geosciences* 31:1241-1248.

Lee, Z., K.L. Carder and R.A. Arnone. 2002. Deriving inherent optical properties from water color: a multiband quasi-analytical algorithm for optically deep waters. *Applied Optics* 41:5755-5772.

Lee, Z., K.L. Carder and R.A. Arnone. 2006. The Quasi-Analytical Algorithm. pp. 73-79 *in*: Z. Lee (Ed.), Remote Sensing of Inherent Optical Properties: Fundamental, Tests of Algorithms and Applications, Vol. 5. IOCCG. Dartmouth, Canada.

Lee, Z.-P. (Ed.). 2006. Remote Sensing of Inherent Optical Properties: Fundamental, Tests of Algorithms and Applications. (Vol. 5). IOCCG. Dartmouth, Canada.

Lentz, S.J. and C.D. Winant. 1986. Subinertial currents on the southern California shelf. *Journal of Physical Oceanography* 16:1737-1750.

Lynn, R.J. and J.J. Simpson. 1987. The California Current System: The seasonal variability of its physical characteristics. *Journal of Geophysical Research-Oceans* 92:12947-12966.

Maritorena, S., Z. Lee, K. Du, H. Loisel, R. Doerffer, C.S. Roesler, P.E. Lyon, A. Tanaka, M. Babin and O.V. Kopelevich. 2006. Synthetic and in situ data sets for algorithm testing. pp. 13-18 *in*: Z. Lee (Ed.), Remote Sensing of Inherent Optical Properties: Fundamental, Tests of Algorithms and Applications, Vol. 5. IOCCG. Dartmouth, Canada.

Mertes, L.A.K., M. Hickman, B. Waltenberger, A.L. Bortman, E. Inlander, C. McKenzie and J. Dvorsky. 1998. Synoptic views of sediment plumes and coastal geography of the Santa Barbara Channel, California. *Hydrological Processes* 12:967-979.

Mertes, L.A.K., M.O. Smith and J.B. Adams. 1993. Estimating suspended sediment concentrations in surface waters of the Amazon River wetlands from Landsat images. *Remote Sensing of Environment* 43:281-301.

Mertes, L.A.K. and J.A. Warrick. 2001. Measuring flood output from 110 coastal watersheds in California with field measurements and SeaWiFS. *Geology* 29:659-662.

Miller, R.L. and B.A. McKee. 2004. Using MODIS Terra 250 m imagery to map concentrations of total suspended matter in coastal waters. *Remote Sensing of Environment* 93:259-266.

Miller, S.N., W.G. Kepner, M.H. Mehaffey, M. Hernandez, R.C. Miller, D.C. Goodrich, K.K. Devonald, D.T. Heggem and W.P. Miller. 2002. Integrating landscape assessment and hydrologic modeling for land cover change analysis. *Journal of the American Water Resources Association* 38:915-929.

Monahan, E.C. and M.J. Pybus. 1978. Colour, UV absorbance and salinity of the surface waters off the west coast of Ireland. *Nature* 274:782-784.

Moore, K.D., K.J. Voss and H.R. Gordon. 2000. Spectral reflectance of whitecaps: Their contribution to water-leaving radiance. *Journal of Geophysical Research-Oceans* 105:6493-6499.

Morel, A. and L. Prieur. 1977. Analysis of variations in ocean color. *Limnology and Oceanography* 22:709-722.

Muller-Karger, F.E., C.R. McClain, T.R. Fisher, W.E. Esaias and R. Varela. 1989. Pigment distribution in the Caribbean Sea: Observations from space. *Progress in Oceanography* 23:23-64.

Munchow, A.K. and R.W. Garvine. 1993. Buoyancy and wind forcing of a coastal current. *Journal of Marine Research* 51:293-322.

National Research Council. 1990. Monitoring southern California's coastal waters. National Academy Press. Washington, DC.

Nezlin, N.P. and P.M. DiGiacomo. 2005. Satellite ocean color observations of stormwater runoff plumes along the San Pedro Shelf (southern California) during 1997 to 2003. *Continental Shelf Research* 25:1692-1711.

Nezlin, N.P., P.M. DiGiacomo, E.D. Stein and D. Ackerman. 2005. Stormwater runoff plumes observed by SeaWiFS radiometer in the Southern California Bight. *Remote Sensing of Environment* 98:494-510.

Nezlin, N.P. and J.C. McWilliams. 2003. Satellite data, Empirical Orthogonal Functions, and the 1997-1998 El Nino off California. *Remote Sensing of Environment* 84:234-254.

Nezlin, N.P. and E.D. Stein. 2005. Spatial and temporal patterns of remotely-sensed and field-measured rainfall in southern California. *Remote Sensing of Environment* 96:228-245.

Nezlin, N.P., S.B. Weisberg and D.W. Diehl. 2007. Relative availability of satellite imagery and ship-based sampling for assessment of stormwater runoff plumes in coastal southern California. *Estuarine, Coastal and Shelf Science* 71:250-258.

Noble, M.A., H.F. Ryan and P.L. Wiberg. 2002. The dynamics of subtidal poleward flows over a narrow continental shelf, Palos Verdes, CA. *Continental Shelf Research* 22:923-944.

Noble, R.T., I.M. Lee and K.C. Schiff. 2004. Inactivation of indicator bacteria from various sources of fecal contamination in seawater and freshwater. *Journal of Applied Microbiology* 96:464-472.

Noble, R.T., S.B. Weisberg, M.K. Leecaster, C.D. McGee, J.H. Dorsey, P. Vainik and V. Orozco-Borbon. 2003. Storm effects on regional beach water quality along the southern California shoreline. *Journal of Water and Health* 1:23-31.

Ohlmann, J.C., P.F. White, A.L. Sybrandy and P.P. Niiler. 2005. A new kind of drifter to observe the coastal ocean. *Bulletin of the American Meteorological Society* 86:1219-1221.

Oliver, M.A. and R. Webster. 1990. Kriging: a method of interpolation for geographical information system. *International Journal of Geographical Information Systems* 4:313-332.

Opsahl, S. and R. Benner. 1998. Photochemical reactivity of dissolved lignin in river and ocean waters. *Limnology and Oceanography* 43:1297-1304.

Otero, M.P. and D.A. Siegel. 2004. Spatial and temporal characteristics of sediment plumes and phytoplankton blooms in the Santa Barbara Channel. *Deep-Sea Research II* 51:1129-1149.

Pinones, A., A. Valle-Levinson, D.A. Narvaez, C.A. Vargas, S.A. Navarrete, G. Yuras and J.C. Castilla. 2005. Wind-induced diurnal variability in river plume motion. *Estuarine, Coastal and Shelf Science* 65:513-525.

R Development Core Team. 2006. R: A Language and Environment for Statistical Computing. R Foundation for Statistical Computing. Vienna, Austria.

Ragan, M.A. 2003. Response of inherent optical properties to stormwater runoff in Santa Monica Bay, California. Unpublished Master of Science Thesis, University of Southern California. Los Angeles, CA.

Reid, J.L., Jr. and A.W. Mantyla. 1976. The effect of the geostrophic flow upon coastal sea elevations in the northern North Pacific ocean. *Journal of Geophysical Research* 81:3100-3110.

Richards, J.A. 1999. Remote Sensing Digital Image Analysis. Springer-Verlag. Berlin.

Roesler, C.S., M.J. Perry and K.L. Carder. 1989. Modeling in situ phytoplankton absorption from total absorption spectra in productive inland marine waters. *Limnology and Oceanography* 34:1510-1523.

Rosenfeld, L.K., C.D. McGee, G.L. Robertson, M.A. Noble and B.H. Jones. 2006. Temporal and spatial variability of fecal indicator bacteria in the surf zone off Huntington Beach, CA. *Marine Environmental Research* 61:471-493.

Roughan, M., E. Terrill, J.L. Largier and M.P. Otero. 2005. Observations of divergence and upwelling around Point Loma, California. *Journal of Geophysical Research-Oceans* 110:doi:10.1029/2004JC002662.

Ruddick, K.G., F. Ovidio and M. Rijkeboer. 2000. Atmospheric correction of SeaWiFS imagery for turbid coastal and inland waters. *Applied Optics* 39:897-912.

Sathyendranath, S. (Ed.). 2000. Remote Sensing of Ocean Colour in Coastal and Other Optically-Complex Waters. (Vol. 3). IOCCG. Dartmouth, Canada.

Schiff, K.C., M.J. Allen, E.Y. Zeng and S.M. Bay. 2000. Southern California. *Marine Pollution Bulletin* 41:76-93.

Schiff, K.C., S.B. Weisberg and V.E. Raco-Rands. 2002. Inventory of Ocean Monitoring in the Southern California Bight. *Environmental Management* 29:871-876.

Schnetzer, A., P.E. Miller, R.A. Schaffner, B.A. Stauffer, B.H. Jones, S.B. Weisberg, P.M. DiGiacomo, W.M. Berelson and D.A. Caron. 2007. Blooms of *Pseudo-nitzschia* and domoic acid in the San Pedro Channel and Los Angeles harbor areas of the Southern California Bight, 2003-2004. *Harmful Algae* 6:372-387.

Schueler, T.R. and H.K. Holland. 2000. The Practice of Watershed Protection. Center for Watershed Protection. Ellicott City, MD.

Siddorn, J.R., D.G. Bowers and A.M. Hoguane. 2001. Detecting the Zambezi River plume using observed optical properties. *Marine Pollution Bulletin* 42:942-950.

Siegel, D.A., S. Maritorena, N.B. Nelson, D.A. Hansell and M. Lorenzi-Kayser. 2002. Global distribution and dynamics of colored dissolved and detrital organic materials. *Journal of Geophysical Research-Oceans* 107:3228, doi:3210.1029/2001JC000965.

Siegel, D.A., M. Wang, S. Maritorena and W. Robinson. 2000. Atmospheric correction of satellite ocean color imagery: the black pixel assumption. *Applied Optics* 39:3582-3591.

Smayda, T.J. 1997. Harmful algal blooms: Their ecophysiology and general relevance to phytoplankton blooms in the sea. *Limnology and Oceanography* 42:1137-1153.

Southern California Association of Governments; Regional Data & Maps; <http://www.scag.ca.gov>.

SSI. 2004. SYSTAT for Windows. SYSTAT Software, Inc. Richmond, CA.

State Water Resources Control Board. 2005. California Ocean Plan. SWRCB. Sacramento, CA.

Stein, E.D., L.L. Tiefenthaler and K.C. Schiff. 2006. Watershed-based sources of polycyclic aromatic hydrocarbons in urban storm water. *Environmental Toxicology and Chemistry* 25:373-385.

Strub, P.T. and C. James. 2000. Altimeter-derived variability of surface velocities in the California Current System: 2. Seasonal circulation and eddy statistics. *Deep-Sea Research II* 47:831-870.

Stumpf, R.P., G. Gelfenbaum and J.R. Pennock. 1993. Wind and tidal forcing of a buoyant plume, Mobile Bay, Alabama. *Continental Shelf Research* 13:1281-1301.

Sverdrup, H.U. and R.H. Fleming. 1941. The waters off the coast of southern California, March to July 1937. *Bulletin of the Scripps Institution of Oceanography* 4:261-378.

Toole, D.A. and D.A. Siegel. 2001. Modes and mechanisms of ocean color variability in the Santa Barbara Channel. *Journal of Geophysical Research-Oceans* 106:26985-27000.

US EPA. 1995. Short-term methods for estimating the chronic toxicity of effluents and receiving waters to West Coast marine and estuarine organisms (First ed.). Office of Research and Development, U.S. Environmental Protection Agency. Cincinnati, OH.

Vasilkov, A.P., V.I. Burenkov and K.G. Ruddick. 1999. The spectral reflectance and transparency of river plume waters. *International Journal of Remote Sensing* 20:2497-2508.

Vodacek, A., N.V. Blough, M.D. DeGrandpe, E.T. Peltzer and R.K. Nelson. 1997. Seasonal variation of CDOM and DOC in the Middle Atlantic Bight: Terrestrial inputs and photooxidation. *Limnology and Oceanography* 42:674-686.

Walker, N.D. 1996. Satellite assessment of Mississippi river plume variability: Causes and predictability. *Remote Sensing of Environment* 58:21-35.

Wang, M. 2002. The Rayleigh lookup tables for the SeaWiFS data processing: Accounting for the effects of ocean surface roughness. *International Journal of Remote Sensing* 23:2693-2702.

Wang, M. 2007. Remote sensing of the ocean contributions from ultraviolet to near-infrared using the shortwave infrared bands: simulations. *Applied Optics* 46:1535-1547.

Wang, M. and S. Bailey. 2001. Correction of sun glint contamination on the SeaWiFS ocean and atmosphere products. *Applied Optics* 40:4790-4798.

Wang, M. and W. Shi. 2005. Estimation of ocean contribution at the MODIS near-infrared wavelengths along the east coast of the U.S.: Two case studies. *Geophysical Research Letters* 32:L13606.

Wang, M. and W. Shi. 2006. Cloud masking for ocean color data processing in the coastal regions. *IEEE Transactions on Geoscience and Remote Sensing* 44:3196-3205.

Wang, M., J. Tang and W. Shi. 2007. MODIS-derived ocean color products along the China east coastal region. *Geophysical Research Letters* 34:L06611.

Warrick, J.A. and D.A. Fong. 2004. Dispersal scaling from the world's rivers. *Geophysical Research Letters* 31:doi:10.1029/2003GL019114.

Warrick, J.A., L.A.K. Mertes, D.A. Siegel and C. MacKenzie. 2004a. Estimating suspended sediment concentrations in turbid coastal waters of the Santa Barbara Channel with SeaWiFS. *International Journal of Remote Sensing* 25:1995-2002.

Warrick, J.A., L.A.K. Mertes, L. Washburn and D.A. Siegel. 2004b. A conceptual model for river water and sediment dispersal in the Santa Barbara Channel, California. *Continental Shelf Research* 24:2029-2043.

Warrick, J.A., L.A.K. Mertes, L. Washburn and D.A. Siegel. 2004c. Dispersal forcing of southern California river plumes, based on field and remote sensing observations. *Geo-Marine Letters* 24:46-52.

Warrick, J.A. and J.D. Milliman. 2003. Hyperpycnal sediment discharge from semiarid southern California rivers: Implications for coastal sediment budgets. *Geology* 31:781-784.

Warrick, J.A., L. Washburn, M.A. Brzezinski and D.A. Siegel. 2005. Nutrient contributions to the Santa Barbara Channel, California, from the ephemeral Santa Clara River. *Estuarine, Coastal and Shelf Science* 62:559-574.
10

Washburn, L., K.A. McClure, B.H. Jones and S.M. Bay. 2003. Spatial scales and evolution of stormwater plumes in Santa Monica Bay. *Marine Environmental Research* 56:103-125.

Whitney, M.M. and R.W. Garvine. 2005. Wind influence on a coastal buoyant outflow. *Journal of Geophysical Research-Oceans* 110:C03014.

Willis, C.M. and G.B. Griggs. 2003. Reductions in fluvial sediment discharge by coastal dams in California and implications for beach sustainability. *Journal of Geology* 111:167-182.

Winant, C.D. and A.W. Bratkovich. 1981. Temperature and currents on the southern California shelf: A description of the variability. *Journal of Physical Oceanography* 11:71-86.

Winant, C.D. and C.E. Dorman. 1997. Seasonal patterns of surface wind stress and heat flux over the Southern California Bight. *Journal of Geophysical Research-Oceans* 102:5641-5653.

Yankovsky, A.E. and D.C. Chapman. 1997. A simple theory for the fate of buoyant coastal discharges. *Journal of Physical Oceanography* 27:1386-1401.

ZoBell, C.E. 1941. The occurrence of coliform bacteria in oceanic water. *Journal of Bacteriology* 42:284.

APPENDIX A

ftp://ftp.sccwrp.org/pub/download/DOCUMENTS/TechnicalReports/528_B03_WQ_Appendix_A.pdf

APPENDIX B

ftp://ftp.sccwrp.org/pub/download/DOCUMENTS/TechnicalReports/528_B03_WQ_Appendix_B.pdf

APPENDIX C

ftp://ftp.sccwrp.org/pub/download/DOCUMENTS/TechnicalReports/528_B03_WQ_Appendix_C.pdf

APPENDIX D

ftp://ftp.sccwrp.org/pub/download/DOCUMENTS/TechnicalReports/528_B03_WQ_Appendix_D.pdf

APPENDIX E

ftp://ftp.sccwrp.org/pub/download/DOCUMENTS/TechnicalReports/528_B03_WQ_Appendix_E.pdf

APPENDIX F

ftp://ftp.sccwrp.org/pub/download/DOCUMENTS/TechnicalReports/528_B03_WQ_Appendix_F.pdf

APPENDIX G

ftp://ftp.sccwrp.org/pub/download/DOCUMENTS/TechnicalReports/528_B03_WQ_Appendix_G.pdf

APPENDIX H

ftp://ftp.sccwrp.org/pub/download/DOCUMENTS/TechnicalReports/528_B03_WQ_Appendix_H.pdf

APPENDIX I

ftp://ftp.sccwrp.org/pub/download/DOCUMENTS/TechnicalReports/528_B03_WQ_Appendix_I.pdf

APPENDIX J

ftp://ftp.sccwrp.org/pub/download/DOCUMENTS/TechnicalReports/528_B03_WQ_Appendix_J.pdf

APPENDIX K

ftp://ftp.sccwrp.org/pub/download/DOCUMENTS/TechnicalReports/528_B03_WQ_Appendix_K.pdf